Final Report
F-B2300-1

Technical Report

COMPUTER CONTROL STUDY FOR A MANNED CENTRIFUGE

by

John Stone
Ke-Cheong Taui
Eugene Peck

June 1965

Prepared for

NATIONAL AERONAUTICS & SPACE ADMINISTRATION
Manned Spacecraft Center
Houston, Texas

Contract NAS 9-2570

Final Report

F-B2300-1

Technical Report

COMPUTER CONTROL STUDY FOR A MANNED CENTRIFUGE

by

John Stone
Ka-Cheung Tsui
Eugene Pack

June 1965

Prepared for

NATIONAL AERONAUTICS & SPACE ADMINISTRATION
Manned Spacecraft Center
Houston, Texas

Contract NAS 9-3570

THE FRANKLIN INSTTUTE RESEARCH LABORATORIES

BENJAMIN FRANKLIN PARKWAY AT 20TH STREET, PHILA. 3, PA.

TABLE OF CONTENTS

LIST OF FIGURES

LIST OF FIGURES (Cont.)

Page

LIST OF FIGURES (Concl.)

INTRODUCTION

The purpose of this analog simulation study of the man-rated centrifuge is to determine the capabilities of the centrifuge in producing various g level versus time effects on a subject riding in the gondola. A control computer is necessary to convert g versus time input into command signals for the main arm drive, gimbal ring drive and gondola drive systems. The computer has been developed in analog form for this simulation and is written in a digital flow diagram form for use in the actual system control computer. The approach to this simulation project was to reduce the information supplied into a form suitable for analog simulation. Each of the main control systems has been checked separately to determine the effects of nonlinear components on frequency response and phase shift in that particular system. Limit circuits have been included and a study made to determine their effect since command signals are in some cases large enough to drive portions of the system beyond the linear range of gain. The effects of gyroscopic forces upon each of the systems has been analyzed and the resulting effect of these forces recorded during the simulation. Equations and methods for solving these equations have been developed for the control computer and the effectiveness demonstrated in the analog simulation runs. The methods for solving the complex equations in the analog computer simulation of the control computer have required the concept of special analog circuit configurations.

TECHNICAL DISCUSSION OF SYSTEM STUDIES

A. Inertia Changes

Before the analog simulations could be written for the computer, new values of inertia had to be inserted into the load equations for each of the control systems. In the gimbal ring and gondola control systems, these new inertias were relatively simple. The reflected load inertia to the motor drive shaft is computed by

$$S\theta_1 = nS\theta_2 \tag{1}$$

$$T_1 S\theta_1 = T_2 S\theta_2 \tag{2}$$

$$T = JS^2\theta \tag{3}$$

$$\frac{T_2}{T_1} = \frac{J_2 S^2\theta_2}{J_1 S^2\theta_1} = \frac{S\theta_1}{S\theta_2} \tag{4}$$

$$\frac{J_2}{J_1} = \frac{S(S\theta_1)^2}{S(S\theta_2)^2} = n^2 \tag{5}$$

From this we find that the inertia load reflected back to the motor shaft is multiplied by the inverse of the gear ratio squared.

The inertia loads specified for each system and the value

reflected back to the motor shaft are converted by

$$1b(ft)^2 \left[12/n^2 (32.2)\right] = 1b\text{-}in\text{-}sec^2 \qquad (6)$$

in order to apply the values to the motor torque equations.

Gimbal Ring Reflected Inertia

In the gimbal ring system the gondola load must also be included in the various relative positions since it is not a symmetrical load. Since the Y axis of the gimbal ring is always in line with either the Y axis or the Z axis of the gondola, we shall use the rms value to simulate the load inertia in this study. The specified inertias and reflected inertias are therefore calculated as:

Gimbal Ring Inertias Specified (with gondola load)

$$J_{GR(Y)} = 385,876\ 1b\text{-}ft^2 \qquad (7)$$

$$J_{G(Y)} = 172,377\ 1b\text{-}ft^2 \qquad (8)$$

$$J_{G(Z)} = 209,291\ 1b\text{-}ft^2 \qquad (9)$$

$$J_{G(rms)} = 191,834\ 1b\text{-}ft^2 \qquad (10)$$

Gimbal ring reflected inertia is expressed as

$$J_R = \left(\frac{1}{66}\right)^2 (385,876 + 191,834) \left(\frac{12}{32.2}\right) = 49,4\ 1b\text{-}in\text{-}sec^2 \qquad (11)$$

This information substituted into the motor equations provides the transfer function for θ_m/T_m

$$\theta_m/T_m = 1/K + 1/JS^2 \qquad (12)$$

$$\theta_m/T_m = .812 \times 10^{-4} + .02025/S^2 \qquad (13)$$

Gondola Reflected Inertia

The gondola system involves only the inertia load of the gondola about the X axis of the gondola. This calculation is expressed as:

Gondola Inertia Specified

$$J_{G(X)} = 85,706 \text{ lb-ft}^2 \qquad (14)$$

Gondola Reflected Inertia

$$J_R = \left(\frac{1}{58.5}\right)^2 (85,706) \left(\frac{12}{32.2}\right) = 9.33 \text{ lb-in-sec}^2 \qquad (15)$$

From this the motor transfer equation can be expressed as

$$\theta_m/T_m = .704 \times 10^{-4} + .107/S^2 \qquad (16)$$

Consideration of Shaft Spring Rate

Equation (12) is the expression of motor shaft position

and motor torque. To accurately simulate the output load shaft position we must consider the spring rate of the shaft that is inserted between the motor shaft and the load.

Figure 1 illustrates schematically the system to be considered. The transfer function of motor shaft position θ_m to load position θ_R is developed as follows:

$$T_m = K(\theta_m - n\theta_R) = \frac{J}{n^2} S^2(n\theta_R) \tag{17}$$

$$\theta_R \left[\frac{J}{n} S^2 + K_n\right] = K\theta_m \tag{18}$$

$$\frac{\theta_R}{\theta_m} = \frac{1}{n}\left[\frac{1}{(1/K)(J/n^2)S^2+1}\right] \tag{19}$$

In the simulation of the systems it is more important for us to know P_m instead of θ_m since P_m must be limited at a specified value. From information supplied for this simulation we have

$$\theta_m = d_m \left(\frac{\theta_m}{T_m}\right) P_m \tag{20}$$

and

$$\frac{\theta_m}{T_m} = \frac{1}{K} + \frac{1}{\left(\frac{J}{n^2}\right) S^2} \tag{21}$$

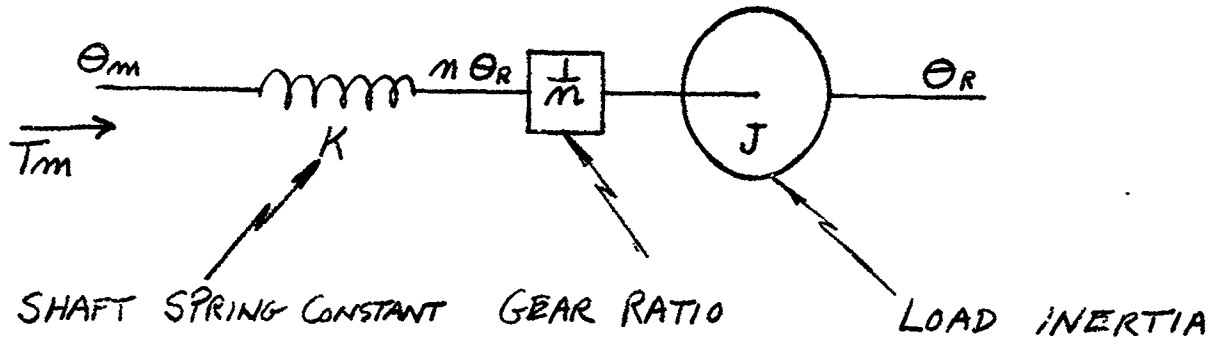

Figure 1 - Schematic Illustration of Load Coupling Shaft

$$\frac{\theta_m}{T_m} = \frac{\left(\frac{J}{n^2}\right) S^2 + K}{K\left(\frac{J}{n^2}\right) S^2} \tag{22}$$

then

$$\frac{\theta_R}{T_m} = \frac{1}{n}\left[\frac{1}{(1/K)(J/n^2)S^2+1}\right]\left[\frac{(1/K)(J/n^2)S^2+1}{(J/n^2)S^2}\right] \tag{23}$$

$$\frac{\theta_R}{T_m} = \frac{n}{JS^2} \tag{24}$$

Since $T_m = P_m d_m$

$$\frac{\theta_R}{P_m} = \frac{nd_m}{JS^2} \tag{25}$$

also from equation (20)

$$d_m = \frac{\theta_m}{P_m}\frac{T_m}{\theta_m} \tag{26}$$

which provides a transfer equation of θ_R/θ_m in terms of θ_m/T_m as

$$\frac{\theta_R}{\theta_m} = \frac{n}{JS^2}\left(\frac{T_m}{\theta_m}\right) \tag{27}$$

Main Arm Load Inertia

Changes in inertia of the gimbal ring and gondola create a complex change in the load equation for the main arm due to the shift in vibration modes of the main arm structure. Using the same equations as used in the Rucker Report No. 412, we find that the inertia coefficient at

LUMP-9 $J_9 = 352 \times 10^3$ lb-in-sec^2

Radius of gyration = 92.6 in

$Z_9 = 600$ in

$$m_9 Z_9^2 \doteq \frac{J_9}{(Rg)^2} (Z_9)^2 = 14.8 \times 10^6 \text{ lb-in-sec}^2 \qquad (28)$$

LUMP-10 $J_{10} = 78 \times 10^3$ lb-in-sec^2

Sphere Radius = 6 ft

$Z_{10} = 600$ in

$$m_{10} Z_{10}^2 = \frac{J_{10}}{\frac{2}{5}(R)^2} (Z_{10})^2 = 13.6 \times 10^6 \text{ lb-in-sec}^2 \qquad (29)$$

Summing all of the inertia torques (mZ) from LUMP-2 to LUMP-10 we have the following:

(HUB) $m_2 Z_2 = 0$ lb-sec^2

$$m_3 Z_3 = 2.65 \times 10^3$$

$$m_4 Z_4 = 1.96 \times 10^3$$

$$m_5 Z_5 = 2.72 \times 10^2$$

$$m_6 Z_6 = 3.54 \times 10^3$$

$$m_7 Z_7 = 4.80 \times 10^3$$

(FORK) $m_8 Z_8 = 3.74 \times 10^3$

(GIMBAL) $m_9 Z_9 = 24.60 \times 10^3$

(GONDOLA) $m_{10} Z_{10} = 22.60 \times 10^3$

TOTAL 66.61×10^3 lb-sec^2 (30)

The counter weight mass is located 95 inches from the shaft on the side diametrically opposite from the main arm. To obtain static balance such that

$$\sum_{1}^{10} m_i Z_i = 0 \tag{31}$$

$$\text{(CWT)}\ m_1 = \frac{66.61}{95} \times 10^3 = 701\ \frac{\text{lb-sec}^2}{\text{in}} \tag{32}$$

This is considerably larger than the initial CWT mass of 626 lb-sec^2/in as specified in the Rucker Report No. 412, p. 324. Assuming no other inertia changes and using the new (CWT) mass the total moment of inertia is expressed as

$$J_T = J_R + \sum_{2,10} J_i + \sum_{1}^{10} m_i Z_i^2 \tag{33}$$

$$J_T = (1.53 + .573 + 42.3)\ 10^6 = 44.4 \times 10^6 \text{ lb-in-sec}^2 \quad (34)$$

$$J_T = 119 \times 10^6 \text{ lb-ft}^2 \quad (35)$$

This value differs from the value of 115×10^6 lb-ft^2 that was given to us along with other inertia changes. These inertia changes will cause different modes of vibration to be reflected back to the main arm drive system. The solution of these vibration effects requires the use of 22 equations. This was discussed, and it was felt that the inertia changes are not great enough to justify solving these equations again with the new values of inertia. Therefore, the value of 115×10^6 lb-ft^2 was used in this simulation.

B. Hydraulic Component Simulation

Before simulating the flow control valves some thought was given to valve nonlinearities. To simulate the valve nonlinearity of flow versus spool displacement we may express it by the equation

$$\frac{Q}{y} = \frac{Q_o}{\sqrt{2}} \sqrt{\frac{P_S - P_L}{P_S}} \quad (36)$$

where Q_o is flow at rated valve current

y is spool displacement

P_L is load pressure drop

Carrying this one step further, we consider the case of supply pressure regulation due to flow. The characteristic of the valve including supply pressure regulation is:

$$\frac{Q_a}{I_a} = \frac{K_a}{(1 + ST)^2} \cdot \frac{Q_o}{\sqrt{2}} \sqrt{\left(1-k \frac{Q_a}{Q_o}\right) - \frac{P_L}{P_S}} \qquad (37)$$

where Q_o is flow at rated valve current

K_a is valve gain

k is supply regulation due to load flow

P_L is load pressure drop

Since only small pressure regulation is generally encountered in this type of system design, this effect was not considered to be necessary in this simulation.

The block diagram for both the 1st and 2nd axis control system is shown in Figure 2.

C. 1st Axis, Gimbal Ring System

(1) Linear System Analysis (Paper)

The system performance was studied in both a paper analysis and analog computer study. The paper analysis is a study of the linear system and is used as a means of checking the analog computer simulation. A different configuration of system loops is used in these two studies to provide a means of comparison. Figure 3 is the block diagram for both axes in a loop configuration used in the paper analysis. The frequency

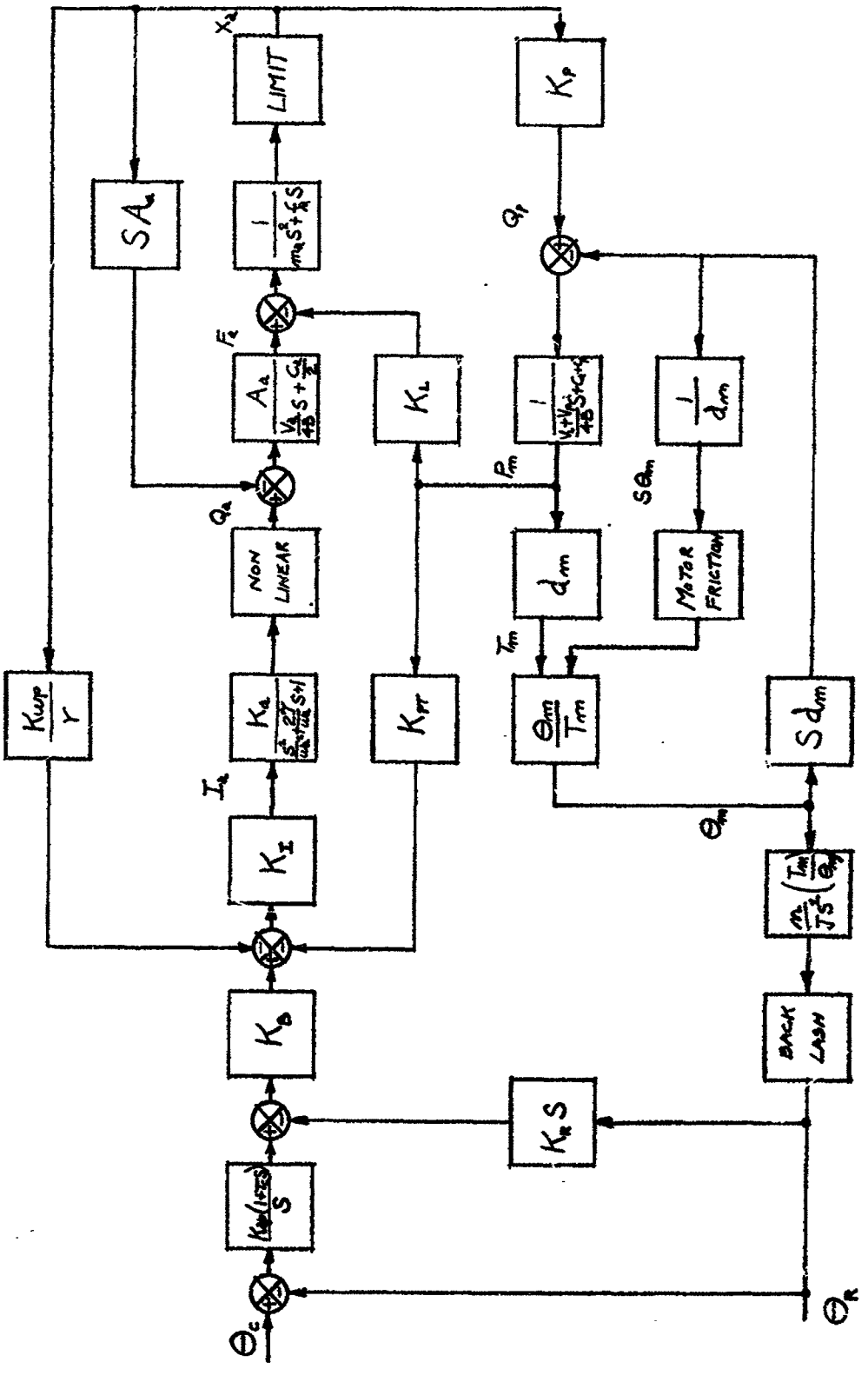

Figure 2

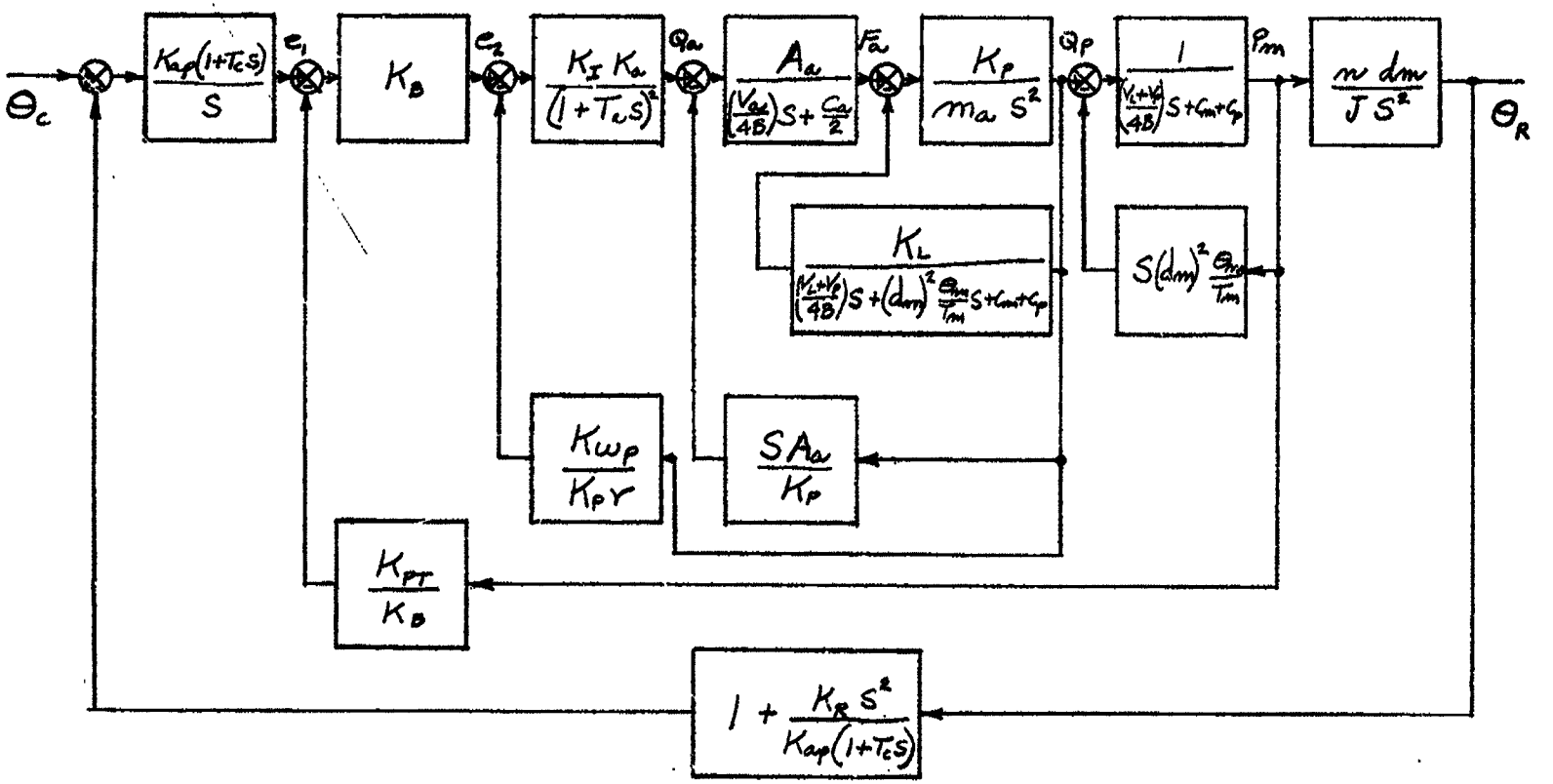
θ_c
$\frac{K_{ap}(1+T_c S)}{S}$
e_1
K_D
e_2
$\frac{K_I K_a}{(1+T_a S)^2}$
Q_a
$\frac{A_a}{\left(\frac{V_{oa}}{4B}\right)S+\frac{C_a}{2}}$
F_a
$\frac{K_p}{m_a S^2}$
Q_p
$\frac{1}{\left(\frac{V_t+V_p}{4B}\right)S+C_m+C_p}$
P_m
$\frac{n\, d_m}{J S^2}$
θ_R
$\frac{K_L}{\left(\frac{V_t+V_p}{4B}\right)S+(d_m)^2\frac{\Theta_m}{T_m}S+C_m+C_p}$
$S(d_m)^2\frac{\Theta_m}{T_m}$
$\frac{K_{\omega p}}{K_{pr}}$
$\frac{SA_a}{K_p}$
$\frac{K_{PT}}{K_D}$
$1+\frac{K_R S^2}{K_{ap}(1+T_c S)}$

Figure 3

response characteristics of each of the major loops of the system are recorded in the following figures. Figure 4 is the open loop gain and phase characteristic of Q_a to Q_p including the feedback gain of SA_a/K_p. Loop gain greater than unity is still evident at 1000 radians per second. Figure 5 is the closed loop characteristic before being multiplied by the 1/H term of K_p/SA_a and is recorded only to show that a high peak in the frequency response does appear at close to 1000 radians per second. This is far removed from the range of system response, and it is proved later in the analog computer study that this characteristic can be replaced by a unity gain without affecting the system frequency response. Figure 6 is the closed loop transfer characteristic of Q_a to Q_p over a frequency range that is related to the majority of the system elements. Figure 7 is a similar characteristic for the loop of e_2 to Q_p and Figure 8 for the loop of e_1 to P_m. Figure 9 is the complete closed loop transfer characteristic for the 1st axis control system in which it becomes apparent that the system response will have a peak of 5.1 db at about 1.2 radians per second which can be expressed as an amplitude ratio of 1.8 with a damping factor of 0.3 and a natural frequency of 0.184 cps.

(2) Linear System Analog Computer Study

The block diagram for the analog computer study of both the 1st and 2nd axis control system is shown in Figure 10. It will be noted that this is the same system as shown in Figure 3 but with a different arrangement of feedback loops thus permitting a method

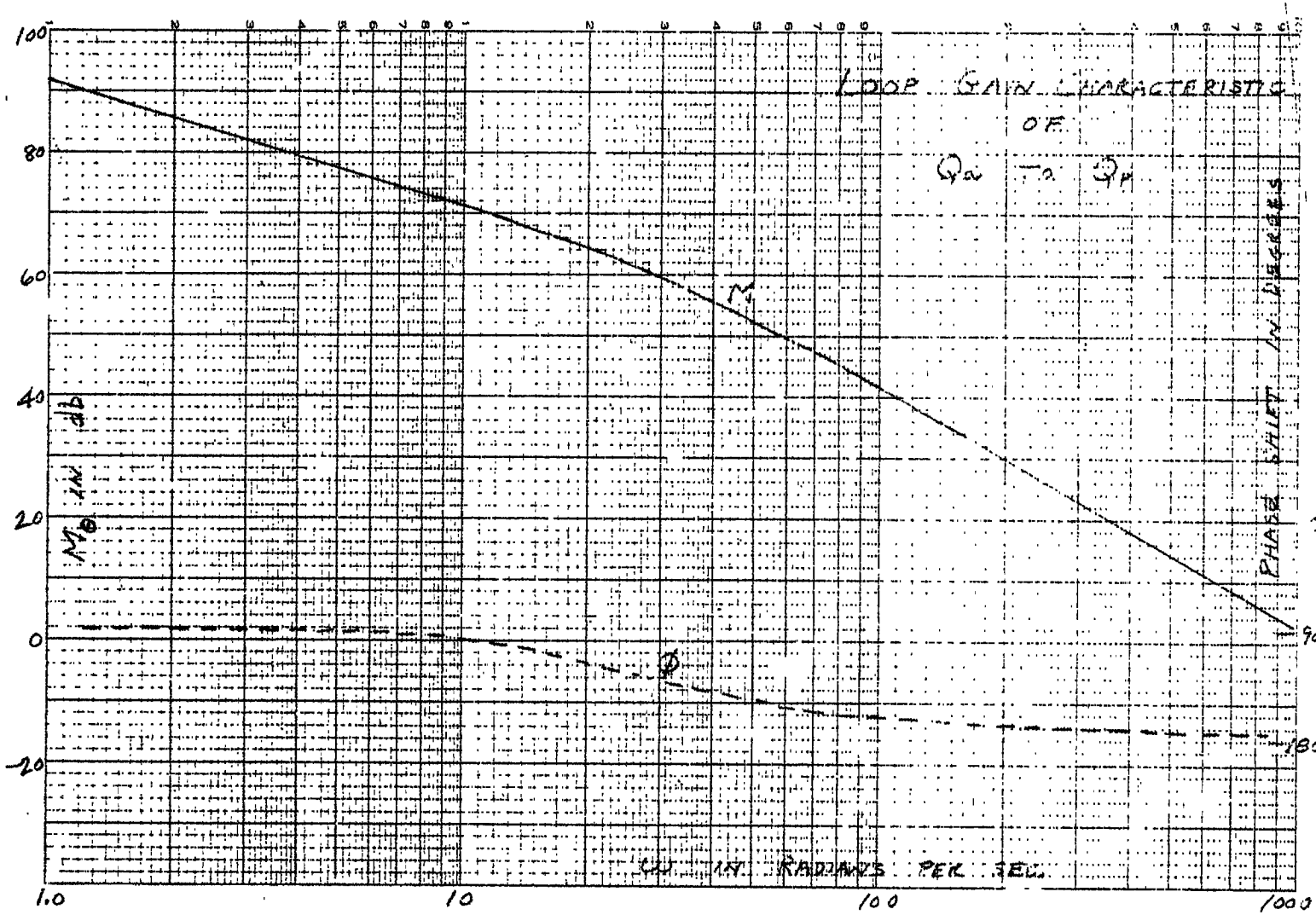
LOOP GAIN CHARACTERISTICS
OF
Q_a TO Q_M
M_Φ IN db
PHASE LAG IN DEGREES
CUT IN RADIANS PER SEC.
100
80
60
40
20
0
-20
1.0
10
100
1000
0°
90°
180°

Figure 4

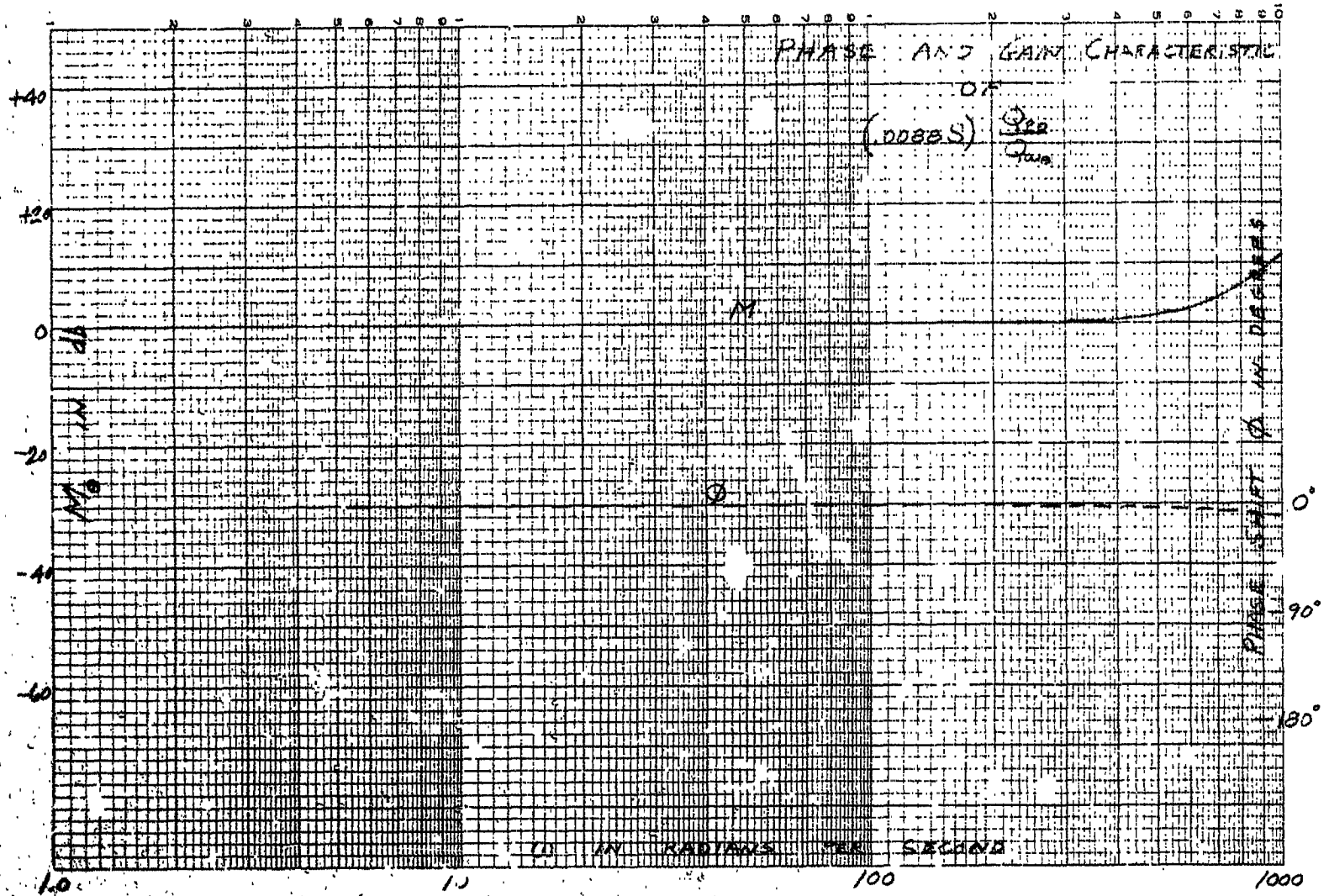
PHASE AND GAIN CHARACTERISTIC
OF
(.0088S) $\frac{S+20}{S+10}$
+40
+20
0
-20
-40
-60
M
Φ
0°
90°
180°
PHASE SHIFT Φ IN DEGREES
ω IN RADIANS PER SECOND
1.0
10
100
1000

Figure 5.

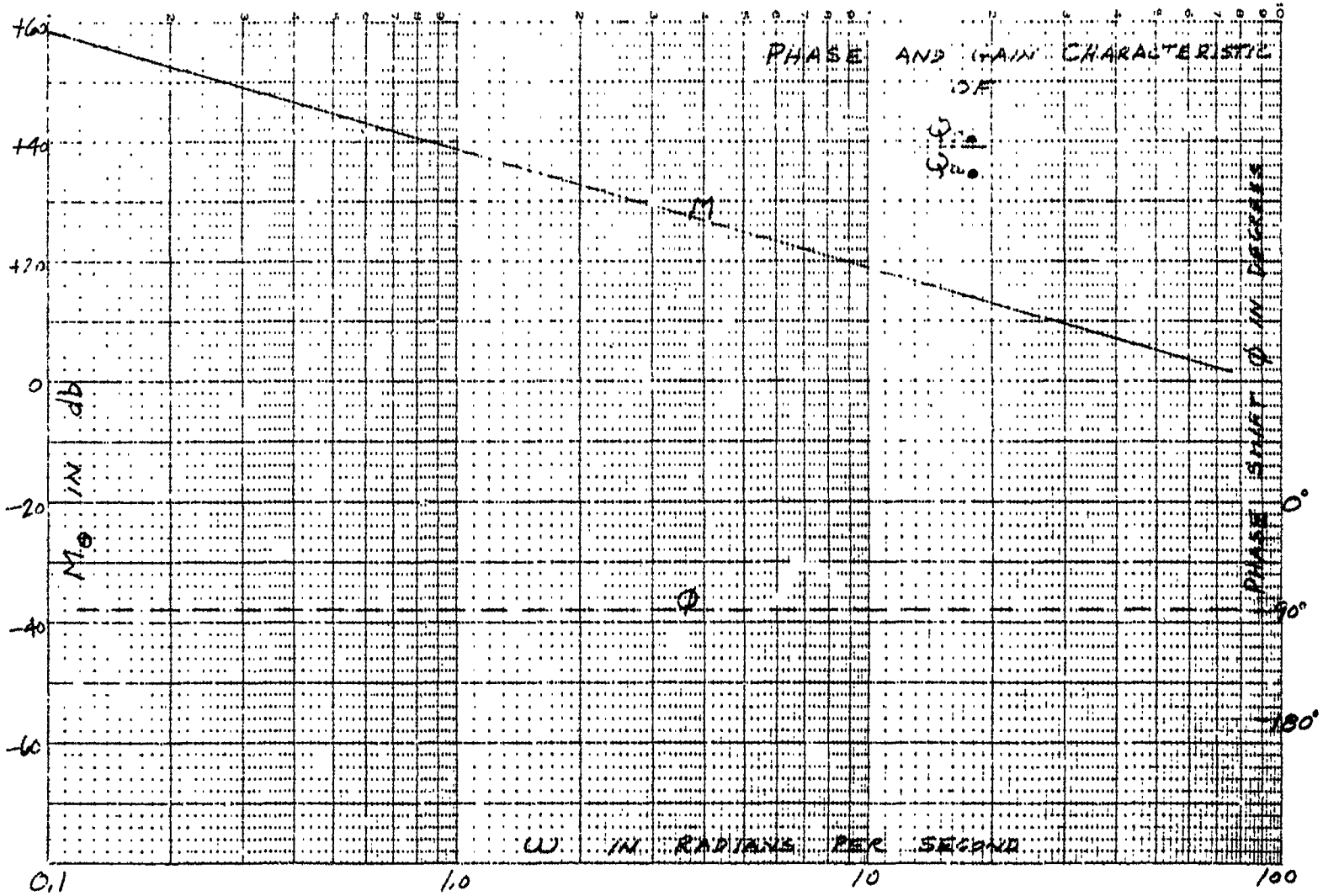
PHASE AND GAIN CHARACTERISTIC
OF
+60
+40
+20
0
-20
-40
-60
db
IN
Mφ
M
φ
0°
-90°
-180°
PHASE SHIFT φ IN DEGREES
0.1
1.0
10
100
ω IN RADIANS PER SECOND

Figure 6

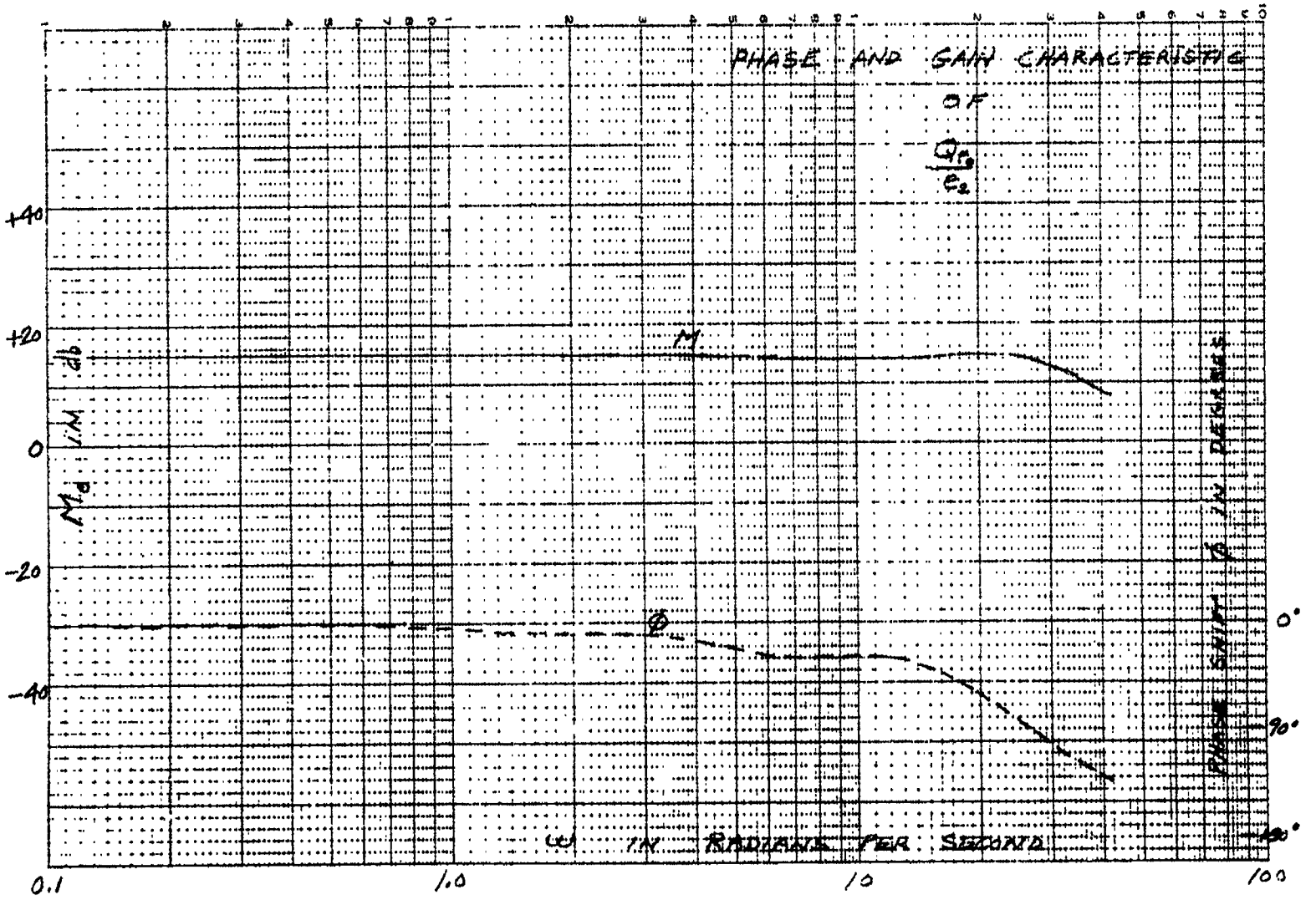
PHASE AND GAIN CHARACTERISTICS
OF
$\frac{Q_2}{e_2}$
+40
+20
0
-20
-40
db
M
M_d
ϕ
0°
90°
0.1
1.0
10
100
RADIANS PER SECOND

Figure 7

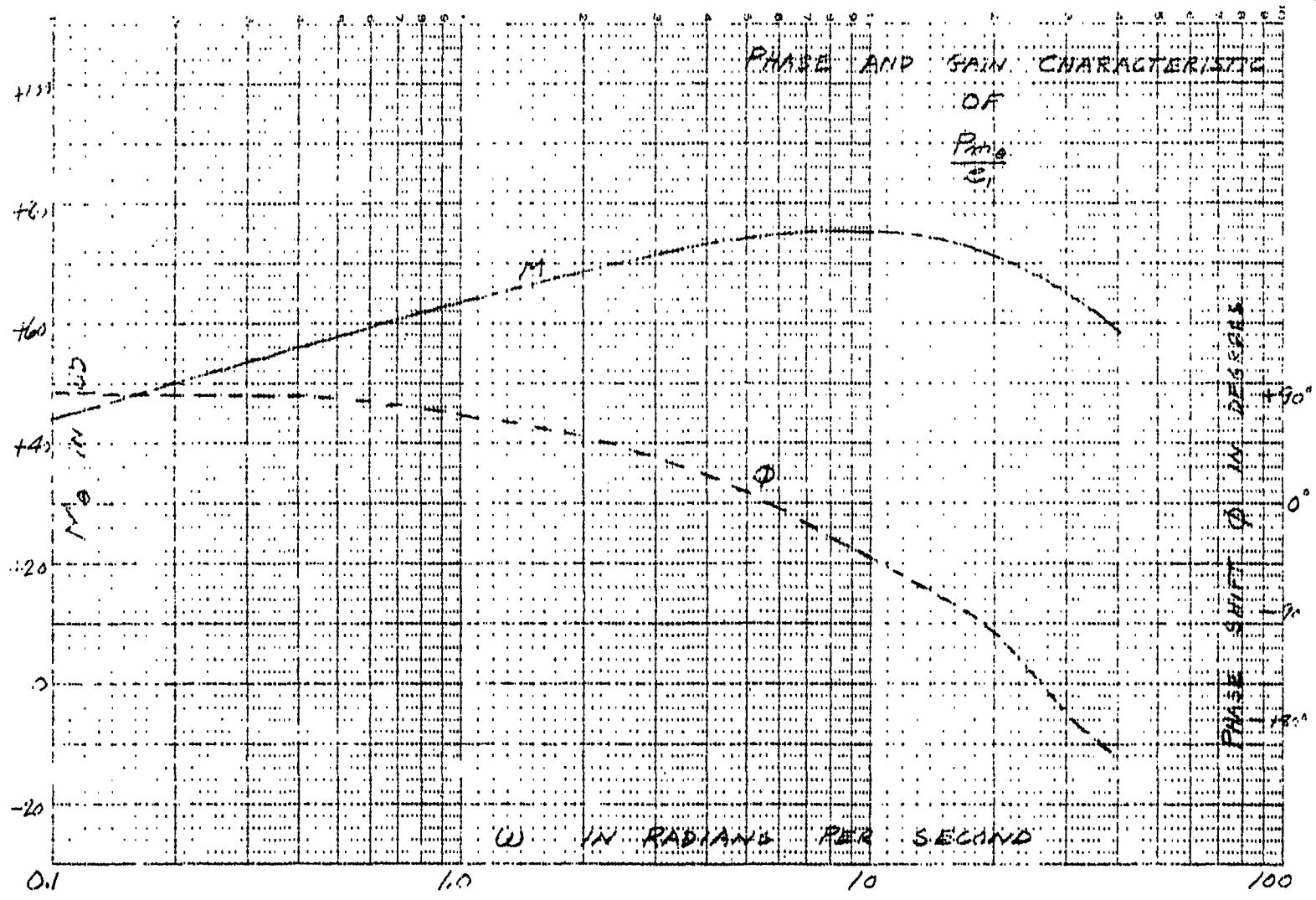
PHASE AND GAIN CHARACTERISTIC
OF
$\frac{P_{m\theta}}{E_1}$
M
Φ
+60
+40
-20
0
-20
0.1
1.0
10
100
ω IN RADIANS PER SECOND
PHASE SHIFT (Φ) IN DEGREES
+90°
0°

Figure 8

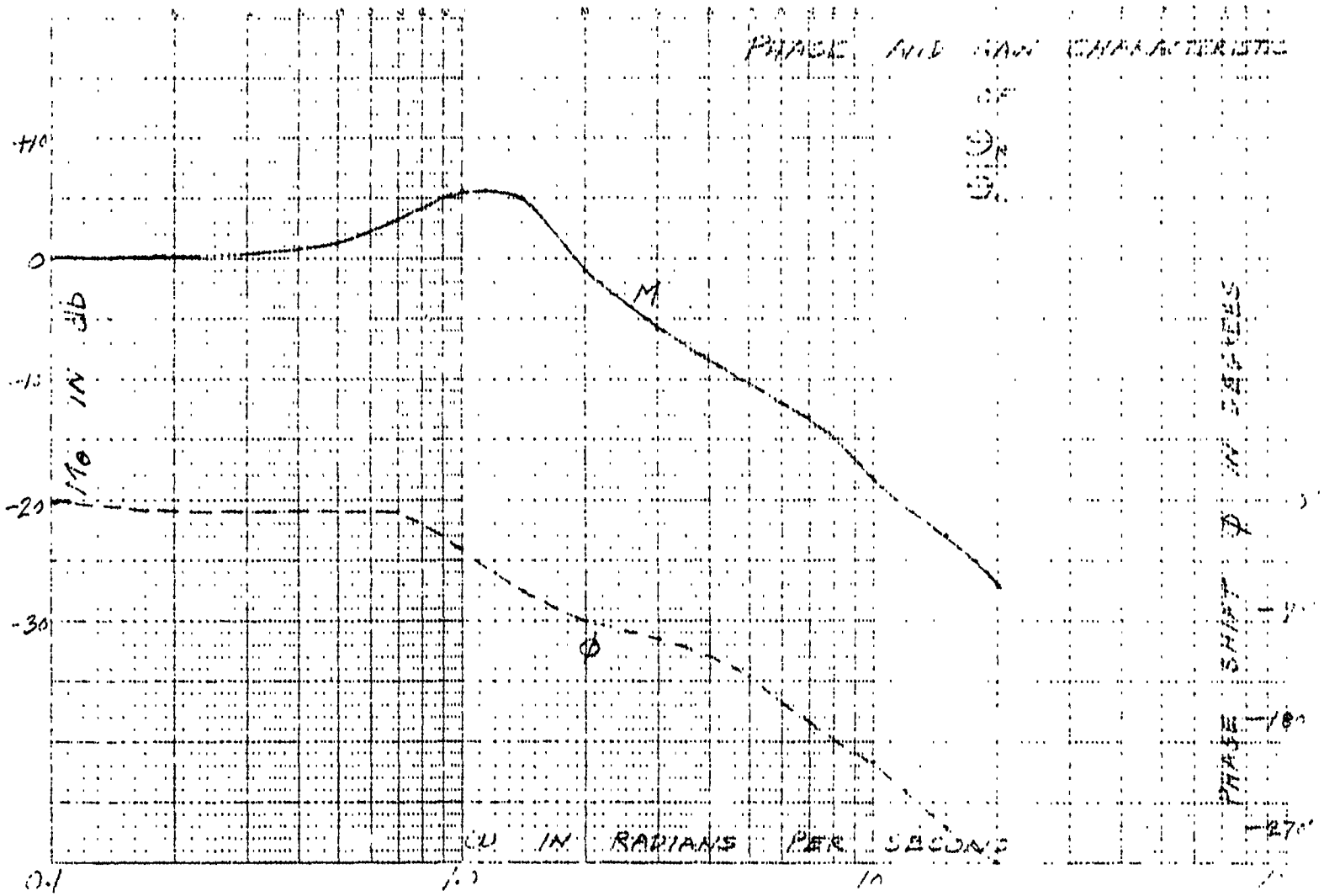

Figure 9

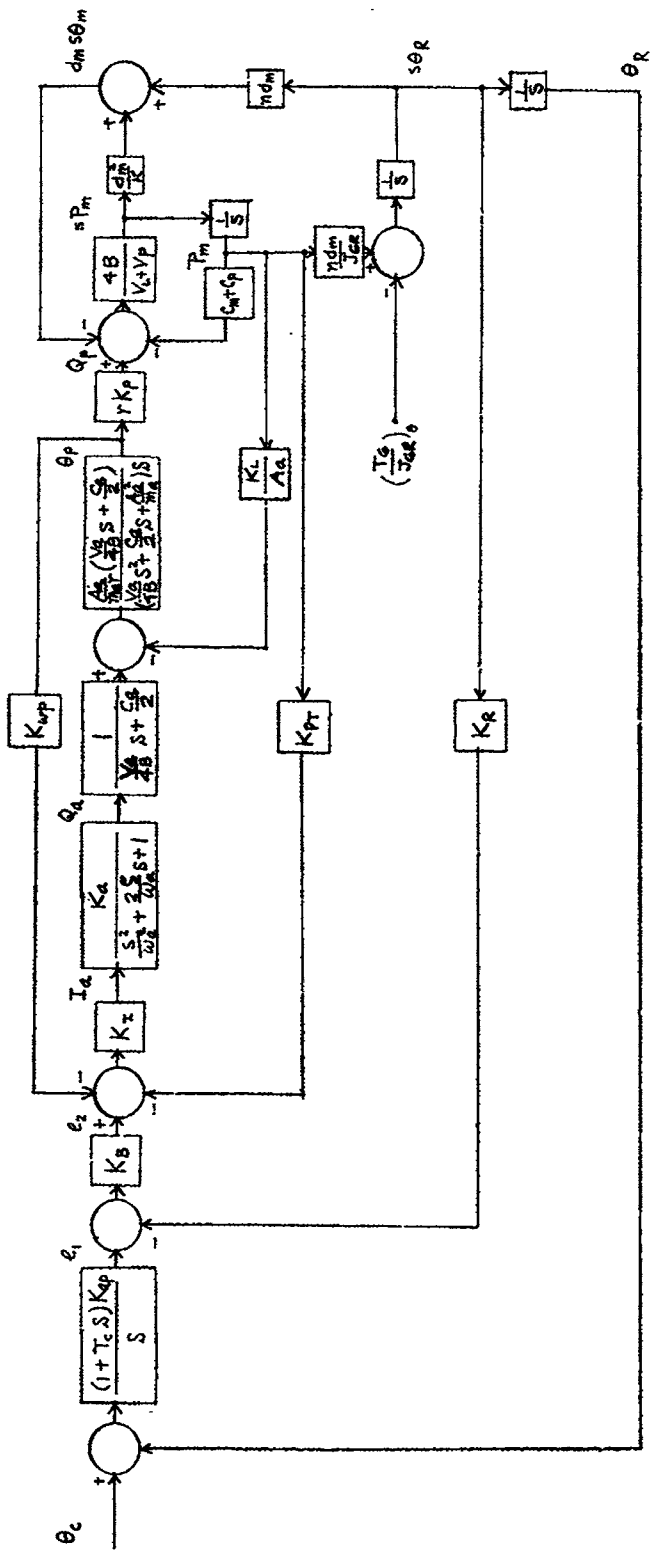

Figure 10 - 1st & 2nd Axes Block Diagram

of checking the system simulated for the centrifuge study. Figure 11 is the block diagram of the 1st axis system with the analog computer diagram shown in Figure 12. The time scale factor used throughout the studies is 1 (real time scale) and a unit volt of analog computer output represents a single unit of the quantity simulated (e.g., 1 rad, 1 lb-in, etc.)

The analog computer test result of the frequency response for the 1st axis system without nonlinear elements is plotted in Figure 13. This indicates a peak amplitude ratio of output to input as expressed in decibels of approximately 5.2 db at a frequency of 0.175 cps and a crossover frequency of 0.195 cps. Beyond this frequency the ratio decreases with a slope slightly in excess to 20 db per decade. The phase shift plot starts at zero for zero frequency indicating that the system is a position controlled system as required for this application.

The response to a step input for the 1st axis system is shown in Figure 14. Each recording channel corresponds to the circled number in Figure 12. These recordings show that for a step input the output position has about a 50% overshoot and reaches a steady-state in approximately 9.6 seconds.

(3) Comparison of Paper Study and Analog Study

The phase and gain characteristic of the paper analysis and the analog computer study have been plotted on a single graph shown in Figure 15. These graphs show very good agreement and indicate that the system simulated is a good representation of the actual hardware.

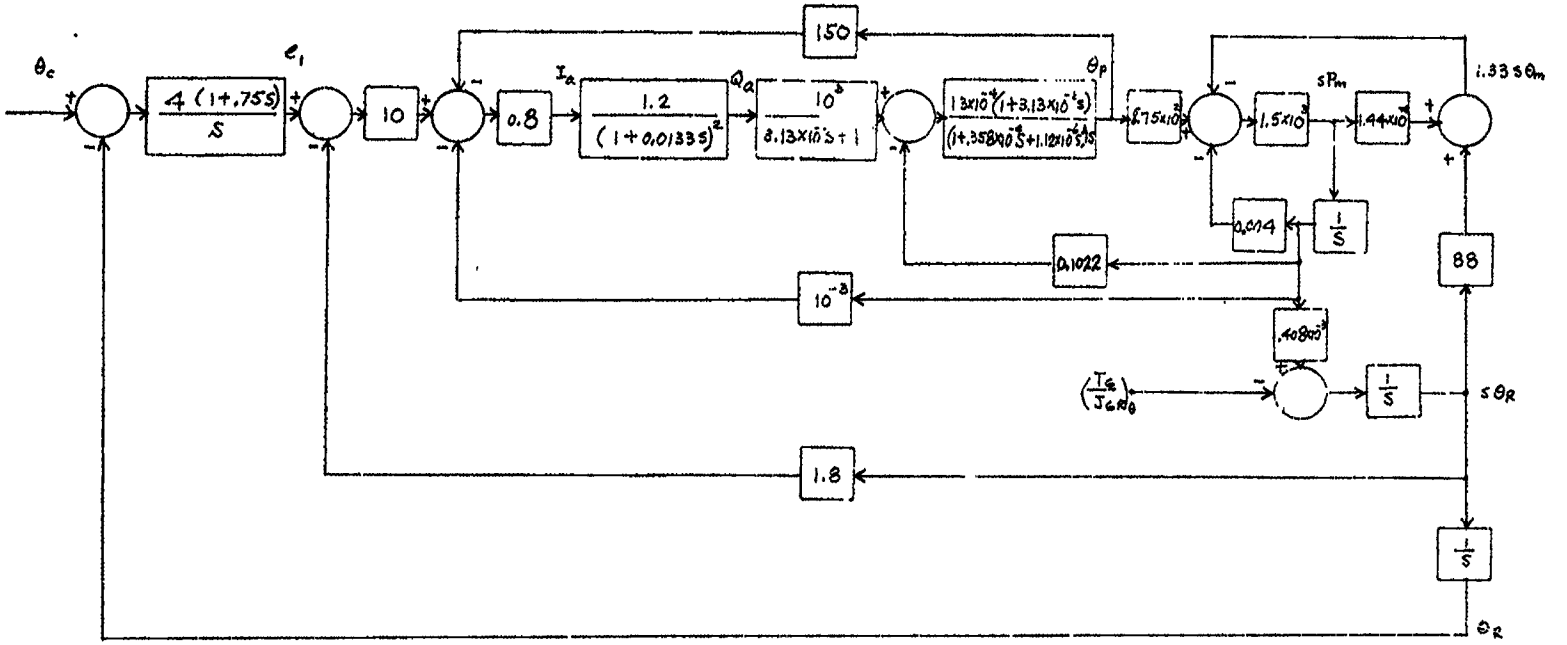

Figure 11 - 1st Axis Block Diagram

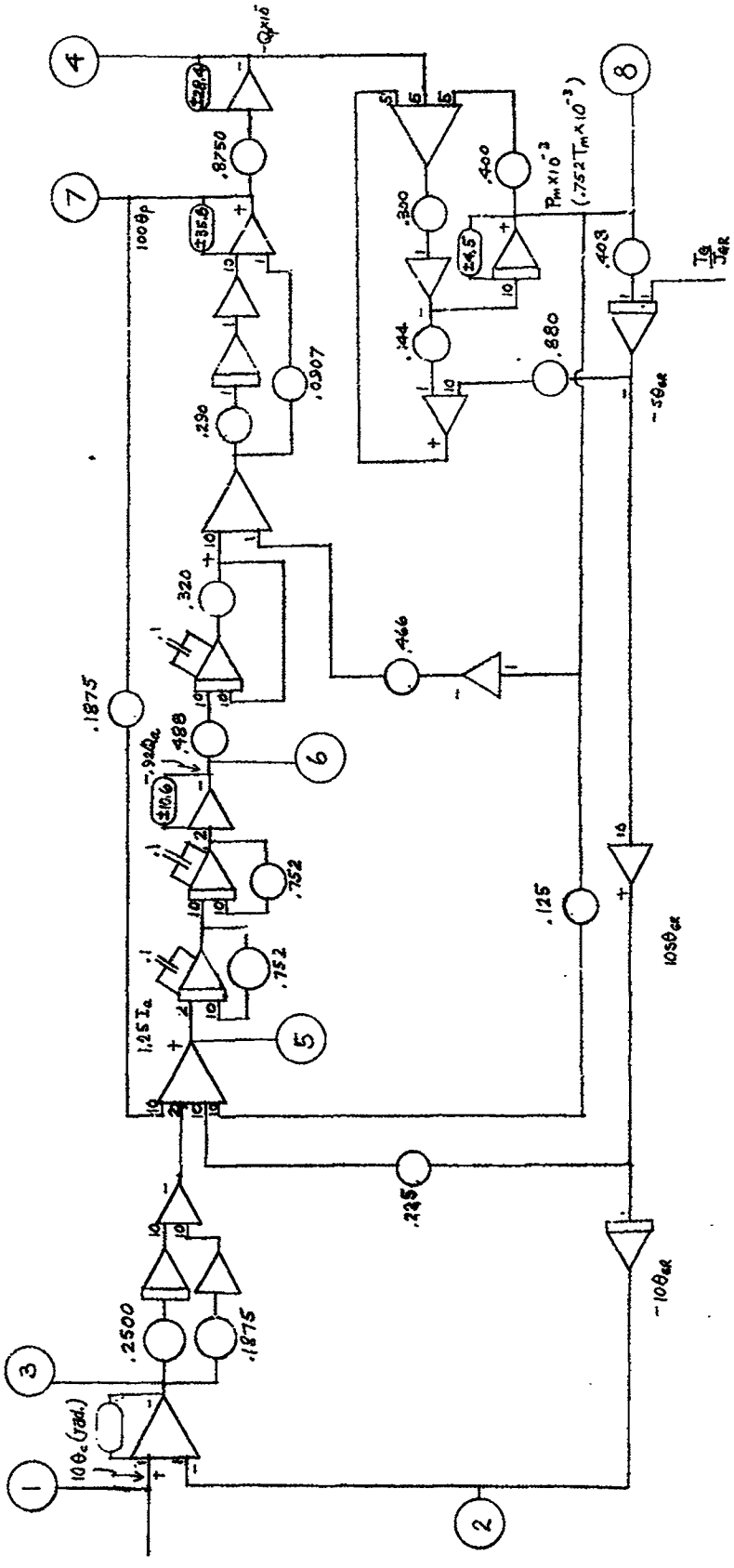

Figure 12 - 1st Axis Analog Circuit

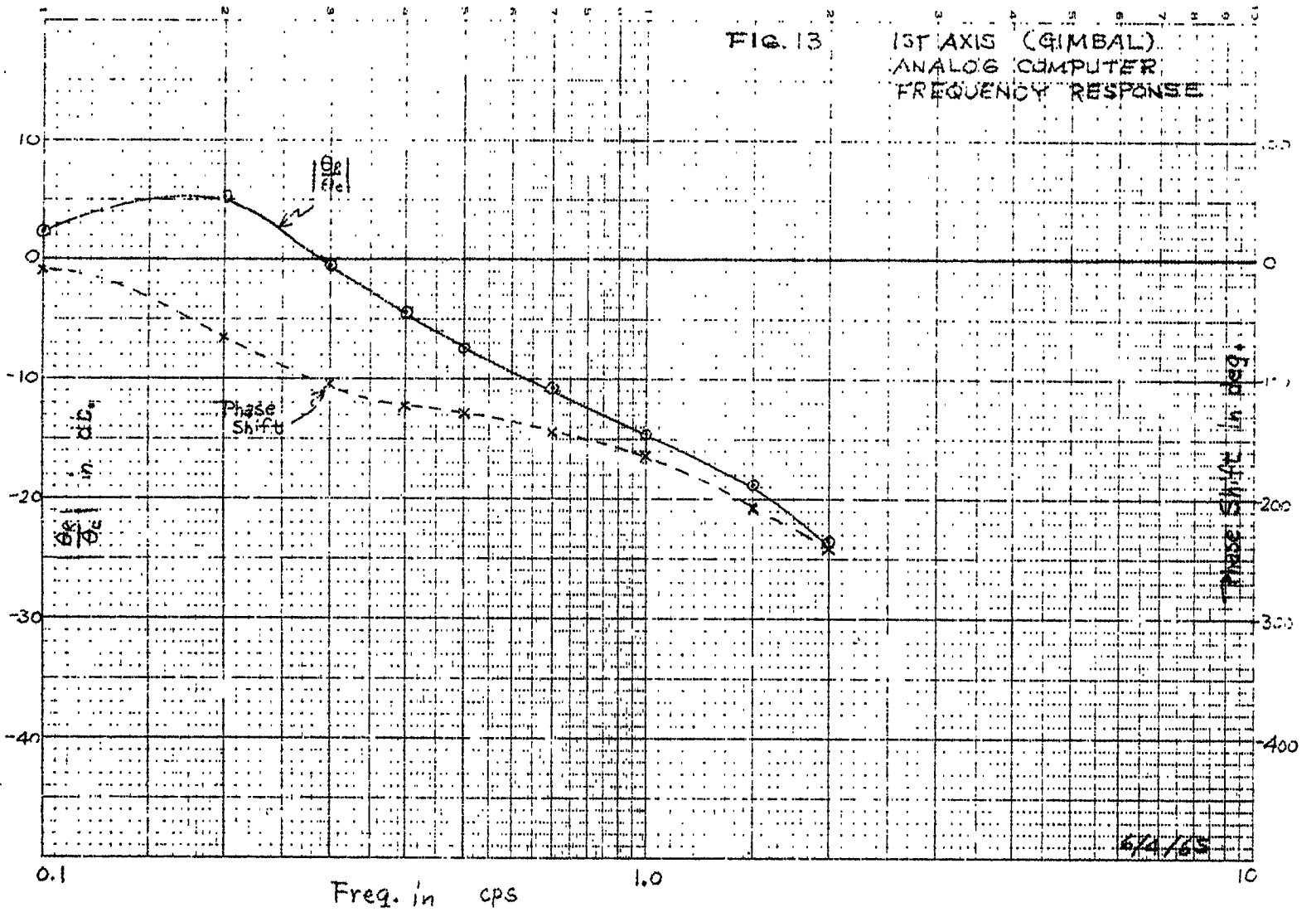
FIG. 13
1ST AXIS (GIMBAL)
ANALOG COMPUTER
FREQUENCY RESPONSE
10
0
-10
-20
-30
-40
Phase Shift
Phase Shift in deg
0.1
1.0
10
Freq. in cps
6/4/65

Figure 13

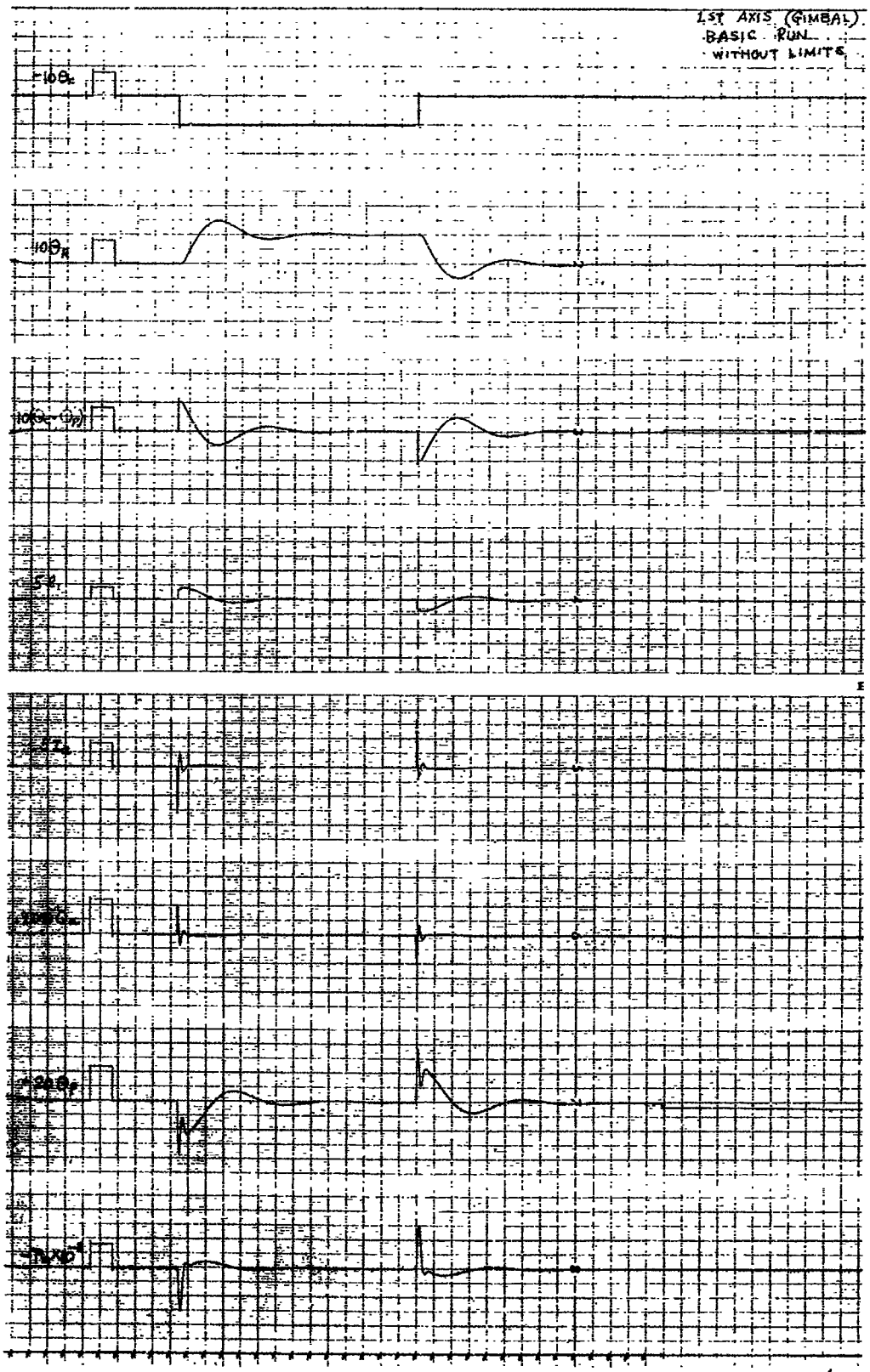

Figure 14

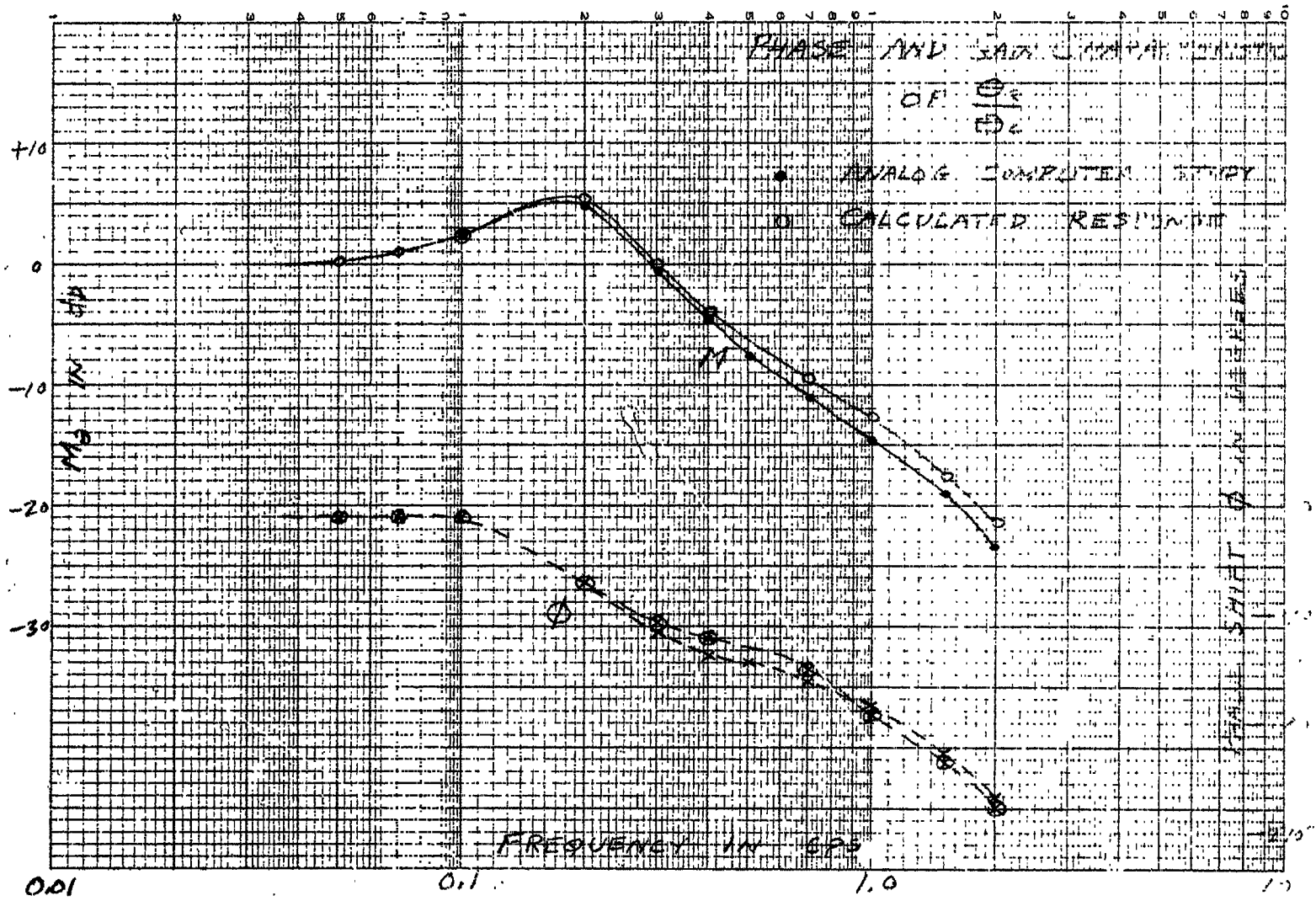

Figure 15

(4) Limit Circuits

The actual hardware system has physical limits which must be simulated in the analog computer study. From information submitted for this study a tabulation has been made for the 1st and 2nd axis systems of the significant limits and is shown in Figure 16.

The effect of these limits in the 1st axis system is shown in Figures 17 and 18. The system is stable for a step input command of 0.5 radians. A step input command of 1.7 radians as shown in Figure 18 will cause the system to become unstable. Command signals in actual system operation can exceed 1.7 radians. Provisions must therefore be made to limit the error signal to a level that will prevent the system from becoming unstable. A error limit set at ± 0.2 rad will permit an input command of 4 radians without becoming unstable. The computer study of this system is shown in Figures 19 and 20. The time to reach steady-state has been extended to 21 and 37.6 sec as compared to the 9.6 seconds settling time for the linear system. This limit has also reduced the velocity of the 1st axis system from approximately 1.26 rad/sec to .85 rad/sec. With the limit set to ± 0.1 rad the settling time increases to 34 seconds for a 2 rad step input and 62 seconds for a 4 rad step input. The error limit used in the final system simulation was 0.1 radians.

(5) Effects of Disturbance Forces

Due to mass unbalance in the systems, forces will be physically coupled between systems and appear in the analog

All these limits are in reference to Rucker Drawing No. 05018 entitled "Hydraulic Circuit 1st Axis & 2nd Axis Drives FAF", and the Rucker Memo AC-1

SYMBOL	DESCRIPTION	1ST AXIS	2ND AXIS	LIMITER USED AT
Q_a	SERVOVALVE FLOW	3GPM (1800 psi) 11.5 in^3/sec	5GPM (1200 psi) 19.2 in^3/sec	1st 2nd
X_a	STROKE OF PISTON	1.625 in	1.813 in	
θ_p	ANGULAR DISPLACEMENT OF WOBBLE PLATE	.358 rad	.362 rad	1st 2nd
Q_p	HYDRAULIC PUMP FLOW ($Q_p = X_a K_p$)	74GPM (4500 psi) 284 in^3/sec	180GPM (4500 psi) 690 in^3/sec	1st
P_m	MOTOR PRESSURE	4500 psi	4500 psi	1st 2nd
T_m *	MOTOR TORQUE ($T_m = d_m P_m$)	6000 in-lb ($d_m = 1.33\ in^3/rad$)	15800 in-lb ($d_m = 3.75\ in^3/rad$)	2nd
$\dot{\theta}_m$	MOTOR SPEED	2140 RPM 224.5 rad/sec	1720 RPM 180.5 rad/sec	—

*MOTOR TORQUE LIMITS ARE FROM EXHIBIT F, REF DATA GRAPH GR-470-Z AND EXHIBIT H, p.14, DATA GR-482-Z

Figure 16 - Component Limitations of the 1st & 2nd Axes System

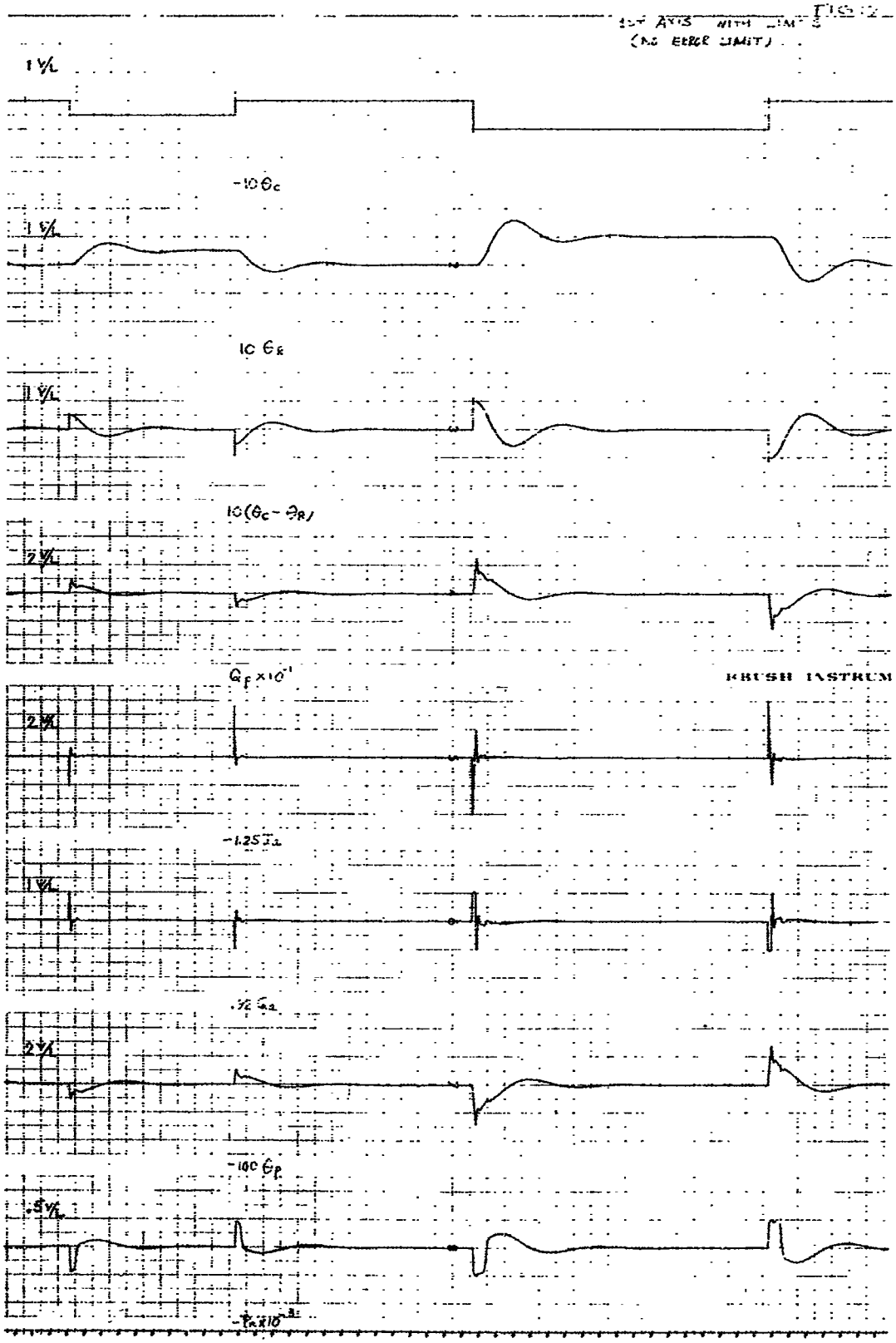
1 V/L
-10 θc
1 V/L
10 θε
1 V/L
10(θc - θR)
2 V/L
Qf x10
2 V/L
-1.25 Ia
1 V/L
2 V/L
-100 θp
.5 V/L

Figure 17

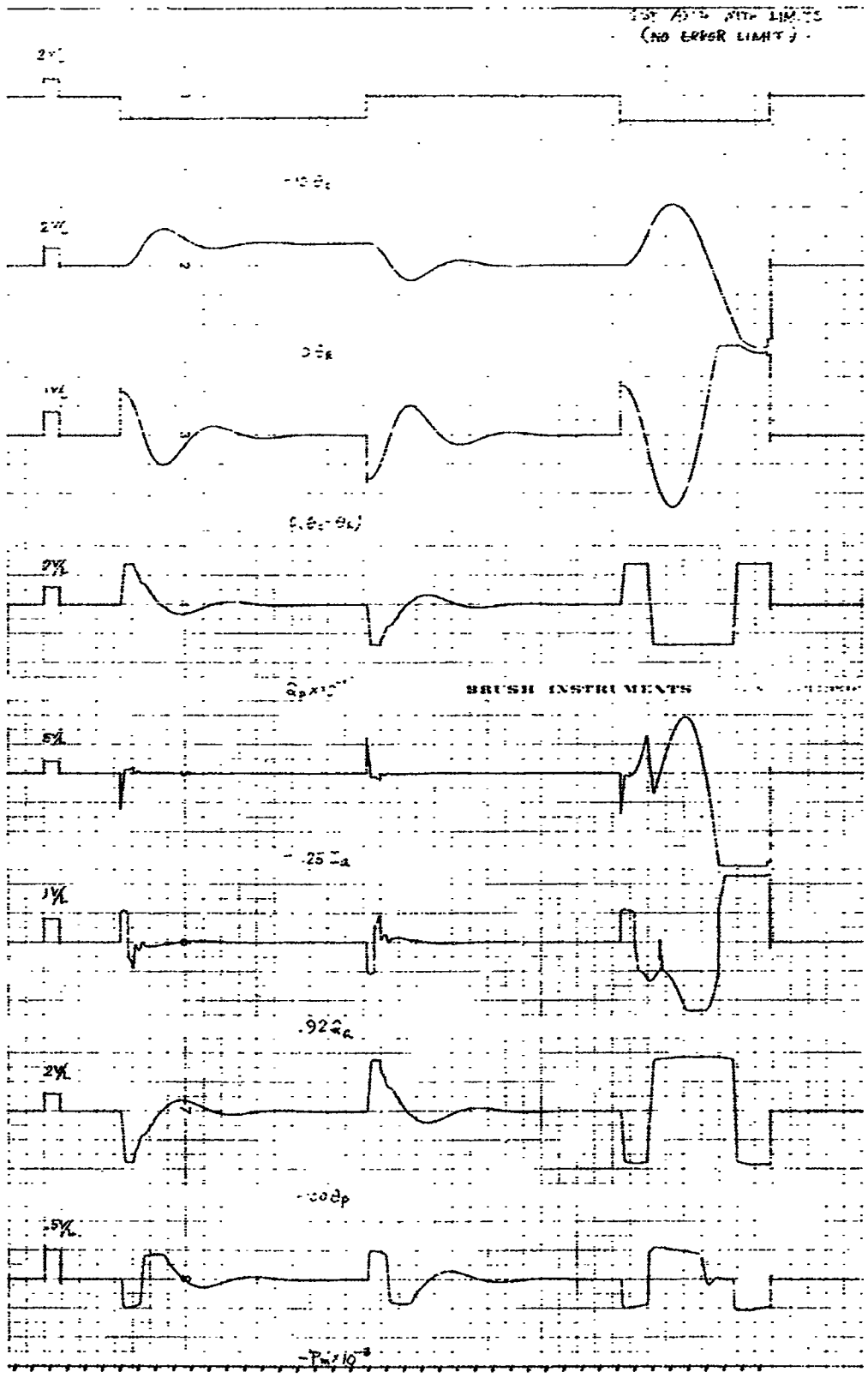

Figure 18

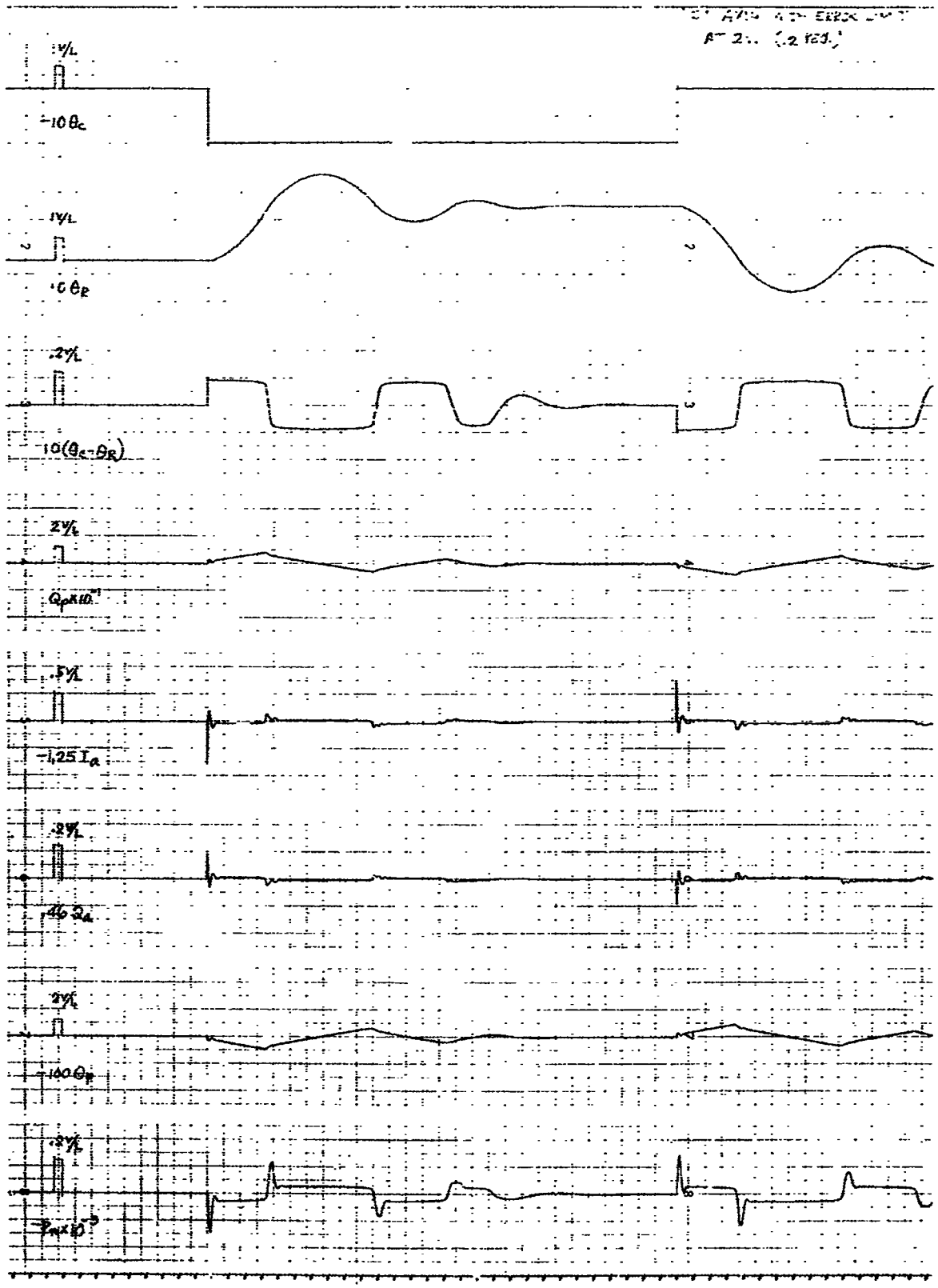
1V/L
10 θc
1V/L
10 θR
2V/L
10(θc-θR)
2V/L
Qp x10
5V/L
1,25 Ia
2V/L
40 Qa
2V/L
100 θR
2V/L

Figure 19

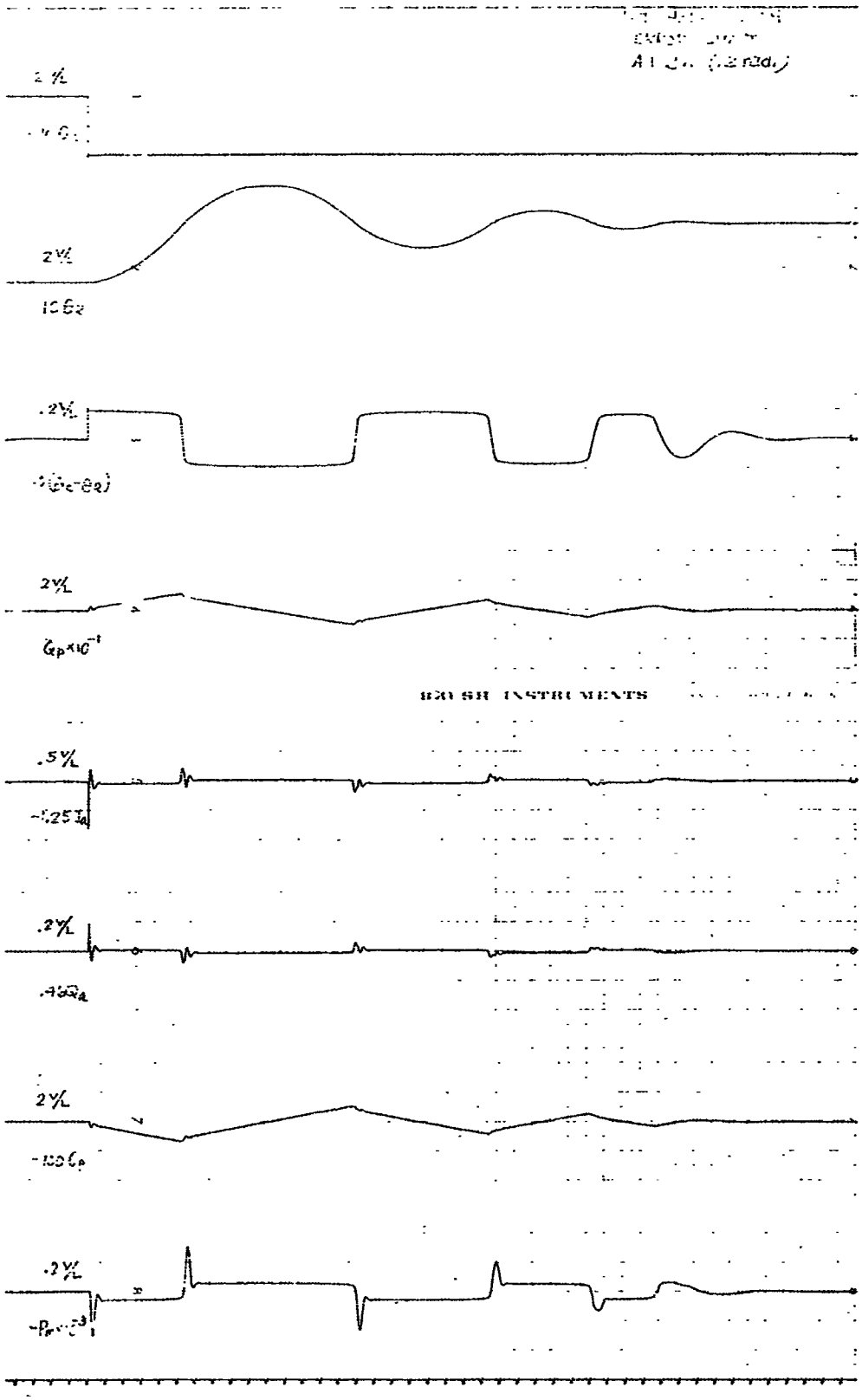

Figure 20

simulation as T_G/J_{GR} as shown in Figure 1C. In order to keep the system stable for a step disturbance, $T_G/J_{GR} = D$, in the steady-state, the equation to be satisfied is

$$P_m = \frac{J_{GR}}{nd_m}(-D) \tag{38}$$

and

$$P_m = \frac{T_G}{nd_m} \tag{39}$$

where T_G is the disturbance torque at the load side and is assumed to be a step function.

In making this study the following cases arise:

(1) When $\left|P_m\right|_{max} > \left|\frac{T_G}{nd_m}\right|$

the system goes to steady-state with no error in position of θ_R as shown in Figure 21.

(2) When $\left|P_m\right|_{max} = \left|\frac{T_G}{nd_m}\right|$

the system becomes stable with possible error in position of θ_R.

(3) When $\left|P_m\right|_{max} < \left|\frac{T_G}{nd_m}\right|$

the system becomes unstable depending on the time duration of the disturbing force.

Case 3 is a condition that could cause serious trouble in the performance of the centrifuge and will therefore be studied more closely.

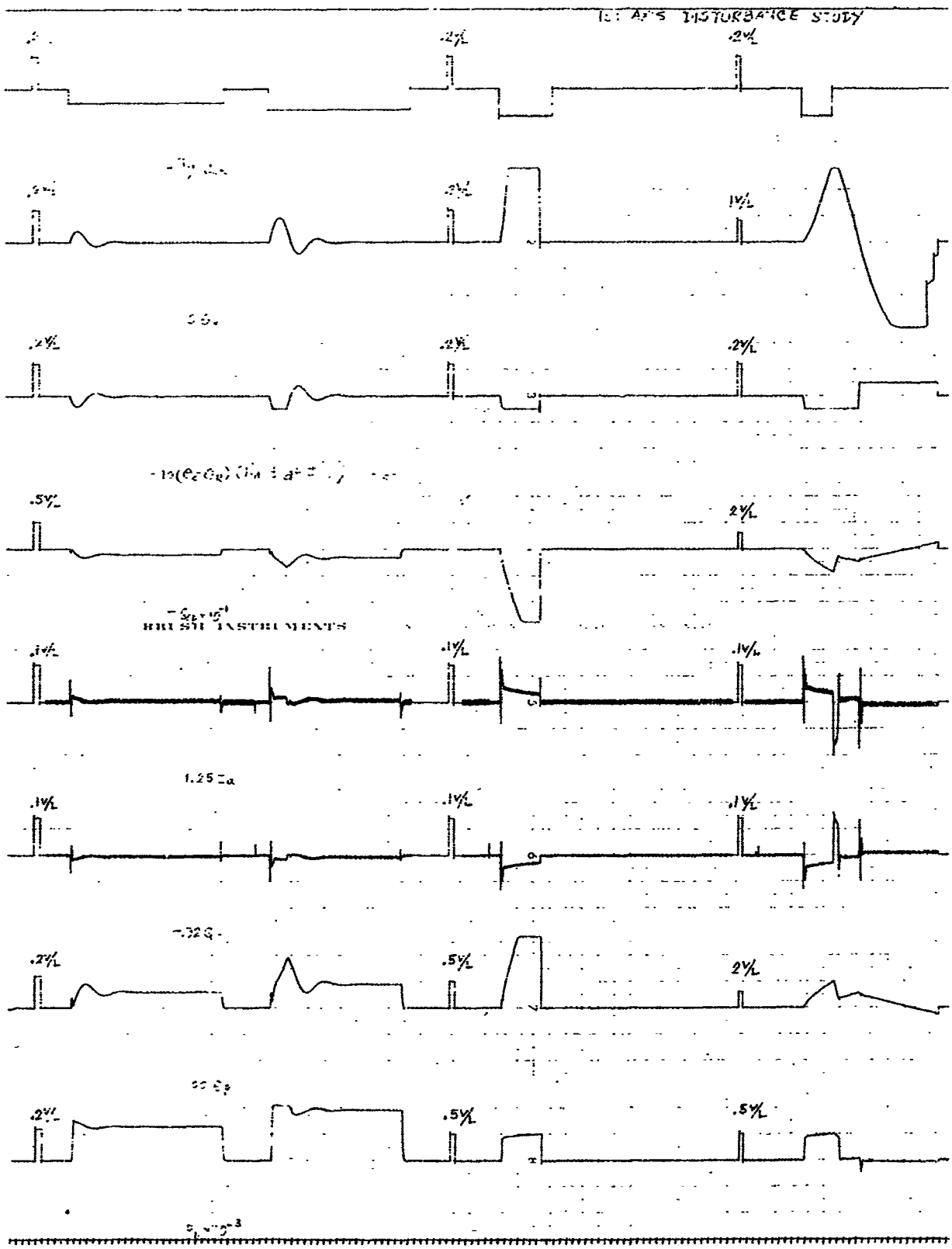
APS DISTURBANCE STUDY
.2%
.2%
.2%
1%
.2%
.2%
.2%
.5%
2%
BRUEL INSTRUMENTS
.1%
.1%
.1%
1.25 Ω
.1%
.1%
.1%
.2%
.5%
2%
.2%
.5%
.5%

Figure 21

If we let

$$\frac{1}{J_G}\,(T_G - nd_m P_m) = C \tag{40}$$

$$\theta_R(s) = \frac{1}{s^2}\cdot\frac{C}{s} = \frac{C}{s^3} \tag{41}$$

$$\therefore\ \theta_R(t) = \frac{1}{2}\,Ct^2 \tag{42}$$

From Figure 10 between Q_p and sP_m, we may write,

$$[Q_p - d_m s\theta_m - (C_m+C_p)P_m]\,\frac{4B}{V_L+V_p} = sP_m \tag{43}$$

where

$$d_m s\theta_m = \frac{d_m^2}{K}\,sP_m + nd_m s\theta_R$$

Let $sP_m = 0$ at $t > \varepsilon$, where ε is small positive number. Then we have

$$Q_p - nd_m s\theta_R - (C_m+C_p)P_m = 0$$

$$Q_p = nd_m s\theta_R + (C_m+C_p)P_m \tag{44}$$

Since $s\theta_R = \frac{C}{s^2}$ and $P_m = \frac{P_{max}}{S}$

$$Q_p(s) = nd_m\,\frac{C}{s^2} + (C_m+C_p)\,\frac{P_{max}}{S} \tag{45}$$

Therefore,

$$Q_p(t) = nd_m Ct + (C_m+C_p)P_{max} \tag{46}$$

For the 1st axis (Gimbal)

$n = 66$

$d_m = 1.33$

$C_m = 0.002$

$C_p = 0.002$

$P_{max} = 4.5 \times 10^3$

$$\therefore Q_p(t) = 88Ct + 18 \tag{47}$$

But $Q_{pmax} = 284$. If we substitute this value into the above, we have

$$t = \frac{284-18}{88C} = 3.02\ J_{GR}\ \frac{1}{T_G - nd_m P_{max}}$$

where

$$J_{GR} = 215.5 \times 10^3,\ nd_m P_{max} = 396 \times 10^3$$

$$\therefore t = \frac{650 \times 10^3}{T_G - 396 \times 10^3} \tag{48}$$

This t indicates the time when Q_p reaches maximum, and after this t, the system (1st axis) becomes unstable (see the following $t - T_G$ curve).

The comparisons between $t - T_G$ curve (Fig. 22) and actual analog computer results are made as follows: Figure 23:

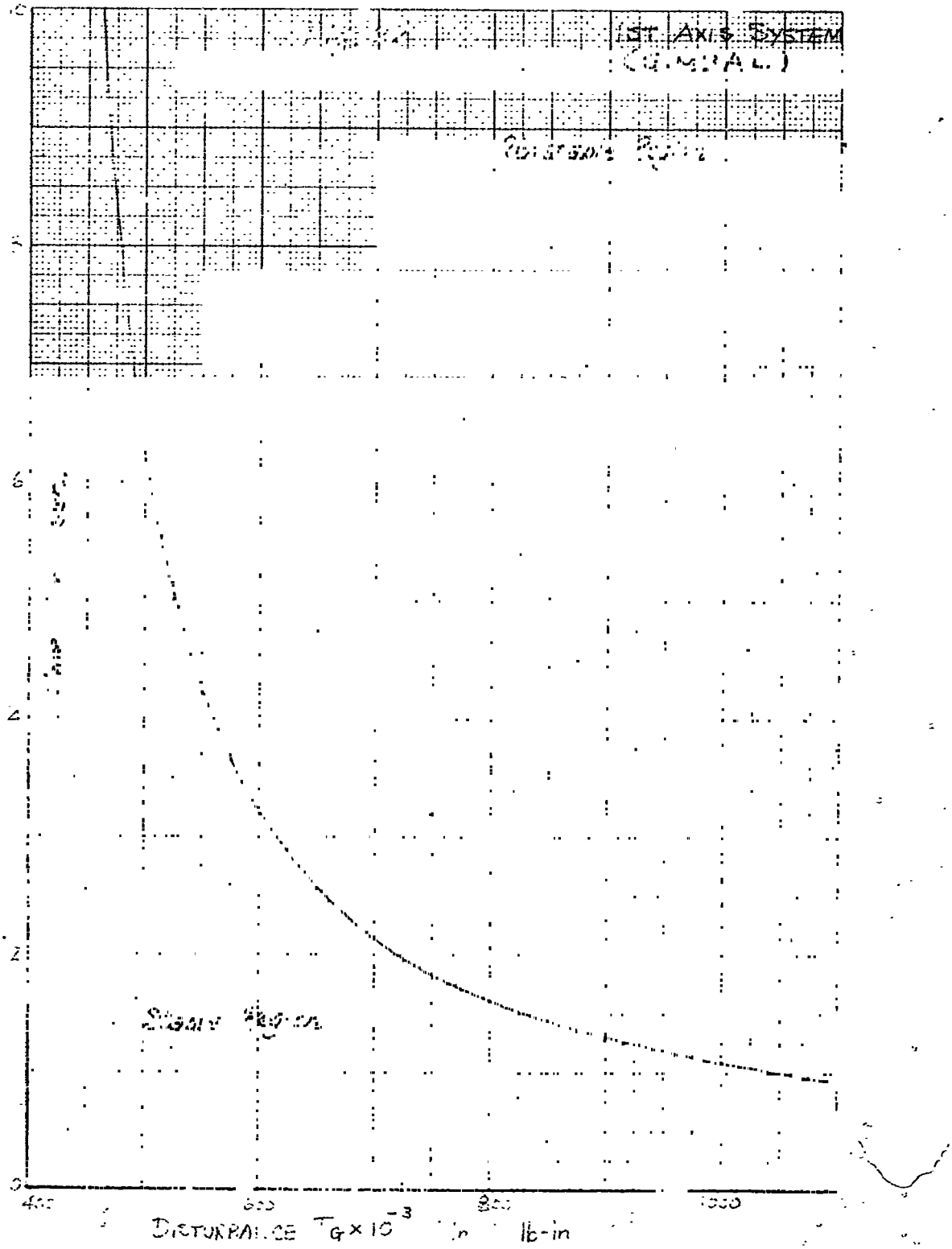
ST. AXIS SYSTEM
(GIMBAL)
6
4
2
0
400
600
800
1000
DISTURBANCE $T_G \times 10^{-3}$ in lb-in

Figure 22

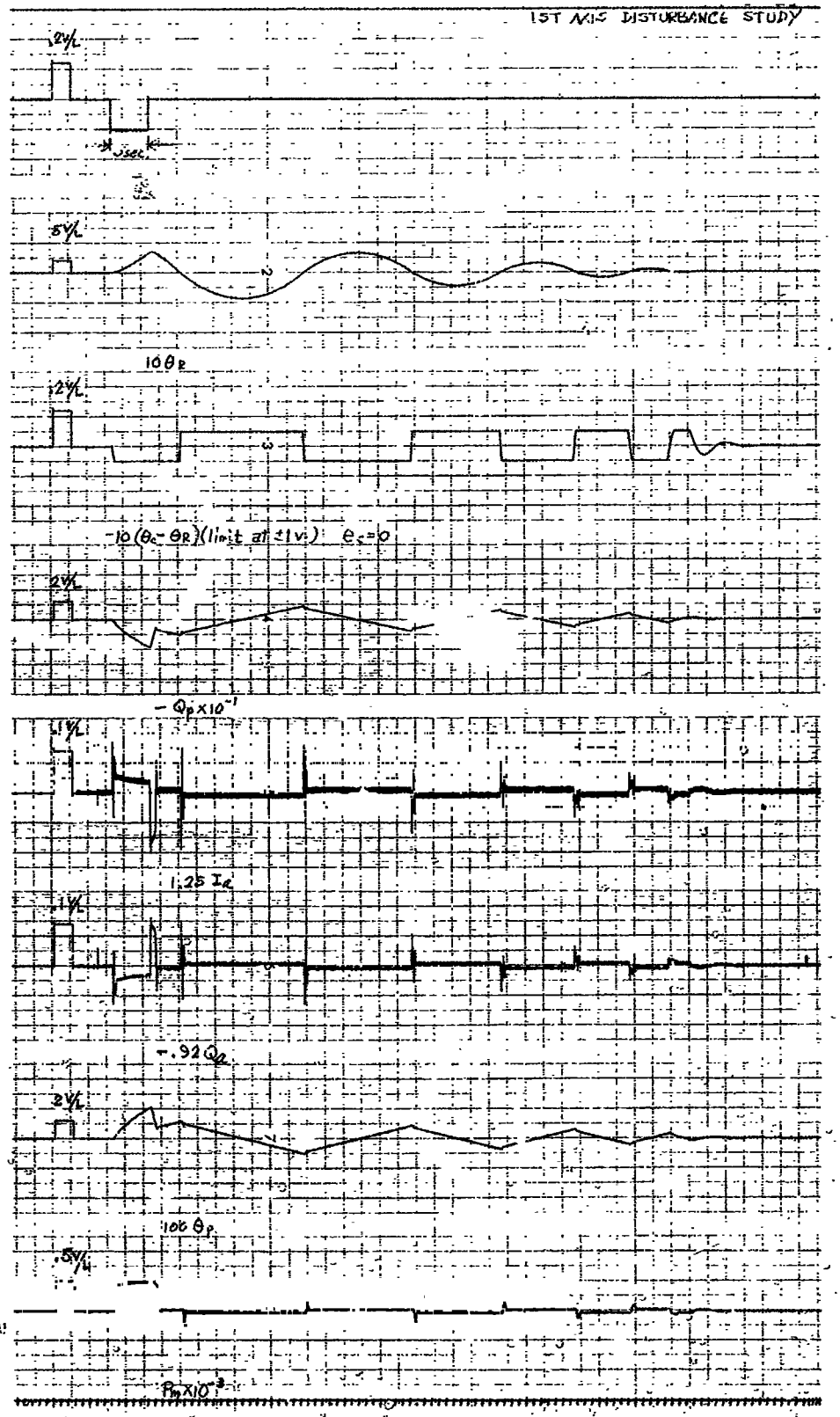
1ST MIC DISTURBANCE STUDY
2V/L
1 sec
5V/L
10θR
2V/L
-10(θc-θR)(limit at ±1v.) ec=0
2V/L
-Qp×10⁻¹
1V/L
1.25 Ic
1V/L
-.92Qc
2V/L
10θp
.5V/L
Pm×10⁻³

Figure 23

$$\frac{T_G}{J_{GR}} = .2 \times 10.5 = 2.1$$

$$\therefore T_G = 2.1 \times 215.5 \times 10^3 = 452 \times 10^3$$

$$t = 5$$

The analog result shows the system is stable, which checks with the curve. Figure 24:

$$T_G = 452 \times 10^3$$

$$t = 10$$

Stable by both results. Figure 25:

$$T_G = .2 \times 15.3 \times 215.5 \times 10^3 = 670 \times 10^3$$

(A) $t = 6$

unstable by both results.

(B) $t = 3$

unstable by both results.

(c) $t = 2$

stable by both results.

We therefore have been able to analyze and predict the effects of disturbance torques to the 1st axis system and verify these results by use of the analog computer.

D. 2nd Axis, Gondola Ring System

(1) Linear System Analysis (Paper)

As in the 1st axis, this system was studied in both a paper analysis and analog computer study. The transfer

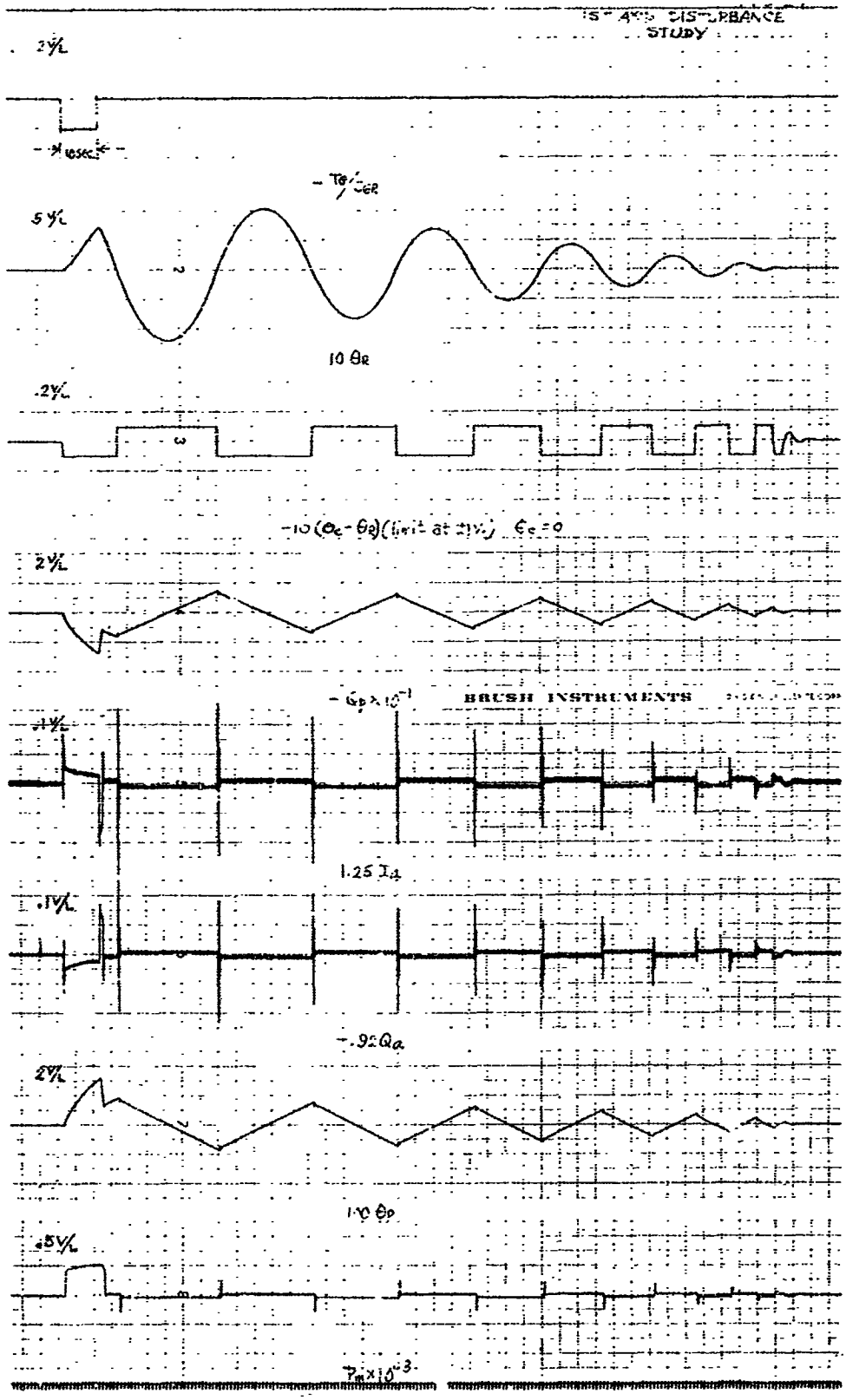

Figure 24

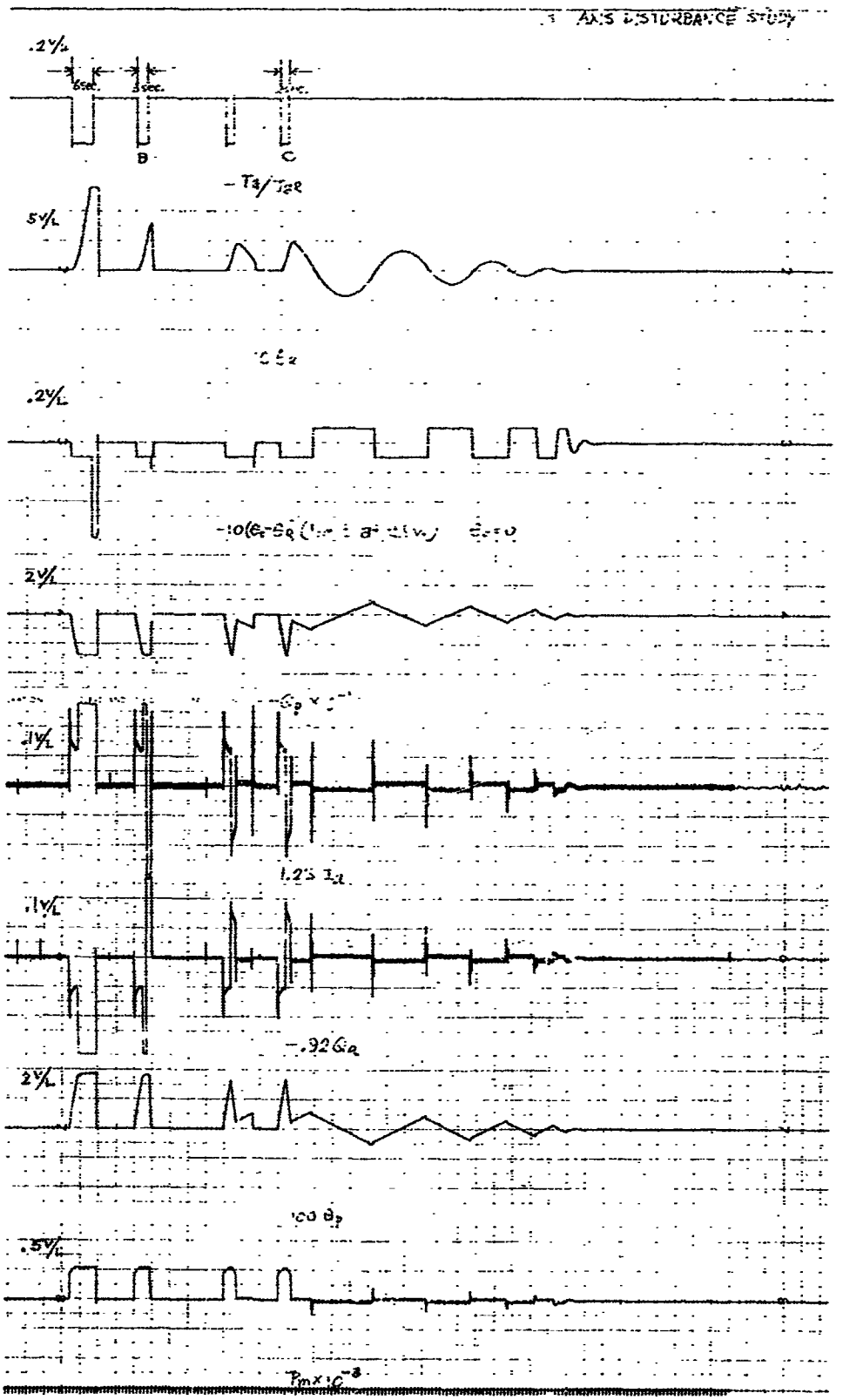

Figure 25

characteristics of phase and gain of the linear system paper analysis is included for the indicated loops of this system. Figure 26 is the closed loop characteristic of Q_a to Q_p. Figure 27 is the closed loop characteristic of e_2 to Q_p and Figure 28 is for e_1 to P_m. Figure 29 is the transfer characteristic for the closed loop response of the complete 2nd axis system which indicates that in the frequency spectrum the system response will have a 5.5 db peak at approximately 0.8 cps with a damping ratio of 0.3 from which we would expect an overshoot of 1.35 for a step input.

(2) Linear System Analog Computer Study

The block diagram for the analog computer study of the second axis system is shown in Figure 30 with the computer diagram shown in Figure 31. As in the study of the first axis system, the simulation is made in real time with unity scale factors.

The analog computer test result of the frequency response for the 2nd axis system without nonlinear elements is plotted in Figure 32. This indicates a peak amplitude ratio of output to input, as expressed in decibels of approximately 6.8 db at a frequency of 0.8 cps and a crossover frequency of 1.85 cps. The phase shift plot starts at zero for zero frequency indicating that the system is a position controlled system as required for this application.

The response to a step input for the 2nd axis system is shown in Figure 33. Each recording channel corresponds to the circled number in Figure 31. These recordings show that for

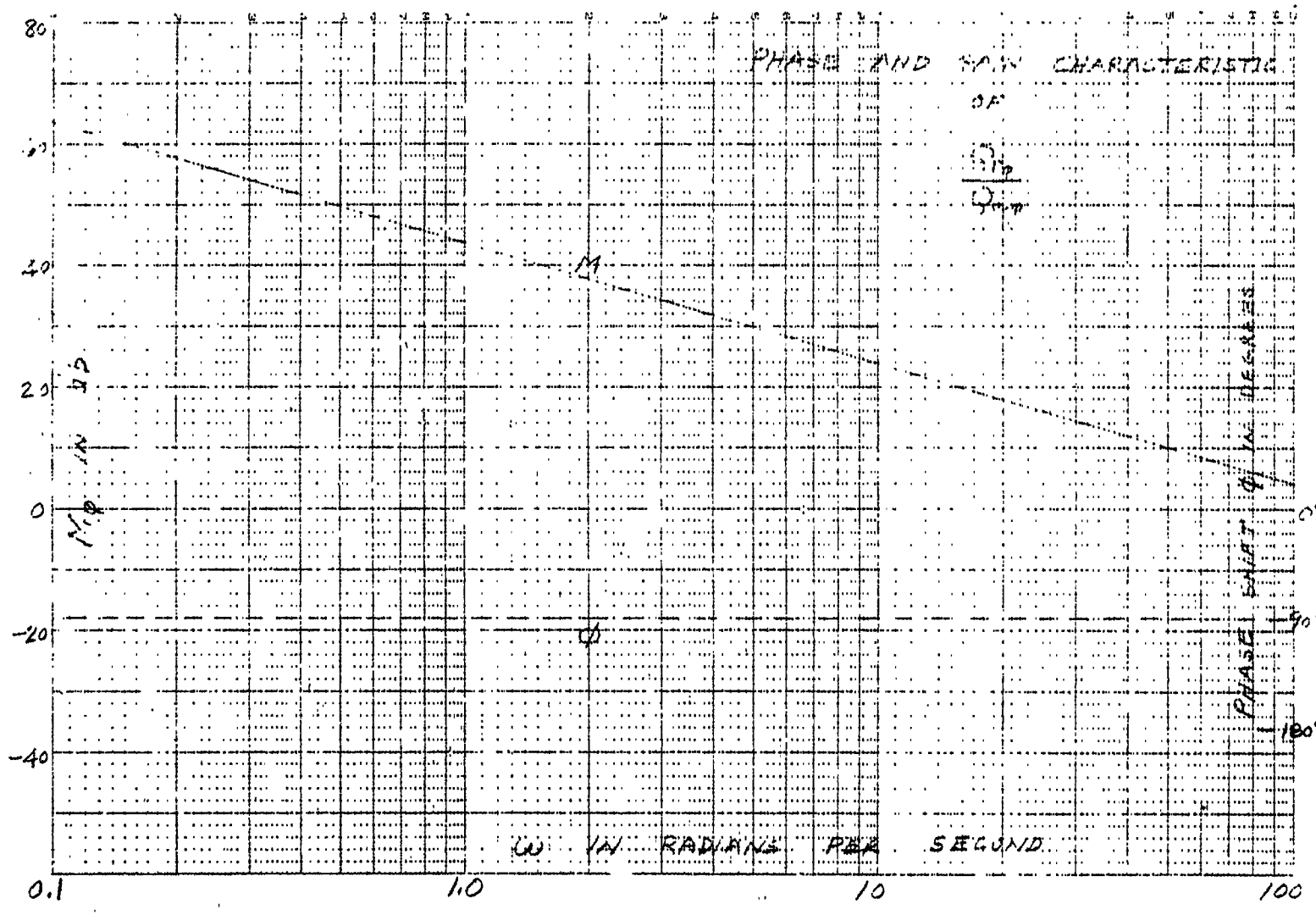
PHASE AND GAIN CHARACTERISTIC
80
40
20
0
-20
-40
0.1
1.0
10
100
0°
-90°
-180°
PHASE LAG IN DEGREES
ω IN RADIANS PER SECOND

Figure 26

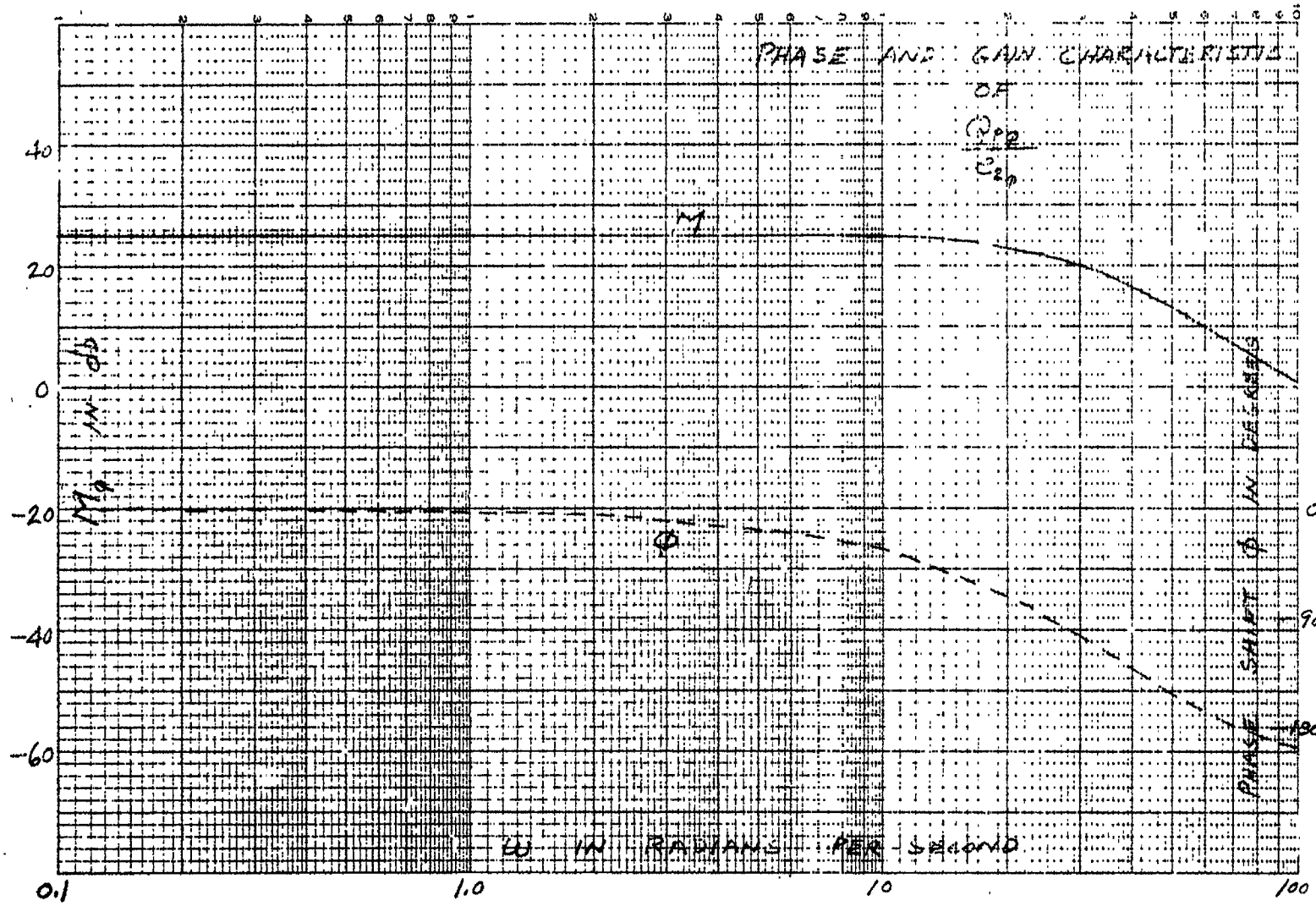
PHASE AND GAIN CHARACTERISTICS
OF
$\frac{e_{op}}{e_{ip}}$
40
20
0
-20
-40
-60
M db
M
φ
0.1
1.0
10
100
ω IN RADIANS PER SECOND
0°
90°
180°
PHASE SHIFT φ IN DEGREES

Figure 27

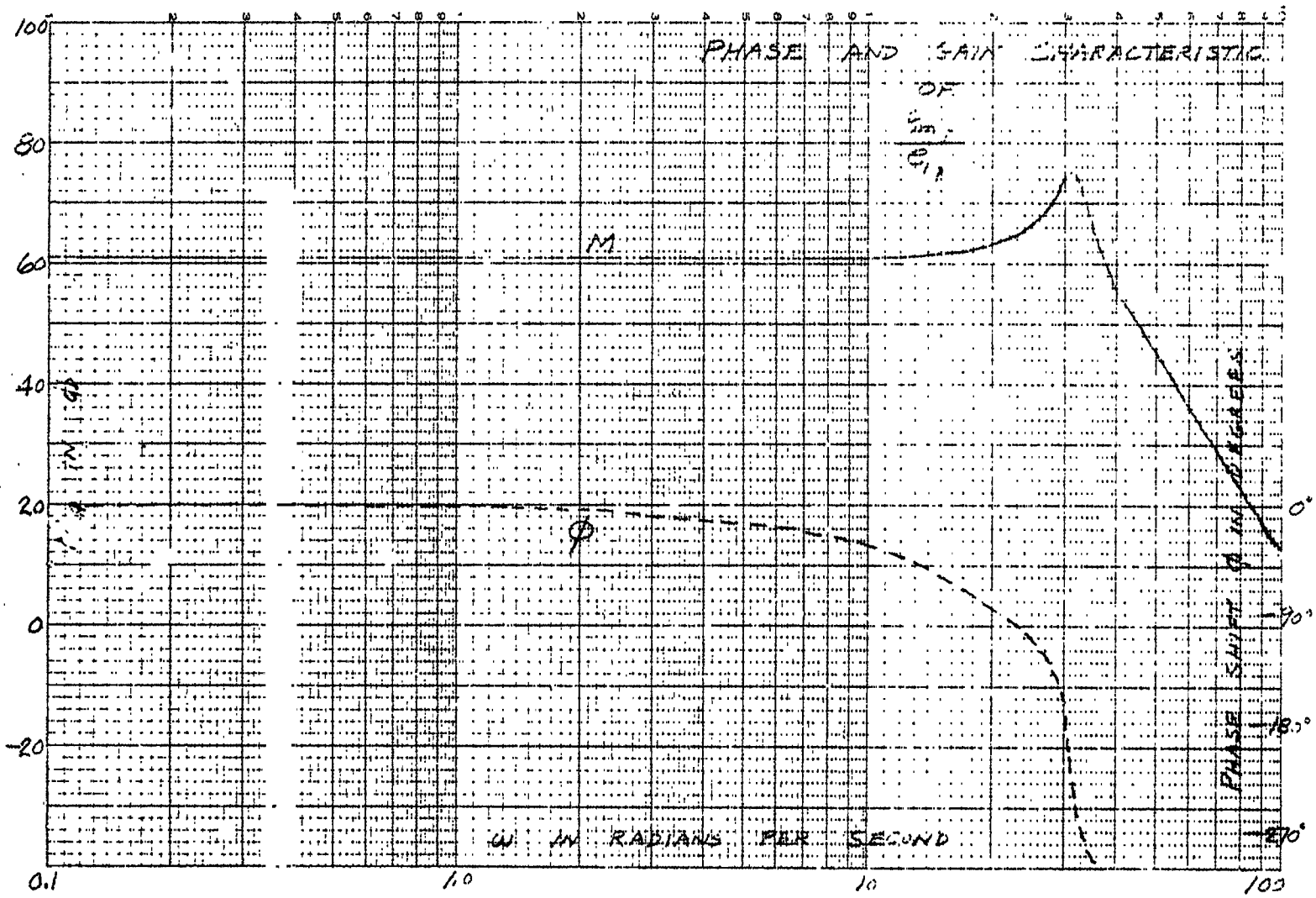
PHASE AND GAIN CHARACTERISTIC
OF
M
100
80
60
40
20
0
-20
0.1
1.0
10
100
0°
-90°
-180°
-270°
PHASE SHIFT IN DEGREES
ω IN RADIANS PER SECOND

Figure 28

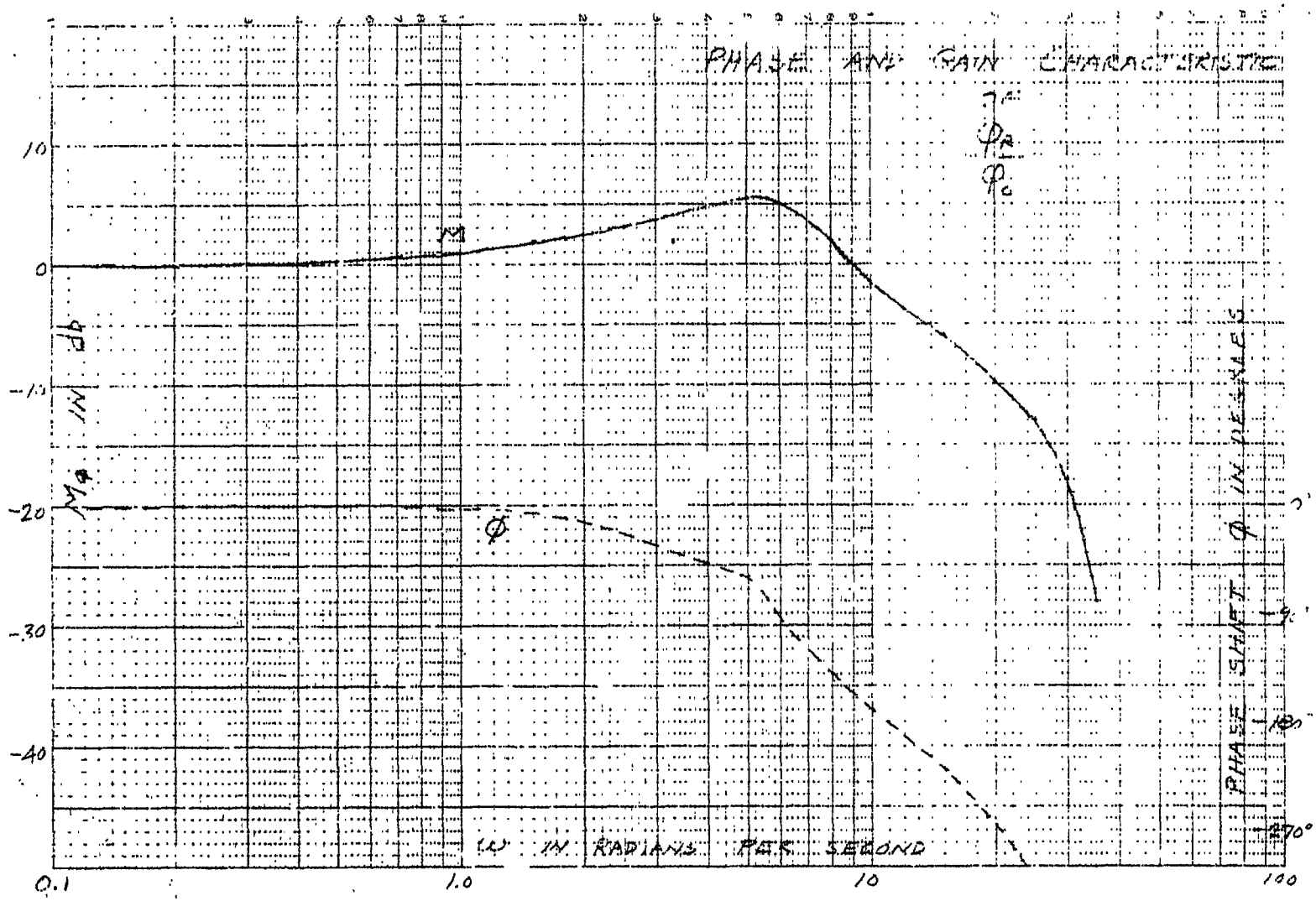
PHASE AND GAIN CHARACTERISTIC
10
0
-10
-20
-30
-40
M
Mφ IN db
φ
φR
φo
PHASE SHIFT φ IN DEGREES
-90°
-180°
-270°
ω IN RADIANS PER SECOND
0.1
1.0
10
100

Figure 29

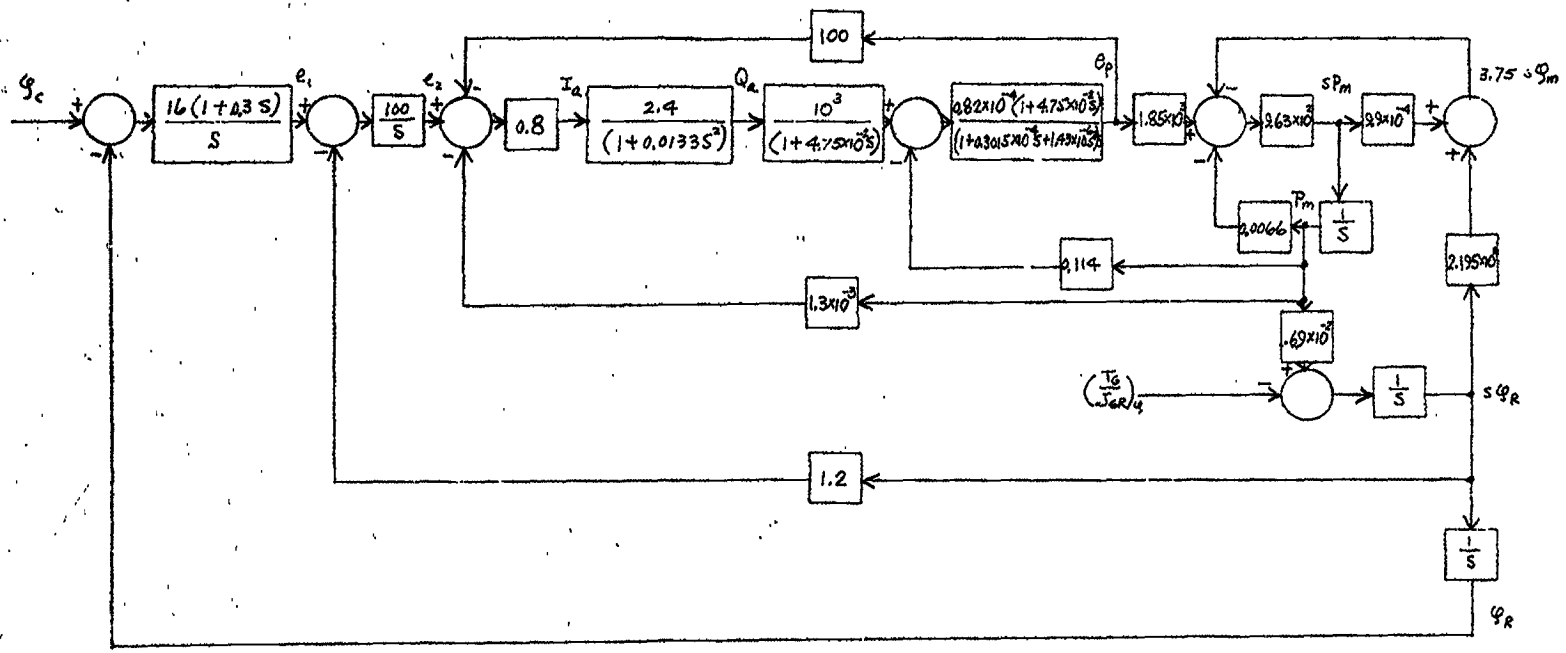

Figure 30 - 2nd Axis Block Diagram

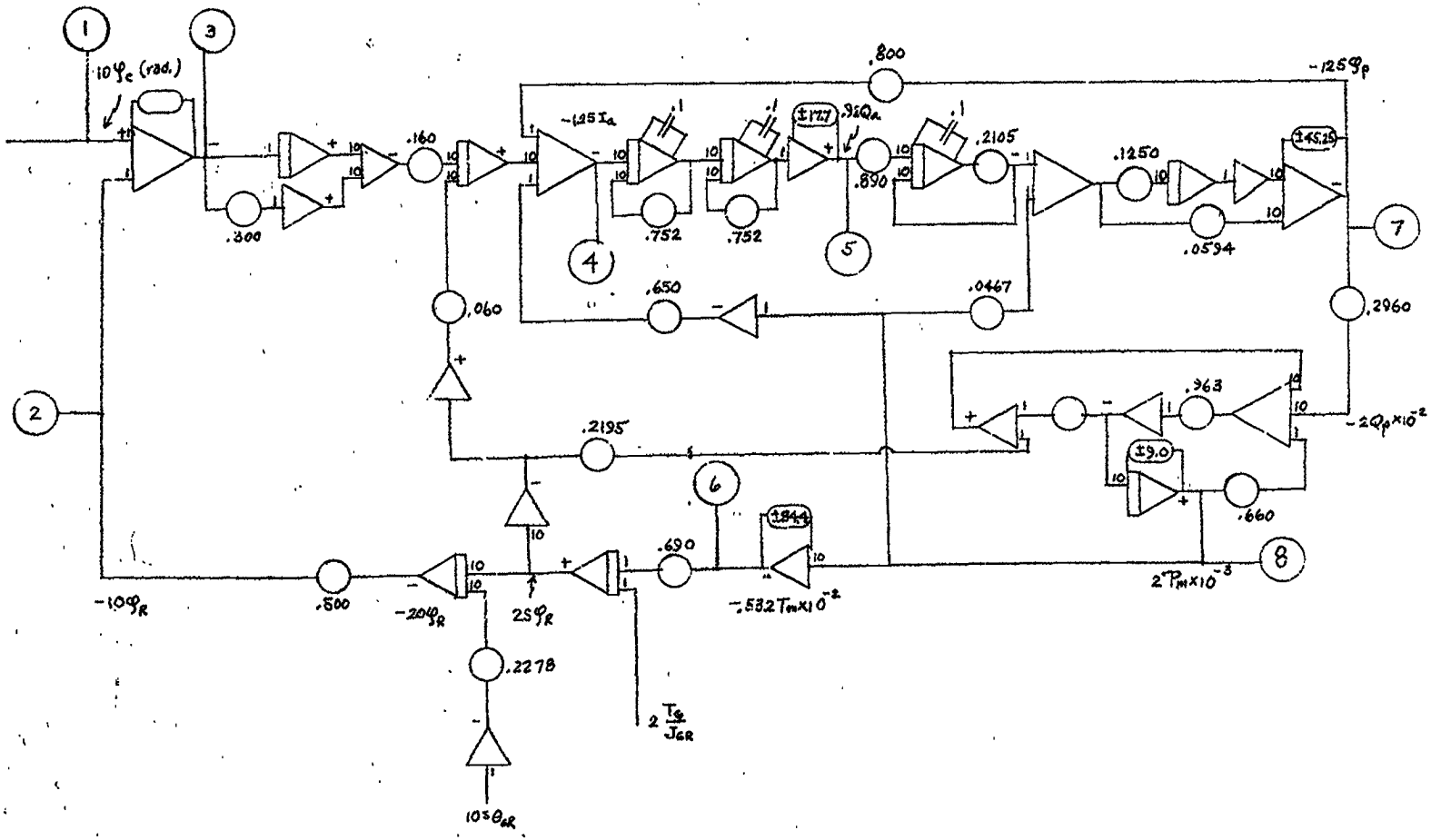

Figure 31 - 2nd Axis Analog Circuit

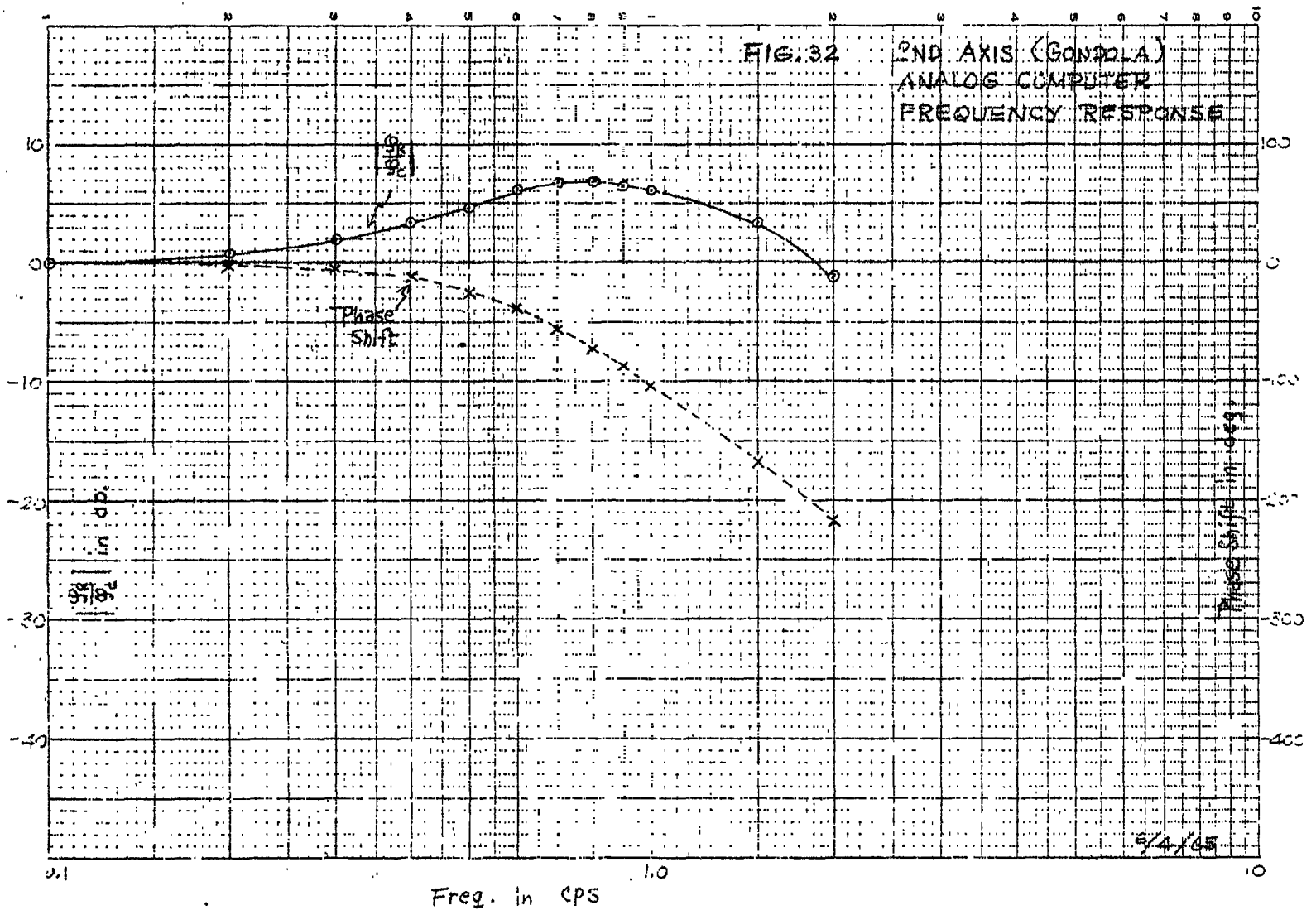
FIG. 32 2ND AXIS (GONDOLA)
ANALOG COMPUTER
FREQUENCY RESPONSE
10
0
-10
-20
-30
-40
100
0
-100
-200
-300
-400
Phase Shift
Phase Shift in degrees
Phase Shift
6/4/65
0.1
1.0
10
Freq. in CPS

Figure 32

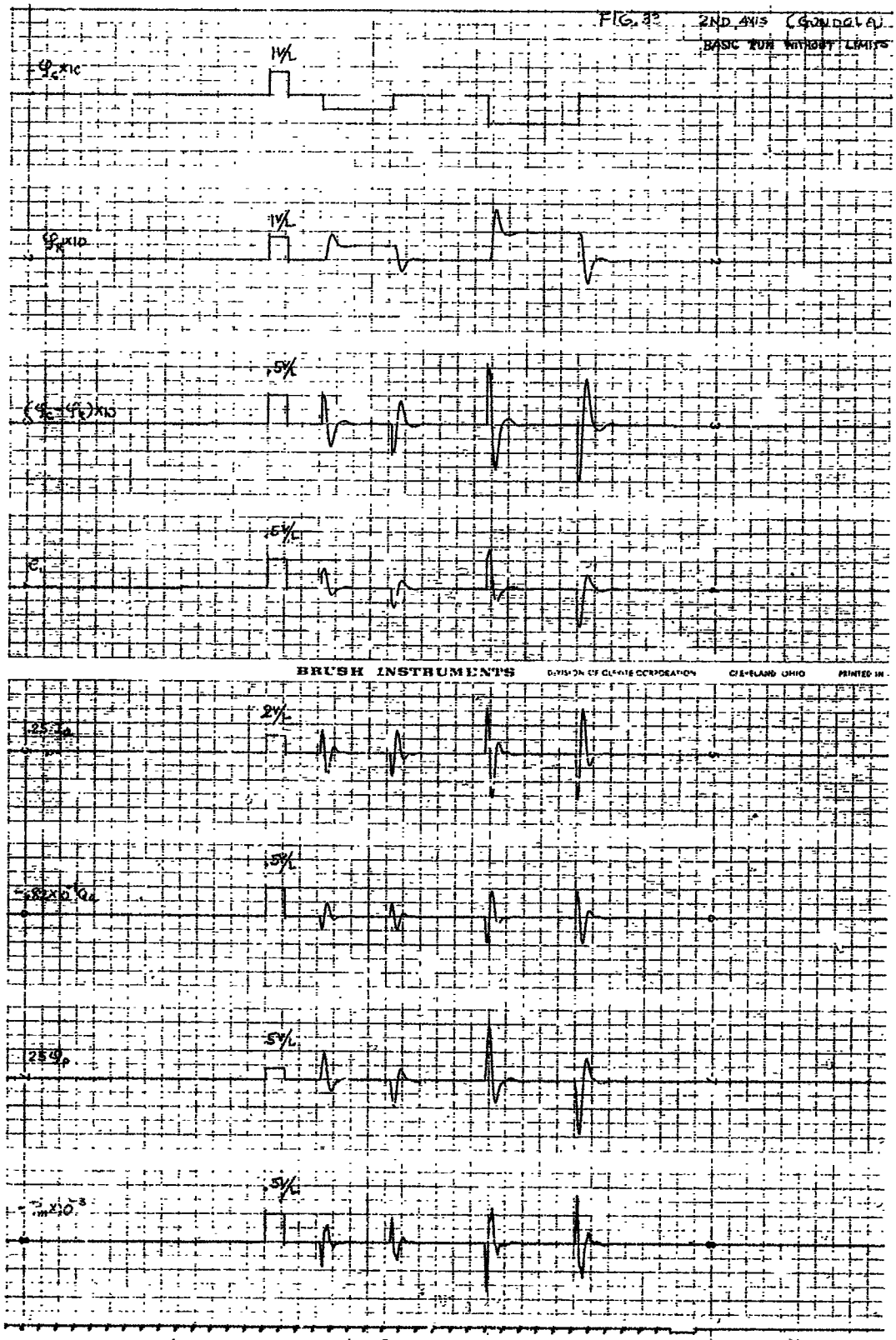
FIG. 3
2ND AXIS (GROUND)
BASIC RUN WITHOUT LIMITS
1V/L
1V/L
.5V/L
.5V/L
BRUSH INSTRUMENTS
2V/L
.5V/L
.5V/L
.5V/L

Figure 33

a step input the output position has about an 80% overshoot and a settling time of about 1.4 seconds. In comparison to the 1st axis system, the percent overshoot is 1 6 times larger and the settling time 0.146 times less.

(3) Comparison of Paper Study and Analog Study

The phase and gain characteristic of the paper analysis and the analog computer study have been plotted on a single graph shown in Figure 34. These graphs show very good agreement and indicate that the system simulated is a good representation of the actual hardware.

(4) Limit Circuits

The limit as determined from information submitted for this study are shown in Figure 16.

The effect of these limits in the 2nd axis system is shown in Figure 35. The system is stable for a step input command of 0.2 rad. A step input command of 0.4 rad will cause the system to become unstable. Provisions must therefore be made to limit the error signal to a level that will prevent the system from becoming unstable. An error limit of ±0.2 rad will permit a command of 1.85 rad to be applied. Command angles as large as 3.14 radians or greater will be subjected to this axis. With an error limit set for ±0.1 radians a command signal of 3.2 radians can be applied as shown in the computer results of Figure 36. This has increased the settling time to 13.4 seconds as compared to the 1.4 seconds for the linear system. This limit has very little effect on the maximum velocity of approximately 2.0 radians per second

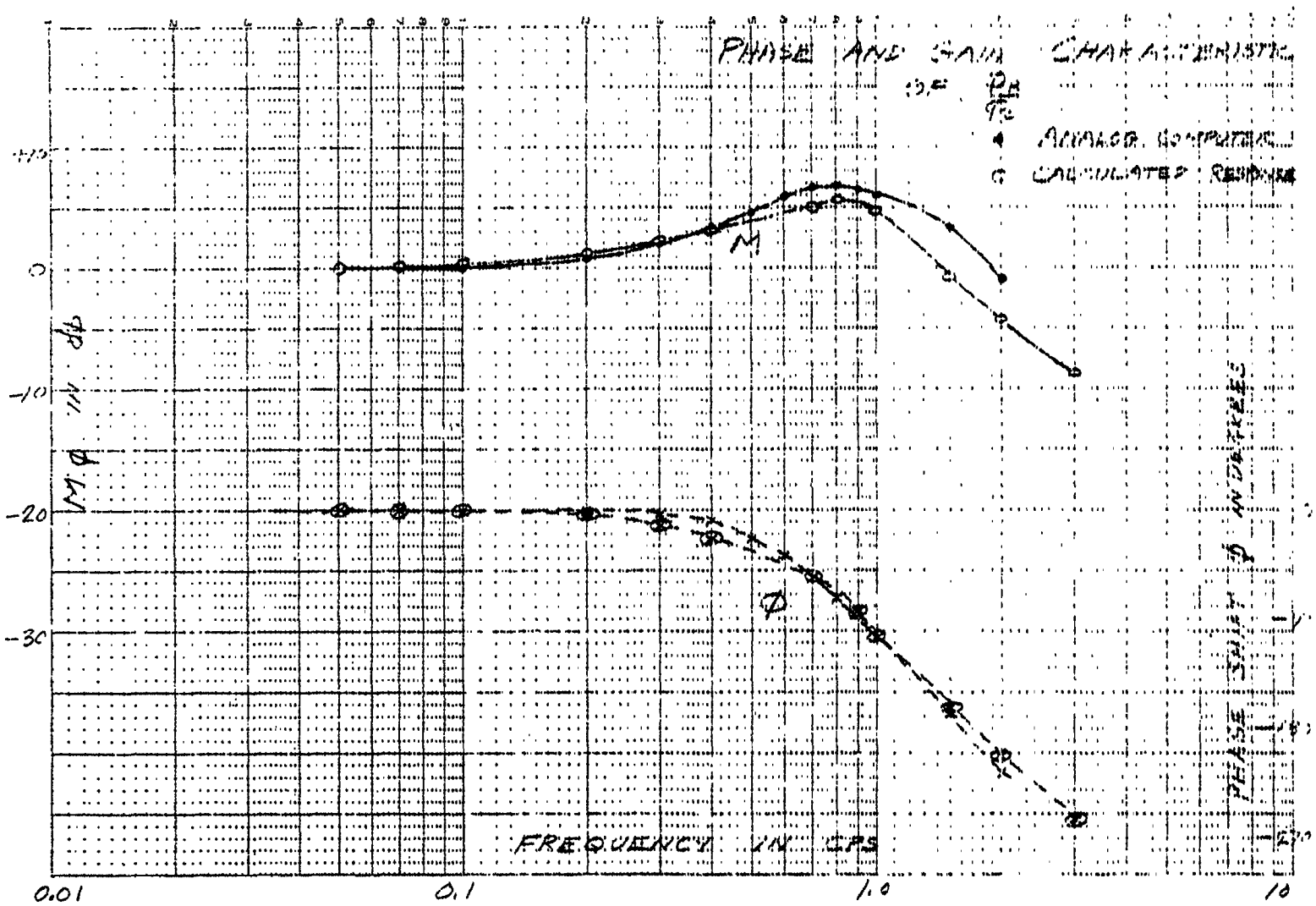
PHASE AND GAIN CHARACTERISTIC
0
-10
-20
-30
0.01
0.1
1.0
10
FREQUENCY IN CPS

Figure 34

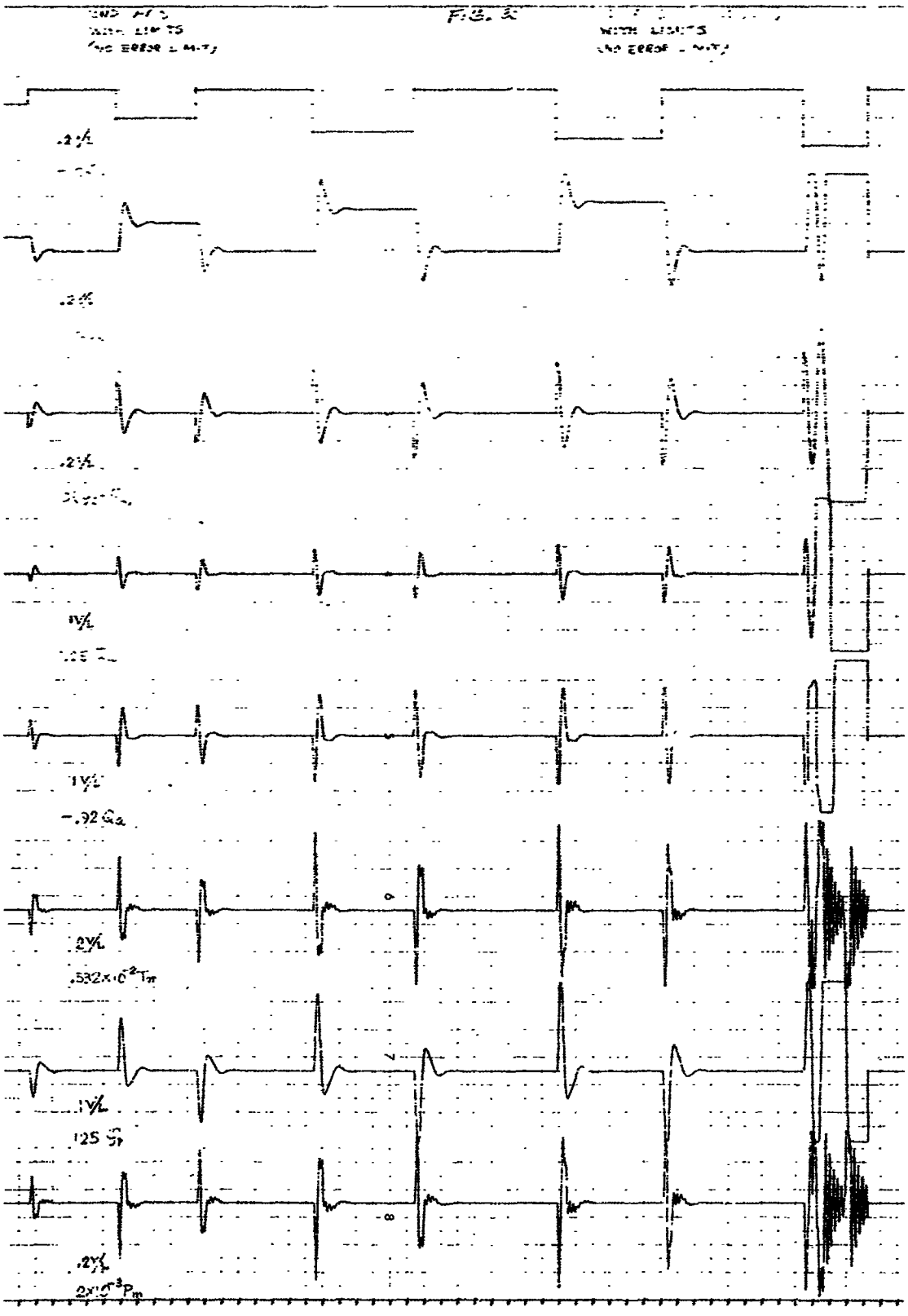

Figure 35

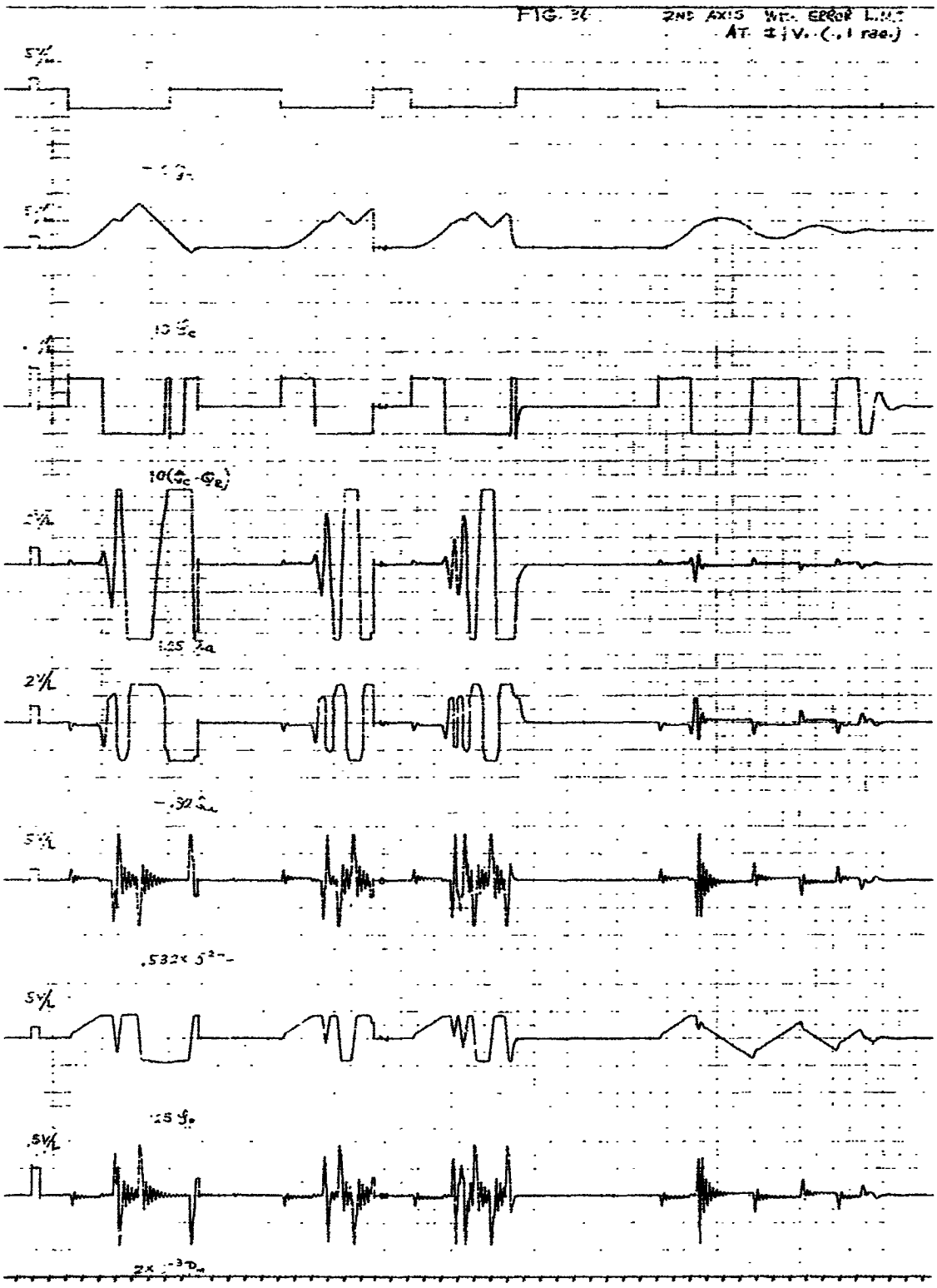
FIG. 36
2ND AXIS WT. ERROR LIMIT
AT ±1 V. (.1 rad.)
5%
10 θc
10(θc - θe)
.05 θa
2%
-.32 θa
5%
.532 × 5²
5%
.25 θe
.5%

Figure 36

for the second axis system.

(5) Effects of Disturbance Forces

A discussion similar to that used for the disturbance forces in the 1st axis system may be applied to the 2nd axis system. From given maximum condition we can solve for the maximum value of time for which these conditions can be sustained. Solving for Q_{pmax}, we have (using equation 46)

$$Q_p(t) = nd_mCt + (C_m+C_p)P_{max}$$

Here

$$Q_p(t) = rK_p\theta_p(t)$$

$$= 4.812 \times 385\ \theta_p(t)$$

$$= 1850\ \theta_p(t)$$

and $Q_{pmax} = 690$ and $\theta_{pmax} = .362$

Therefore, we have

$$1850.\theta_p(t) = nd_mCt + (C_m+C_p)P_{max}$$

where

$$n = 58.5$$

$$d_m = 3.75$$

$$C_m = 0.0033$$

$$C_p = 0.0033$$

$$P_{max} = 4.5 \times 10^3$$

$$\theta_{pmax} = .362$$

$$\therefore\ t = \frac{670-29.7}{219.5G} = 1.4\ J_{GR}\ \frac{1}{T_G - nT_{max}}$$

where

$$J_{GR} = 32 \times 10^3 \qquad nT_{max} = 925 \times 10^3$$

$$\therefore\ t = \frac{44.8 \times 10^3}{T_G - 925 \times 10^3} \tag{49}$$

Therefore, for the 2nd axis system, the above expression of t represents the maximum limit for system stability.

In addition to the cases considered so far, the following case should be also considered for the 2nd axis system.

Pressure and torque response to a step disturbance torque has, in its transient period, damped oscillation. This oscillation is more evident in the 2nd axis system than in the first axis system due to the 15 db peak in amplitude of the pressure loop at approximately 5 cps. Comparison of Figures 8 and 28 shows this large peak in the second axis system where the first axis system is relatively flat.

Therefore, if the torque difference (response overshoots and step disturbance) remains above a certain value for a certain period, the system would become unstable for the same reason applied previously, even though the disturbance is less than the maximum system torque.

The curve of time and torque difference which divides stable and unstable regions is drawn as shown in Figure 37.

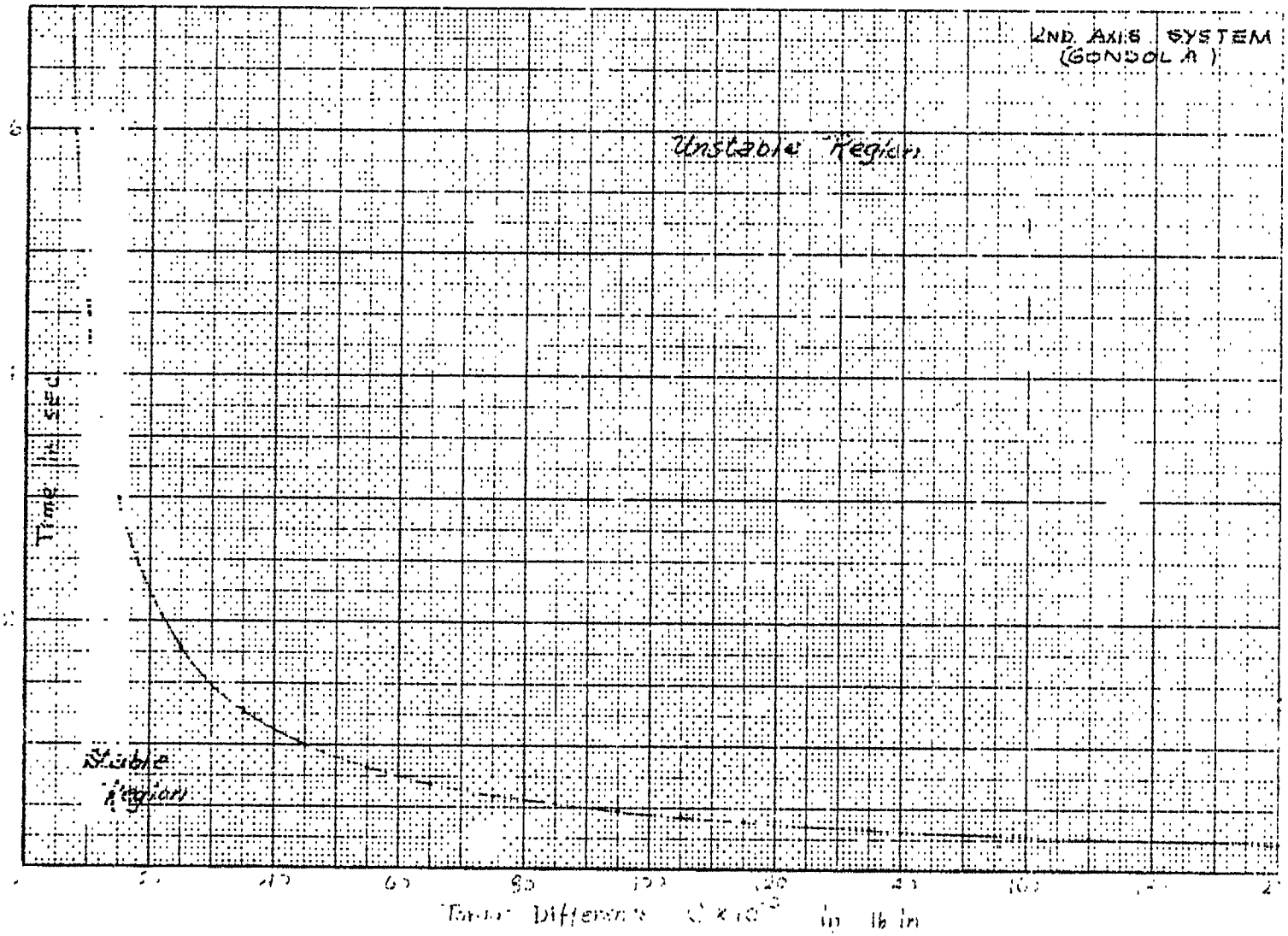
2ND. AXIS SYSTEM
(GONDOLA)
Unstable Region
Stable
Region
Time in SEC
Torque Difference
in lb in

Figure 37

From this curve, the following data are obtained:

Time t(sec)	Torque Difference $C \times 10^{-3}$ (lb-in)	Disturbances $T_G \times 10^{-3} = (925 - C \times 10^{-3})$ (lb-in)
.7	65	860
.6	75	850
.5	90	835
.4	110	815
.3	150	775
.22	200	725

Accordingly, the stable and unstable regions for the 2nd axis system will be drawn as shown on the following page, Figure 38.

The analog computer studies show instability occurs at $T_G \times 10^{-3} = 740$ (Figure 39). For Figure 39 A:

$$2 \frac{T_G}{J_{GR}} = 5 \times 9.5 = 47.5$$

$$\therefore T_G = 23.75 \times 32 \times 10^3 = 760 \times 10^3$$

$$t = 2.8$$

Unstable by both results.

For Figure 39 B:

$$T_G = 760 \times 10^3$$

$$t = .15$$

Stable by both results.

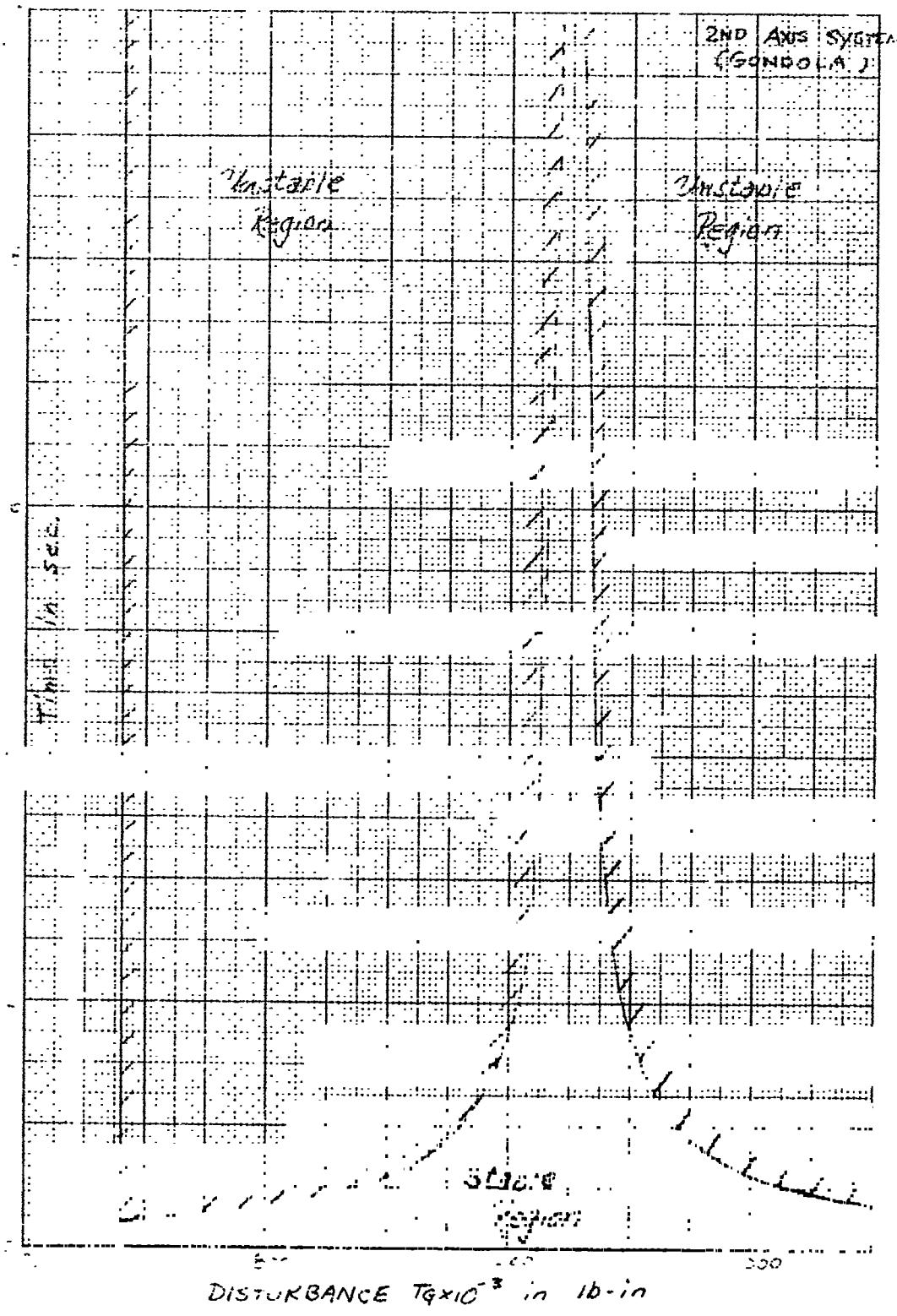
2ND AXIS SYSTEM
(GONDOLA)
Unstable
Region
Unstable
Region
Stable
Region
DISTURBANCE TG x 10⁻³ in lb-in

Figure 38

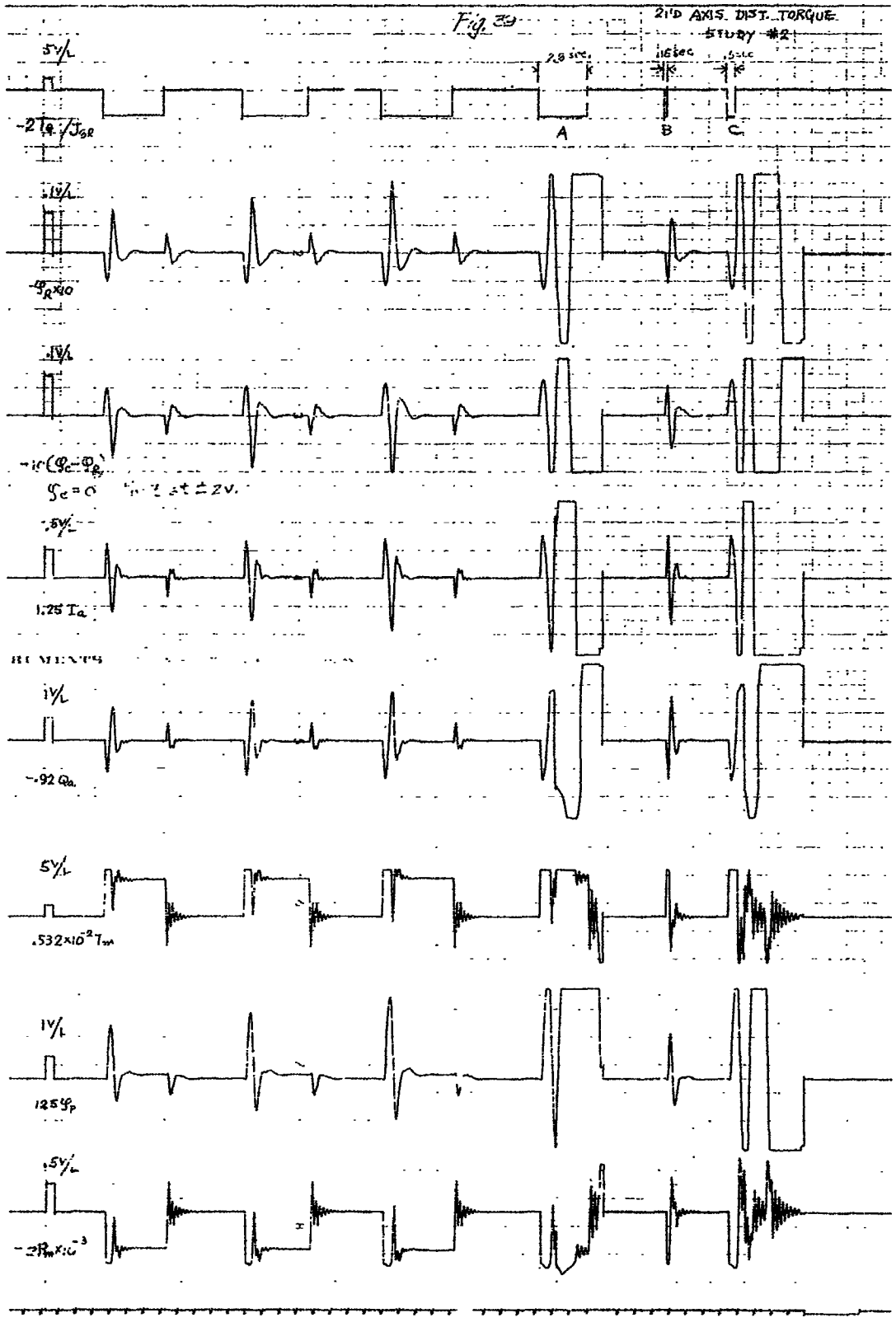
Fig. 39
2ND AXIS DIST. TORQUE
STUDY #2
2.8 sec.
.116sec
.5sec
A
B
C
5V/L
-2Tq/JqR
1V/L
-φR×10
1V/L
-10(φc-φR)
φc=0
.5V/L
1.25 Ia
1V/L
-.92 Qa
5V/L
.532×10⁻²Tm
1V/L
1.25φp
.5V/L
-2Rm×10⁻³

Figure 39

For Figure 39 C:

$T_G = 760 \times 10^3$

$t = .5$

Unstable by both results.

Again we have been able to analyze and predict the effects of disturbance torques to the 2nd axis system, and verify these results by use of the analog computer.

(6) Coupling Torques

Due to the physical arrangement of the drive input to each of the systems, there are coupling torques that interact on both the 1st and 2nd axis systems. This information supplied as a supplement to the initial specifications stated that the torque applied at the 1st axis by the 2nd axis drive must be counterbalanced by the 1st axis drive by $-.3884\ T$. The method of simulating this effect is as follows:

$$T_{m1} = (P_{m1})(d_{m1})$$

$$T_{m2} = (P_{m2})(d_{m2})$$

$$T_{m1}' = .3884\ T_{m2}$$

$$P_{m1}' = .3884\ \frac{P_{m2} d_{m2}}{d_{m1}}$$

The value of P_{m1}' is then summed in with P_{m1} to produce the 1st axis torque which is now a function of both the 1st and 2nd axis systems due to the coupling effect.

Compensation for the coupling torques was included in this computer simulation. The first axis velocity was summed in with the second axis velocity through the proper gain factor. With the second axis input command at zero, a torque will be developed in the second axis system due to the mechanical coupling of the first axis to the second axis. This torque is coupled back to the first axis system through the proper gain constant. The second axis system has therefore been forced to assume a new output shaft position due to the first axis velocity. This new output shaft position is compensated by feeding in an input command position that is a function of the first axis command position. This will hold the second axis position steady for changes in the first axis position. The coupling effect of the first axis upon the second axis position is shown in Figure 40.

E. 3rd Axis Main Arm Drive System

(1) System Configuration

The main arm drive system is basically a Ward Leonard configuration consisting of 2-2500 KW direct current generators connected in parallel to deliver driving power to a 6700 HP, 11/48 rpm shunt type direct current motor. The control system is designed to permit maximum torque delivery from the motor over a speed range of zero to 11 rpm. Above this speed constant horsepower limit is achieved by weakening of the motor field thus permitting operation up to a top speed of 48 rpm. The control system is a velocity type in which the motor shaft speed is proportional to an input command signal.

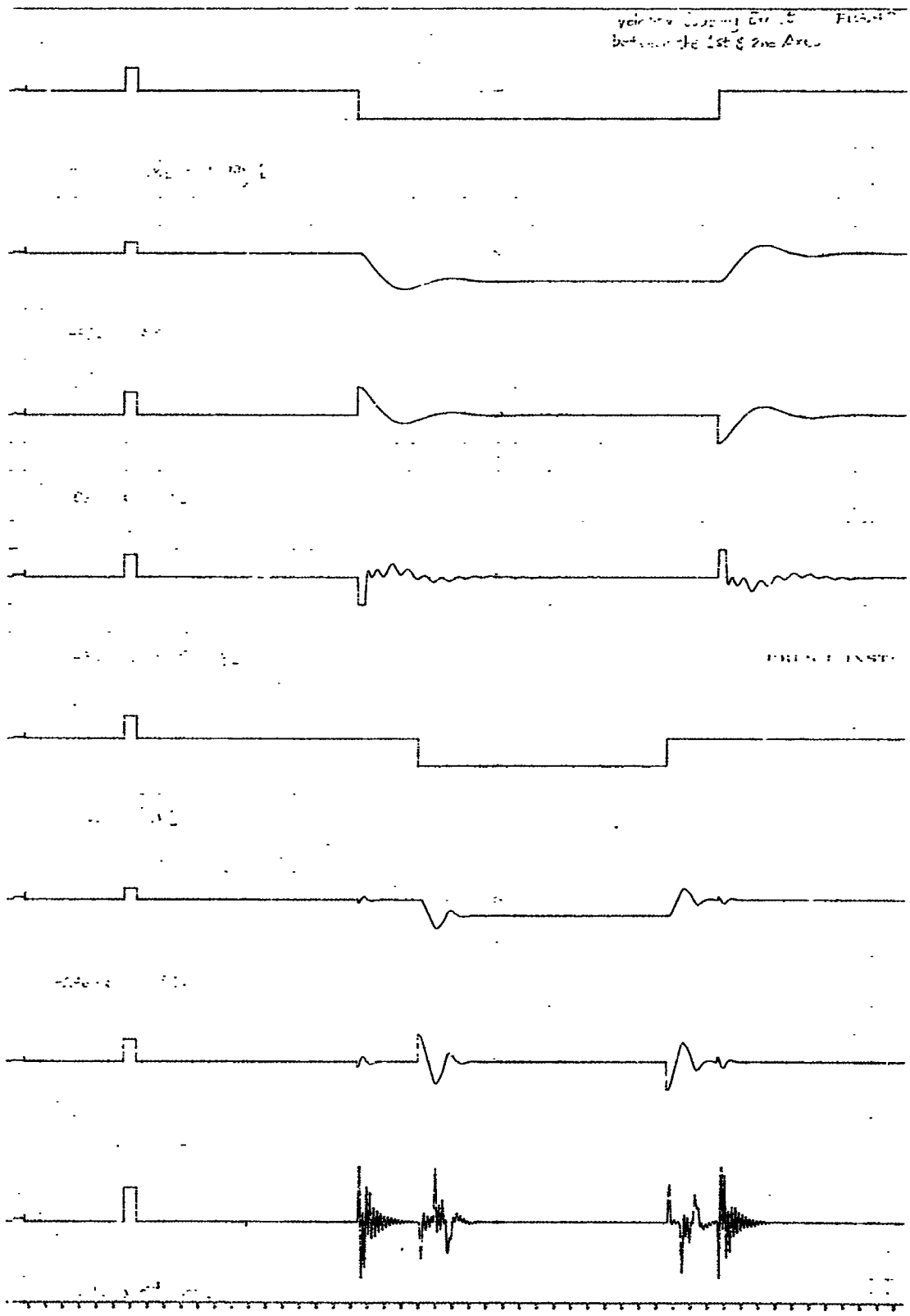

Figure 40

The block diagram for this system is shown in Figure 41.

(2) Confirmation of Final Parameters

Considerable effort was expended in checking the hardware information against circuit diagrams in order to insure an accurate simulation. As a basis of comparison the zero mode load simulation as performed by the Westinghouse Corporation was used. The specific test cited here is the Westinghouse Figure 8-6 which is a ramp starting at 1.15 rad/sec and rising to 2.7 rad/sec in a period of 2 sec. The results of the analog computer test as performed at The Franklin Institute Laboratories using the computer program of. Figure 42 are shown in Figure 43. These curves show good similarity with the exception of the current peak magnitude. The current reaches a peak of 18,400 amperes. According to the specifications, this current is not to exceed 15,000 amperes. The same slope of ramp was used with the upper level extended to 3.9 rad/sec as shown in Figure 44. The current has definitely limited at 19,200 amperes which is considerably in excess of the design value. An attempt was made to limit this current to 15,000 amperes by adjusting the voltage limit of E_a. Figure 45 shows the results of this approach when an input command equivalent to the maximum g profile is used. It is quite evident that the system becomes unstable. It was found that the limit for V_1 had been improperly specified. By using the proper limit value for V_1 it was possible to produce the maximum g profile without exceeding the 15,000 ampere limit and without the system becoming unstable. These results are shown in Figure 46.

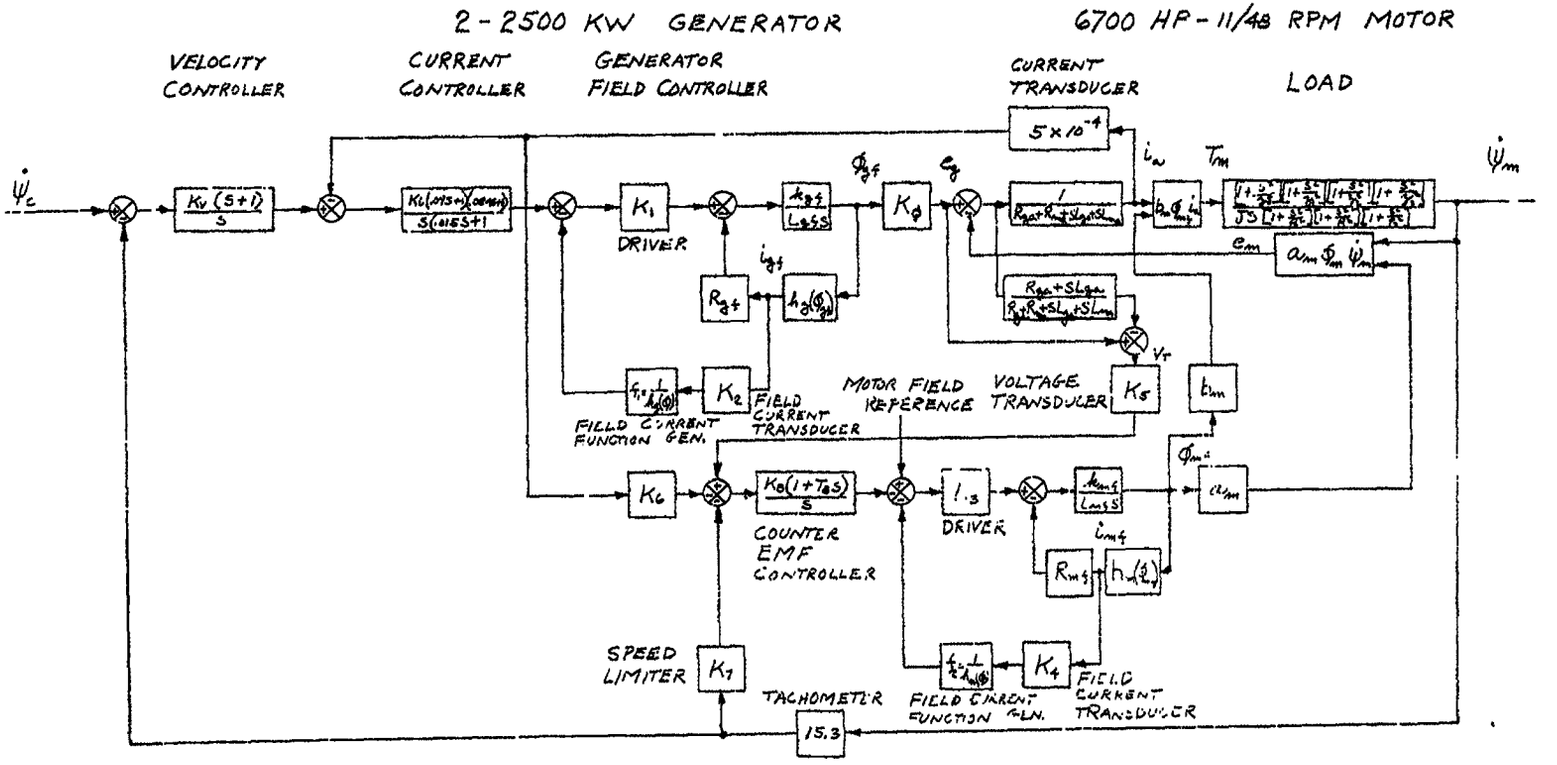

Figure 41 - Main Axis Control System Block Diagram

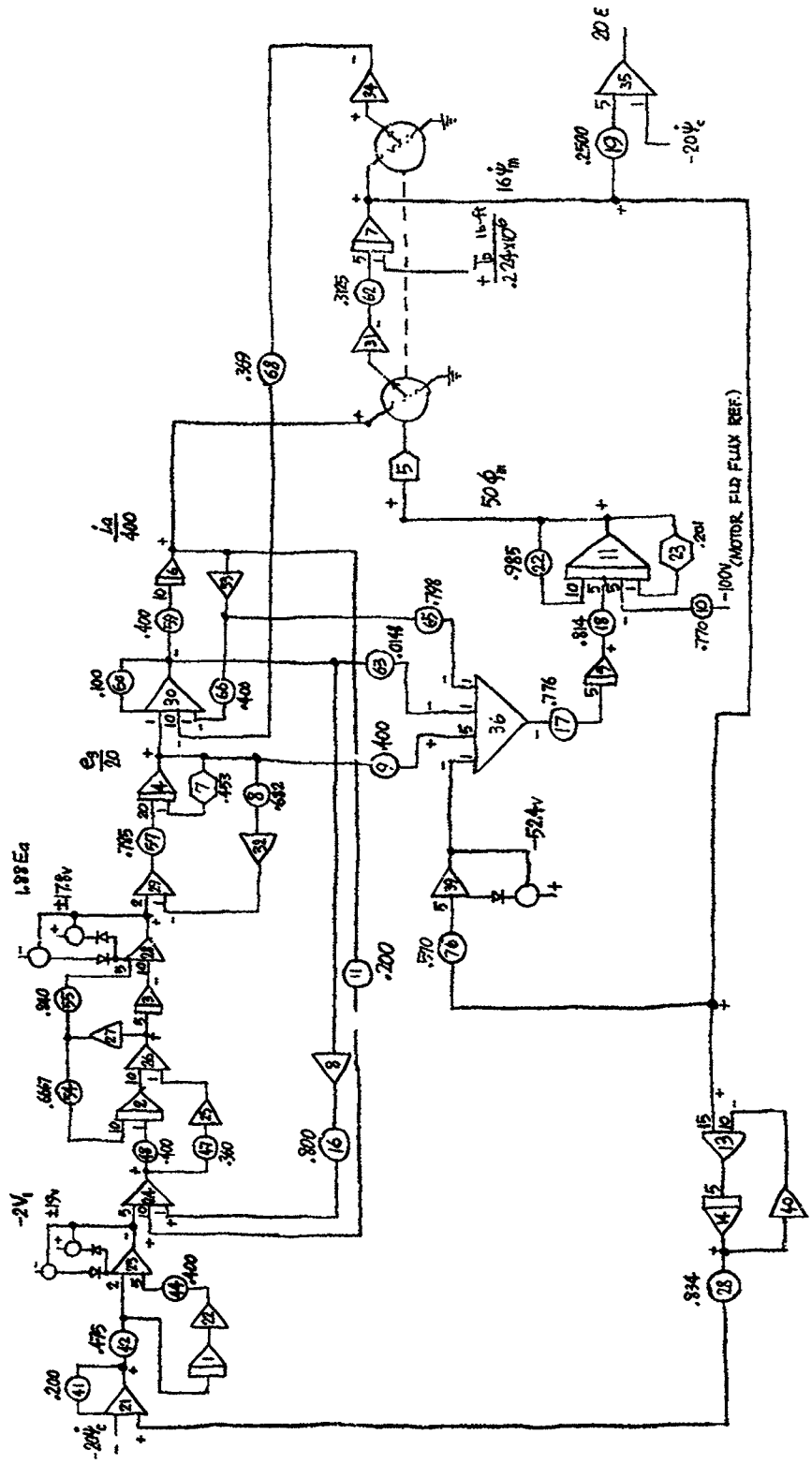

Figure 42 - NASA Centrifuge Main Arm Control System Computer Simulation Circuit

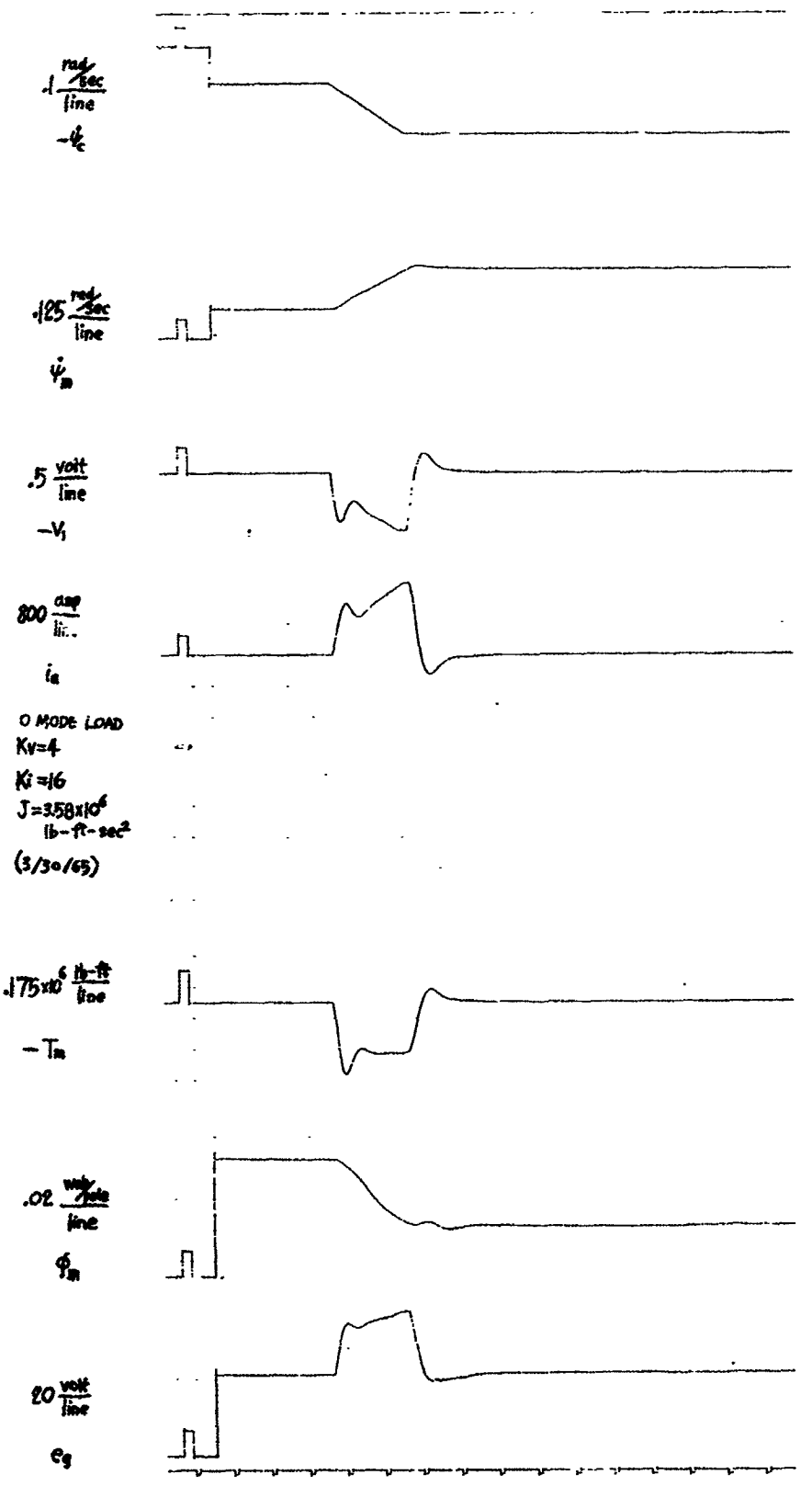

41, 4C

Figure 43

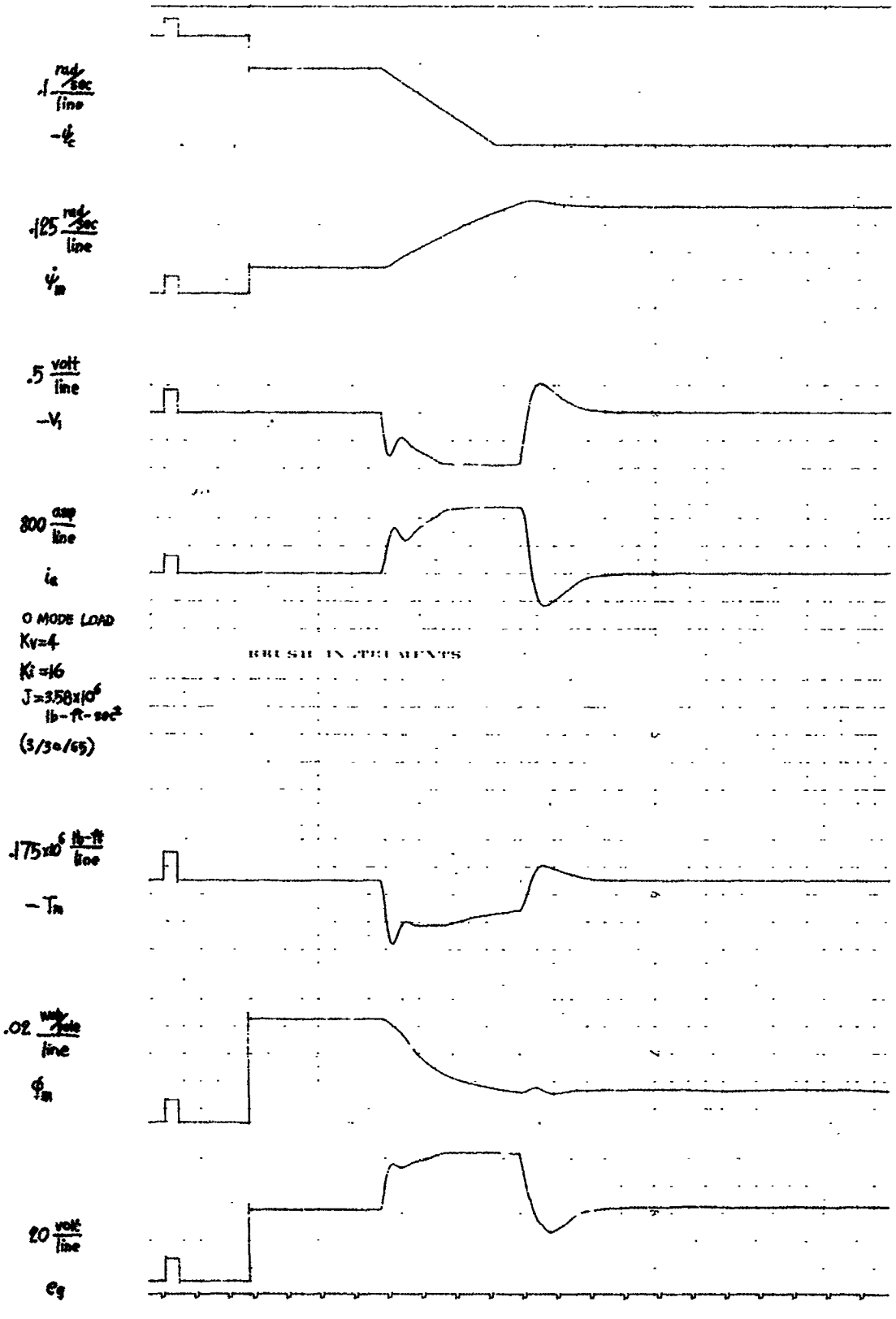

Figure 44

41, 40

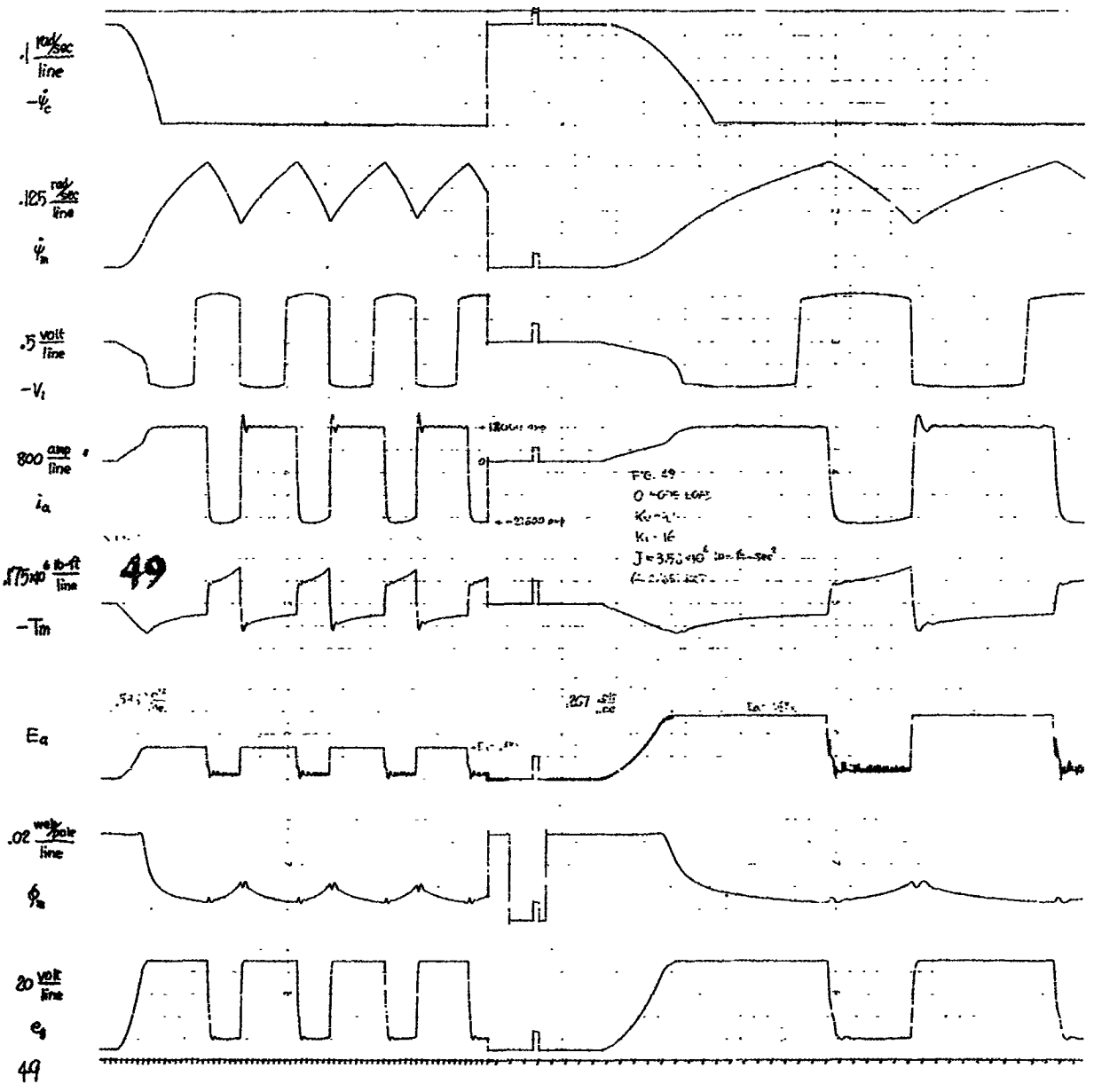
.1 rad/sec line
$-\dot{\psi}_c$
.125 rad/sec line
$\dot{\psi}_m$
.5 volt line
$-V_t$
800 amp line
i_a
.175x10^6 lb-ft line
$-T_m$
49
E_a
.02 weber/pole line
ϕ_a
20 volt line
e_g
49

Figure 45

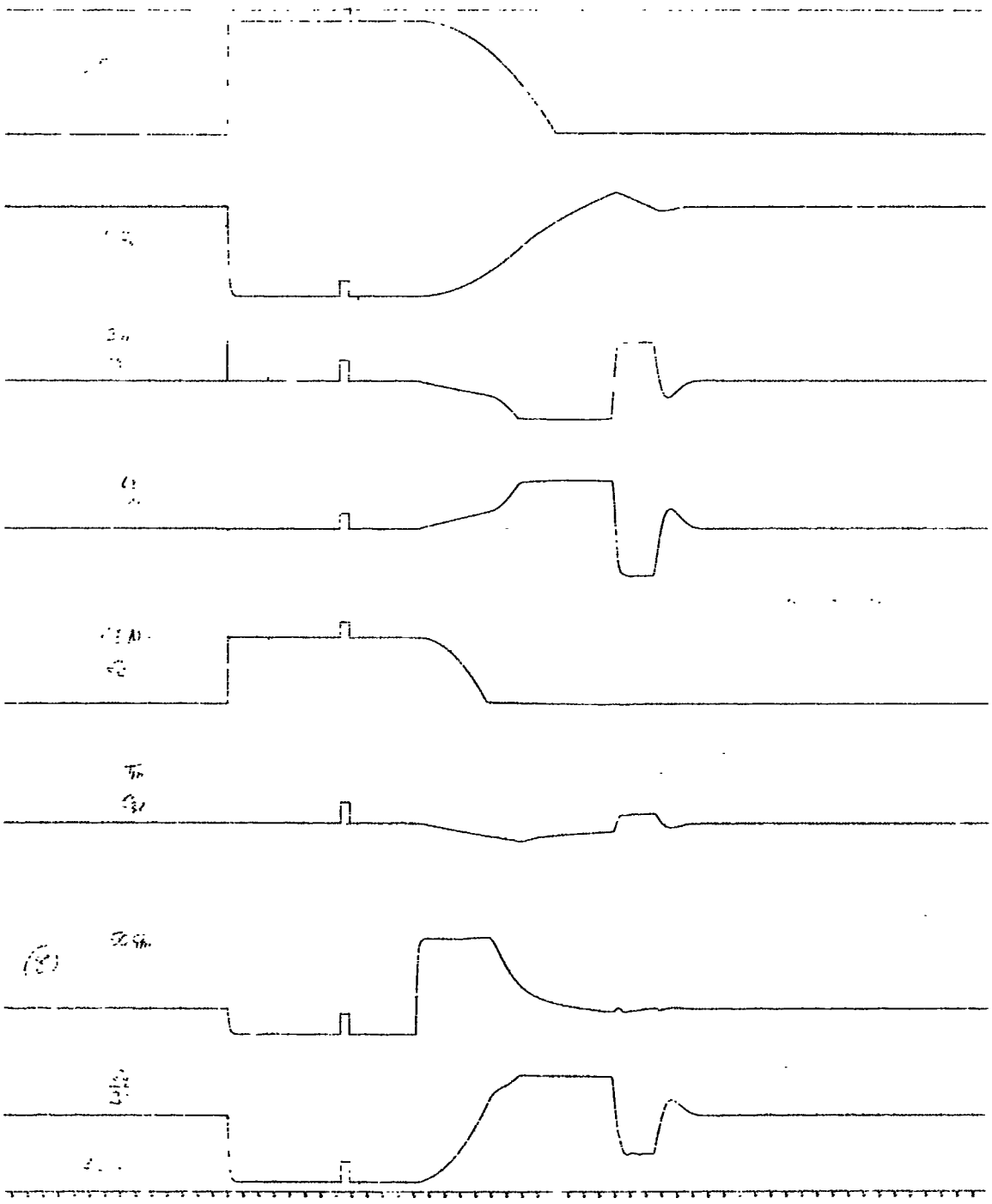

Figure 46

(3) Effect of Step Change in Velocity Command

The ramp input has been studied, and the results indicate that the system will perform satisfactorily for this type of command. The effect of step changes in input command are also of considerable importance. Tests showing these effects are recorded in Figures 47 and 48 where the initial velocity is 1.15 rad/sec and the step change 0.1 rad/sec and 0.15 rad/sec. For these small changes the output has settled to the new level in slightly less than 1 second with approximately a 60% overshoot.

(4) Effects of Disturbance Forces

The disturbance torques subjected to the main arm have been considered in order to determine the effect upon the main arm velocity and thus determine the necessity for feed forward torque compensation.

Computer studies were made of the main arm control system during which time disturbance torques were applied as step functions and sinusoidal functions of different amplitudes. A tabulation of the applied torque and the resultant change in main arm velocity is shown in Figure 49.

By assuming the maximum conditions for each of the variables, we can determine the extreme forces that will be developed working against the main arm. The equation for the disturbance is

$$T_{G\psi} \times 10^{-3} = -32 \ddot{\phi}_R \sin \theta + 331 \ddot{\psi}$$

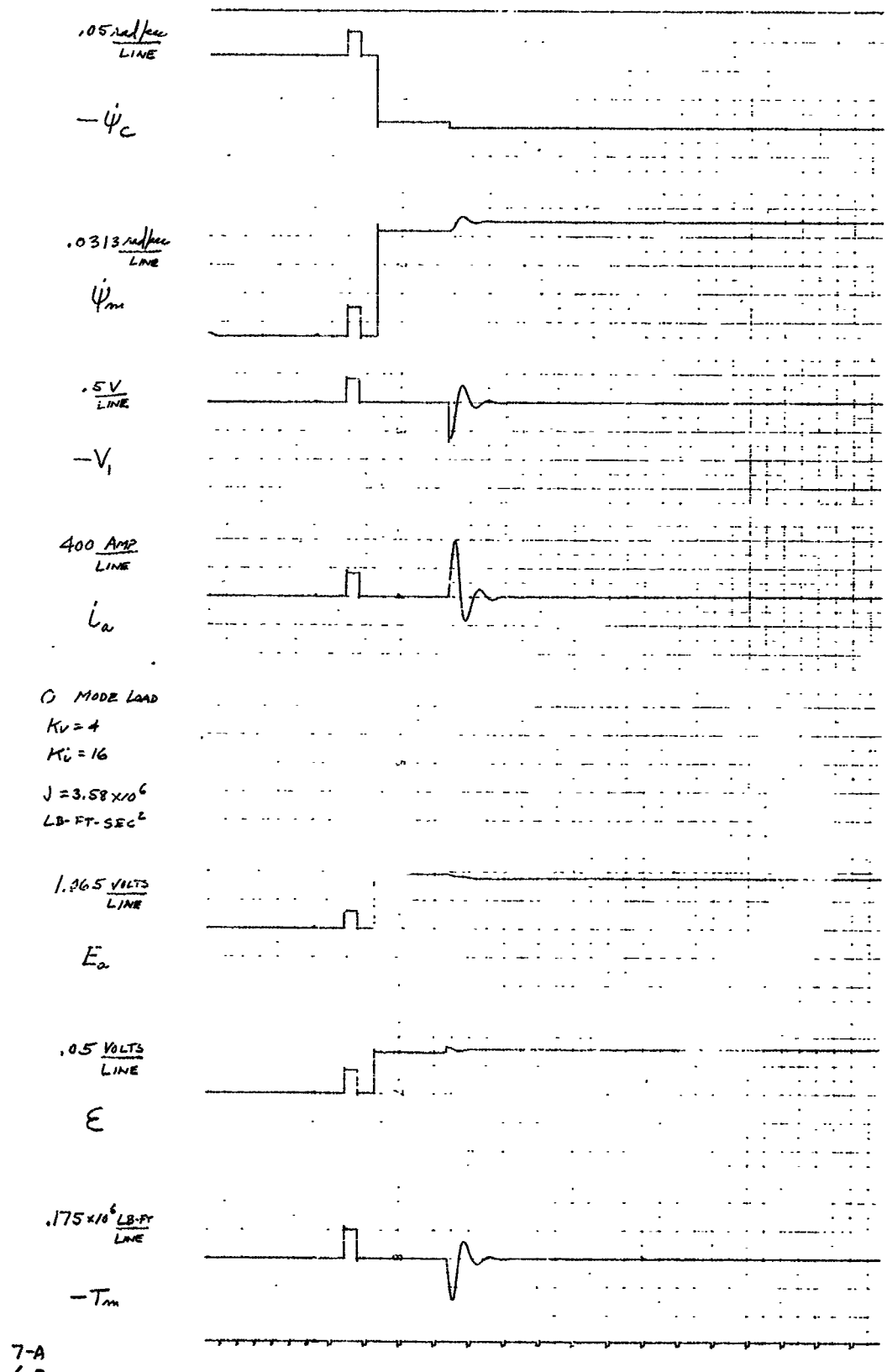
.05 rad/sec LINE
$-\dot{\psi}_c$
.0313 rad/sec LINE
$\dot{\psi}_m$
.5 V LINE
$-V_1$
400 AMP LINE
i_a
0 MODE LOAD
$K_V = 4$
$K_i = 16$
$J = 3.58 \times 10^6$ LB-FT-SEC^2
1.965 VOLTS LINE
E_a
.05 VOLTS LINE
ε
$.175 \times 10^6$ LB-FT LINE
$-T_m$
7-A
6-B

Figure 47

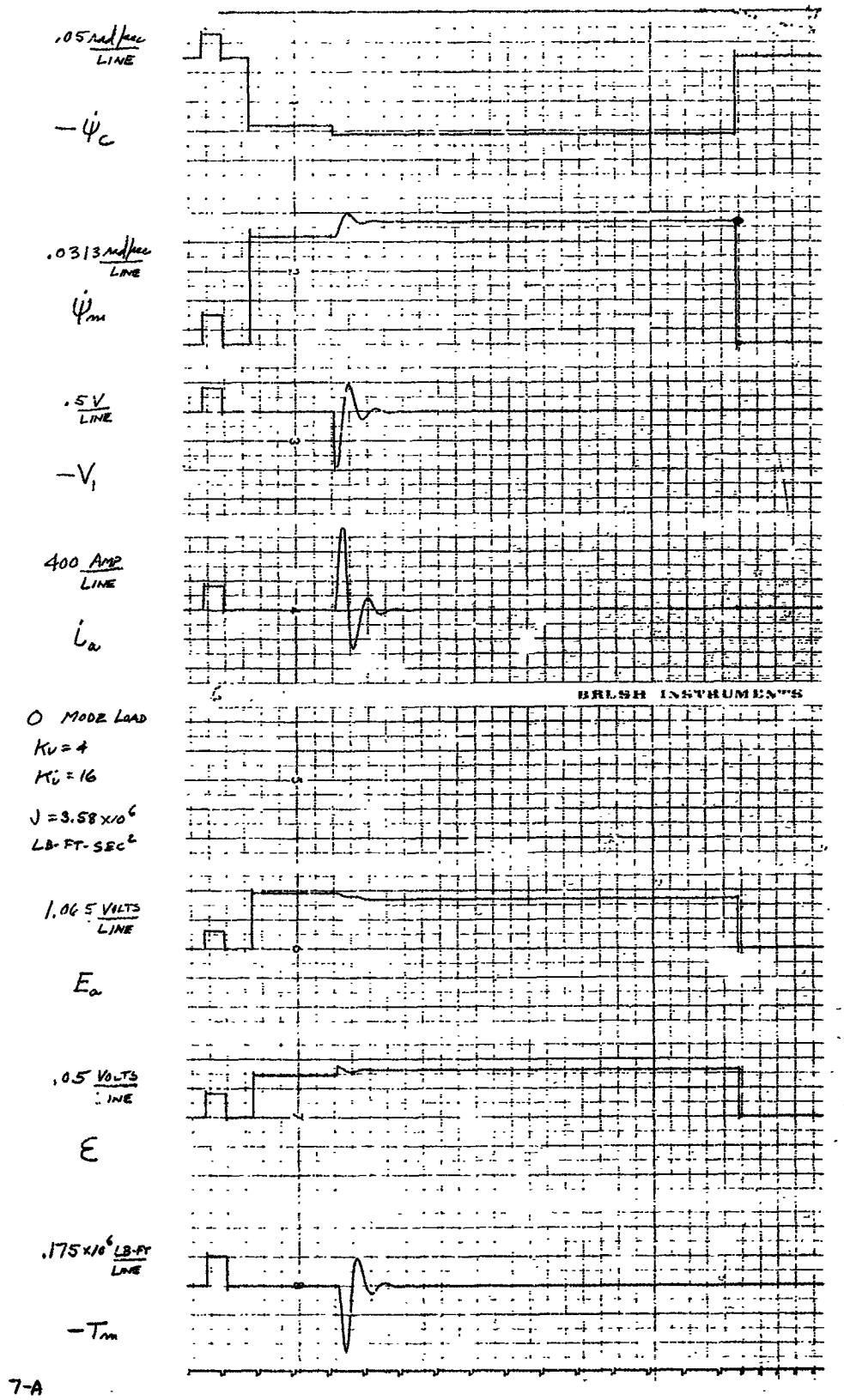
.05 rad/sec LINE
$-\dot{\psi}_c$
.0313 rad/sec LINE
$\dot{\psi}_m$
.5 V LINE
$-V_1$
400 AMP LINE
i_a
BRUSH INSTRUMENTS
0 MODE LOAD
$K_V = 4$
$K_i = 16$
$J = 3.58 \times 10^6$ LB-FT-SEC^2
1.065 VOLTS LINE
E_a
.05 VOLTS LINE
ϵ
$.175 \times 10^6$ LB-FT LINE
$-T_m$
7-A
6-B

Figure 48

RUN No.	$\dot{\psi}_c$	T_D	$\dot{\psi}_m$
17	0 RAD./SEC.	1.12×10^6 LB-FT	.0375 RAD./SEC.
18	0	2.24	.075
19	0	4.48	.1562
20	0	5.6	.2
21	1.15	1.12	.0313
22	1.15	2.24	.0937
23	1.15	4.48	.156
24	1.15	5.6	.313 *
25	3.0	1.12	.075
26	3.0	2.24	.125
27	3.0	4.48	.156 *
28	0	1.12×10^6 LB-FT PEAK	.025 [SIN 2t]
29	0	1.12	.063 [SIN 10t]
30	0	2.24	.138 [SIN 10t]
31	0	2.24	.038 [SIN 2t]
32	0	4.48	.113 [SIN 2t]
33	0	4.48	.225 [SIN 10t]
34	3.0	1.12	.05 [SIN 10t]
35	3.0	1.12	.094 [SIN 2t]
36	3.0	2.24	.219 [SIN 2t]
37	3.0	2.24	.081 [SIN 10t]
38	3.0	4.48	.144 [SIN 10t]
39	3.0	4.48	.78 [SIN 2t]

NOTE:- (*) INDICATES SYSTEM BECAME UNSTABLE.

Figure 49 - Effect of Disturbance Torque on Motor Shaft Speed

$$-13.7\ \ddot{\theta}_R \sin\phi \cos\phi \cos\theta$$
$$-370\ \dot{\psi}\dot{\theta}_R \sin\theta \cos\theta - 32\ \dot{\phi}\dot{\theta} \cos\theta$$
$$+13.7\ \dot{\theta}_R^2 \sin\phi \cos\phi \sin\theta$$
$$-27.4\ \dot{\psi}\dot{\phi}_R \sin\phi \cos\phi \cos^2\theta \qquad (50)$$

Using the maximum values of

$$\dot{\theta}_R = .85 \text{ rad/sec}$$
$$\dot{\phi}_R = 2.0 \text{ rad/sec}$$

$$\ddot{\vartheta}_R = \frac{6.65 \times 10^3 \times 58.5 \text{ lb in}}{13.7 \times 10^3 \text{ lb in sec}^2} = 28.4 \text{ rad/sec}^2$$

$$\ddot{\phi}_R = \frac{15.5 \times 10^3 \times 66 \text{ lb in}}{32 \times 10^3 \text{ lb in sec}^2} = 32 \text{ rad/sec}^2$$
$$\ddot{\psi}_R = .7 \text{ rad/sec}^2$$
$$\ddot{\psi}_R = 4.4 \text{ rad/sec}$$

we obtain a value for $T_{G\psi}$ of

$$T_{G\psi} = -.435 \times 10^6 - 1.02 \times 10^6 \sin\theta - .247 \times 10^6 \cos\theta$$
$$-.1205 \times 10^6 \cos^2\theta \text{ lb in} \qquad (51)$$

Computing this torque for angles of θ varying from 0 to 90 degrees, we obtain values of disturbance torque which are plotted in the curve shown in Figure 50. This indicates that the maximum disturbance torque will be approximately 0.125×10^6 lb-ft. Referring to Figure 49 we find that the change in main arm shaft velocity ($\dot{\psi}_m$) will be less than .01 rad/sec. A change in velocity of .01 rad/sec is equivalent to an acceleration of

$$a = \frac{.01 \times .01 \times 50}{32} = .00016 \text{ g}$$

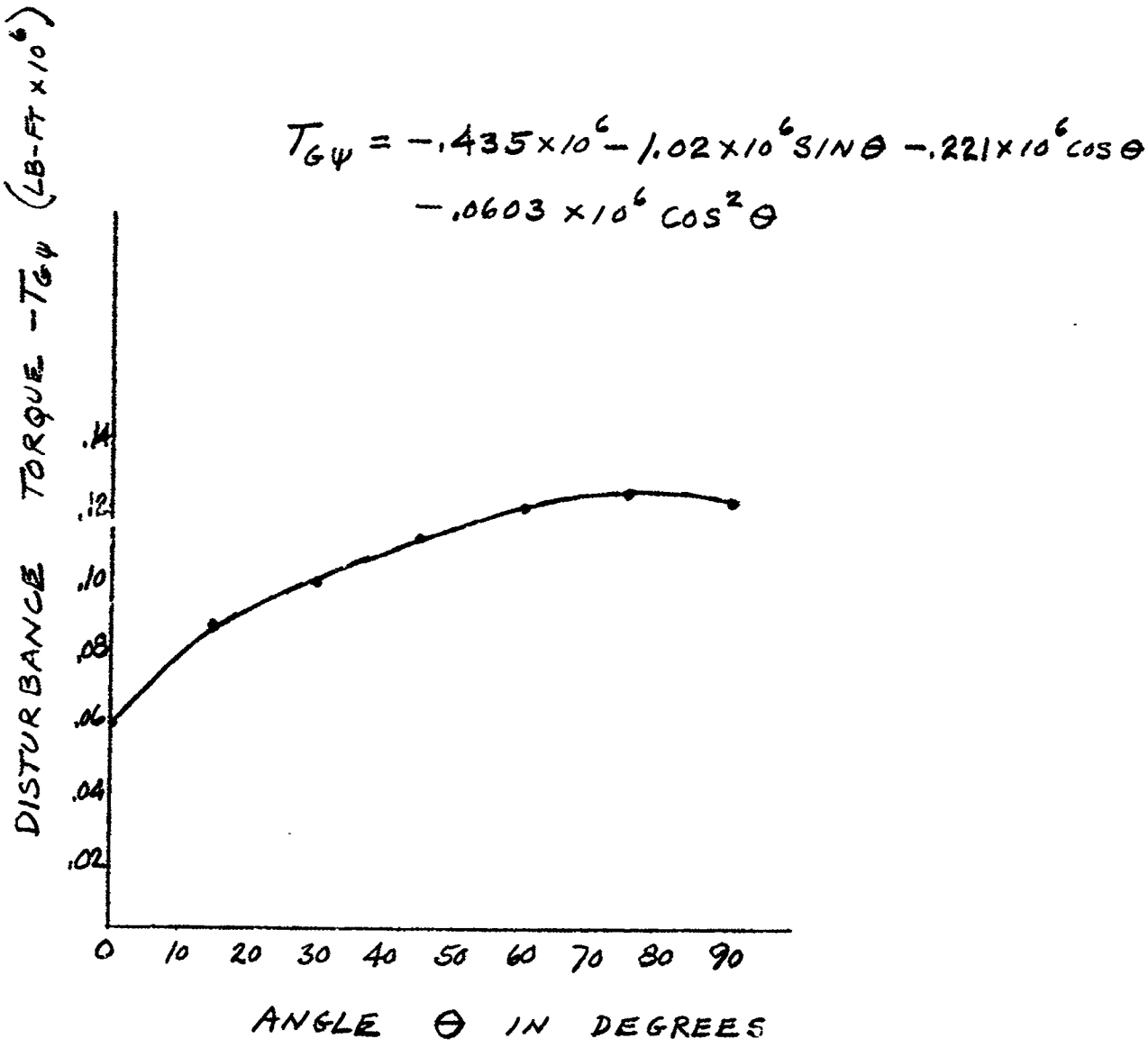
$T_{G\psi} = -.435\times10^6 - 1.02\times10^6 \sin\theta - .221\times10^6 \cos\theta$
$- .0603\times10^6 \cos^2\theta$
DISTURBANCE TORQUE $-T_{G\psi}$ (LB-FT $\times10^6$)
.14
.12
.10
.08
.06
.04
.02
0
10
20
30
40
50
60
70
80
90
ANGLE θ IN DEGREES

Figure 50

These torques will produce very little effect upon the main arm velocity and are therefore not included in the simulation. This also indicates that feed forward compensation is not needed in the main arm drive system.

CONTROL COMPUTER

I. INTRODUCTION

The main control function of the centrifuge is implemented by the control computer, which is so called to be a computing device to compute the proper control signals to the centrifuge control systems.

The objective of the control computer is to coordinate the centrifuge control systems with respect to the design values of the centrifuge acceleration inputs A_x, A_y, A_z. Therefore, it accepts the acceleration inputs as well as the control system instrumentation output signals and continuously solves a set of equations to provide the command signals to the control systems to generate and orientate the output resultant acceleration vector.

II. CONTROL COMPUTER EQUATIONS

The control computer equations are the equations of motion of the three centrifuge axes derived from the physical related configurations of the three axes. The development of the equations is shown as follows:

CENTRIFUGE CONTROL COMPUTER EQUATIONS

Four right-hand cartesian coordinate systems have been used to define the acceleration vectors in respect to the earth, the main arm, the Gimbal Ring and the Gondola respectively. They are

(X, Y, Z) center at main axis, O; fixed to earth
(U, V, W) center at Gondola O', fixed to main arm
(X_{GR}, Y_{GR}, Z_{GR}) center at O', fixed to Gimbal Ring
(X_G, Y_G, Z_G) center at O', fixed to Gondola

With $OO' = R$ = length of the main arm, their relations can be expressed by

$$[\ddot{i}_x, \ddot{i}_y, \ddot{i}_z] = [\dot{i}_u, \dot{i}_v, \dot{i}_w][\psi] \quad (1)$$

$$[\dot{i}_u, \dot{i}_v, \dot{i}_w] = [\dot{i}_{GRX}, \dot{i}_{GRY}, \dot{i}_{GRZ}][\theta] \quad (2)$$

$$[\dot{i}_{GRX}, \dot{i}_{GRY}, \dot{i}_{GRZ}] = [\dot{i}_{GX}, \dot{i}_{GY}, \dot{i}_{GZ}][\varphi] \quad (3)$$

with

$$[\psi] = \begin{bmatrix} \cos\psi & \sin\psi & 0 \\ -\sin\psi & \cos\psi & 0 \\ 0 & 0 & 1 \end{bmatrix} \quad (4)$$

CONTROL COMPUTER EQUATIONS

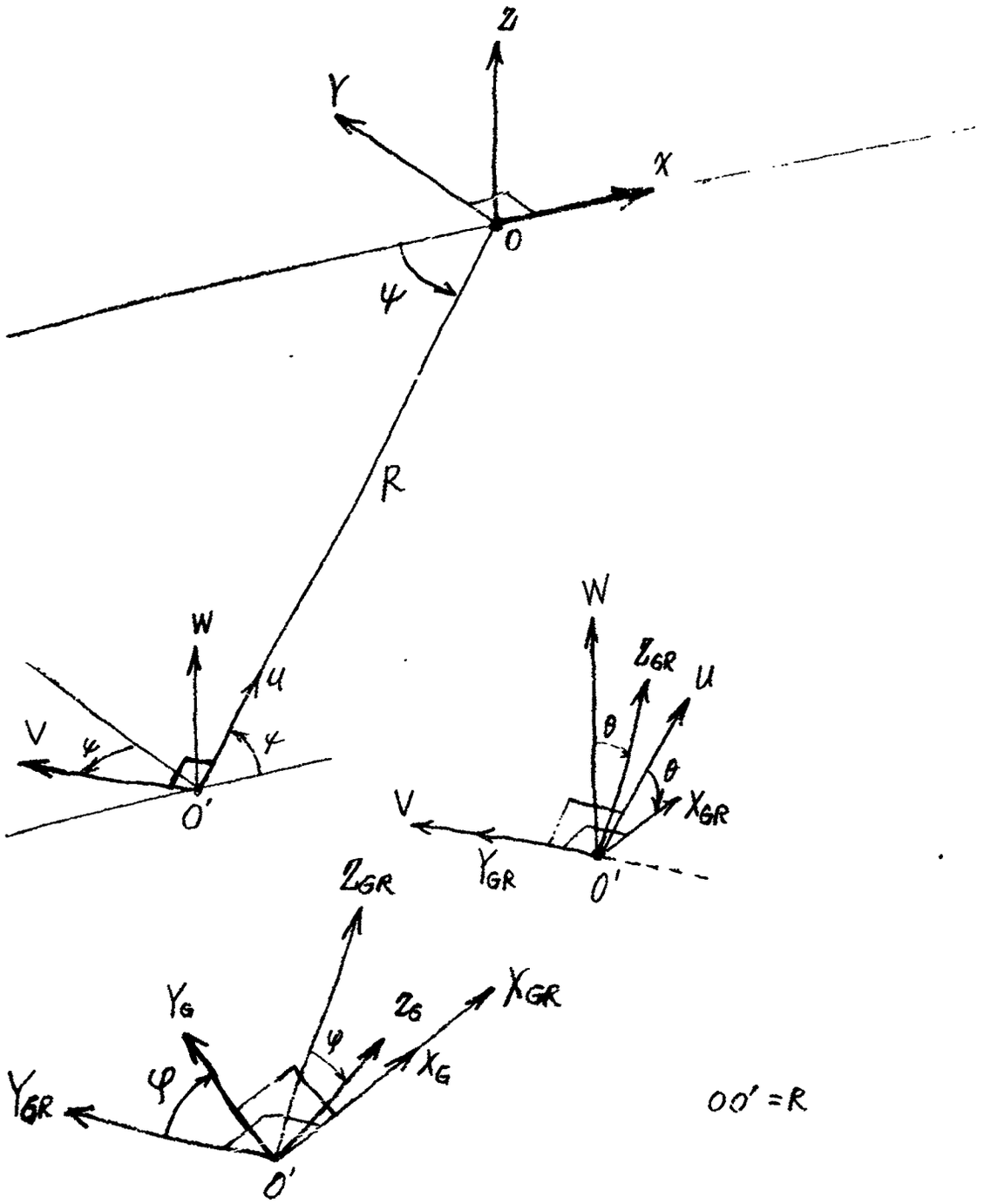

$OO' = R$

CONTROL COMPUTER EQUATIONS

$$[\theta] = \begin{bmatrix} \cos\theta & 0 & -\sin\theta \\ 0 & 1 & 0 \\ \sin\theta & 0 & \cos\theta \end{bmatrix} \tag{5}$$

$$[\varphi] = \begin{bmatrix} 1 & 0 & 0 \\ 0 & \cos\varphi & \sin\varphi \\ 0 & -\sin\varphi & \cos\varphi \end{bmatrix} \tag{6}$$

Initially, when $\psi = \theta = \varphi = 0$,

$$\overset{o}{i}_x = i_u = i_{GRX} = i_{GX}$$
$$\overset{o}{i}_y = i_v = i_{GRY} = i_{GY}$$
$$i_z = i_w = i_{GRZ} = i_{GZ}$$

where i_k is the respective unit vector of coordinate axis k.

CONTROL COMPUTER EQUATIONS

The position of point O' with respect to (X, Y, Z) coordinates is

$$O' = -i_x^o R\cos\psi - i_y^o R\sin\psi \tag{7}$$

The rate of change of O' with respect to time or the velocity of O' is

$$\dot{O}' = +i_x^o R\dot{\psi}\sin\psi - i_y^o R\dot{\psi}\cos\psi \tag{8}$$

The acceleration is

$$\ddot{O}' = i_x^o(R\ddot{\psi}\sin\psi + R\dot{\psi}^2\cos\psi) + i_y^o(R\dot{\psi}^2\sin\psi - R\ddot{\psi}\cos\psi) \tag{9}$$

With the consideration of gravitational acceleration in the i_z^o direction, the acceleration vector A at O' in (x, y, z) coordinates is

$$A = i_x^o(R\ddot{\psi}\sin\psi + R\dot{\psi}^2\cos\psi) + i_y^o(R\dot{\psi}^2\sin\psi - R\ddot{\psi}\cos\psi) + i_z^o g \tag{10}$$

with $g = 32.2\ ^{ft}/_{sec^2}$

Or

$$A = [\hat{i}_x, \hat{i}_y, \hat{i}_z] \begin{bmatrix} R\dot{\psi}^2 \cos\psi + R\ddot{\psi}\sin\psi \\ R\dot{\psi}^2 \sin\psi - R\ddot{\psi}\cos\psi \\ g \end{bmatrix}$$

or

$$A = [\hat{i}_x, \hat{i}_y, \hat{i}_z] \begin{bmatrix} \cos\psi & \sin\psi & 0 \\ \sin\psi & -\cos\psi & 0 \\ 0 & 0 & 1 \end{bmatrix} \begin{bmatrix} R\dot{\psi}^2 \\ R\ddot{\psi} \\ g \end{bmatrix} \qquad (11)$$

Substituting equations (1), (2) and (3) into (11) to get A expressed in Gondola coordinate system (X_G, Y_G, Z_G), we have

$$A = [\hat{i}_{GX}, \hat{i}_{GY}, \hat{i}_{GZ}][\varphi][\theta][\psi] \begin{bmatrix} \cos\psi & \sin\psi & 0 \\ \sin\psi & -\cos\psi & 0 \\ 0 & 0 & 1 \end{bmatrix} \begin{bmatrix} R\dot{\psi}^2 \\ R\ddot{\psi} \\ g \end{bmatrix}$$

$$= [\hat{i}_{GX}, \hat{i}_{GY}, \hat{i}_{GZ}][\varphi][\theta] \begin{bmatrix} 1 & 0 & 0 \\ 0 & -1 & 0 \\ 0 & 0 & 1 \end{bmatrix} \begin{bmatrix} R\dot{\psi}^2 \\ R\ddot{\psi} \\ g \end{bmatrix}$$

CONTROL COMPUTER EQUATIONS

$$A = \left[\ddot{i}_{GX},\ \ddot{i}_{GY},\ \ddot{i}_{GZ} \right] \begin{bmatrix} \cos\theta & 0 & -\sin\theta \\ \sin\theta\sin\varphi & \cos\varphi & \cos\theta\sin\varphi \\ \sin\theta\cos\varphi & -\sin\varphi & \cos\theta\cos\varphi \end{bmatrix} \begin{bmatrix} R\dot{\psi}^2 \\ -R\ddot{\psi} \\ g \end{bmatrix} \qquad (12)$$

Therefore,

$$\begin{cases} A_{GX} = R\dot{\psi}^2\cos\theta - g\sin\theta & (13) \\ A_{GY} = R\dot{\psi}^2\sin\theta\sin\varphi - R\ddot{\psi}\cos\varphi + g\cos\theta\sin\varphi & (14) \\ A_{GZ} = R\dot{\psi}^2\sin\theta\cos\varphi + R\ddot{\psi}\sin\varphi + g\cos\theta\cos\varphi & (15) \end{cases}$$

Solving $\sin\theta$ and $\cos\theta$ from equation (13),

$$(A_{GX} + g\sin\theta)^2 = (R\dot{\psi}^2)^2(1 - \sin^2\theta)$$

$$A_{GX}^2 + g^2\sin^2\theta + 2gA_{GX}\sin\theta + (R\dot{\psi}^2)^2\sin^2\theta - (R\dot{\psi}^2)^2 = 0$$

$$\left[g^2 + (R\dot{\psi}^2)^2\right]\sin^2\theta + 2gA_{GX}\sin\theta + A_{GX}^2 - (R\dot{\psi}^2)^2 = 0$$

$$\therefore \sin\theta = \frac{-2gA_{GX} \pm \sqrt{4g^2A_{GX}^2 - 4\left[g^2A_{GX}^2 + (R\dot{\psi}^2)^2A_{GX}^2 - g^2(R\dot{\psi}^2)^2 - (R\dot{\psi}^2)^4\right]}}{2\left[g^2 + (R\dot{\psi}^2)^2\right]}$$

CONTROL COMPUTER EQUATIONS

$$\sin\theta = \frac{-gA_{GX} \pm (R\dot{\psi}^2)\sqrt{(R\dot{\psi}^2)^2 + g^2 - A_{GX}^2}}{(R\dot{\psi}^2)^2 + g^2} \qquad (16)$$

And from equation (13)

$$R\dot{\psi}^2\cos\theta = A_{GX} + g\sin\theta$$

$$= \frac{(R\dot{\psi}^2)^2 A_{GX} + g^2 A_{GX} - g^2 A_{GX} \pm g(R\dot{\psi}^2)\sqrt{(R\dot{\psi}^2)^2 + g^2 - A_{GX}^2}}{(R\dot{\psi}^2)^2 + g^2}$$

$$\cos\theta = \frac{(R\dot{\psi}^2)A_{GX} \pm g\sqrt{(R\dot{\psi}^2)^2 + g^2 - A_{GX}^2}}{(R\dot{\psi}^2)^2 + g^2} \qquad (17)$$

We may solve for $\sin\varphi$ and $\cos\varphi$ from equations (14) and (15).

$$\begin{cases} A_{GY} = \left[(R\dot{\psi}^2)\sin\theta + g\cos\theta\right]\sin\varphi - (R\ddot{\psi})\cos\varphi \\ A_{GZ} = \left[(R\dot{\psi}^2)\sin\theta + g\cos\theta\right]\cos\varphi + (R\ddot{\psi})\sin\varphi \end{cases}$$

CC EQUATIONS

Let $$a_1 = (R\dot{\psi}^2)\sin\theta + g\cos\theta \tag{18}$$

the equations (14) and (15) become

$$\begin{cases} A_{GY} = a_1 \sin\varphi - (R\ddot{\psi})\cos\varphi & (19) \\ A_{GZ} = (R\ddot{\psi})\sin\varphi + a_1\cos\varphi & (20) \end{cases}$$

Or

$$\begin{cases} a_1 A_{GY} = a_1^2 \sin\varphi - a_1(R\ddot{\psi})\cos\varphi \\ (R\ddot{\psi})A_{GZ} = (R\dot{\psi})^2\sin\varphi + a_1(R\ddot{\psi})\cos\varphi \end{cases}$$

$$\therefore \quad a_1 A_{GY} + (R\ddot{\psi})A_{GZ} = [a_1^2 + (R\dot{\psi})^2]\sin\varphi$$

$$\sin\varphi = \frac{a_1 A_{GY} + (R\ddot{\psi})A_{GZ}}{a_1^2 + (R\dot{\psi})^2} \tag{21}$$

Similarly,

$$\cos\varphi = \frac{a_1 A_{GZ} - (R\ddot{\psi})A_{GY}}{a_1^2 + (R\dot{\psi})^2} \tag{22}$$

Simplifying a_1 in equation (18), we have

CC EQUATIONS

$$a_1 = \frac{-g(R\ddot{\psi}) A_{Gx} \pm (R\dot{\psi}^2)^2 \sqrt{(R\dot{\psi}^2)^2 + g^2 - A_{Gx}^2} + g(R\ddot{\psi}) A_{Gx} \pm g^2 \sqrt{(R\dot{\psi}^2)^2 + g^2 - A_{Gx}^2}}{(R\dot{\psi}^2)^2 + g^2}$$

$$a_1 = \pm \sqrt{(R\dot{\psi}^2)^2 + g^2 - A_{Gx}^2} \qquad (23)$$

$$a_1^2 = (R\dot{\psi}^2)^2 + g^2 - A_{Gx}^2 \qquad (24)$$

$\therefore$

$$\sin\varphi = \frac{(R\ddot{\psi}) A_{Gz} \pm A_{Gy} \sqrt{(R\dot{\psi}^2)^2 + g^2 - A_{Gx}^2}}{(R\dot{\psi}^2)^2 + (R\ddot{\psi})^2 + g^2 - A_{Gx}^2} \qquad (25)$$

$$\cos\varphi = \frac{-(R\ddot{\psi}) A_{Gy} \pm A_{Gz} \sqrt{(R\dot{\psi}^2)^2 + g^2 - A_{Gx}^2}}{(R\dot{\psi}^2)^2 + (R\ddot{\psi})^2 + g^2 - A_{Gx}^2} \qquad (26)$$

CC EQUATIONS

Furthermore, when we multiply equation (19) with $\cos\varphi$ and equation (20) with $\sin\varphi$, we have

$$\begin{cases} A_{GY}\cos\varphi = a_1\sin\varphi\cos\varphi - (R\ddot{\psi})\cos^2\varphi & (27) \\ A_{GZ}\sin\varphi = a_1\sin\varphi\cos\varphi + (R\ddot{\psi})\sin^2\varphi & (28) \end{cases}$$

(28) − (27),

$$\boxed{A_{GZ}\sin\varphi - A_{GY}\cos\varphi = (R\ddot{\psi})} \qquad (29)$$

Substituting equations (25), (26) into (29), we have

$$\frac{A_{GZ}^2(R\ddot{\psi}) + A_{GY}^2(R\ddot{\psi})}{(R\dot{\psi}^2)^2 + (R\ddot{\psi})^2 + g^2 - A_{GX}^2} = R\ddot{\psi}$$

or

$$A_{GX}^2 + A_{GY}^2 + A_{GZ}^2 = (R\dot{\psi}^2)^2 + (R\ddot{\psi})^2 + g^2 \qquad (30)$$

or

$$\boxed{|A| = \sqrt{A_{GX}^2 + A_{GY}^2 + A_{GZ}^2} = \sqrt{(R\dot{\psi}^2)^2 + (R\ddot{\psi})^2 + g^2}} \qquad (31)$$

CONTROL COMPUTER EQUATIONS

More useful equations for the control computer simulation can be obtained from the original equations (13), (14) and (15). From equations (19) and (20), we have

$$A_{GY}\sin\varphi + A_{GZ}\cos\varphi = a_1 \tag{32}$$

Since

$$(R\dot{\psi}^2)\sin\theta + q\cos\theta = a_1 \tag{18}$$

$\therefore$

$$A_{GY}\sin\varphi + A_{GZ}\cos\varphi = (R\dot{\psi}^2)\sin\theta + q\cos\theta = a_1 \tag{33}$$

Differentiating equation (31) with respect to time, we have

$$A_{GX}\dot{A}_{GX} + A_{GY}\dot{A}_{GY} + A_{GZ}\dot{A}_{GZ} = 2R^2\dot{\psi}^3\ddot{\psi} + R^2\dddot{\psi}\ddot{\psi} \tag{34}$$

Differentiating equation (13) with respect to time, we have

$$\dot{A}_{GX} = 2R\dot{\psi}\ddot{\psi}\cos\theta - R\dot{\psi}^2\sin\theta\,\dot{\theta} - q\cos\theta\,\dot{\theta}$$

or

$$\boxed{\dot{\theta} = \frac{2R\dot{\psi}\ddot{\psi}\cos\theta - \dot{A}_{GX}}{(R\dot{\psi}^2)\sin\theta + q\cos\theta}} \tag{35}$$

or

$$\dot{\theta} = \frac{2R\ddot{\psi}\dot{4}\cos\theta - \dot{A}_{GX}}{a_1} \tag{36}$$

Differentiating equation (29) with respect to time, we have

$$\dot{A}_{GZ}\sin\varphi + A_{GZ}\cos\varphi\,\dot{\varphi} - \dot{A}_{GY}\cos\varphi + A_{GY}\sin\varphi\,\dot{\varphi} = R\dddot{\psi}$$

$\therefore$

$$\boxed{\dot{\varphi} = \frac{R\dddot{\psi} + \dot{A}_{GY}\cos\varphi - \dot{A}_{GZ}\sin\varphi}{A_{GY}\sin\varphi + A_{GZ}\cos\varphi}} \tag{37}$$

or

$$\dot{\varphi} = \frac{R\dddot{\psi} - \dot{A}_{GZ}\sin\varphi + \dot{A}_{GY}\cos\varphi}{a_1} \tag{38}$$

III. GENERAL DESCRIPTION

From the control computer equations developed, the assumptions for the design of the control computer were obtained on the basis of the following outlined characteristics of the equations:

(1) The magnitude of the resultant acceleration at the center of the gondola is due only to the angular motion of the main arm and the gravitational acceleration which can be observed by equation (31)

$$\left|A_T\right| = \left|A_R\right| = \sqrt{(R\dot{\psi}_R^2)^2 + (R\ddot{\psi}_R)^2 + g^2}$$

where A_T = simulated total acceleration

R = length of the arm

$\dot{\psi}_R$ = arm angular velocity

$\ddot{\psi}_R$ = arm angular acceleration

g = gravitational acceleration

(2) The major functions of the first and second axes are therefore for the orientation of the resultant acceleration in the proper direction.

(3) The minimum output acceleration is caused by the earth's gravity. Therefore, the total input acceleration, which can be expressed by

$|A|$ = total input acceleration

$$= \sqrt{A_x^2 + A_y^2 + A_z^2} \qquad (39)$$

should be at least 1 g.

(4) From the control computer equations (13), (14) and (15), it is necessary to have, initially

$$A_z = +1$$

$$A_y = A_x = 0$$

at $\theta = \varphi = \psi = 0$ initial condition, if A_{Gz}, A_{Gy}, A_{Gx} are the simulated acceleration components with respect to A_x, A_y, A_z inputs respectively.

(5) The derived equations are very general and capable of giving angular solutions (θ,Φ) covering eight quadrants in three dimensions with respect to the gondola coordinates provided that there are no angular displacement limitations in the two gimbals. This would imply that the control computer is capable of resolving $\pm A_x$, $\pm A_y$, $\pm A_z$ input signals to coordinate the centrifuge control system to provide $\pm A_{Gx}$, $\pm A_{Gy}$, $\pm A_{Gz}$ accordingly if the instrumentation of the centrifuge is capable of doing so.

With reference to these outlined characteristics, we can divide the control computer into three parts for the purpose of simplicity of design study. First, a portion of the control computer circuit will be classified as magnitude controller circuit which will be used to compute simultaneously the control command signal to the main arm control system (3rd axis) so that the motion of the main arm would provide the proper magnitude of the resultant acceleration vector at the center of the gondola. This circuit would include the logics of biasing A_z input to ± 1 g to be used as the forcing function of the control equations.

Second, a computer circuit will be used to solve for the angular solutions of θ and Ψ in sinusoidal functions from the control equations. These solutions are the command inputs to the 1st and 2nd axes control systems to orientate the resultant g vector.

The remaining portion of the control computer circuit will be the circuit to generate the gyroscopic coupling and the velocity coupling compensations for the gimbal axes control systems. These compensating signals may be used by feeding forward to the particular points of interests in the control systems for effective compensations.

IV. CONCEPT OF MAGNITUDE CONTROLLING OF OUTPUT G VECTOR

As was discussed previously, the radial and tangential acceleration components of the simulated resultant g vector are produced by the main arm angular motion. Means for computing the proper velocity command signal to the main arm control system are required. Unfortunately, it is rather difficult to obtain a unique solution for the velocity command $\dot{\psi}_c$ from the nonlinear differential equation

$$|A| = \sqrt{(R\dot{\psi}_c^{\,2})^2 + (R\ddot{\psi}_c)^2 + g^2} \qquad (40)$$

with the correct sign for the rate of change of the angular velocity $\dot{\psi}_c$ simultaneously. Under the circumstances, an alternate method to control the magnitude of the resultant acceleration vector was developed as follows:

The concept of this method utilizes the feedback control theory to control the magnitude of the resultant acceleration vector measured by the main axis instrumentation. The input to this design control loop will be the root-mean-square value of the desirable inputs A_x, A_y, A_z acceleration components. (A_z' is the modified A_z input by ± 1 g which will be discussed in more detail later.) The control parameter will be the computed feedback acceleration A_F which has a steady-state value equal to the output resultant acceleration at constant acceleration g-input. The difference between the input and the feedback accelerations will be the error signal ε_c of this feedback system which will be integrated with a design value of gain G_c to give the main arm velocity input, $\dot{\psi}_c$. The signal $\dot{\psi}_c$ will activate the main arm control system to accelerate the main arm until the main arm velocity and acceleration reach a value such that the magnitude of the feedback acceleration is exactly equal to the desired input acceleration magnitude.

The system equations of this scheme were established as follows:

$$|A_1| = \sqrt{A_x^2 + A_y^2 + A_z'^2} \qquad \text{g's} \qquad (41)$$

$$|A_1| - A_F = \varepsilon_c \qquad \text{g's} \qquad (42)$$

$$\varepsilon_c G_c = \dot{\psi}_c \qquad \text{rad/sec} \qquad (43)$$

$$\dot{\psi}_c G = \dot{\psi}_R \qquad \text{rad/sec} \qquad (44)$$

$$|A_F| = \sqrt{G_R\left(\frac{R}{g}\dot{\psi}_R^2\right)^2 + G_T\left(\frac{R}{g}\ddot{\psi}_R\right)^2 + 1} \qquad \text{g's} \qquad (45)$$

where $|A_I|$ = total desirable input acceleration

$|A_F|$ = magnitude of feedback acceleration

G_c = design system forward gain

G_ψ = main arm control system closed-loop transfer function

G_R = design radial transfer function

G_T = design tangential transfer function

$\dot{\psi}_c$ = computed input

angular velocity of the main arm system

$\dot{\psi}_R$, $\ddot{\psi}_R$ = actual main arm angular velocity and acceleration respectively at the gondola.

The essential design parameters for good system performance are the forward, radial and tangential transfer functions G_c, G_R, G_T respectively. It is expected that (1) the forward gain G_c would directly affect the speed and stability of the system; (2) the radial transfer function G_R would affect the speed and constant g-input steady-state accuracy of the system, and (3) the tangential transfer function G_T would affect the transient or rate of change of "G" performance.

A preliminary analog study on this scheme was made by letting

$$|A_F| = |A_R| = \sqrt{\left(\frac{R}{g}\,\dot{\psi}_R^2\right)^2 + \left(\frac{R}{g}\,\ddot{\psi}_R\right)^2 + 1}$$

where $|A_R|$ = magnitude of the resultant acceleration. This was discussed in the Interim Report I-B2300-1 on pages 63 to 68. The result of this study indicates that the scheme is feasible, and the system is stable for an arbitrary choice of gain constant G_c between .3 and 1.2. However, in the analog study the system

response was not satisfactory with a considerable amount of transient error and several oscillations at the steady-state. Therefore, it was necessary to make a further detailed study on this system.

V. MAGNITUDE CONTROLLER DESIGN STUDY

The design study of the magnitude controller system accomplished for the centrifuge simulation covers a preliminary analog feasibility study in the Advanced-Time-Scale Computer, a preliminary paper analysis on the stability of the system and a detailed analog study to obtain the optimum design values of the system parameters for the final analog computer simulation. Twelve system output responses were recorded with only one system parameter being studied in the preliminary analog study. Tentative stability conditions of the system for the simple case were developed by the phase-plane equation analytical technique. As for the detailed analog study, 116 computer runs were made including the study of system responses at four levels of input signal (6, 10, 15, 30 g's) with 2-6 g's per second ramp rate trapezoidal inputs. It also includes the study of seven design parameters for good system performance. Two particular g-profiles (S-334-10 and the maximum G abort profiles) were simulated as inputs to this system to see the system performance.

In these studies, an approximate main arm control system transfer function was used in order to simplify the manipulation of the problem. This approximate transfer function was used only

for the purpose of studying the nonlinear magnitude controller system performance alone, and it was not used in the final computer simulation. The approximation was made from the linear system block diagram shown in the Rucker Report No. 412, p. 20. System dynamics with natural frequencies higher than 20 radians per second were neglected on the basis of an average system rise time of 0.5 second corresponding to an approximate system resonance frequency of 2 radians per second. The approximate transfer function was calculated to be

$$\frac{\dot{\psi}_R}{\dot{\psi}_c} = \frac{1 + .37s}{1 + 2.6k_2 s + \frac{.26}{k_1} s^2} \text{ (approximately)} \qquad (46)$$

with $k_1 = 2.94$ $k_2 = .140$ for full motor flux

$k_1 = 1.85$ $k_2 = .160$ for half motor flux

$k_1 = 2.94$ $k_2 = .180$ for 1/4 motor flux

The result of the approximation compared quite well to the main arm system responses recorded in the Rucker Report (No. 412, p 33). Details of the approximation procedures were discussed in the Interim Report (I-B2300-1) and will not be repeated here.

To show the magnitude controller system parameters under study, a block diagram was drawn as shown in Figure 51. The corresponding computer circuit was shown in Figure 52. The preliminary system parameters were expressed as follows:

$$G_c = \frac{k_c(1 + T_1 s)}{s(1 + T_2 s)} \qquad (47)$$

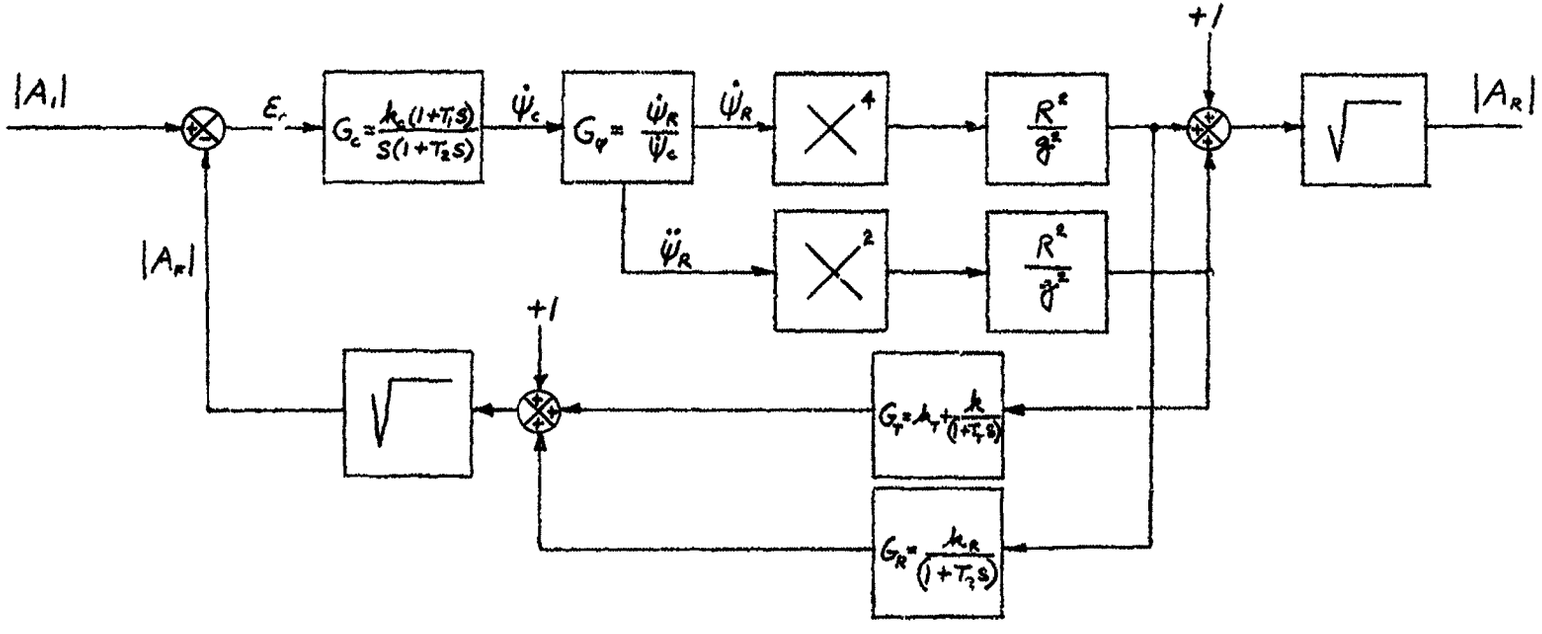

Figure 51 - Control Computer - Magnitude Controller Block Diagram

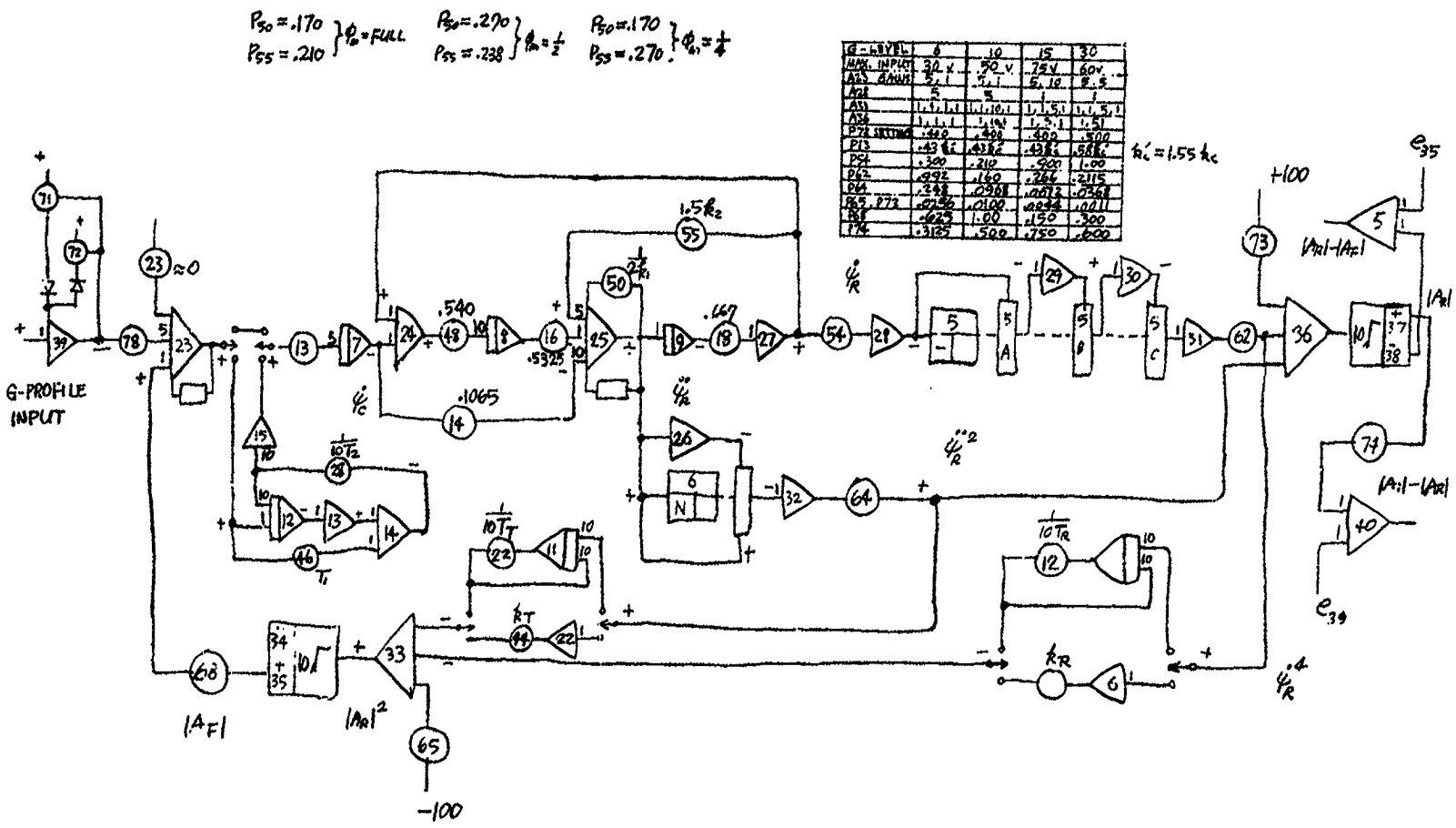

Figure 52 - Analog Circuit for the Study of Magnitude Controller System

$$G_R = \frac{k_R}{1 + T_R s} \tag{48}$$

$$G_T = \frac{k_T}{1 + T_T s} \tag{48}$$

where k_c, k_R, k_T are gain constants of the respective transfer function G_c, G_R, G_T and T_1, T_2, T_R, T_T are the respective time constants.

In the preliminary analog study and paper analysis, the problem was simplified by letting

$$T_1 = T_2 = T_R = T_T = 0,$$

and $k_R = k_T = 1$.

The variable parameter was k_c in determining the stability conditions. It was found that the system was stable for a particular input of 10 g trapezoidal profile at 2 g's per second ramp when k_c was set at 0.8. The system was marginally stable (undamped oscillation in the steady-state) at the condition of half motor flux simulation of the main arm control system.

In order to improve the system's response, a detailed study was made considering the effectiveness of each design parameter. The PACE analog computer was used in this study. In the state of determining the values of the parameters, the reference input used was a trapezoidal signal with different ramp rates as a comparison basis. A brief discussion on the effect of each parameter is summarized as follows:

(1) Effect of k_c (Runs 48, 49, 50)

The values of k_c are of primary importance in determining the stability as well as the performance of the system. With k_c alone, the system may reach the boundary stable condition with k_c higher than 0.8 for a 10 g trapezoidal input of 2 g's per second rate. In general the higher values of k_c will reduce the system's response time but at the same time will introduce a few oscillations in the steady-state if k_c is too large. This is shown in the computer recording Run 50, Channel No. 3 which is the recording of the total resultant acceleration response $|A_R|$. When k_c is small with respect to certain values which are dependent on other system parameters, the system's response is comparatively poor, and there will be no overshoot in the steady-state as shown in Run 49. Run 48 is the compromise of Runs 49 and 50. Four values of k_c[1] were found for four categories of input g-levels as shown in the following table:

Max. g-Level	6	10	15	30
$k_c \left(\frac{\text{rad/sec}}{g}\right)$	.600	.516	.580	.323

(2) Effect of k_T (Runs 70,71, 72)

When the value of k_c is high enough, in the order of k_c = .600, thus making the system dynamics closer to the instability region, the effect of the tangential transfer function gain constant k_T will show distinctly on the system's response.

(1) These values of k_c are optimized in accordance with other system parameters k_T and T_T

For a constant value of k_c equal to .600 and T_T equal to .333, the computer recording Runs 70, 71, 72 shows the effective change of the system's responses for three values of k_T. From these computer runs, we may conclude that the peak value of the tangential acceleration component $R\ddot{\psi}_R$ (shown in Channel 6) decreases as k_T increases from .01 to .20. The $|A_R|$ responses shown in Channel 3 become poorer as k_T increases. It should be stated that the effectiveness of k_T will be insignificant when k_c is small. The suitable values of k_T for four levels of inputs were found as follows:

Input g-Level	6	10	15	30
k_T	.0403	.100	.045	.100

(3) Effect of T_T (Runs 48, 51 and 55, 56)

Similar to k_T, the effectiveness of the time constant T_T is also dependent on the value of k_c. To be more precise, k_T and T_T both affect the response of the tangential acceleration component $R\ddot{\psi}_R$. The combination of these in the latest design of the tangential transfer function G_T has the form

$$G_T = \frac{(k_T+k)\left(1 + \frac{k_T T_T}{k_T+k}\, s\right)}{1 + T_T\, s} \qquad (50)$$

where $k = 1$.

Nevertheless, Runs 48 and 51 were recorded at the condition of full main arm motor flux with

$$k_c = .516$$

$$k_T = .100$$

$$T_T = 2.0 \text{ (Run 48)}$$

$$= 0 \text{ (Run 51)}$$

Therefore,

$$G_T = \frac{1.1\ (1 + .182s)}{1 + 2\ s} \text{ (Run 48)}$$

$$G_T = 1.1 \text{ (Run 51)}$$

Comparing these two runs, we found that when T_T was bigger, the $\ddot{\psi}_R$ peak value was smaller and the $|A_R|$ response was better (lower overshoot and smoother error signal).

For the case of one half main arm motor flux with the same value of k_c except

$$k_T = .05$$

$$T_T = 2.0 \text{ (Run 55)}$$

$$= 10.0 \text{ (Run 56)}$$

or

$$G_T = \frac{1.05\ (1 + .095\ s)}{1 + 2s} \text{ (Run 55)}$$

$$G_T = \frac{1.05\ (1 + .476\ s)}{1 + 10s} \text{ (Run 56)}$$

Comparing Runs 55 to 56, it shows that when T_T is bigger, the $\ddot{\psi}_R$ peak value is bigger and the $|A_R|$ response is poorer which is

exactly opposite to the statement made above. One thing in common for these two cases is that the $|A_R|$ response will be better if the $\ddot{\psi}_R$ peak value is comparitively smaller. Therefore, we conclude that there is a certain range of values of T_T between 0 and 10 that will give a good system performance. The values of T_T were thus found for four levels of input as follows:

Input g-Level	6	10	15	30
T_T (sec)	.100	.00	2.00	2.00
k	.403	.00	.450	1.00

(4) Effects of T_1 and T_2

The original idea of designing T_1 and T_2 in the G_c circuit was to trim the open-loop system response whenever necessary. With T_2 alone ($T_1 = 0$), the system open-loop transfer function would simply be an introduction of one additional time lag. It was found that the system was unstable without compensation when T_2 was equal to 50 milliseconds with

$$k_c = .774 \text{ rad/sec}^2 \text{ per g}$$
$$k_T = 1.0$$
$$T_T = 0$$

With a lower value of k_c, say .387, the system is stable with an even longer delay of 100 milliseconds.

With both T_1 and T_2 in the circuit, several combinations of k_c, T_1, T_2 were tried as follows:

$k_c \left(\frac{rad/sec^2}{s}\right)$	.774	.387	.0645	.0645	.0645	.0645
T_1 (sec)	.50	.50	.50	.10	.80	.80
T_2 (sec)	2.0	2.0	2.0	.50	2.0	.50
$\|A_R\|$ response	over-shoots & unsmooth	2 g's overshoot	1 g over-shoot& poor resp. time	poor resp. time	19 over-shoots & poor resp. time	poor resp. time

The results showed that the output responses of $|A_R|$ were poor with high overshoots in some cases. Therefore, it was decided that T_1, T_2 would not be used as the system parameters in the final simulation.

(5) Effect of T_R (Run 34)

An attempt was made to speed up the $|A_R|$ response by delaying the feedback radial acceleration component $R\dot{\psi}_R^2$. With the system's forward gain, k_c, set effectively at .387, the radial feedback delay time constant T_R was arbitrarily set to be 1.0 second. The system's response was recorded as shown in Run 34. Note that the upper slope of the $|A_R|$ response in Channel 3 is leading the input signal in Channel 1. This phenomenon can also be seen in the first portion of the $|A_1| - |A_R|$ response recorded in Channel 2 which shows a negative signal in the respective time region. This proves the fact that the radial acceleration component dominates the higher level of the resultant acceleration in general cases. The tangential acceleration dominates the lower level of the resultant acceleration. The area in need of improvement is found to be the lower level of the $|A_R|$ response. Since this is taken care of by the design of k_T and T_T, the use of the parameter T_R

would not be necessary and, therefore, it would not be considered in the final simulation.

(6) Effect of k_R

If we choose the gain constant k_R of the radial transfer function G_R to be a value smaller than one, the angular velocity of the main arm $\dot{\psi}_R$ will be higher than it should be for k_R equals one and vice versa. This was examined for two different values of k_c of .774 and .387 and two different values of k_R of .8 and 1.5 at k_T equals 1.0, and the system was stable at each condition. At the present time, these tests are of no significant value for normal performance of the centrifuge. It may be advantageous in the future to do so for the unusual cases particularly for the high g-profile simulation where the main arm system may be driven beyond its capability thus producing undesirable overshoots in the resultant acceleration response. Therefore, it may be necessary to use a k_R value higher than one for the purpose of shaping the resultant acceleration response.

(7) Effect of the Change of Main Arm Motor Field Flux, ϕ_m

Three sets of numbers for the coefficients of the linearized approximation of the main arm system were used in this study to represent three cases of the motor field flux level. The design of the system parameters discussed so far was optimized to cover all these cases as completely as possible. However, there are still some differences between a linearized approximation and the real system with nonlinearities. Therefore, it may be necessary to readjust the values of k_c, k_T and T_T in the operation of the

centrifuge when this control computer scheme is being used. Among the three levels of motor flux simulated in the approximations, the case of half motor flux which corresponds to the main arm system step response at the condition of longer response time with a 25% overshoot was the most difficult one to design for the values of the magnitude controller system parameters. This half motor flux condition is expected to occur for inputs lower than 10 g's. An alternate combination of k_c, k_T and T_T was also found satisfactory, particularly for this case with 10 g's input. These values are

$$k_c = .580 \frac{\text{rad/sec}^2}{g}$$

$$k_T = .05$$

$$T_T = .50 \text{ sec}$$

$$T_1 = T_2 = T_R = 0$$

(8) Effects of Input On-Set Rate (g's/sec) and Input g-Level

The system's performance will be affected by the input on-set rate and the input signal amplitude, since the system components are nonlinear. For a constant input amplitude with constant values of k_c, k_T, T_T, it was found that the higher the rate of change of input, the poorer the system response will be. When the input rate is too high, oscillations may occur in the steady-state response of $|A_R|$. Similar results were observed when the input amplitude increased with constant rate of on-set. The change of system response at high rate of change of input and at high input amplitude is very

similar to an increase in k_c. In order to give better system performances it is apparent that we should limit the region of optimization of the design parameters to a smaller area. Therefore, four sets of system parameters (k_c, k_T, k, T_T) were designed for good system performances at 6, 10, 15 and 30 g's input amplitudes. They proved to be satisfactory for 6 and 15 g inputs respectively.

Input g-Level	6	10	15	30
$k_c \left(\frac{rad/sec^2}{g}\right)$	.600	.516	.580	.323
k_T	.0403	.100	.045	.100
k	.0403	1.00	.450	1.00
T_T (sec)	.100	2.00	2.00	2.00

The values of T_1, T_2 and T_R were studied and found to be insignificant in the equations and therefore considered as zero and the value of k_R as one. This is discussed thoroughly from page 55 to page 66. Each set of parameters was optimized to cover different input rates of on-set from 0 to 6 g's/sec for the particular range of input amplitudes. The definitions of good system performances in these optimizations are that (1) the rate of change of $|A_R|$ with respect to time should follow very closely to the on-set rate of the input signal $|A_1|$, (2) the magnitude of the overshoot in the $|A_R|$ response should be within $\pm$ 5% of the input, and the number of overshoots should be as small as possible with one tenth of a g steady-state error or less.

In the final computer simulation of the centrifuge, only two sets of system parameters were used to cover the 10 g's and 30 g's input ranges. They also worked out satisfactorily for 6 and 15 g inputs respectively. A limiter was required to limit the system error signal, ε_c, for high g inputs. This is to prevent a long time saturation of the main arm system which would cause the magnitude controller system to become unstable. The typical value of the error limit is $\pm$ 2.5 g's which may be adjusted for unusual cases with high rate of on-set and high input g amplitude. The psychological profile (S-334-10) and the maximum g abort profile were used to check the system's performance, and they were found later to be in good correlation with the results of the final simulations.

VI. OUTPUT G VECTOR ALIGNMENT

When the magnitude of the output resultant acceleration is generated by the main arm motion, the next immediate requirement is to align the gimbal and gondola axes properly so that the resultant acceleration components with respect to the gondola coordinates will be in correspondence with the A_x, A_y, A_z inputs simultaneously. The command signals to the 1st and 2nd axes control system are sinusoidal functions of the 1st and 2nd axes angular positions θ, Φ. These command signals can be computed directly from the derived control computer equations (16), (17), (25) and (26) with the substitutions of A_{Gx} by A_x, A_{Gy} by A_v and A_{Gz} by A_z.

In the preliminary simulation of the control computer, the output main arm angular velocity $\dot{\psi}_R$ and angular acceleration $\ddot{\psi}_R$ were used in these equations to compute these command signals (sin θ_c, cos θ_c) (sin Φ_c, cos Φ_c). The objective is to align the gimbals once the main arm is in motion which is indicated by the main arm sensors' signals $\dot{\psi}_R$ and $\ddot{\psi}_R$. Later it was found that it was impossible to compute these signals under these conditions. This is due to the main arm motion always lagging behind the desired input by a small period of time thus producing an output resultant acceleration lagging behind the desired input acceleration. This would develop a resultant acceleration smaller than the input acceleration for any positive rate of increase of input. Under such circumstance, equation (25) or (26) will have a numerator bigger than the denominator which implies a sine or cosine function with a value bigger than one. Another indeterminate condition also occurs in

these alignment equations when their solution becomes an imaginary number for the case of A_x input only.

To overcome these problems, modified assumptions were made for applying these alignment equations. The changes are as follows:

(1) All the variables in these equations will be the desirable input values except for the main arm acceleration, $\dot{\psi}$, which will be the computed main arm acceleration, $\dot{\psi}_c$.

(2) The desirable main arm velocity, $\dot{\psi}$, will be computed approximately by the following equation:

$$R\dot{\psi}_1^2 = \sqrt{|A_1|^2 - g^2 - (R\ddot{\psi}_c)^2} \tag{51}$$

where R = length of main arm

A_1 = root-mean-square of A_x, A_y, A_z' summation

g = earth's gravity

$\ddot{\psi}_c$ = computed main arm angular acceleration

The alignment equations were refined as follows:

$$\sin \theta_c = \frac{1.55\ \dot{\psi}_1^2\ a_1 - A_x}{|A_1|^2 - 2.41\ \ddot{\psi}_c^2} \tag{52}$$

$$\cos \theta_c = \frac{1.55\ \dot{\psi}_1^2\ A_z + a_1}{|A_1|^2 - 2.41\ \ddot{\psi}_c^2} \tag{53}$$

$$\sin \varphi_c = \frac{1.55\ \ddot{\psi}_c\ A_z' + a_1 A_y}{|A_1|^2 - A_x^2} \tag{54}$$

$$\cos \Phi_c = \frac{a_1 A_z' - 1.55 \dot{\Psi}_c A_y}{|A_1|^2 - A_x^2} \tag{55}$$

where $a_1 = \sqrt{|A_1|^2 - 2.41 \dot{\Psi}_c^2 - A_x^2}$ in g's (56)

with A_1, A_x, A_y, A_z in g's, $\dot{\Psi}_1$ in rad/sec and $\dot{\Psi}_c$ in rad/sec^2. The results of the final centrifuge simulation showed that the above alignment equations worked satisfactorily.

VII. FEED FORWARD COMPENSATION TORQUES AND THE CONTROL COMPUTER BLOCK DIAGRAMS

The third part of the control computer is the circuit to develop the feed forward gyroscopic compensation torques and the mechanical coupling compensation. The complete gyroscopic torque equations were developed as shown on page 76. From the conclusion of the final centrifuge simulation, the gyroscopic torque exerted on the 1st axis is expected to be the most serious one. The 2nd and 3rd axes gyroscopic torque disturbances are not serious and therefore do not require compensation. The feed forward compensation signal will be for only the 1st axis control system. The programming of this compensation torque will be in reference to the following approximated equation:

$$10^{-3}\, T_{G\theta}' = 2.79\, \dot{\psi}_R^2 \sin\theta_R \cos\theta_R + .2765\, \dot{\varphi}_R \dot{\psi}_R \cos\theta_R + .415\, \dot{\varphi}_R \dot{\psi}_R \cos\theta_R \sin^2\varphi_R \text{ (lb-in)} \qquad (57)$$

where $T_{G\theta}'$ = approximate reflected gyroscopic torque at the 1st axis

θ_R, φ_R = angular positions of the 1st and 2nd axes

$\dot{\varphi}_R$ = angular velocity of the 2nd axis

The necessary compensation for the 2nd axis due to the mechanical coupling between the 1st and 2nd axes is a velocity signal proportional to the 1st axis velocity. This was discussed previously in this report and was determined to be

$$\dot{\varphi}_{cc} = \frac{11.39}{n}\, \dot{\theta}_R \qquad (58)$$

where $\dot{\Phi}_{cc}$ = computed 2nd axis compensated velocity

n_{Φ} = output gear ratio of the 2nd axis system

$\dot{\theta}_R$ = angular velocity of the 1st axis

It was found from the final centrifuge simulation that the compensation for the 1st axis gyroscopic disturbance was not successful because of the limitations of the control system components. The compensation for the mechanical coupling is satisfactory.

A complete drawing of the control computer in block diagram representation is shown in Figures 53, 54 and 55. These figures were drawn in flow diagram form for simplicity with alphabetical representation of the functions to be computed. Figure 53 is part 1 of the control computer including the computations of the 1st, 2nd and 3rd axes control system commands with respect to the control computer inputs A_x, A_y, A_z. Figure 54 is part 2 of the control computer for the computation of 1st axis feed forward gyroscopic compensation. Figure 55 is part 3 of the control computer for the computation of 2nd axis mechanical coupling compensation.

As an example, the flow diagram representation in the computation of $|A_F|$ can be expressed by the following equation

$$|A_F| = \sqrt{A_R^2 + .1\ A_T^2 + T + 1} \qquad (59)$$

We can compute A_R^2, A_T^2 and T separately as follows:

$$A_R^2 = 2.411\ \dot{\psi}_R^4$$

$$A_T^2 = 2.411\ \dot{\psi}_R^2$$

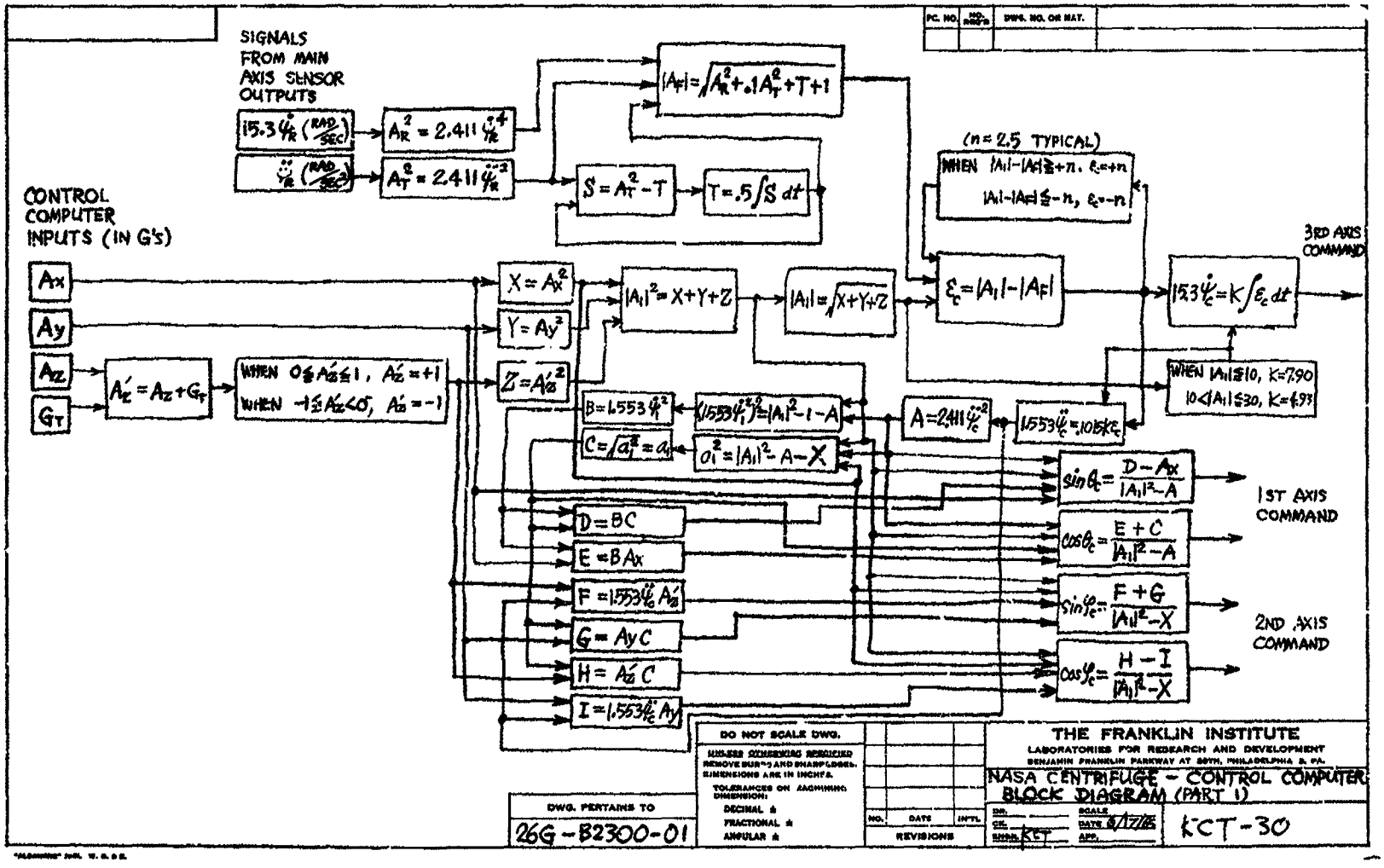

Figure 53 - NASA Centrifuge - Control Computer Block Diagram (Part 1)

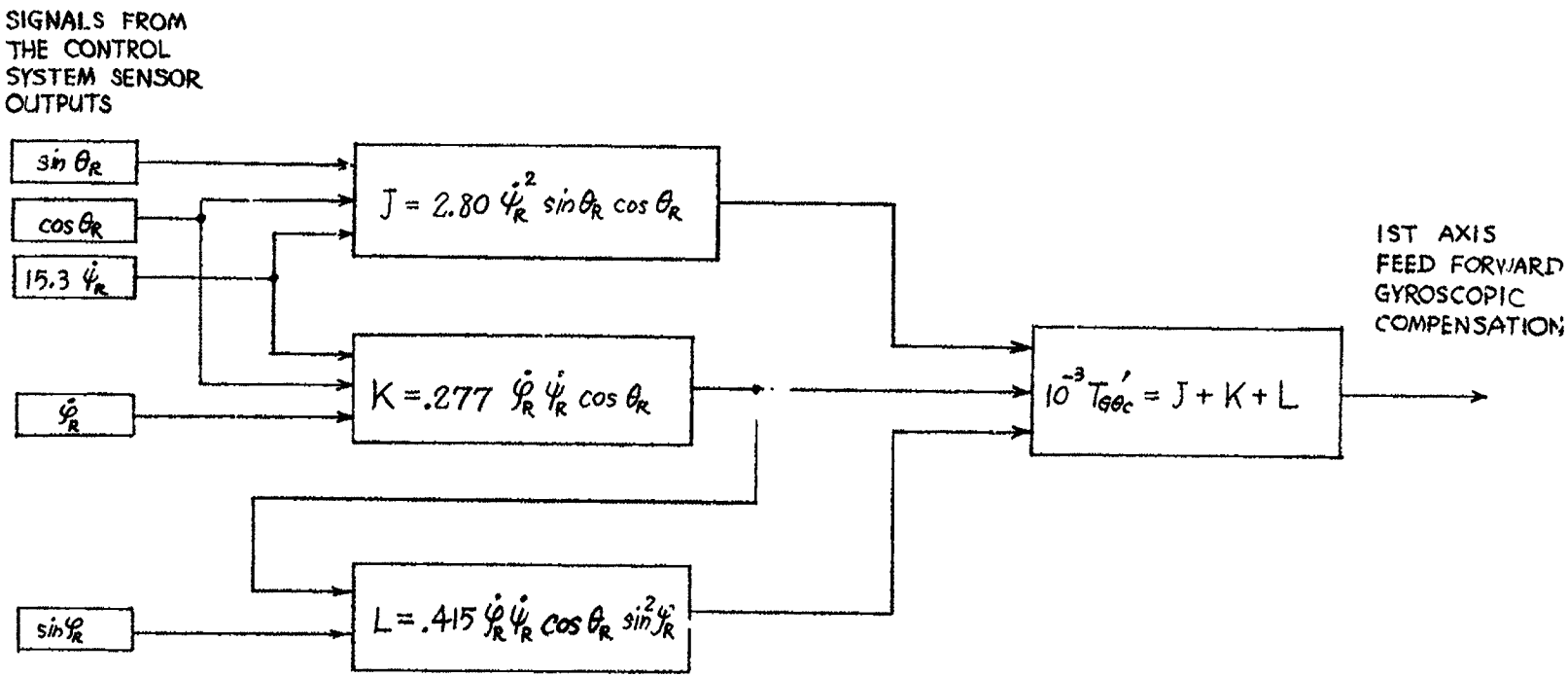

Figure 54 - NASA Centrifuge - Control Computer Block Diagram (Part 2)

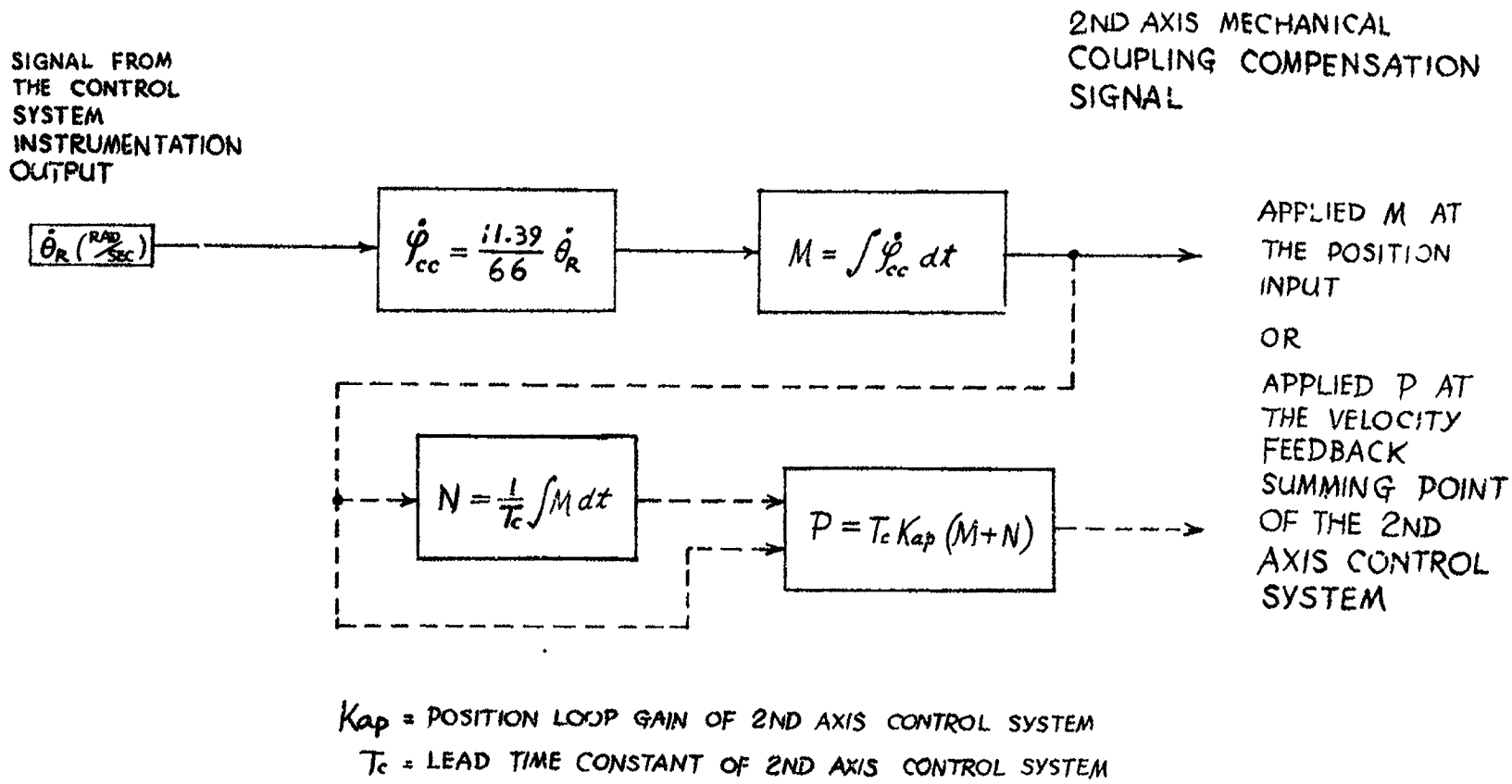

Figure 55 - NASA Centrifuge - Control Computer Block Diagram (Part 3)

$$T = .5 \int (A_T^2 - T)\, dt,$$

G. Profile Converter

The g versus time profiles were submitted in the form of graphs with the exception of 2 profiles that were recorded on a magnetic tape. A total of 33 profiles had to be recorded in the form of an electrical signal as converted from the g profile graphs. To convert the profile graphs into volts proportional to g level, an X-Y plotting table was converted into a photoformer type of device from which the Y axis feedback potentiometer would produce a voltage proportional to g level and the x axis would be driven at a speed proportional to time. The circuit to accomplish this is shown in Figure 56. The photoresistor is electrically connected in a bridge circuit and physically mounted to the pen holder on the Y axis system.

A small light is mounted next to the photoresistors in order to keep the light intensity constant throughout the traverse of the graph. The input to the X axis is a triangular waveform thus providing a constant sweep rate in the X direction. The output signal

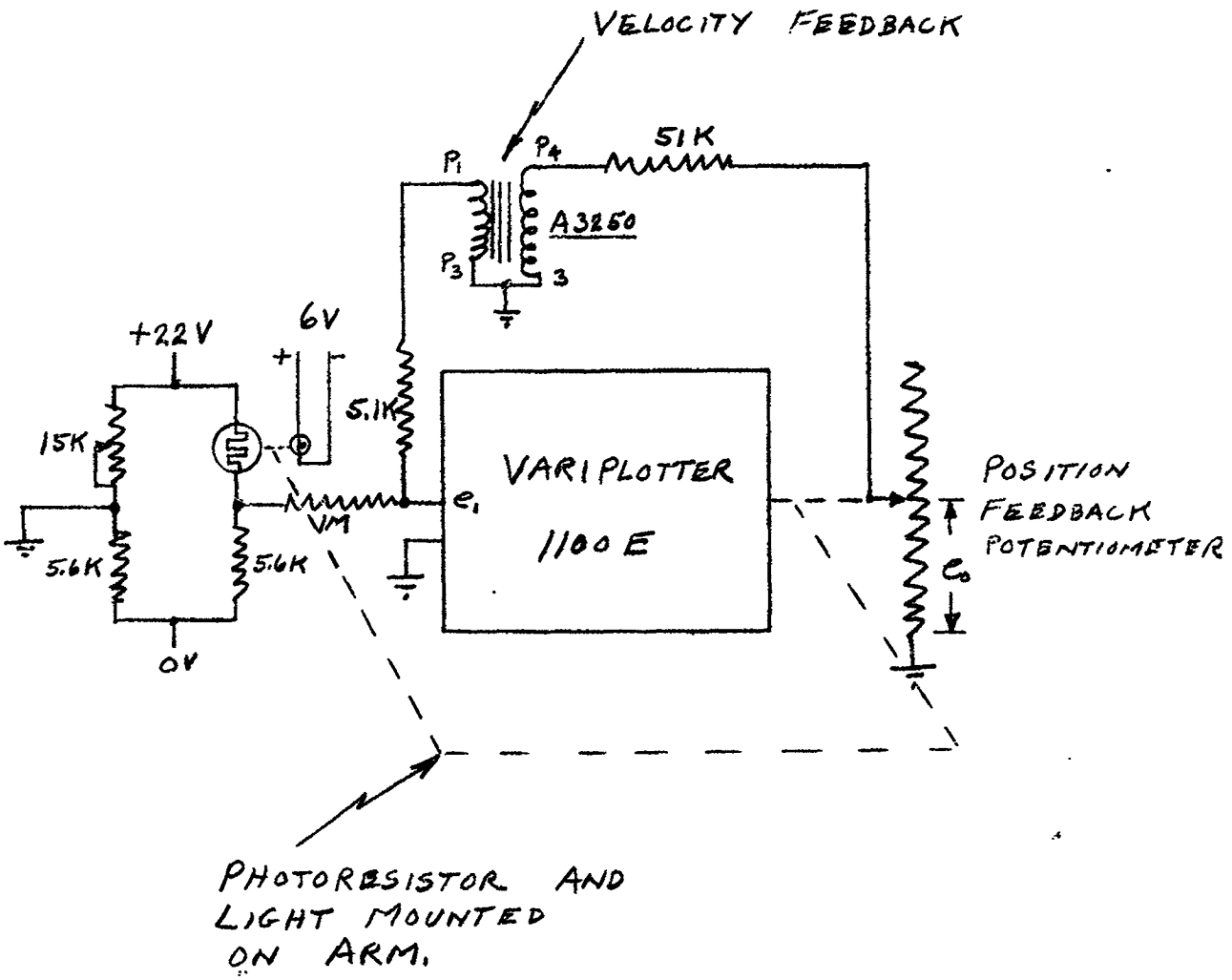

NOTE:- e_1 IS INPUT NORMALLY CONNECTED TO FEEDBACK POT. WIPER

Figure 56 - "g" Profile Generator Schematic Diagram

was recorded on an FM tape thus storing all of the profiles in the form of an electrical signal proportional to g level.

H. Centrifuge Simulation

(1) Output Acceleration g Vector Simulation

The output acceleration g vector A_G is composed of three vectors A_{Gz}, A_{Gy}, A_{Gx}. As shown in Figure 57, the parameters for each of these vectors are obtained from output quantities of acceleration, velocity, and angular position as measured by appropriate instrumentation of the centrifuge. The square root of the sum of the squares of these vectors then produces the resultant vector. The mathematical expression for these vectors is:

$$A_{Gz} = [(R\dot{\psi}_r^2) \sin \theta_r + g \cos \theta_r] \cos \phi_r + (R\ddot{\psi}_r) \sin \phi_r$$

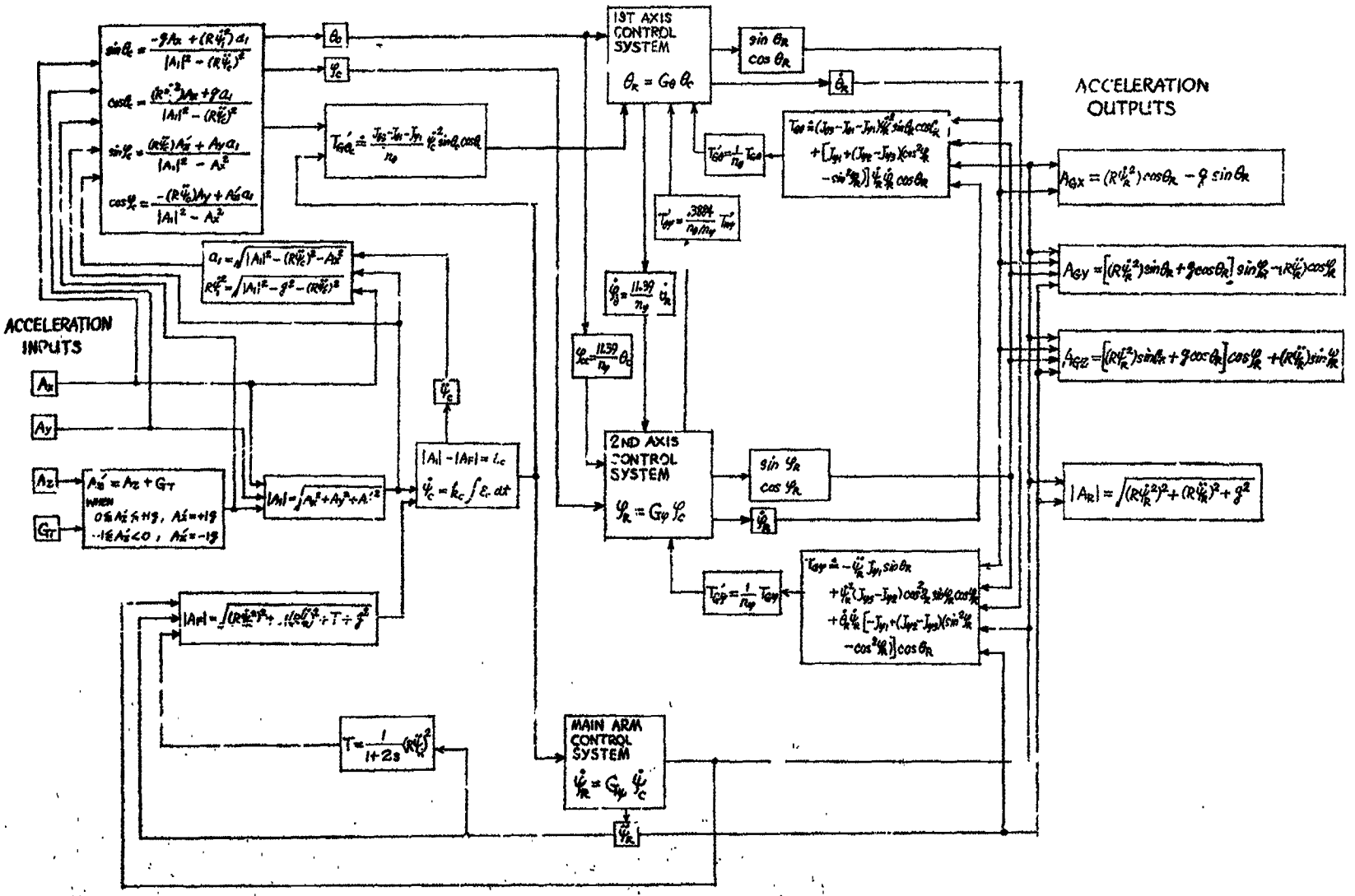

Figure 57 - NASA Centrifuge Simulation Block Diagram

$$A_{Gy} = [(R\dot{\psi}_r^2) \sin \theta_r + g \cos \theta_r] \sin \phi_r - (R\ddot{\gamma}_r) \cos \phi_r$$

$$A_{Gx} = (R\dot{\psi}_r^2) \cos \phi_r - g \sin \theta_r$$

$$A_G = \sqrt{A_{Gx}^2 + A_{Gy}^2 + A_{Gz}^2}$$

(2) Block Diagram of Centrifuge Simulation

The block diagram of the complete centrifuge simulation is shown in Figure 57. This includes the various torque couplings between systems and the means for compensating for such.

(3) Computer Diagram

The complete computer diagram for the analog simulation is shown in Figures 58 to 72. Two sets of diagrams are required in order to cover the 0 to 10 g range and the 0 to 30 g range.

(4) Method and Need for Angle Biasing in Simulation

The command angle for the gimbal and gondola system must be able to go to 180° for some of the g profiles included in these studies. The normal computer resolver will permit $\pm$ 180° input commands. Since the systems simulated in this study do have overshoot, the angle must be capable of exceeding 180°. A method of biasing was therefore employed such that the angle could swing +270° and -90°. The sine of the angle can be simulated as the cosine of the angle minus 90°. This is proved mathematically by

$$\cos (\theta - 90°) = \cos \theta \cos 90° + \sin \theta \sin 90°$$

$$\cos 90° = 0$$

$$\sin 90° = 1$$

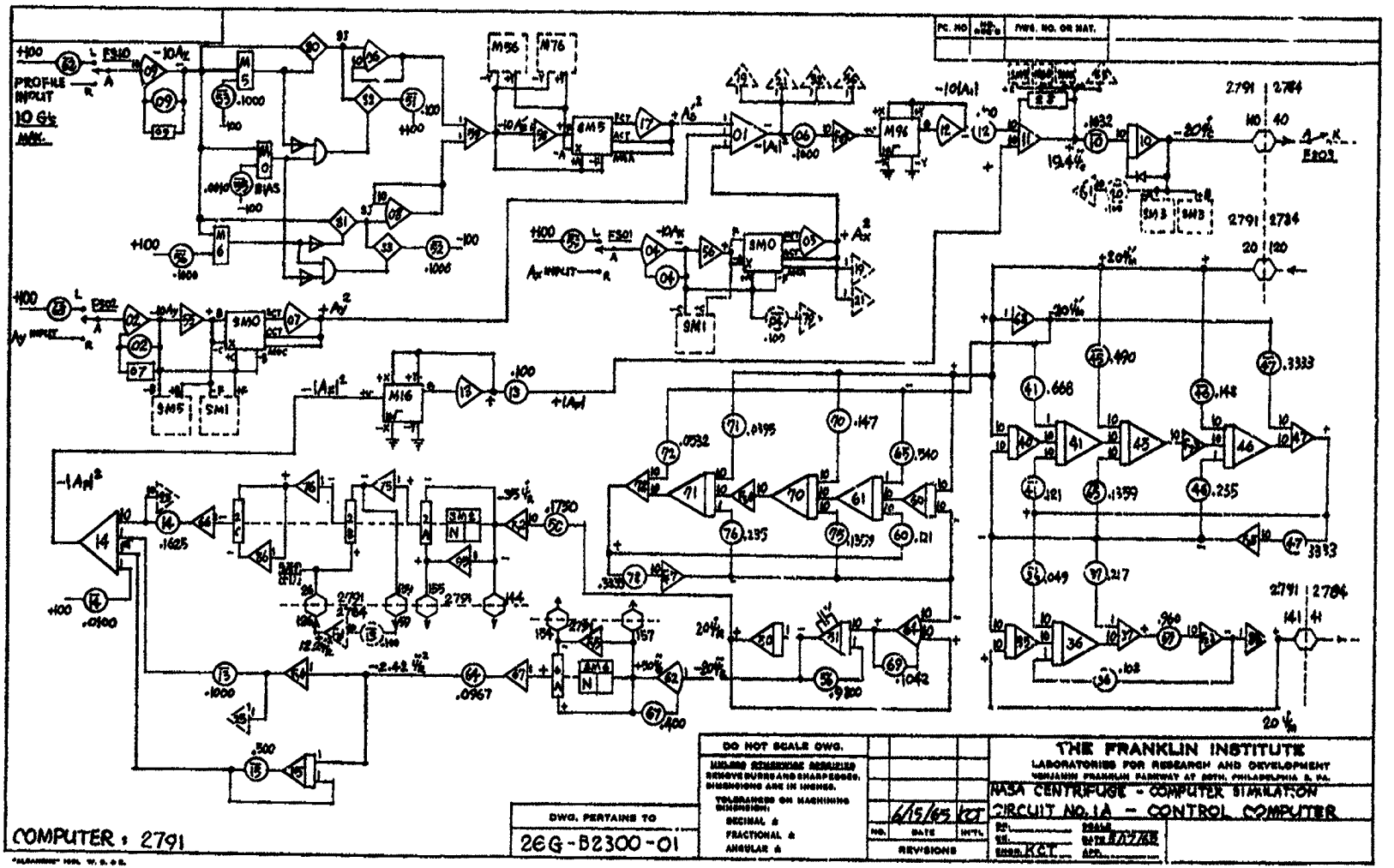

Figure 58 - NASA Centrifuge - Computer Simulation Circuit No. 1A - Control Computer

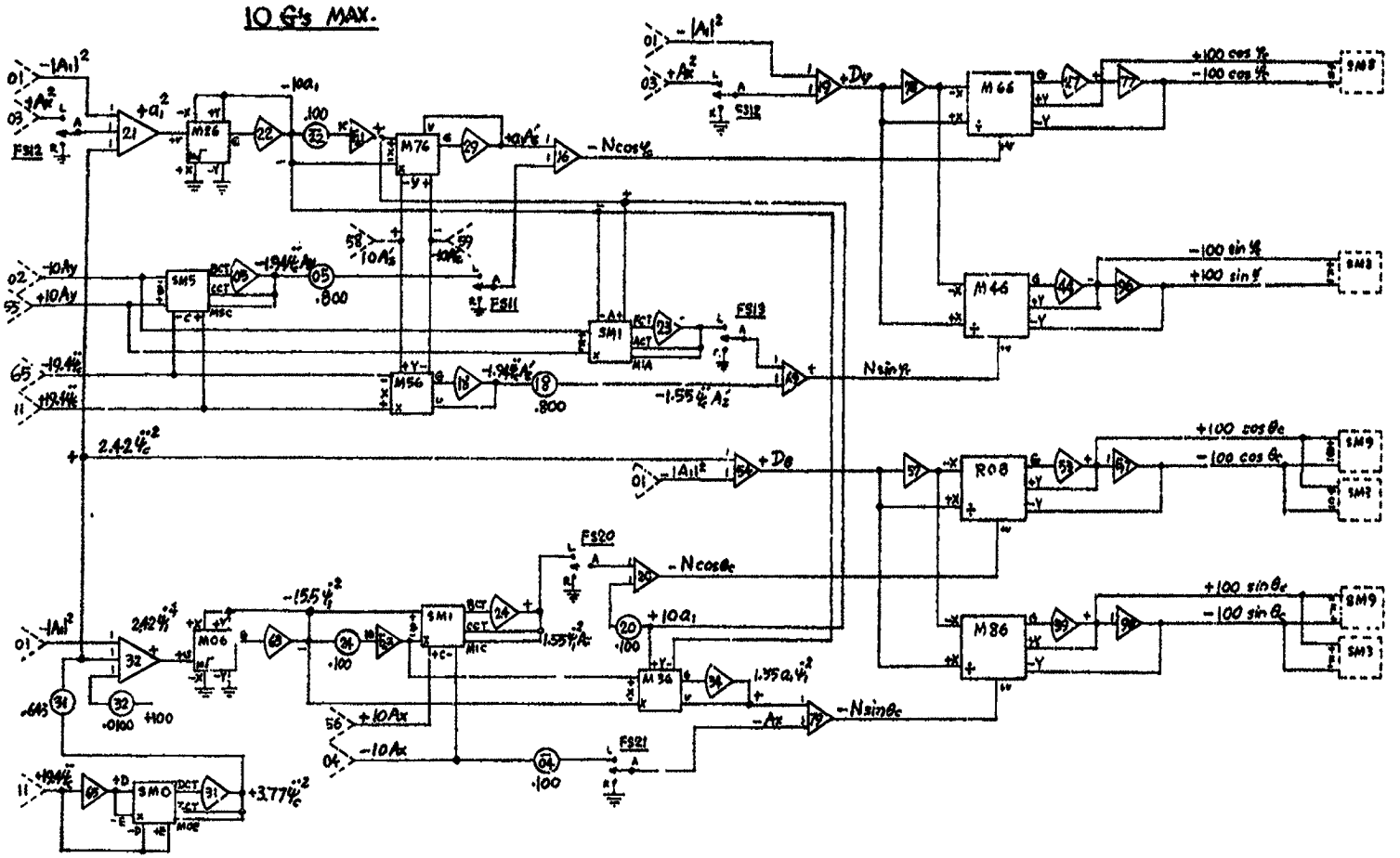

Figure 59 - NASA Centrifuge - Computer Simulation Circuit No. 2A - Vector Alignment

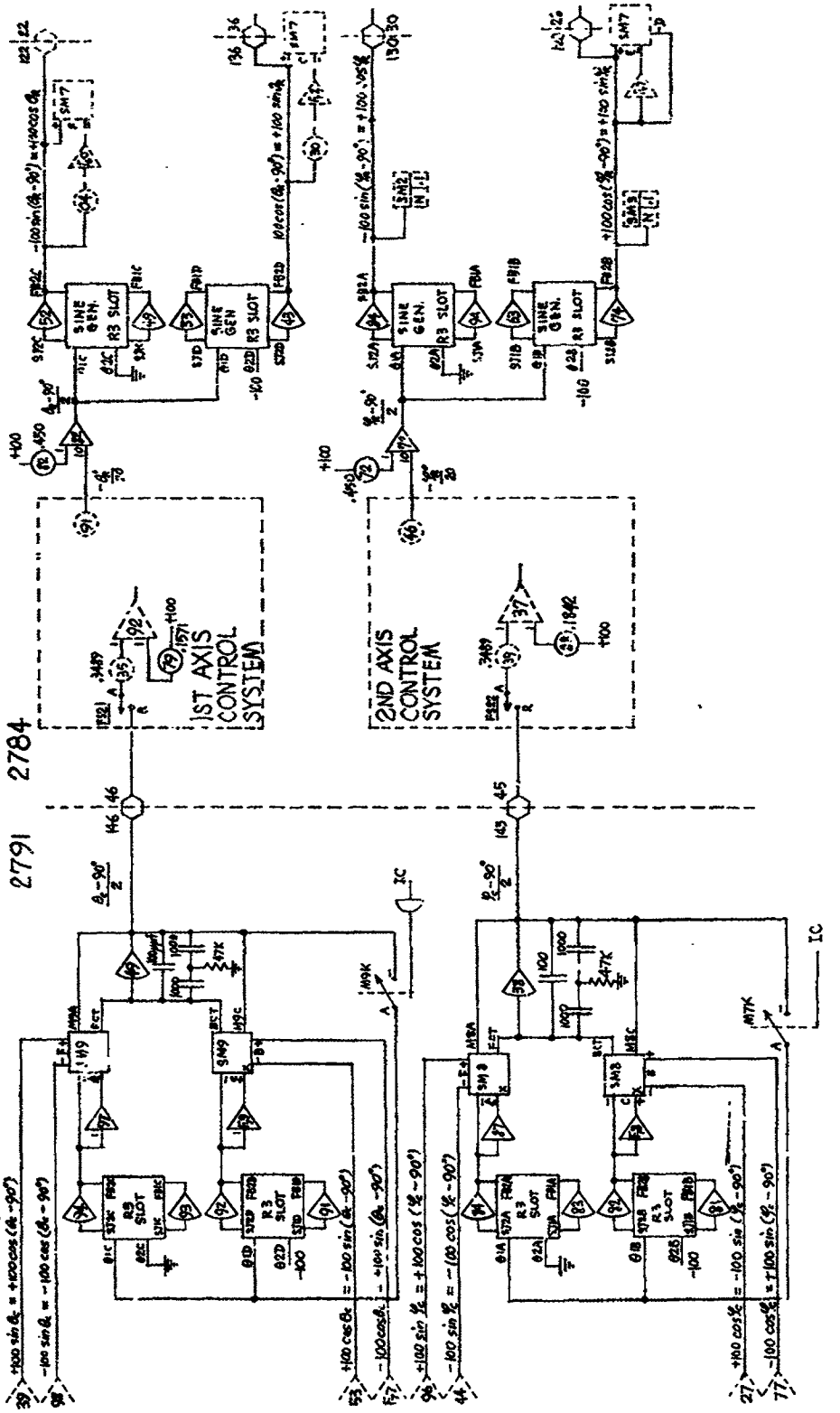

Figure 60 - NASA Centrifuge - Computer Simulation Circuit No. 3 - Trigonometric Funct. Gen.

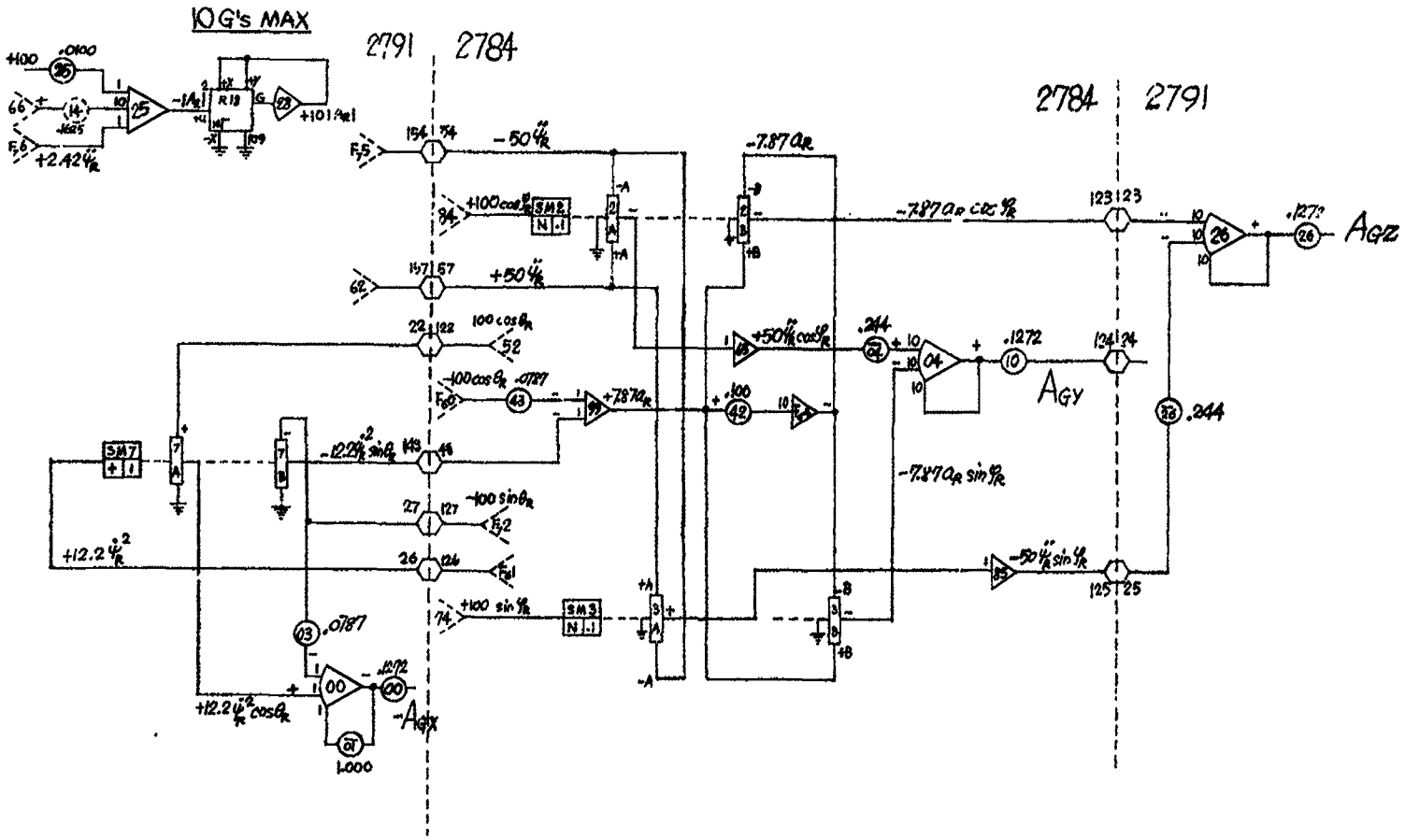

Figure 61 - NASA Centrifuge Computer Simulation Circuit No. 4A - Output G Accelerations

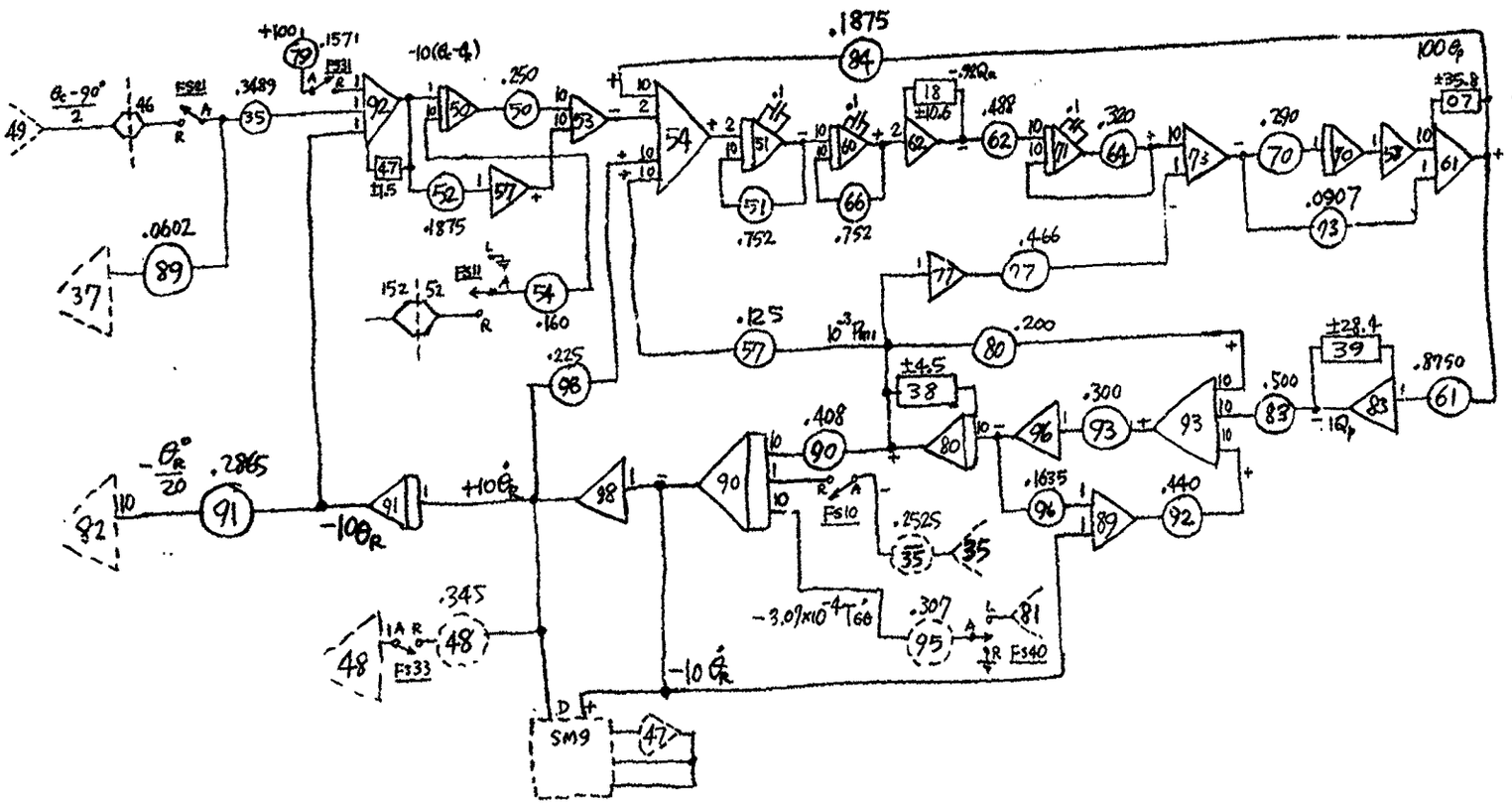

COMPUTER = 2784

Figure 62 - 1st Axis Computer Ckt

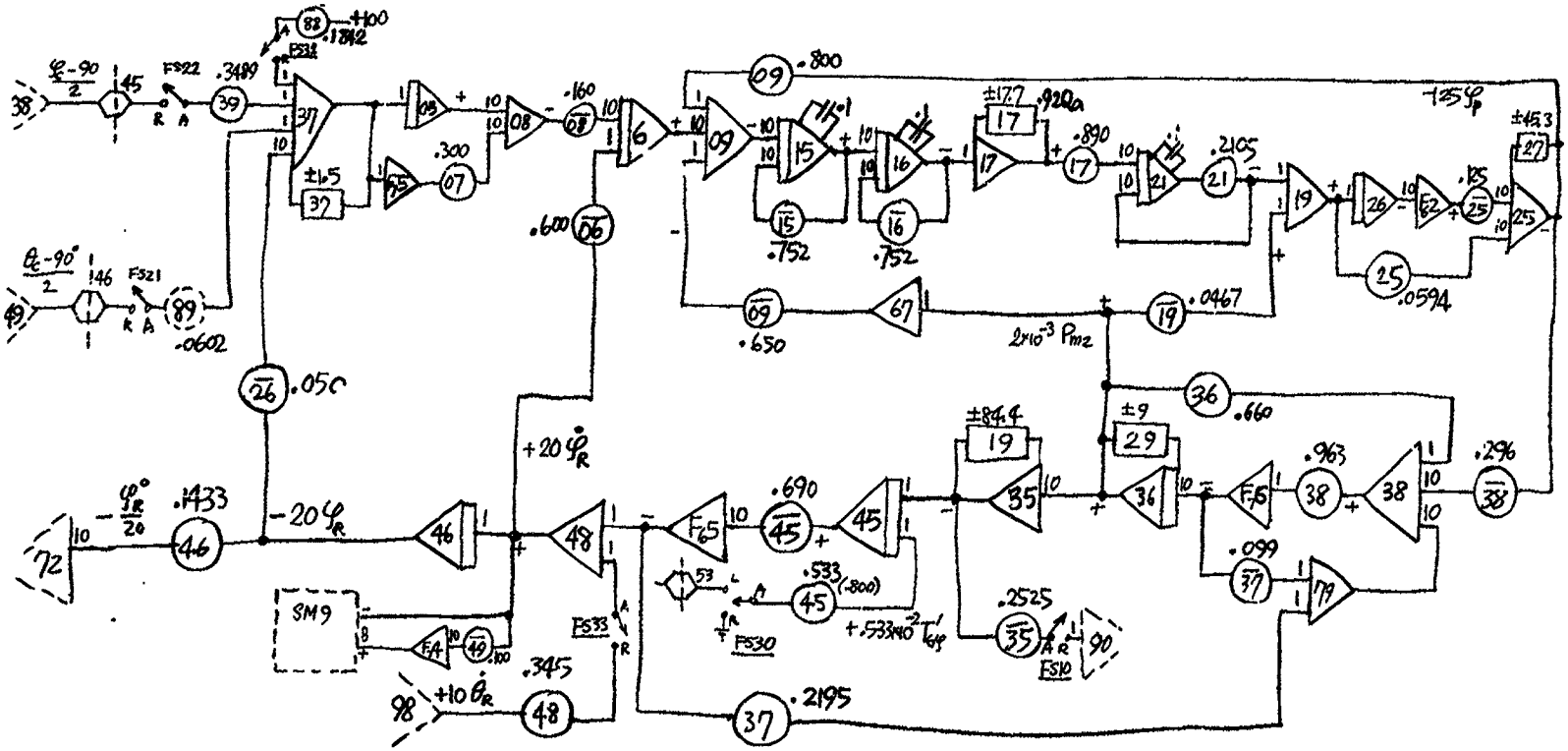

Figure 63 – 2nd Axis Computer Ckt

ELECTRONIC ASSOCIATES, INC.
RESEARCH AND COMPUTATION DIV.
BOX 608, PRINCETON, N. J.

BY_____ SUBJECT THIRD AXIS SHEET NO.____ OF____

DATE_____ PROJ. NO.____

2784

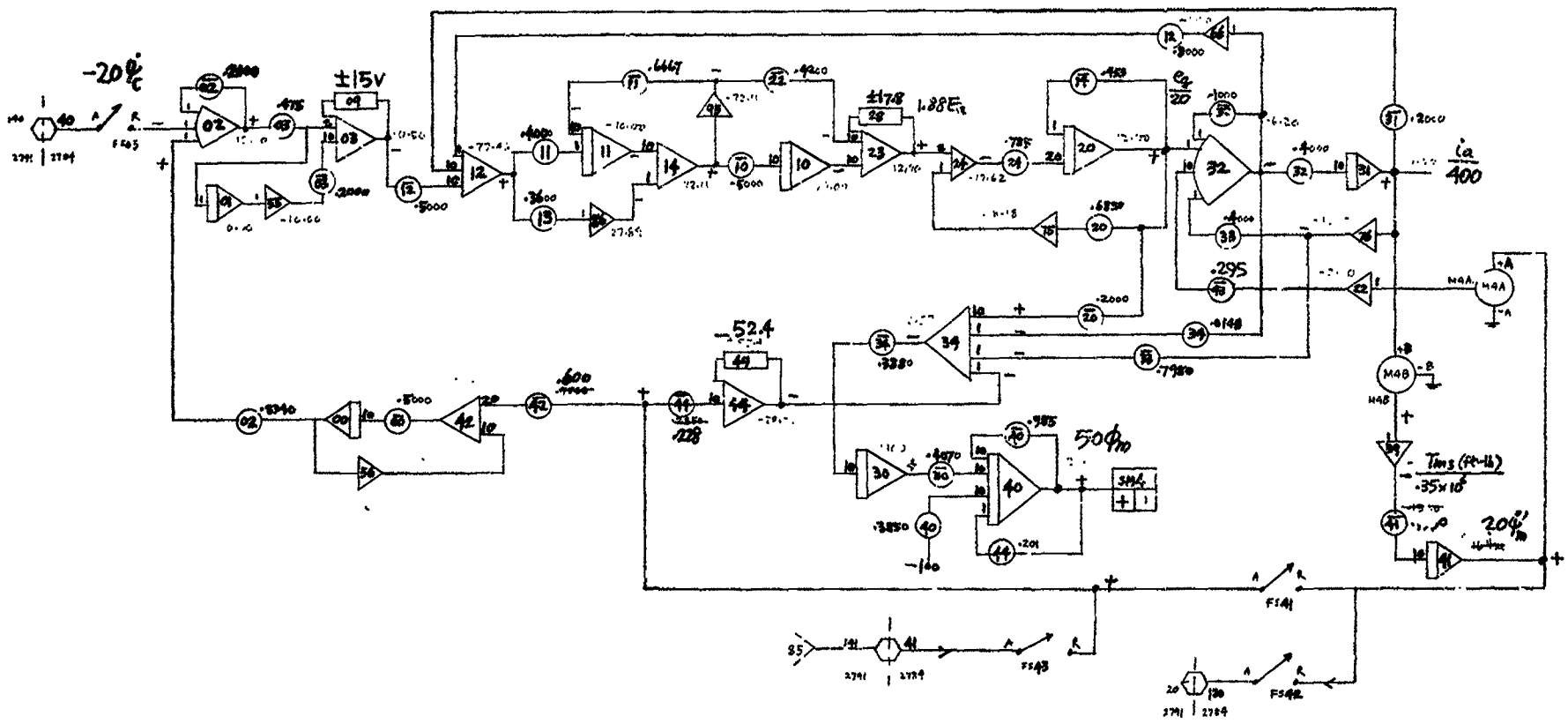

Rev. 6/15/65 KCF

Figure 64

50

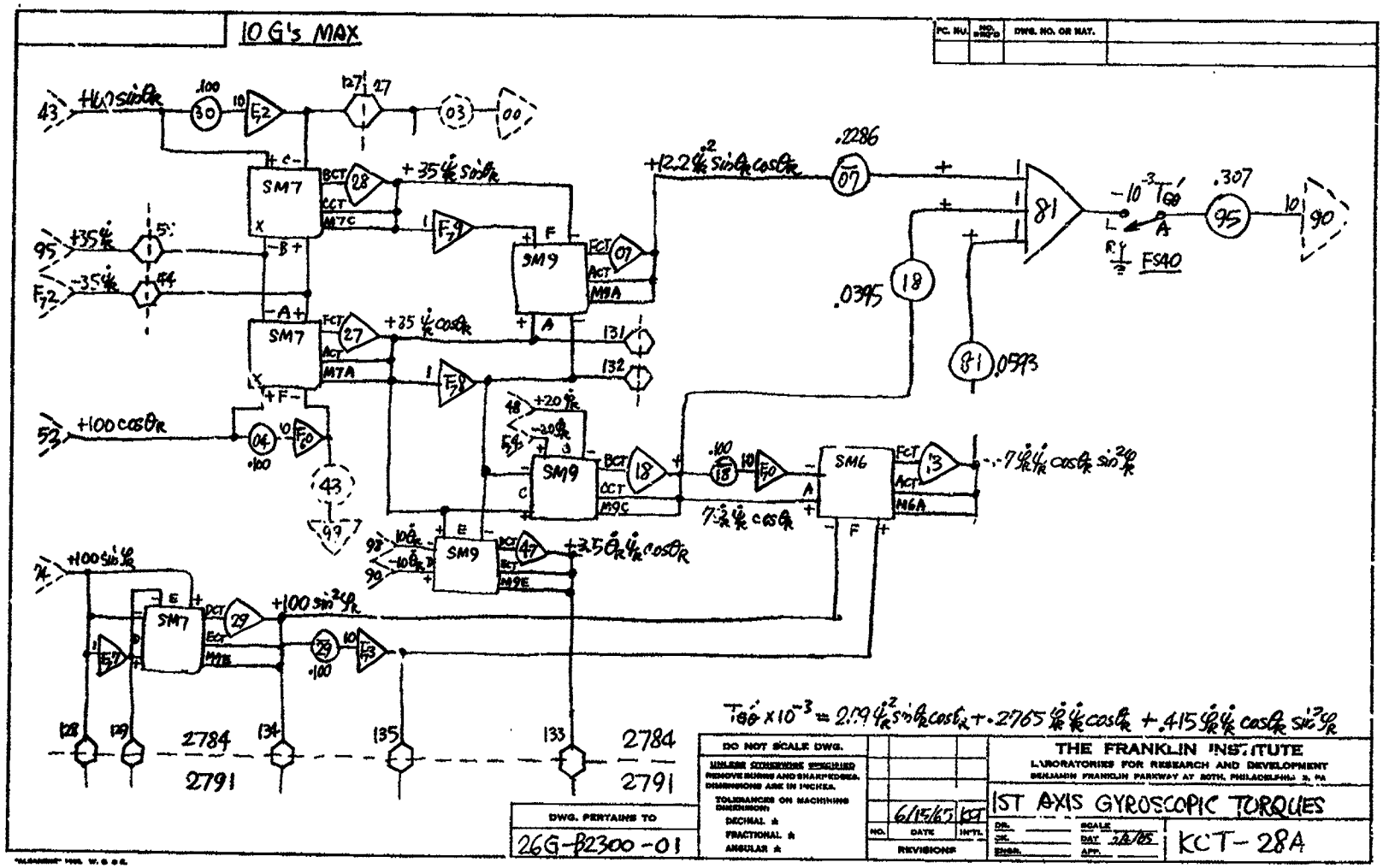

Figure 65 - 1st Axis Gyroscopic Torques

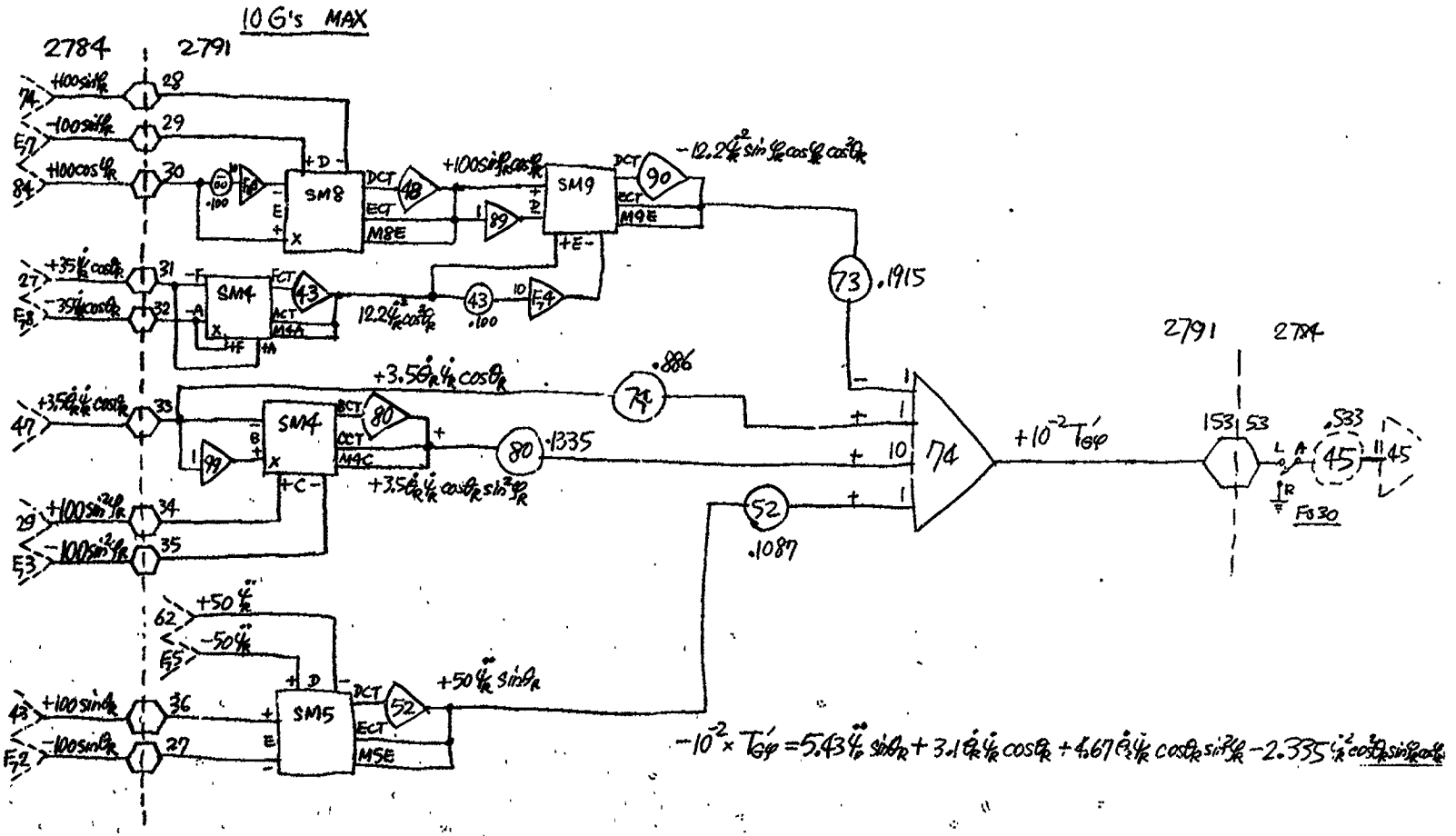

Figure 66 - 2nd Axis Gyroscopic Torques

ELECTRONIC ASSOCIATES, INC.
RESEARCH AND COMPUTATION DIV.
BOX 582, PRINCETON, N. J.

BY J. STONE
DATE
SUBJECT 1ST AXIS COMP. TORQUE
SHEET NO. OF
PROJ. NO.

2791

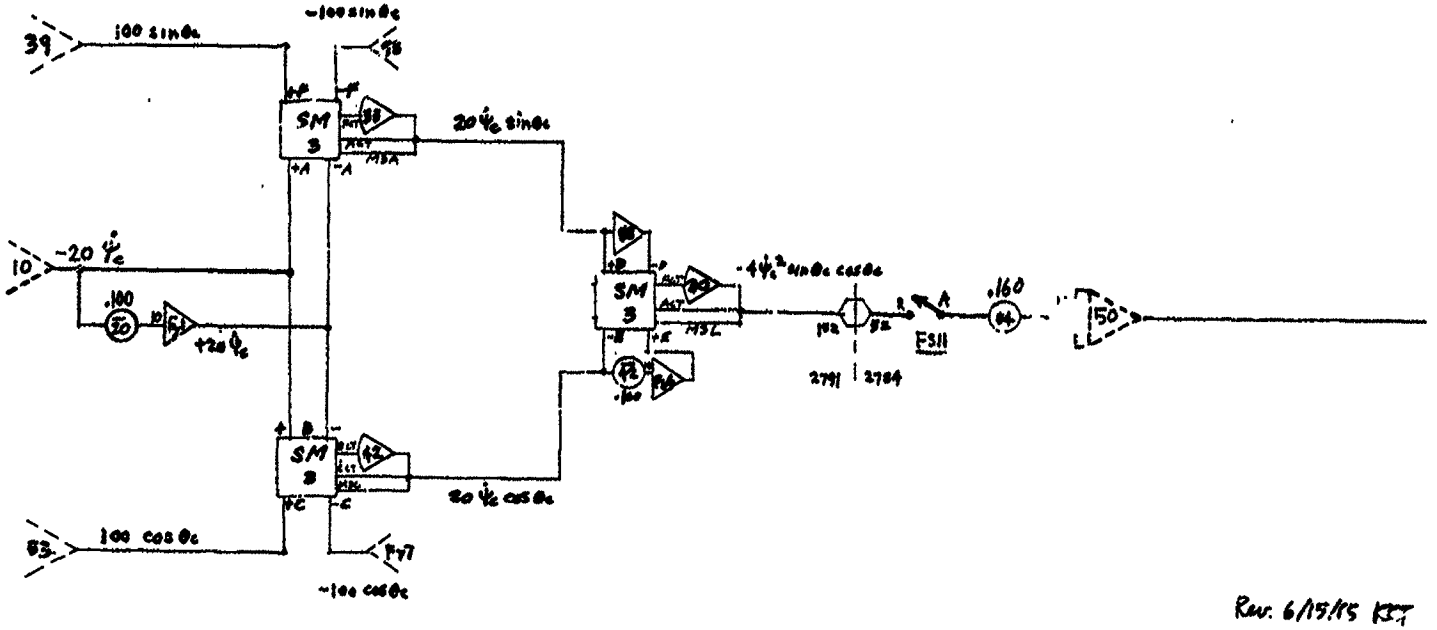

Rev. 6/15/15 KT

Figure 67 - 1st Axis Comp. Torque

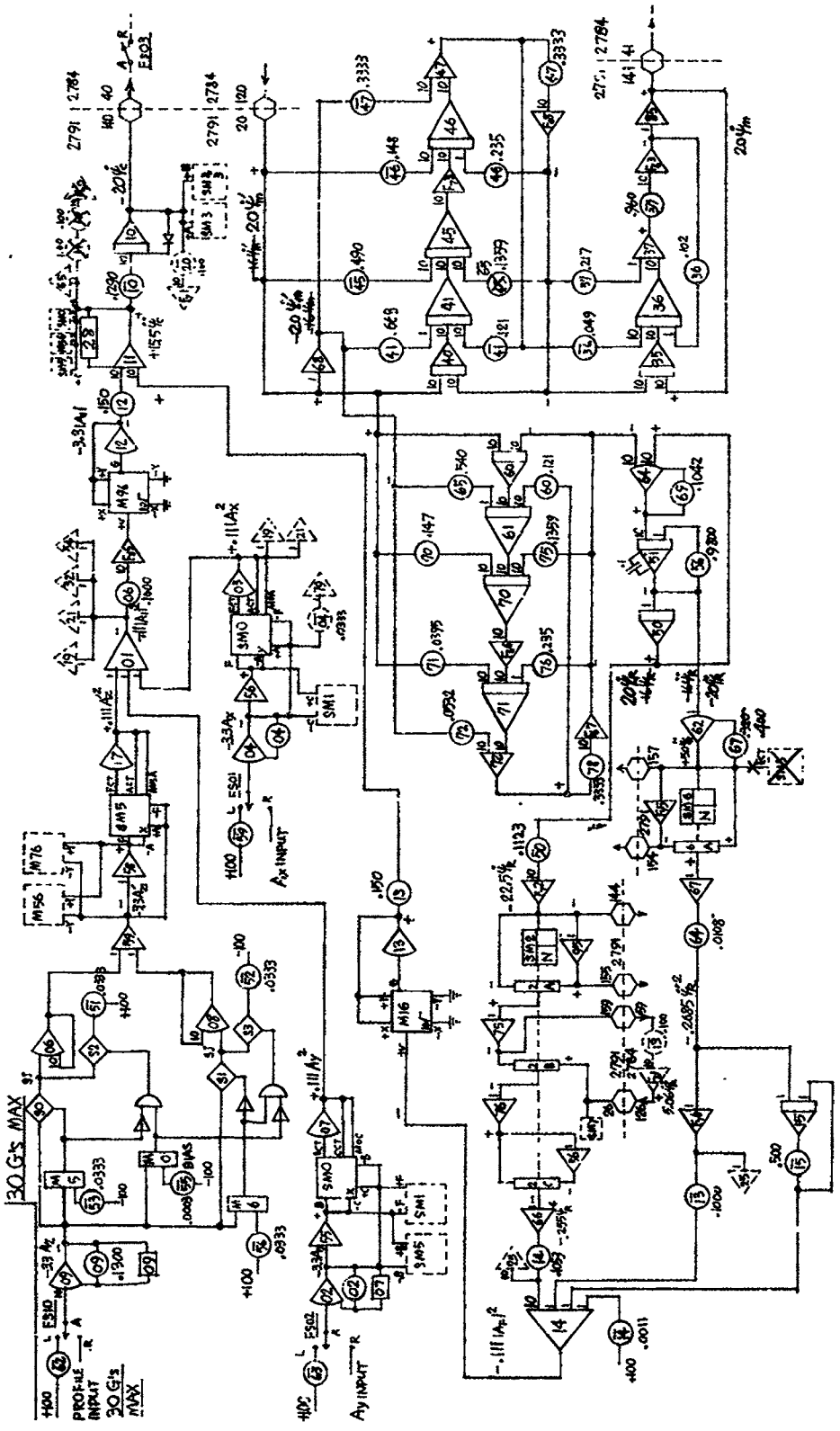

Figure 68 - NASA Centrifuge - Computer Simulation Circuit No. 1B - Control Computer

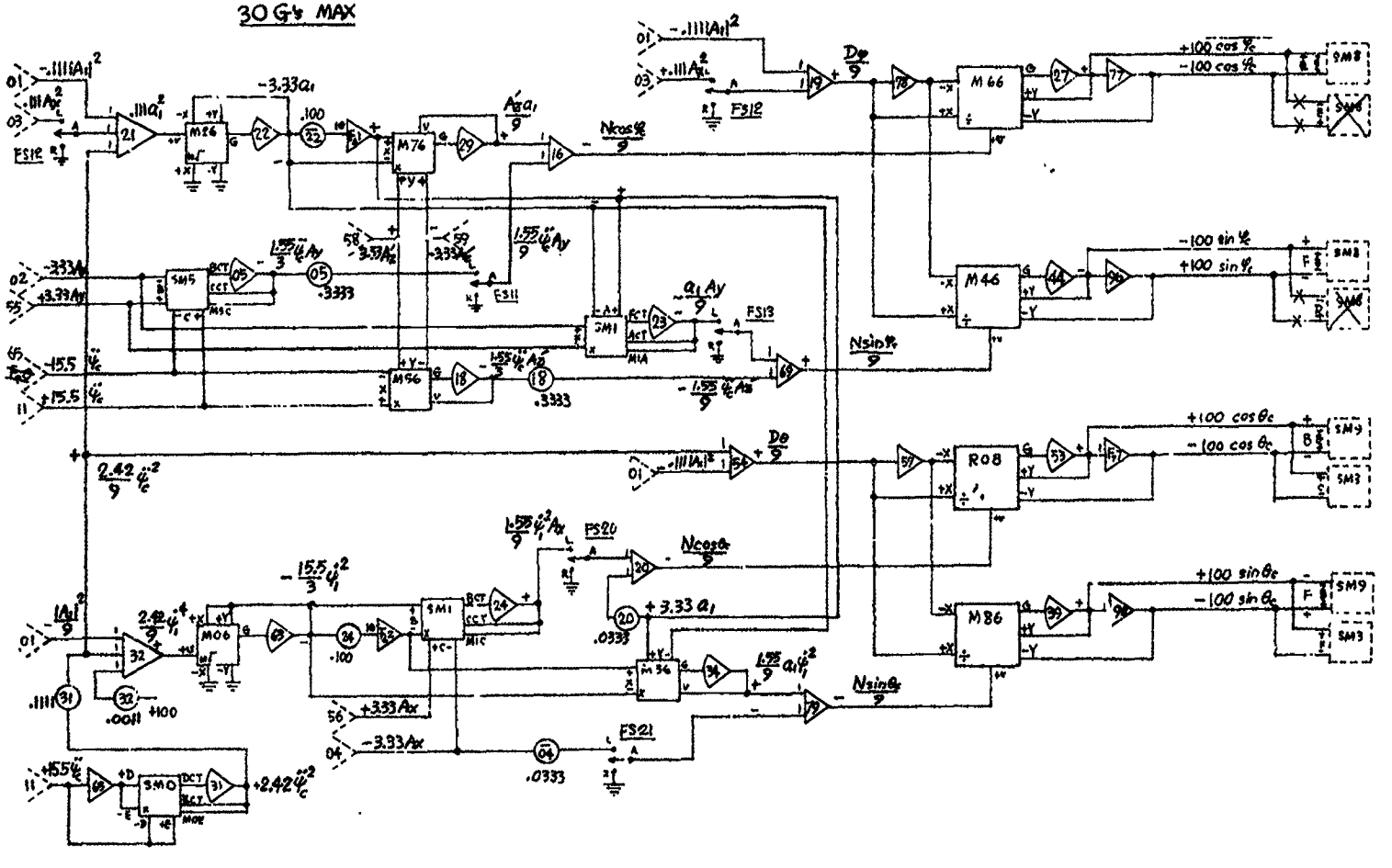

Figure 69 - NASA Centrifuge - Computer Simulation Circuit No. 2B - Vector Orientation

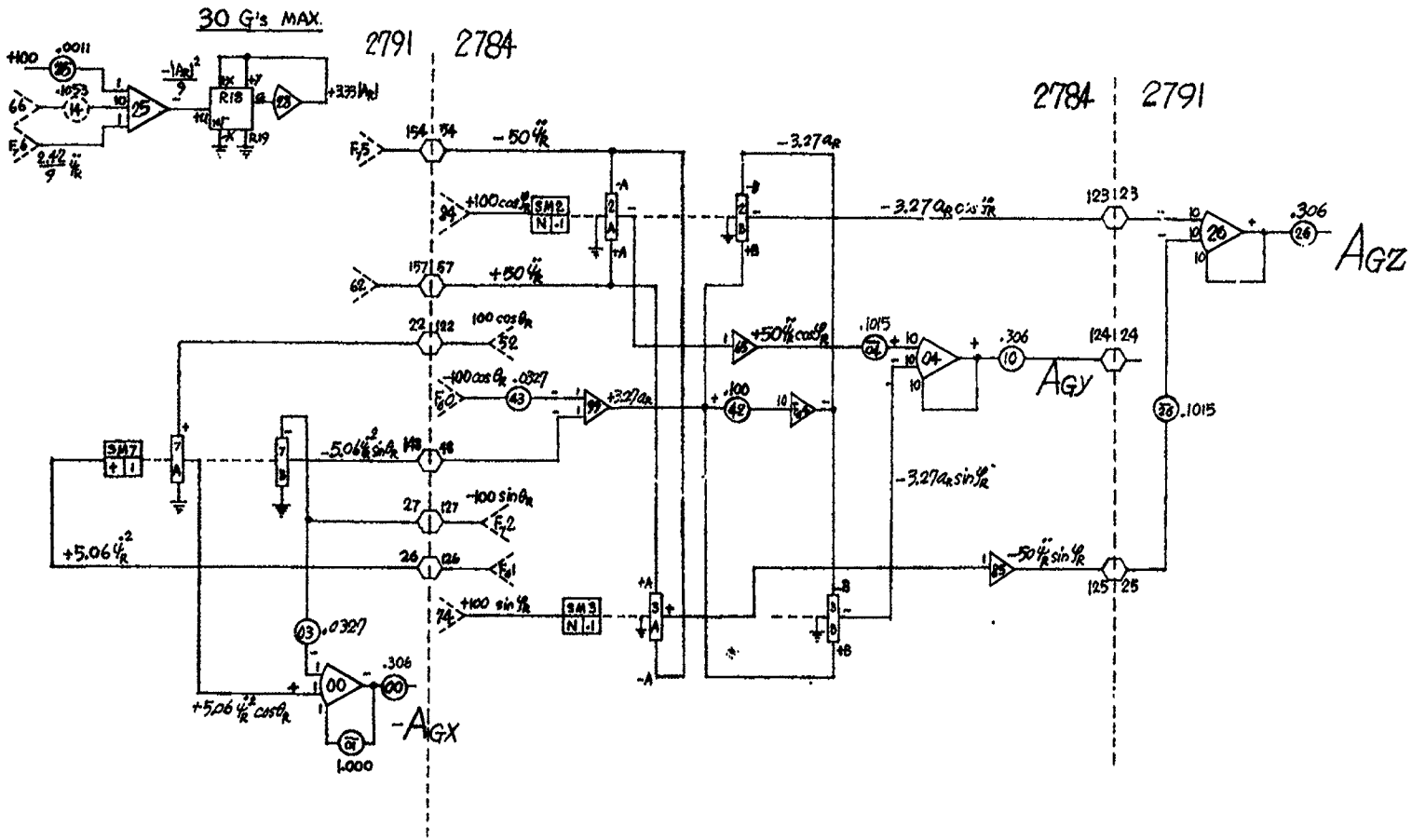

Figure 70 - NASA Centrifuge Computer Simulation Circuit No. 4B - Output G Accelerations

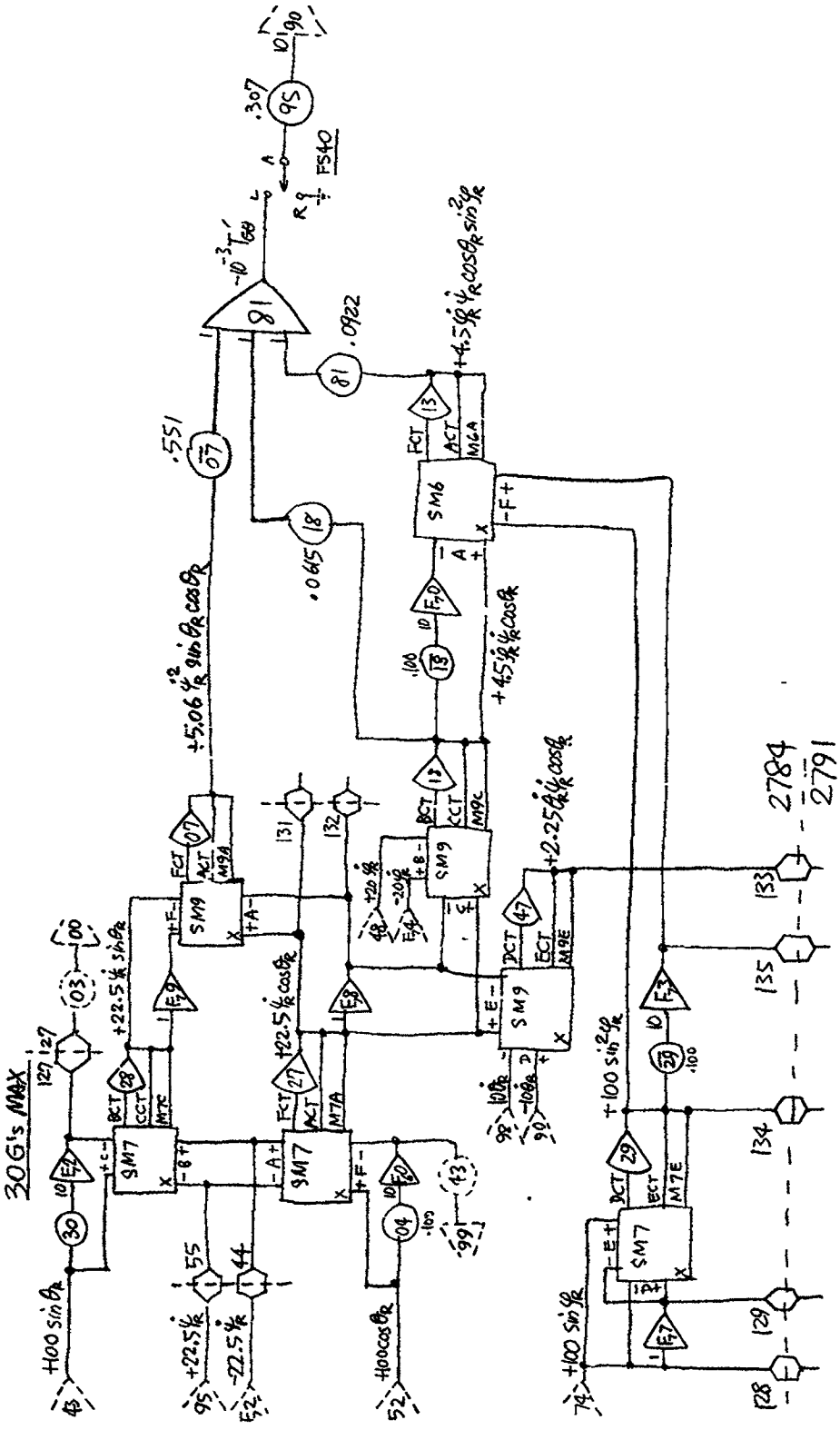

Figure 71 - 1st Axis Gyroscopic Torque Ckt

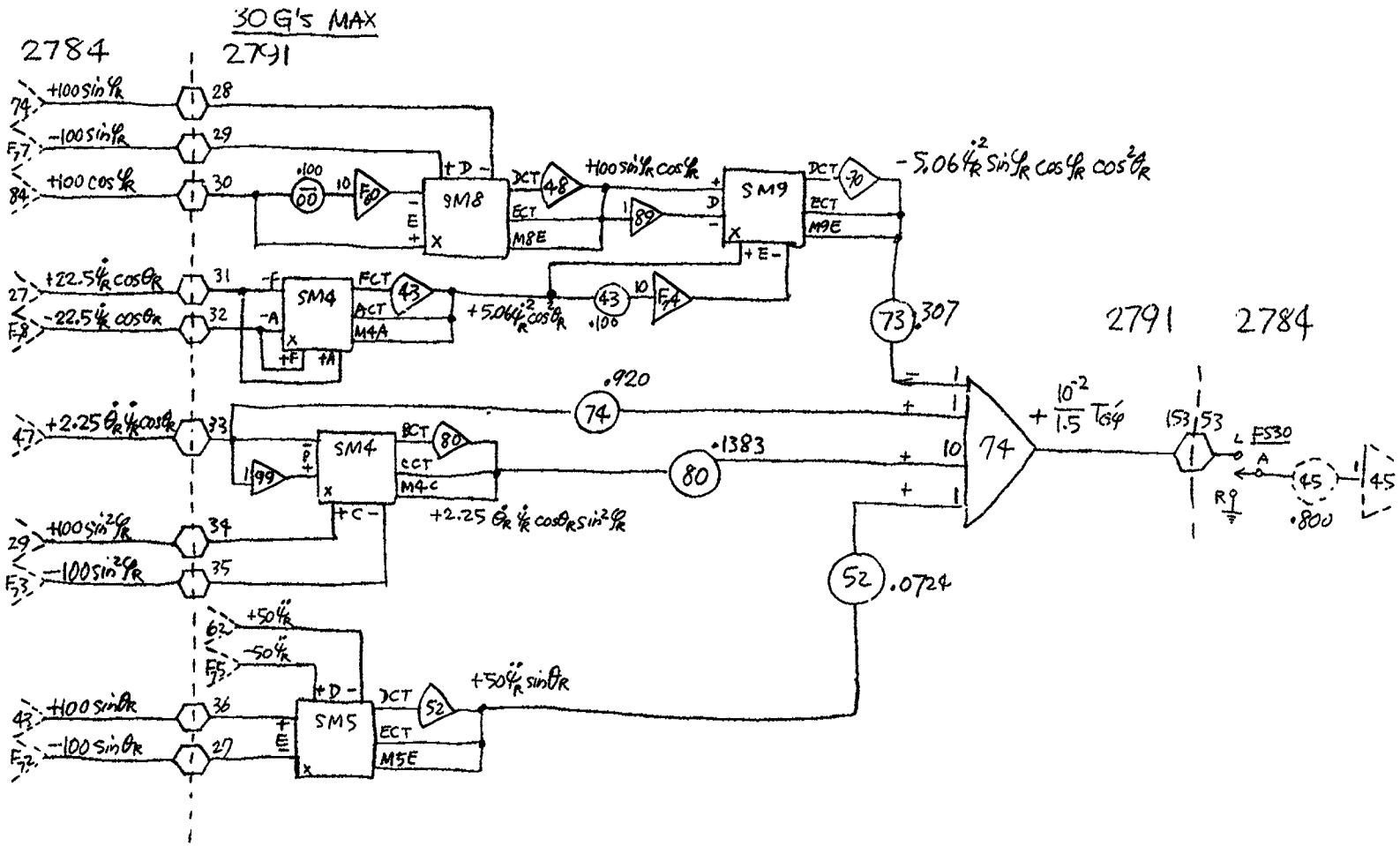

Figure 72 - 2nd Axis Gyroscopic Torque Ckt

$$\cos (\theta - 90°) = \sin \theta$$

The computer simulation is such that 180° = 90 V or 2° = 1 V. When the angle θ is zero a bias voltage must be fed in equivalent to 90° × 1 V/2° = 45 V. Therefore by the proper biasing of the angle fed into the resolver and compensating for this by a bias at the resolver output, the output angle can be made to swing between -90° and +270°. This method of biasing is shown in Figure 60.

(5) According to the results of centrifuge simulation studies, effect of disturbance forces on the 1st axis control system (gimbal ring) is serious, while it is very minor on the 2nd axis control system (gondola).

Therefore, a closer look only at the 1st axis system will be made for further analysis of this effect.

For simplicity's sake, only one predominant term of disturbance torque is considered as follows: (see the following page for the complete torque equations).

$$T_{G\theta} \times 10^{-3} = 185.15 \dot{\psi}_R^2 \sin \theta_R \cos \theta_R$$

$$= 92.575 \dot{\psi}_R^2 \sin 2\theta_R \text{ lb-in}$$

Since θ_R is a function of time, this disturbance torque has a plus sign when $n\pi < \theta < (n + 1/2)\pi$; has a minus sign when $(n + 1/2)\pi < \theta_R < (n + 1)\pi$, where n = 0, 1, 2 .... (see figure of quadrants below).

F-B2300-1

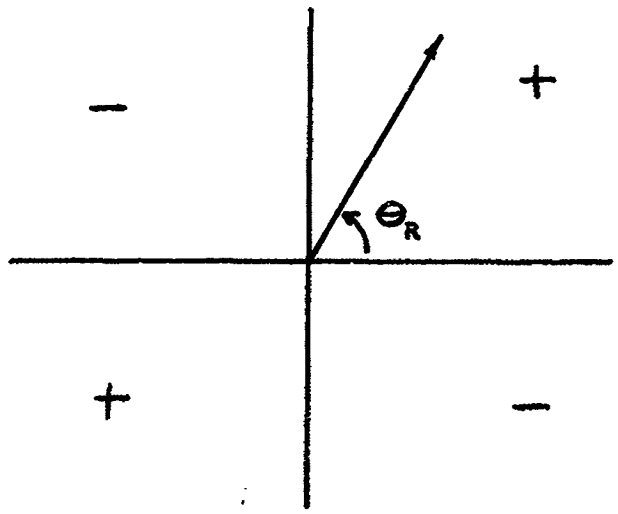

The complete gyroscopic torque equations for the first and second axis are:

$$T_{G\theta} = \ddot{\theta}_r \left[J_{\theta 2} + J_{\phi 2} \cos^2 \phi_r + J_{\phi 3} \sin^2 \phi_r\right]$$

$$+ \ddot{\psi}_r \left[J_{\phi 2} - J_{\phi 3}\right] \cos \theta_r \sin \phi_r \cos \phi_r$$

$$+ \dot{\theta}_r \dot{\phi}_r \left[2 \left(J_{\phi 3} - J_{\phi 2}\right)\right] \sin \varphi_r \cos \varphi_r$$

$$+ \dot{\psi}_r \dot{\phi}_r \left[J_{\phi_1} + \left(J_{\phi_2} - J_{\phi_3}\right) \left(\cos^2 \phi_r - \sin^2 \phi_r\right)\right]$$

$$\cos \theta_r + \dot{\psi}_r \left[\left(J_{\theta 3} - J_{\theta 1}\right) - J_{\phi_1} + J_{\phi_2} \sin^2 \phi_r\right.$$

$$\left. + J_{\phi 3} \cos^2 \phi_r\right] \sin \theta_r \cos \theta_r$$

$$T_{G\phi} = - \ddot{\psi}_r J_{\phi_1} \sin \theta_r + \dot{\psi}_r^2 \left(J_{\phi 3} - J_{\phi 2}\right)$$

$$\cos^2 \theta_r \sin \phi_r \cos \phi_r$$

$$+ \dot{\theta}_r^2 \left(J_{\varphi_2} - J_{\phi_3}\right) \sin \phi_r \cos \phi_r$$

$$+ \dot{\theta}_r \dot{\psi}_r \left[- J_{\phi_1} + \left(J_{\phi_2} - J_{\phi_3}\right) \left(\sin^2 \phi_r - \cos^2 \phi_r\right)\right] \cos \theta_r$$

Figure 73A and B shows curves for No. 3 g profile input. The command signal to the 1st axis system appears to be $\theta_c = 78°$. The responded main arm velocity is $\psi_R = 1.65$ rad. (Figure 73A; Channel 8).

The 1st axis system responds to an almost step input of 78° and overshoots up to $\theta_R = 130°$, which is 67% above the input level.

The disturbance torque becomes

$$T_{G\theta} \times 10^{-3} = 92.6 \times (1.65)^2 \times \sin 2\theta_R$$

$$= 252 \sin 2\theta_R \text{ lb-in}$$

Therefore,

when $\theta_R = 90°$ $\quad T_{G\theta} \times 10^{-3} = 0$

$= 130°$ $\quad = -248$

In other words the disturbance torque is subtractive from the motor torque until θ_R becomes 90° and when θ_R remains above 90° up to 130°, the disturbance torque is additive to the motor torque.

Since at the peak of overshoot, $T_{G\theta} \times 10^{-3} = -24$ lb-in which is within the range of system stability (see "Disturbance Torque Studies for the 1st and 2nd Axes," E. Pack, 6/11/65), the system overcomes this disturbance and tries to follow the command signal. However, as soon as the response θ_R passes below 90°, the disturbance torque changes its sign again and works subtractively this time, bringing the response further down. At the first valley of the response, it appears $\theta_R = 30°$, which gives us $T_{G\theta} \times 10^{-3} =$

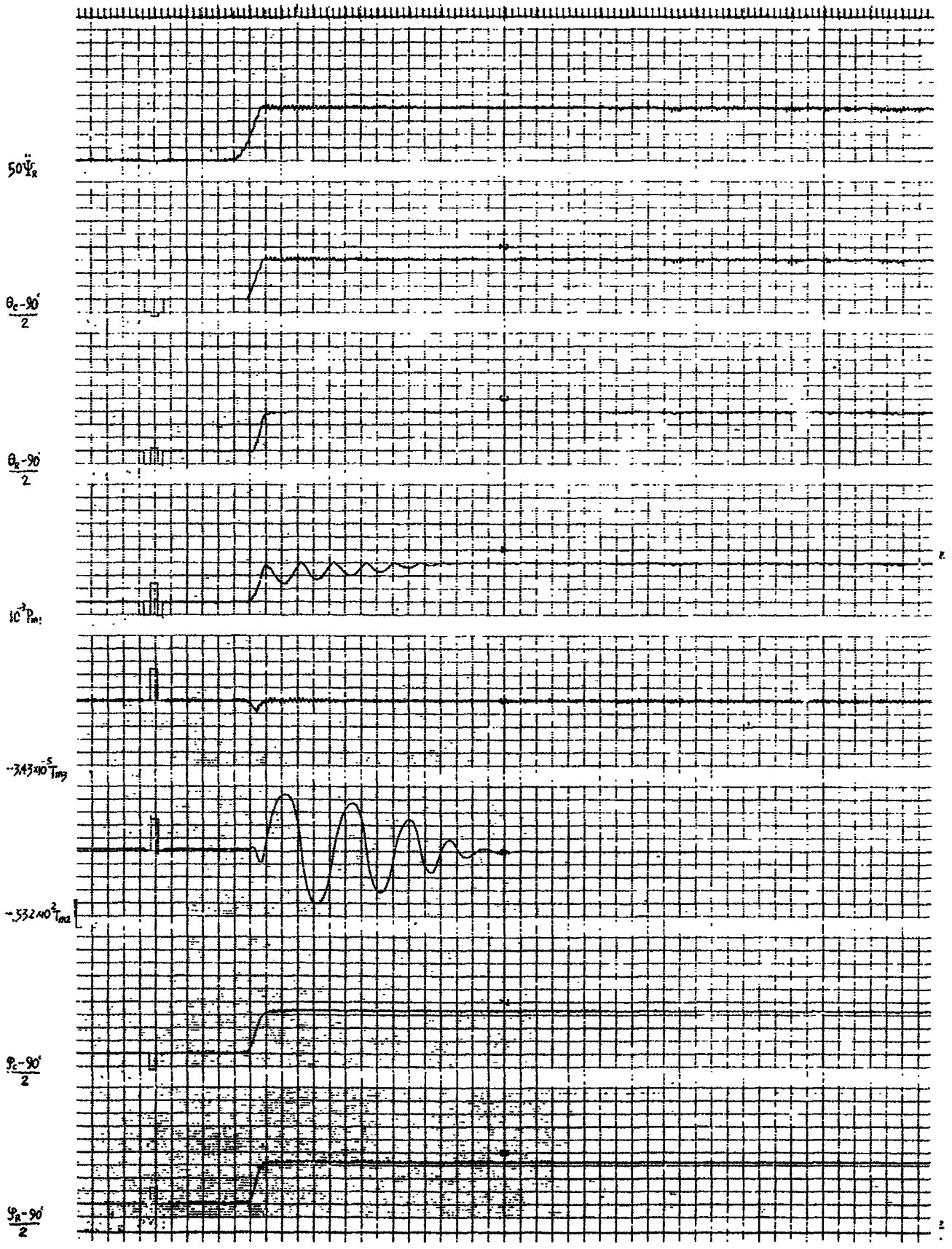
$50\ddot{\psi}_R$
$\frac{\theta_c - 90^\circ}{2}$
$\frac{\theta_R - 90^\circ}{2}$
$10^{-3} P_m$
$-3.43 \times 10^{-5} T_{m3}$
$-3.32 \times 10^{-2} T_{m2}$
$\frac{\varphi_c - 90^\circ}{2}$
$\frac{\varphi_R - 90^\circ}{2}$

Figure 73A

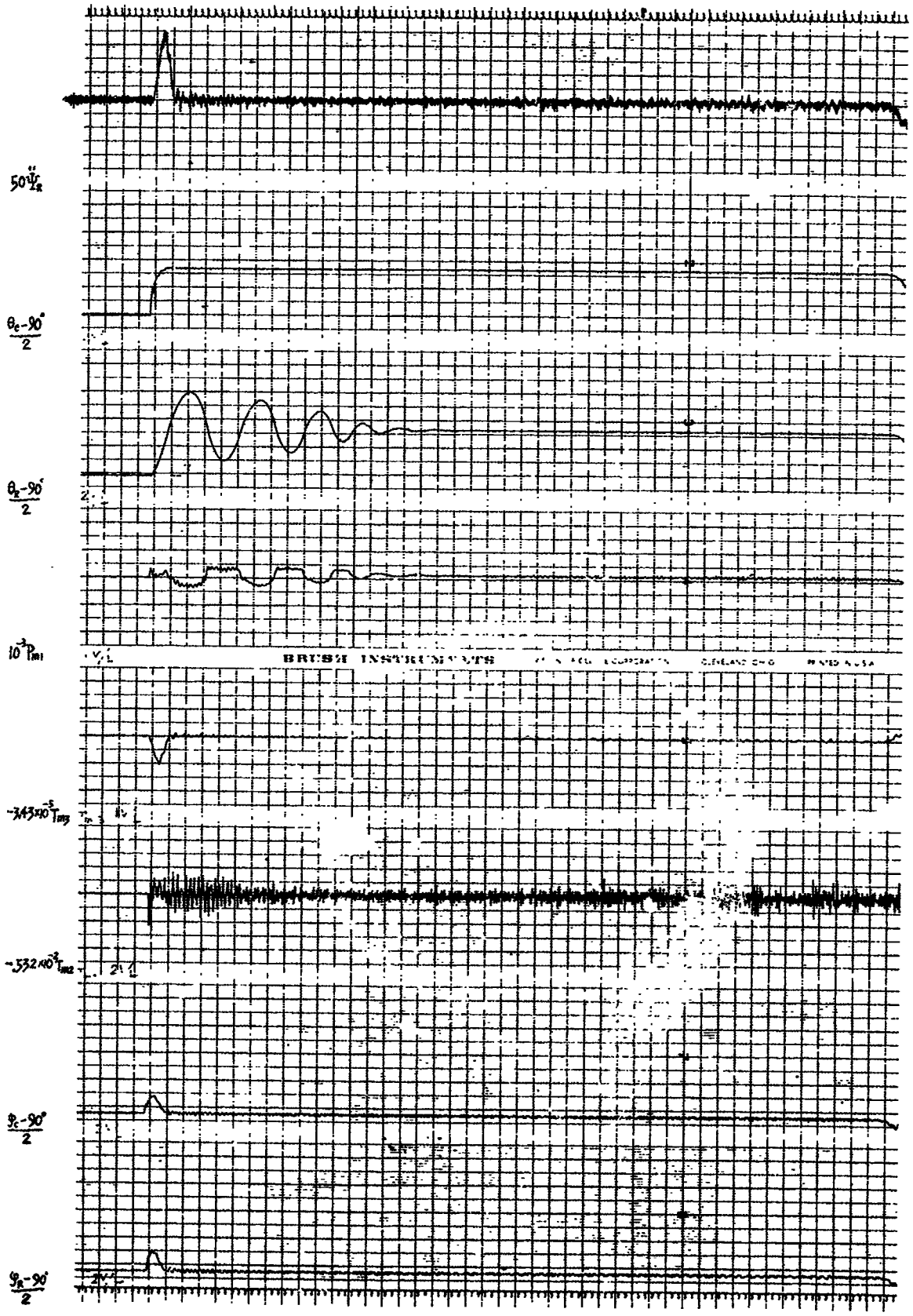
50 $\ddot{\psi}_E$
$\frac{\theta_c - 90^\circ}{2}$
$\frac{\theta_E - 90^\circ}{2}$
$10^{-2} P_{m1}$
BRUSH INSTRUMENTS
$-343 \times 10^{-5} T_{m3}$
$-332 \times 10^{-3} T_{m2}$
$\frac{\varphi_c - 90^\circ}{2}$
$\frac{\varphi_E - 90^\circ}{2}$

Figure 73B

218 lb-in. Therefore, the disturbance is still within the stability limit and the system overcomes it.

So it continues until the system reaches steady-state in about 48 seconds.

The damped oscillation of the 1st axis response is reflected in g-profile response curves as shown in Figure 73A.

Figure 74A and B shows the result of an analog computer run with disturbance torque coupled in and Figure 75A and B shows one without the 1st axis gyroscopic torque, for the g-profile No. 4.

For this g-profile, the command signal for the 1st axis system is 82° (Figure 74B, Figure 75B; Channel 2). Without the gyroscopic torque, the first axis response to this input overshoots to 114°, which is 39% overshoot as shown in Figure 75B, Channel 3.

However, the gyroscopic torque, at this point, would be, since Ψ_R = 2.05 rad (Figure 74A, Figure 75A; Channel 8),

$$T_{G\theta} \times 10^{-3} = 390 \sin 2\theta_R$$

$\therefore$ When $\theta_R = 114°$ $\quad T_{G\theta} \times 10^{-3} = -290$ lb-in

$= 135°$ $\quad = -390$

$= 166°$ $\quad = -183$

Therefore, if the gyroscopic torque is coupled in as in Figure 74, when θ_R reaches overshoot peak of about 114°, the torque works additively and helps the overshoot of the response further up until it reaches a peak of 166° as shown in Figure 74B. The maximum value of disturbance torque is 390×10^{-3} lb-in which occurs at $\theta_R = 135°$.

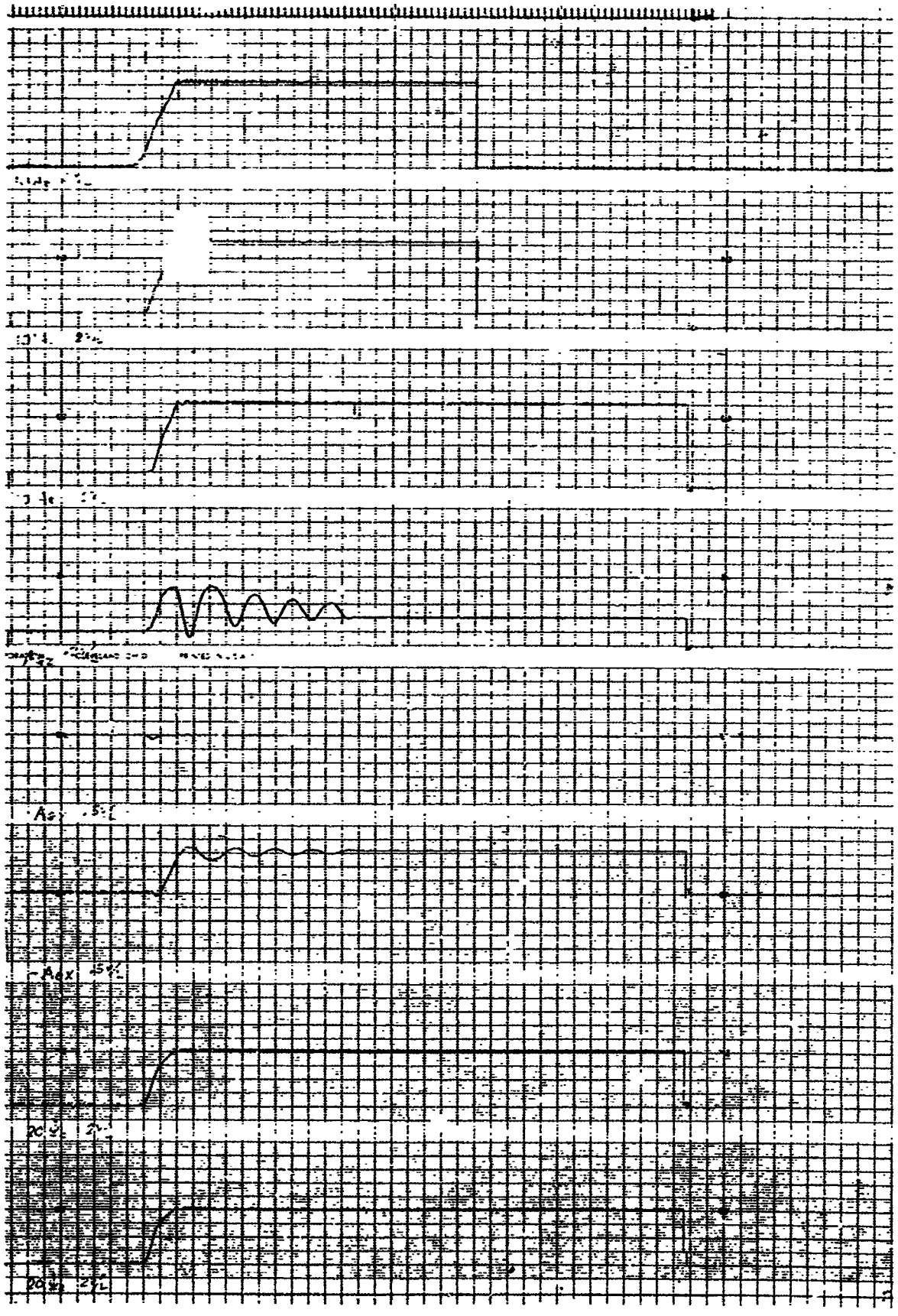

Figure 74A

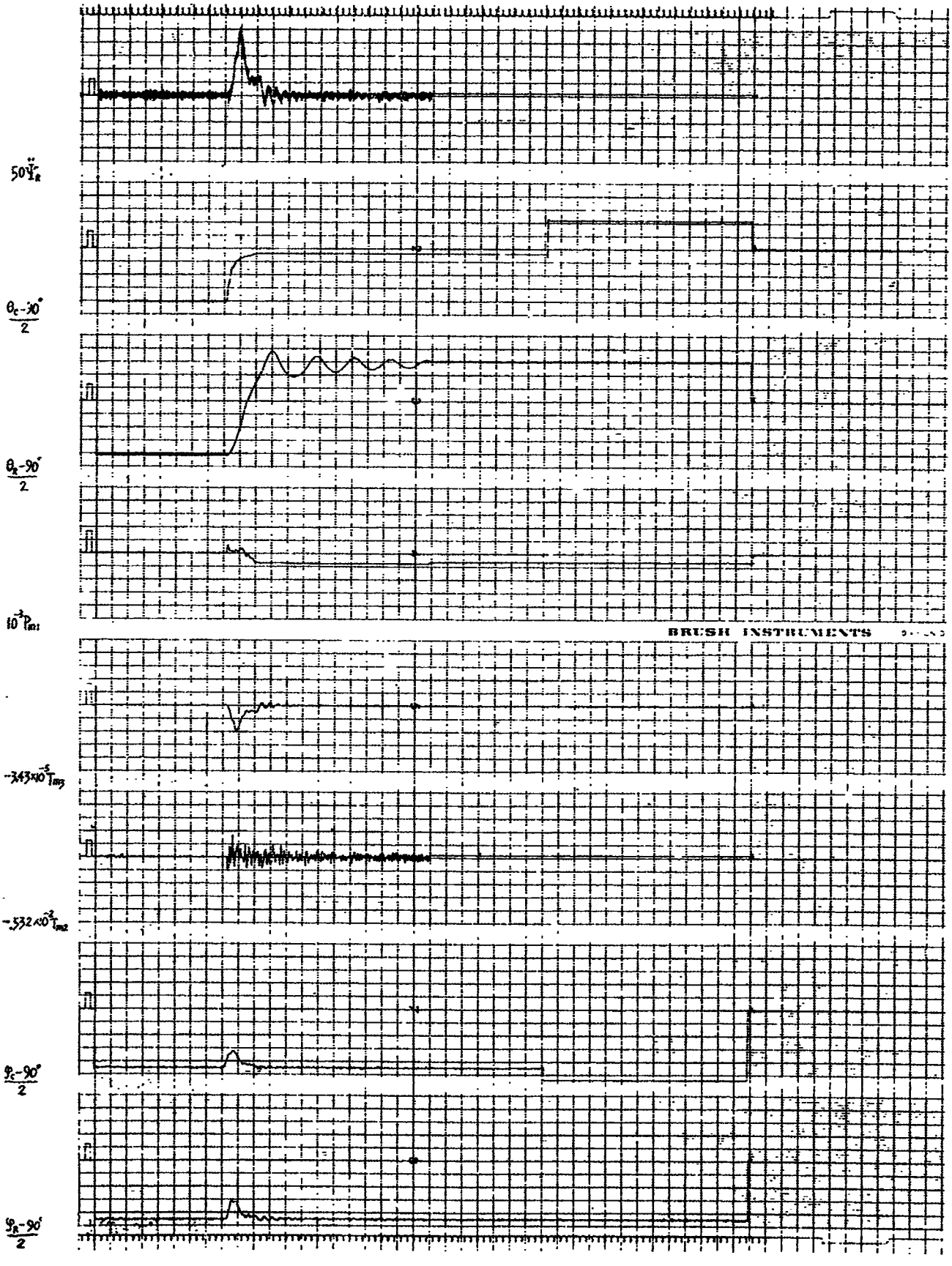
$50\ddot{\psi}_R$
$\frac{\theta_c - 30^\circ}{2}$
$\frac{\theta_R - 90^\circ}{2}$
$10^{-3} P_{m1}$
BRUSH INSTRUMENTS
$-343\times10^{-5} T_{m3}$
$-532\times10^{-2} T_{m2}$
$\frac{\psi_c - 90^\circ}{2}$
$\frac{\psi_R - 90^\circ}{2}$

Figure 74B

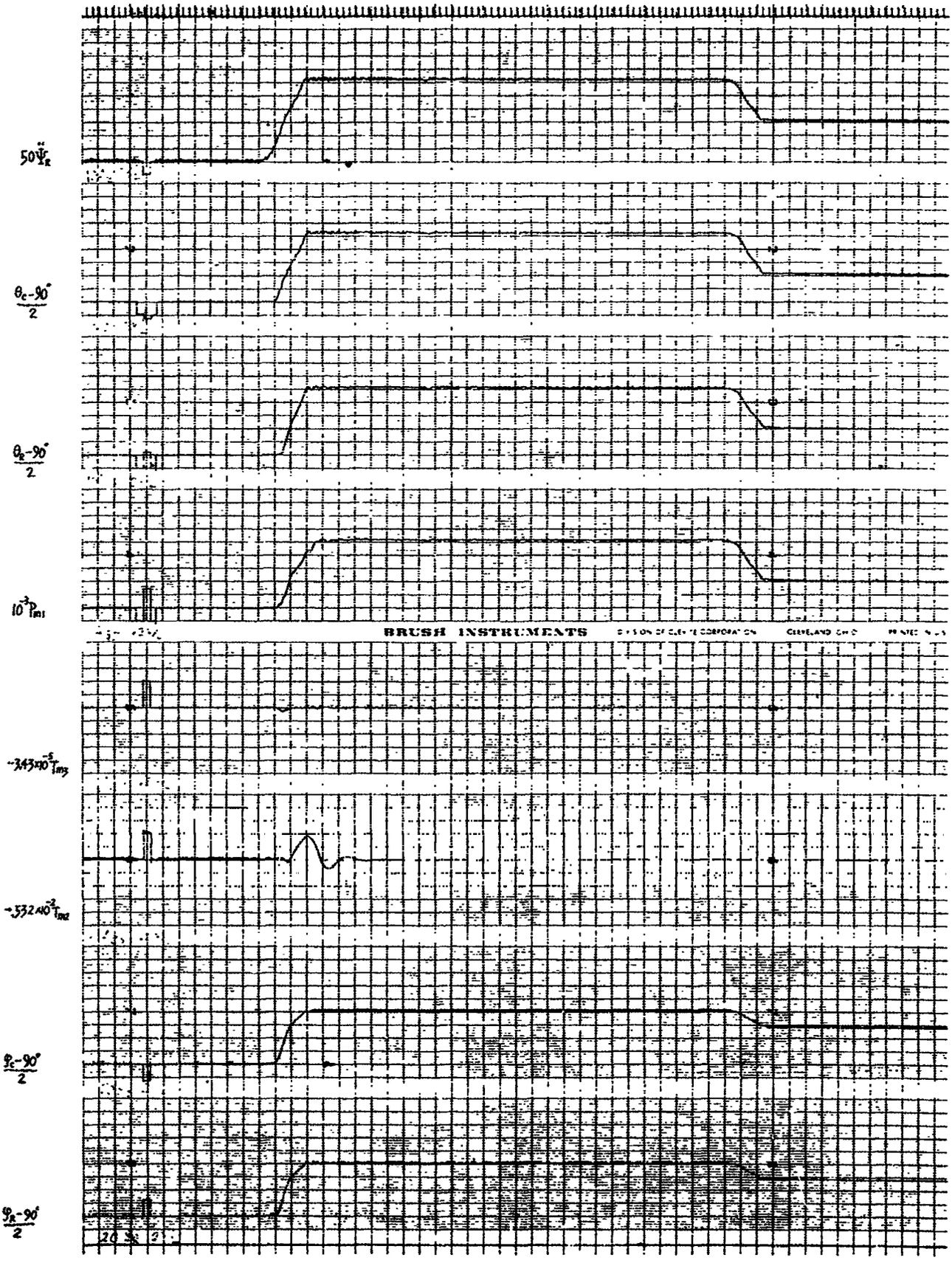
$50\ddot{\psi}_R$
$\frac{\theta_c - 90^\circ}{2}$
$\frac{\theta_R - 90^\circ}{2}$
$10^{-3} p_{ins}$
BRUSH INSTRUMENTS
$-343 \times 10^{-5} r_{ins}$
$-332 \times 10^{-3} r_{ins}$
$\frac{\phi_c - 90^\circ}{2}$
$\frac{\phi_R - 90^\circ}{2}$

Figure 75A

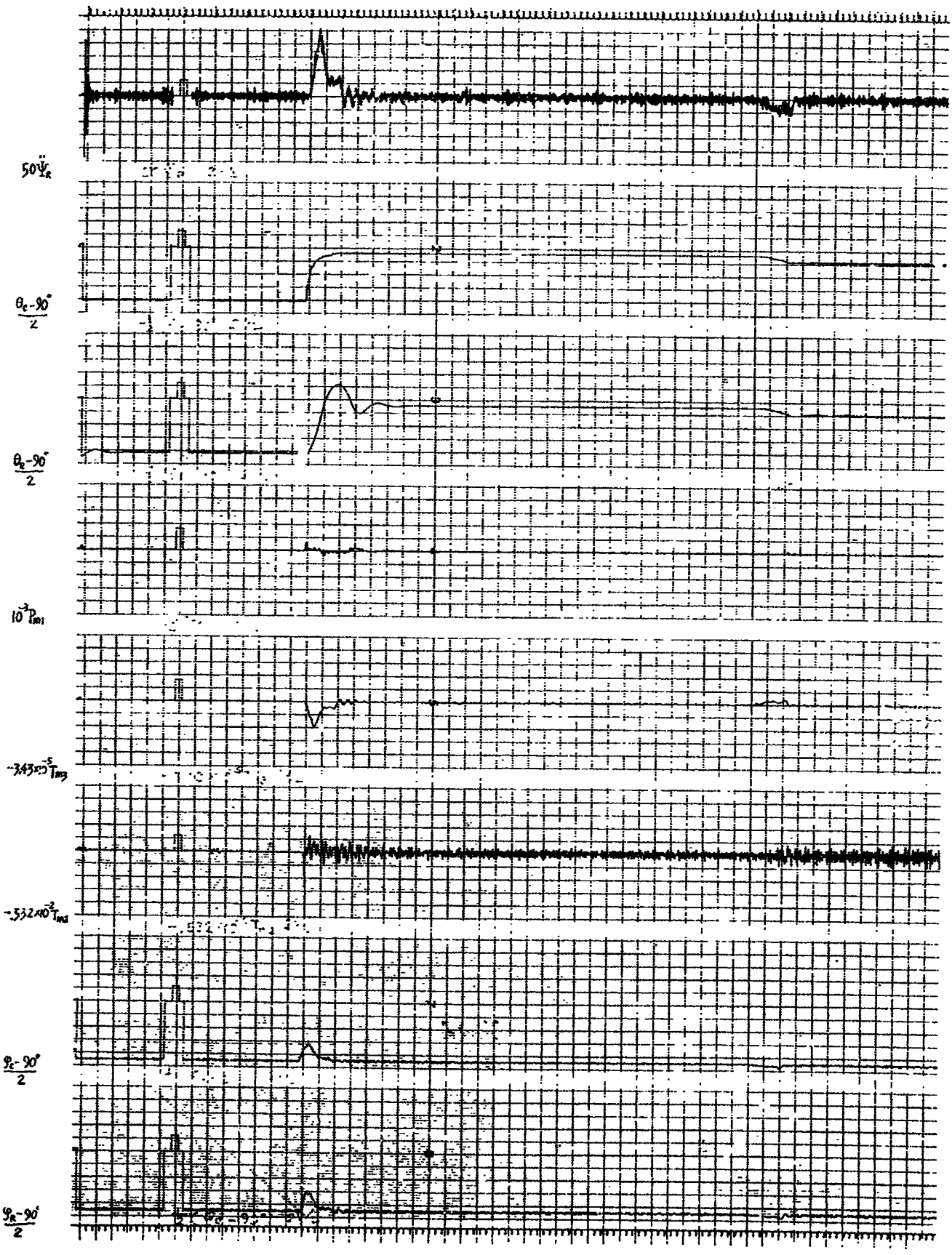
$50\ddot{\psi}_R$
$\frac{\theta_c - 90^\circ}{2}$
$\frac{\theta_R - 90^\circ}{2}$
$10^{-3} P_{m1}$
$-343\times10^{-5} T_{m3}$
$-532\times10^{-2} T_{m2}$
$\frac{\varphi_c - 90^\circ}{2}$
$\frac{\varphi_R - 90^\circ}{2}$

Figure 75B

This maximum value of disturbance torque is very close to the maximum value of system motor torque. Therefore, considering the accuracy of analog computer limiter circuits, the system could either be stable or unstable.

In the case of Figure 74, the system is found unstable, because the disturbance torque is more than the system could handle.

After the first overshoot of θ_R up to 166°, it comes down to 12..8° at the first valley, at which point, the disturbance torque becomes 375×10^3 lb-in (additive), and the system can not overcome it, the response being overshot again. Meanwhile, the pressure of system motor is kept at maximum output and this brings the wobble plate to the maximum position, thus making the system saturate.

In general, therefore, we may assume that when $92.6\ \dot{\psi}_R^2 < 360$, the system is able to overcome gyroscopic torque. That is, when $\dot{\psi}_R < 1.94$, the system is within the stable region with gyroscopic torques.

With a trapezoidal g-profile input, if we let h be the top level in g, the following relationship is valid in steady-state opproximation.

$$\left[\left(\frac{R}{g}\,\dot{\psi}_R^2\right)^2 + 1\right]^{1/2} = h$$

Substituting $\frac{R}{g} = 1.55$ gives:

$$2.42\ \dot{\psi}_R^4 + 1 = h^2$$

$$\therefore \dot{\psi}_R^2 = \sqrt{\frac{h^2 - 1}{2.42}}$$

For $\dot{\psi}_R^2 < 3.89$, we have

$$\frac{h^2 - 1}{2.42} < 15.2$$

$$h < 6.14$$

This indicates that the system is capable of handling disturbance forces when a g-profile input level is less than 6.14 g.

Approximately 1% of the safety margin for other terms of gyroscopic forces has been taken into consideration.

In order to lessen the effect of disturbances and improve the system's performance for a high g-level input, a compensation for disturbance may be helpful. For this purpose, the compensation may be computed using responded values rather than commands for each system for effective results, because of differences between command and response, particularly of the 1st axis system.

The compensation signal may be fed into the summing point of the system's pressure feedback.

(6) "g" Profile Test Results

The centrifuge test results are shown for 30 profiles. Additional runs are included to indicate the type of difficulties encountered by the system just before becoming unstable. For every run, a recording is included of the gyroscopic torques developed in both the first and second axis systems. The output g profile has been superimposed upon the input g profile in the form of a dashed

line. This also applies for the $\dot{\psi}$ and $\ddot{\psi}$ recordings as superimposed upon the same input g profile in which $\dot{\psi}$ is a dashed line and $\ddot{\psi}$ is a dash-dot line.

I. Digital Flow Diagram for Control Computer

The flow diagram for the control computer is shown in Figure 53. This is shown in block diagram form in which each block indicates the information received, the operation to be performed upon this information and where the information is to be sent. Figure 54 is the flow diagram for computing the feed forward compensation for gyroscopic forces in the first axis where these forces do not exceed the torque limitations of the system.

J. Conclusions and Recommendations

The analysis of the first and second axis systems indicates that they have relatively low damping and due to this some difficulties in the generation of g profiles by the centrifuge are encountered. Further limitations were necessarily imposed upon these two systems in order to prevent loss of control due to system saturation incurred by large command signals. The large unbalance in the inertia load of the first axis system has caused excessive gyroscopic torques to be subjected to the first axis system thus limiting the combined factor of g rate, maximum g level and length of time in the g rate period. Once the gimbal position is past the critical angle of 45 degrees these factors are greatly reduced as can be observed in several of the recorded profiles.

Of particular interest in this respect is profile No. 4 in which the effect of the gyroscopic forces on the first axis system

are very close to the maximum that the system can sustain. The gimbal axis oscillates violently but does manage to dampen to a final angle close to 90 degrees. Later in the same profile the same g rate is required to go to an even higher g level. The command angle of the gimbal system remains close to 90 degrees, and it can be observed that no violent oscillations appear in the output g profile. The output g level matches very closely to the input command g profile.

The main axis drive system is capable of meeting the maximum g rate specified for these tests. As in the first and second axes drive systems a limit circuit is necessary to prevent loss of control due to input commands that would saturate the system. The system was tested with a ramp similar to the special profile which reaches a maximum level of 30 g. The main arm drive system performed this profile with the current limiting solidly at both $\pm$ 15,000 amperes. However in the centrifuge simulation the special profile caused the main arm system to become unstable during the deceleration portion of the profile. It was found in the preliminary studies that the system would not settle until approximately 3 seconds after the 30 g level had been reached by the input command signal. During this 8 second period, the armature current is first in the +15,000 ampere limit followed by a rapid excursion to the -15,000 ampere limit. The special profile has a dwell time of only 2 seconds at the 30 g level after which a rapid deceleration is required by the command signal. It is possible that the system became unstable due to this excessive deceleration command which would cause saturation. Reduction in the control computer system error limit would maintain

stability for this particular profile. In this same profile (No. 12), the 1st and 2nd axes angle commands suddenly drives the angle to 180° out of phase. This is caused by possible malfunction of computer elements used in the special circuits of the control computer and also by the inability of the main arm to follow the input command. The acceleration signal $\ddot{\psi}_c$ becomes excessively large in the negative direction thereby causing the angle command to move out of phase by 180°.

The main arm drive system in conjunction with the control computer is capable of producing an acceleration vector that is in very close agreement with the input acceleration command. The concept of using the main arm drive system and control computer in a closed loop system provides for an extremely tight system with minimum error.

Since limitations were met in the effect of gyroscopic forces and also control system response, not all of the 35 profiles were run. Instead some 30 profiles were recorded out of a total of 57 runs. In these recordings the gyroscopic torque is shown for both the first and second axes. In cases where the gyroscopic forces would cause system instability, the forces were recorded even though the effect was not coupled into the simulation. In this manner the configuration of g profile that is satisfactory for this particular centrifuge design can be determined.

The analog simulation of this centrifuge required the use of many multipliers. Several of these are of the servo type in which the measured time delay was approximately 0.1 second. The

simulation therefore includes a delay similar to that expected in the digital control of the actual centrifuge system.

In final summation it can be stated that:

(1) the centrifuge can produce a 30 g maximum acceleration;

(2) first and second axis systems have considerable overshoot which is detrimental to the centrifuge performance;

(3) error limits on the 1st and 2nd axis systems are necessary to prevent saturation and loss of control. These error limits cause loss in speed of response for these systems;

(4) an error limit is required in the control computer system to prevent instability of the main arm drive system.

(5) gyroscopic forces are not of sufficient magnitude in the gondola system or the main arm drive system to be considered of importance.

(6) gyroscopic forces are extremely important in the gimbal system. In many profiles the motor torque limit is reached due to these forces thus negating the use of compensation to correct for these effects.

(7) the control computer has been successfully developed and in conjunction with the main arm system the acceleration profiles can be accurately followed within the limits of the capabilities of the hardware.

Recommendations for this centrifuge design are as follows:

(1) Since the first axis system is underdamped and its effect upon the output g profile is quite serious, the input command to the first axis system should be in the form of a ramp thereby reducing the amplitude of overshoot.

(2) The gyroscopic forces developed in the first axis system are very serious when the first axis angle is less than 45°. By limiting the g level to approximately 2 g until the first axis has reached 45° the effect of gyroscopic forces can be minimized.

(3) It may be possible to develop equations for the control computer to limit the gyroscopic forces effect on the 1st axis system.

John Stone
Project Leader

Approved by:

W. C. Reisener, Jr., Manager
Control Systems Laboratory

C. W. Hargens, III
Technical Director

J. R. Feldmeier
Director of Laboratories

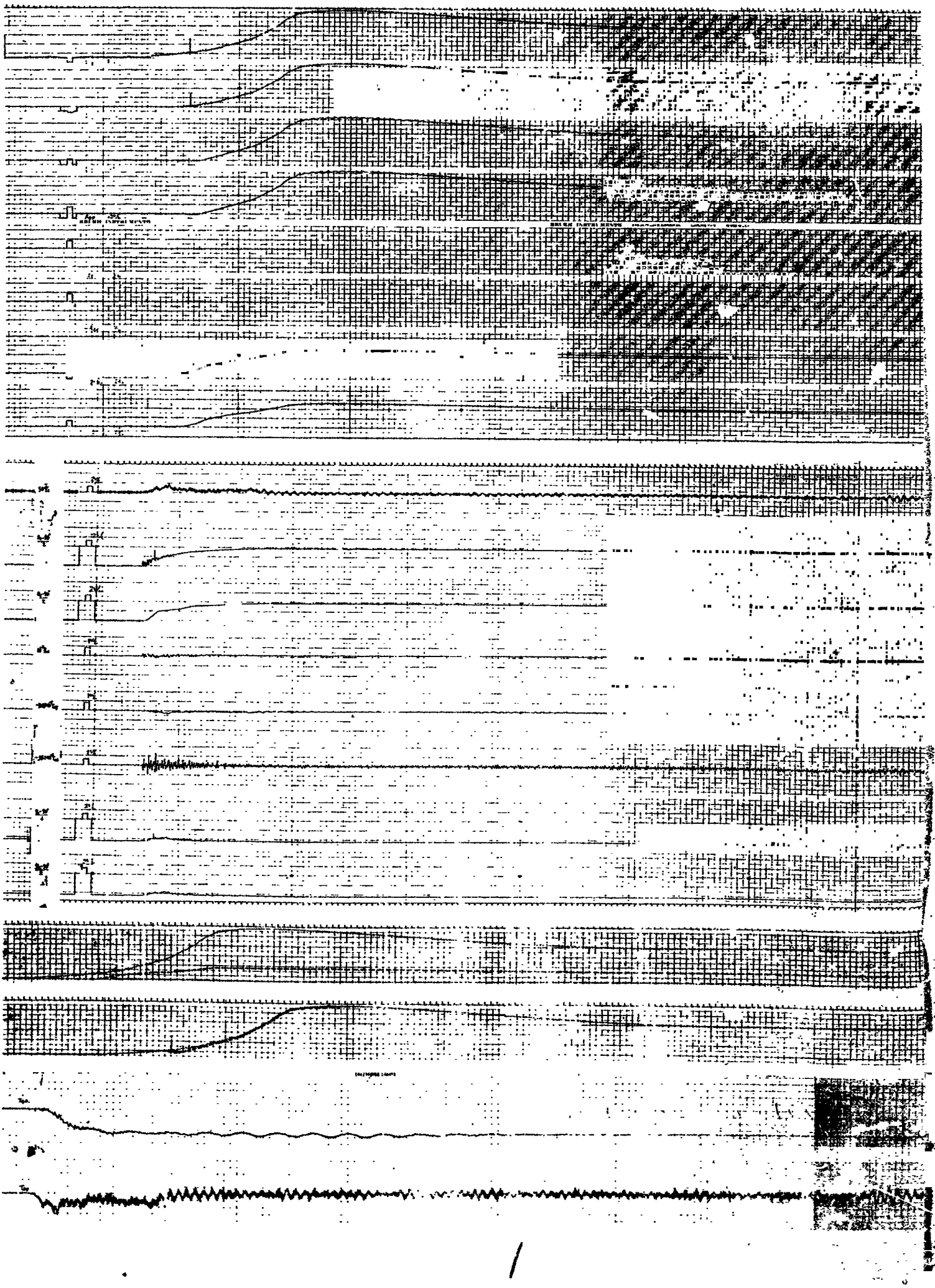

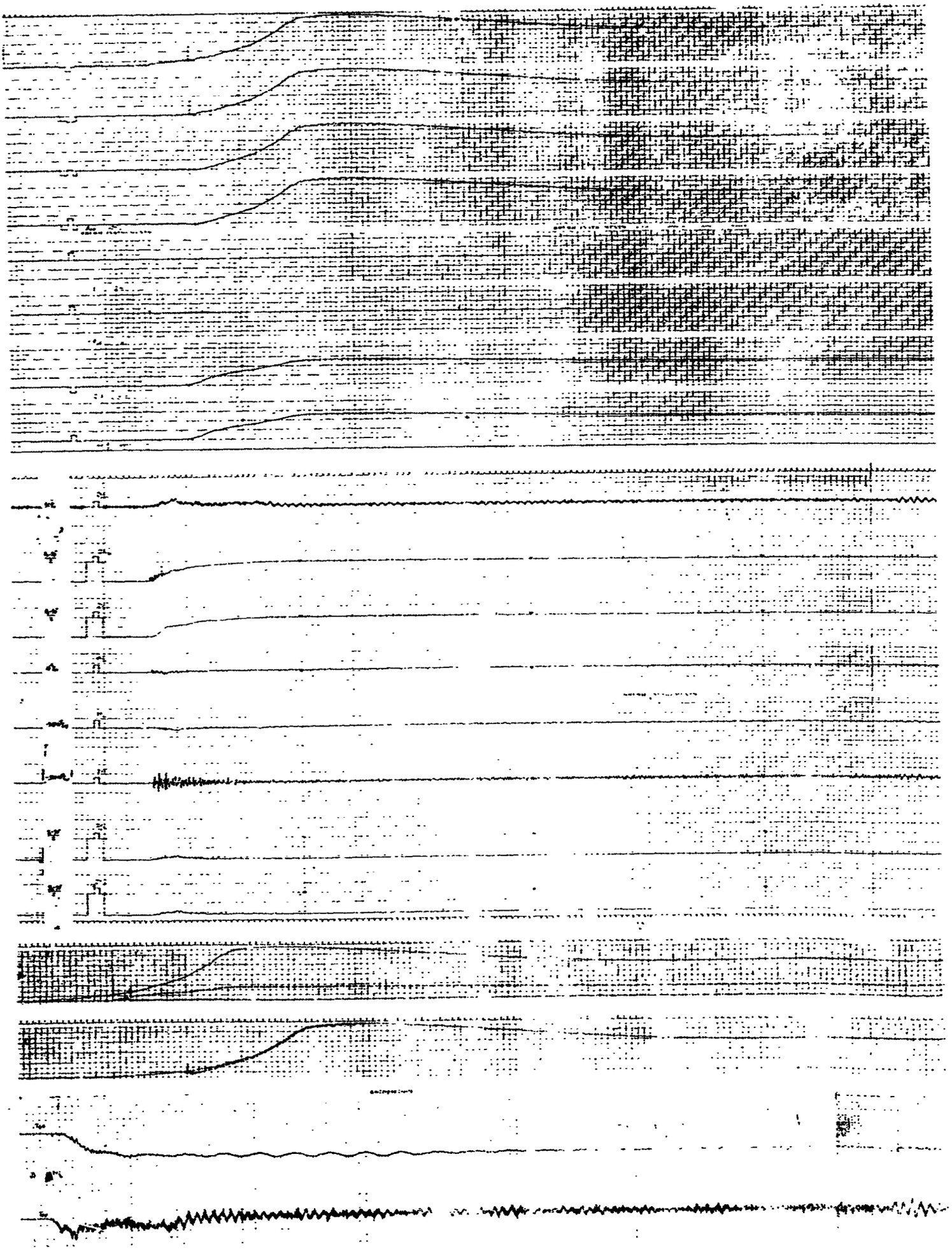

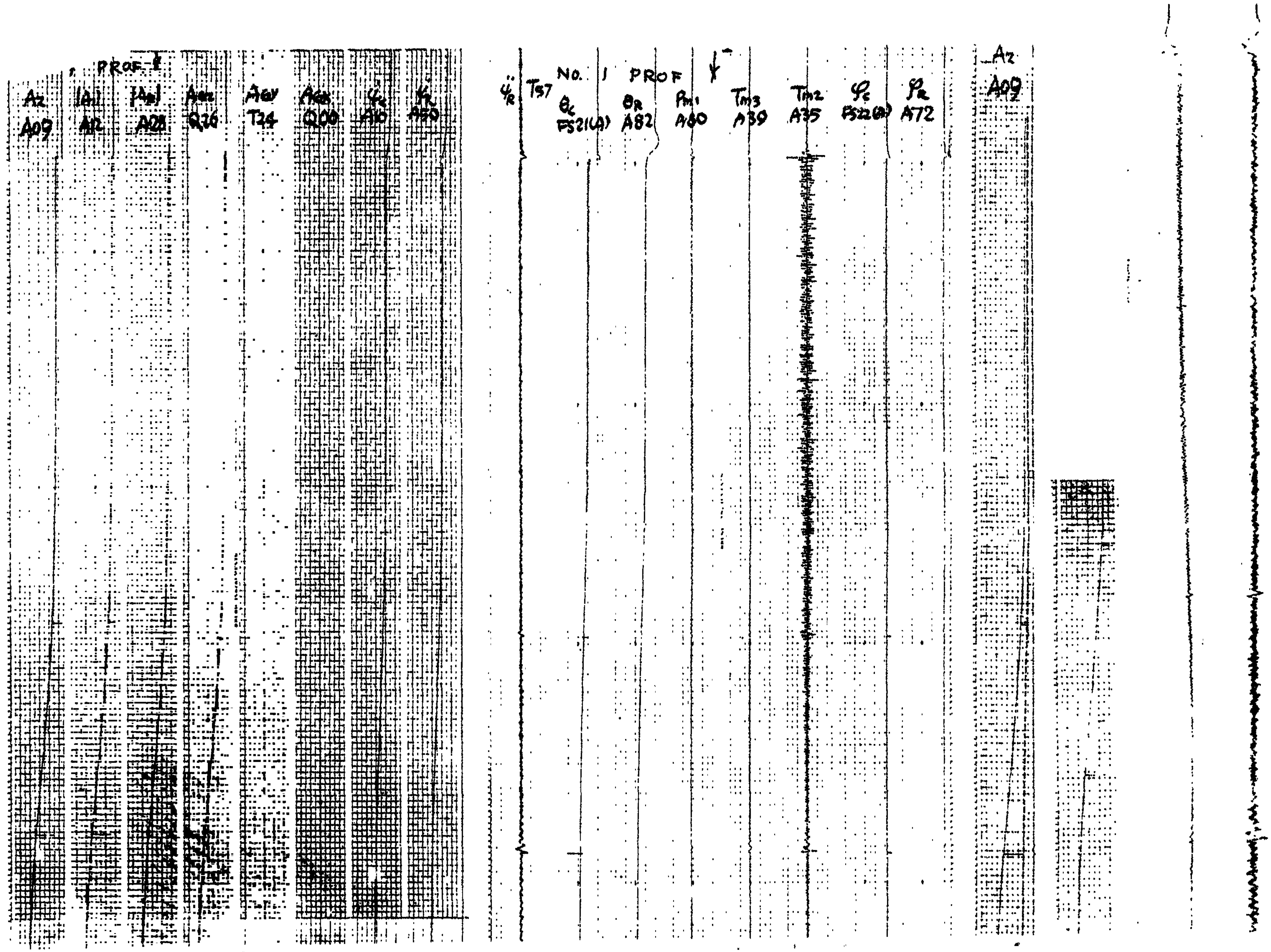
PROF
No. 1 PROF
A09
A12
A28
Q36
T24
Q00
A10
A80
T57
F521(A)
A82
A60
A39
A35
F522(B)
A72
A09

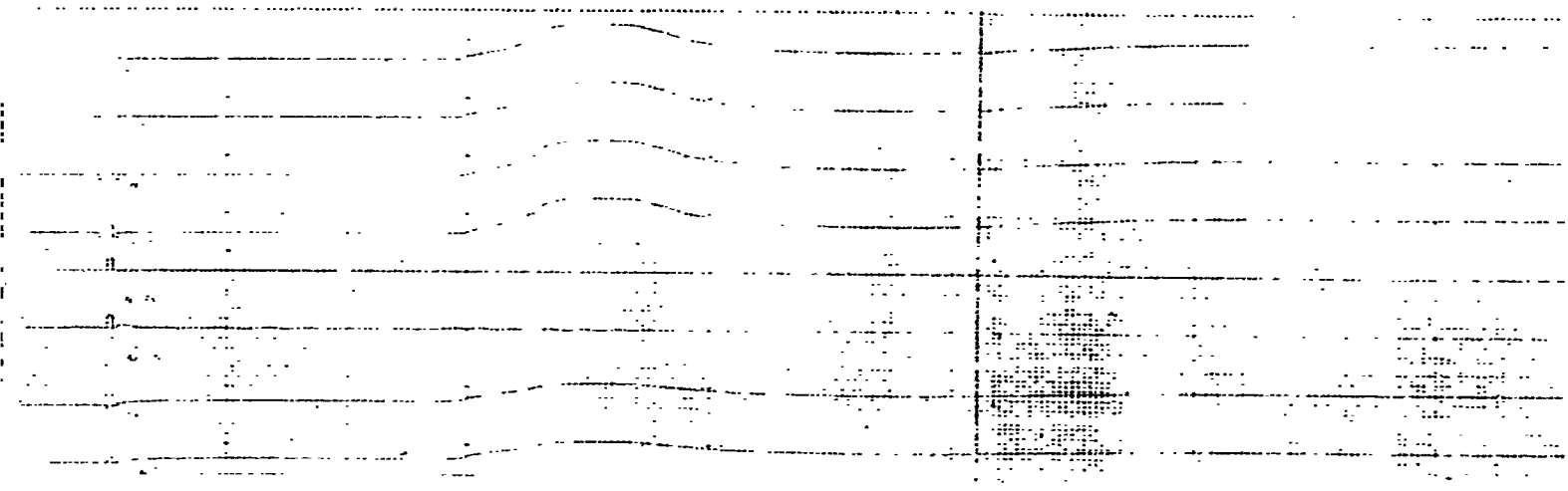

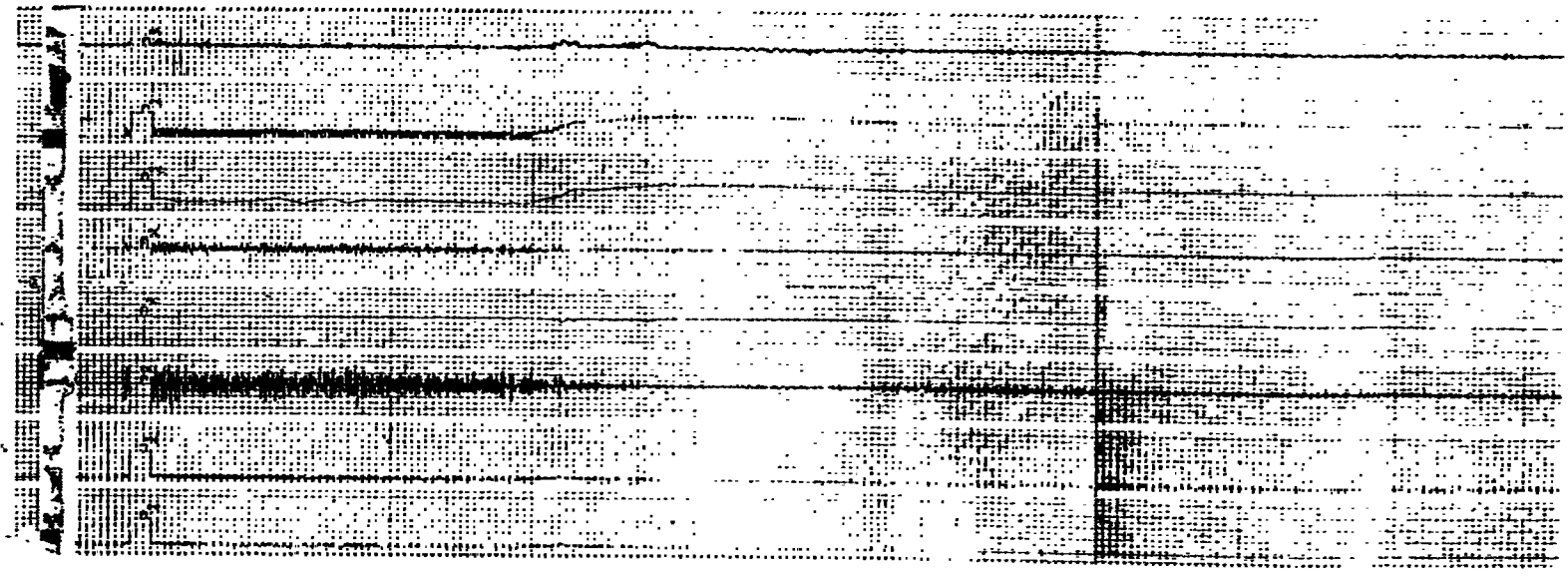

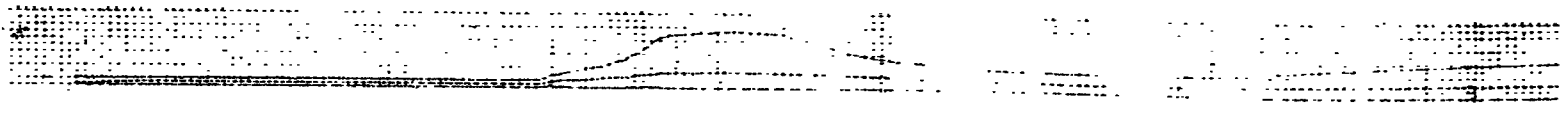

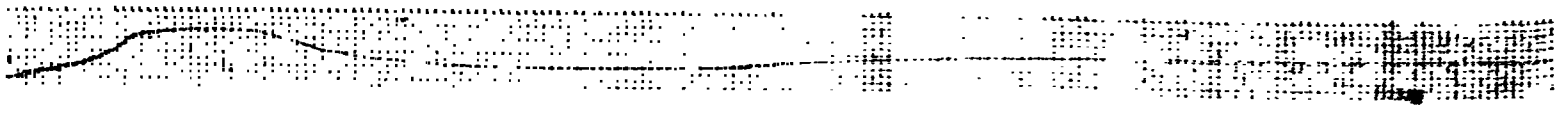

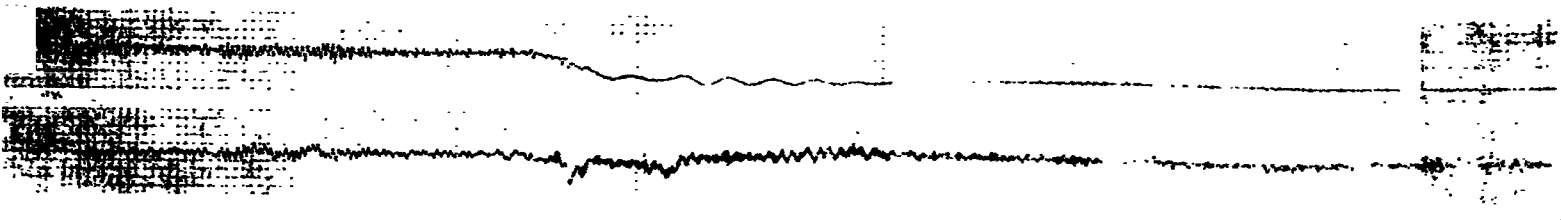

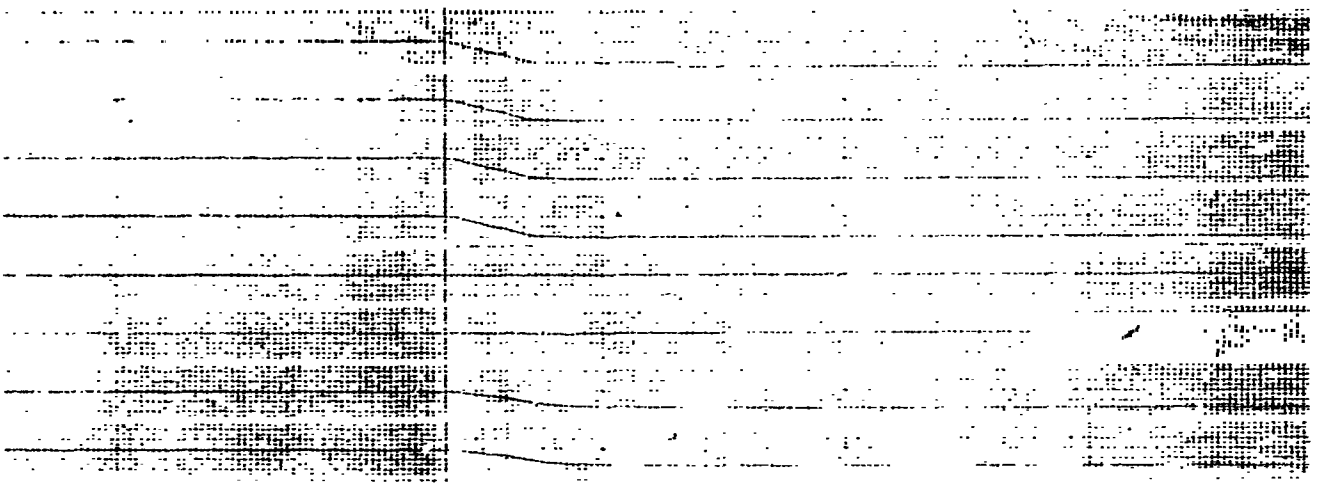

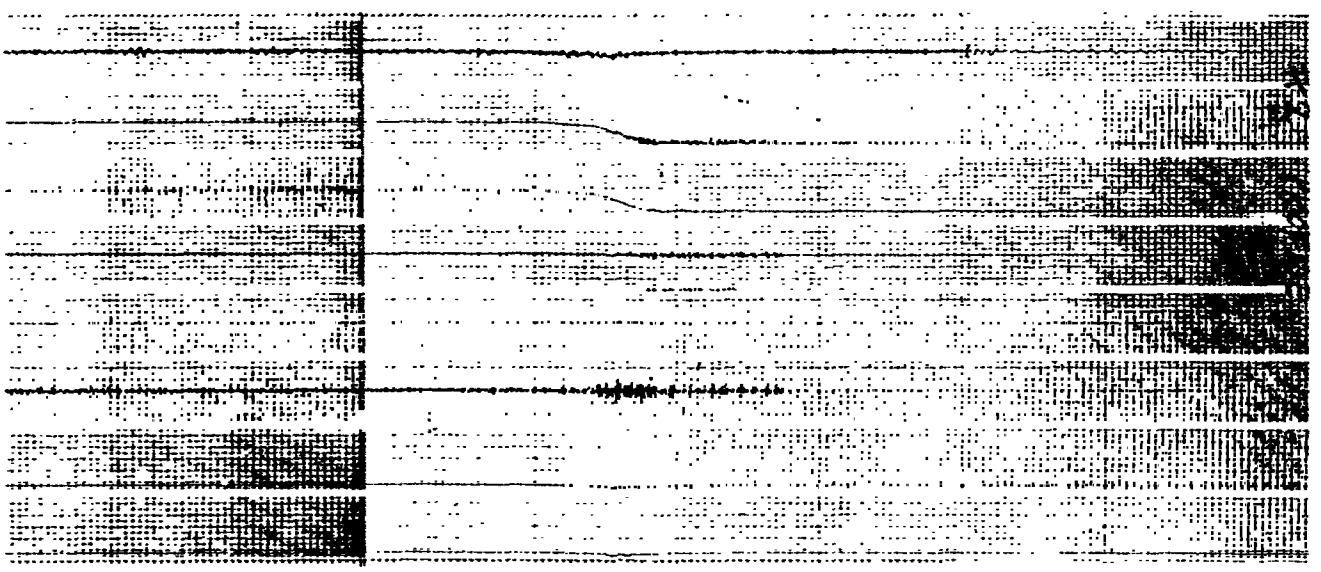

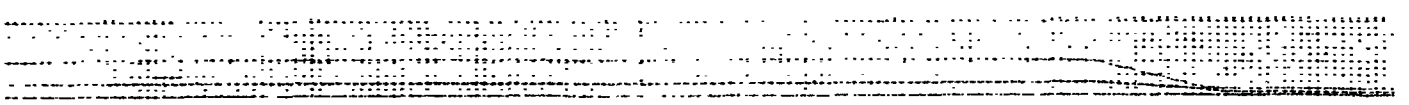

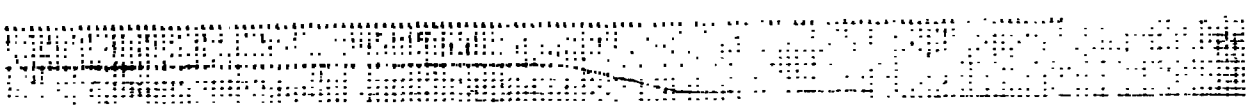

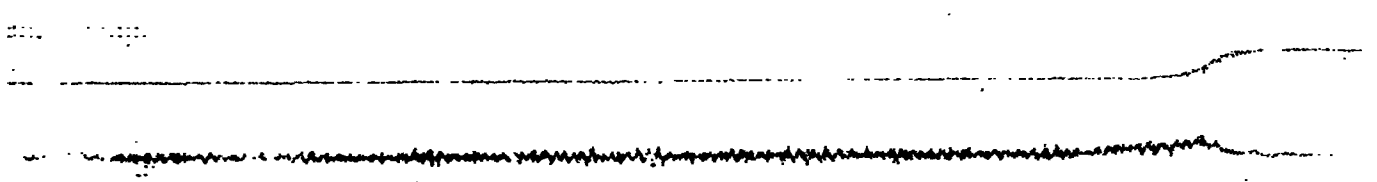

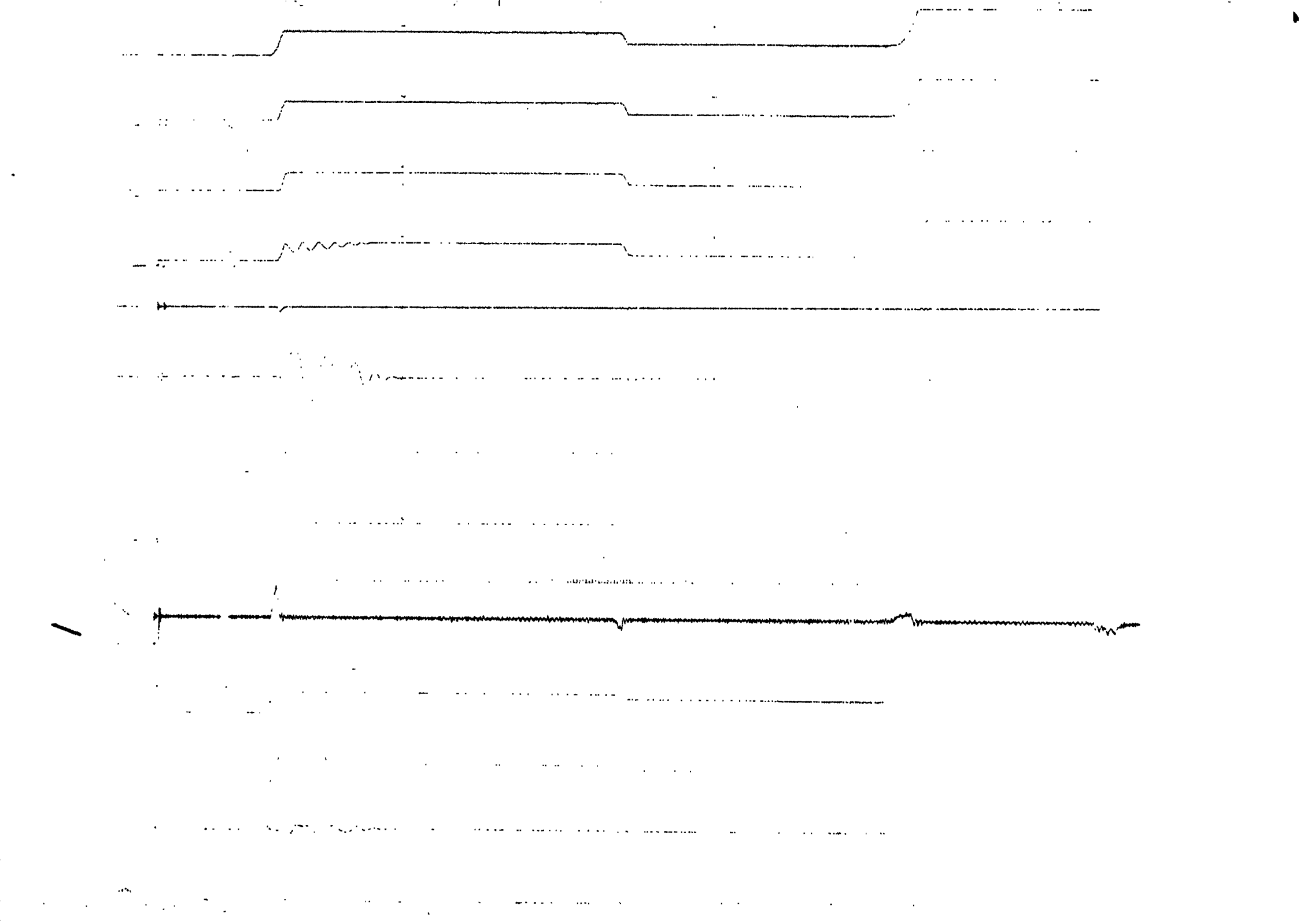

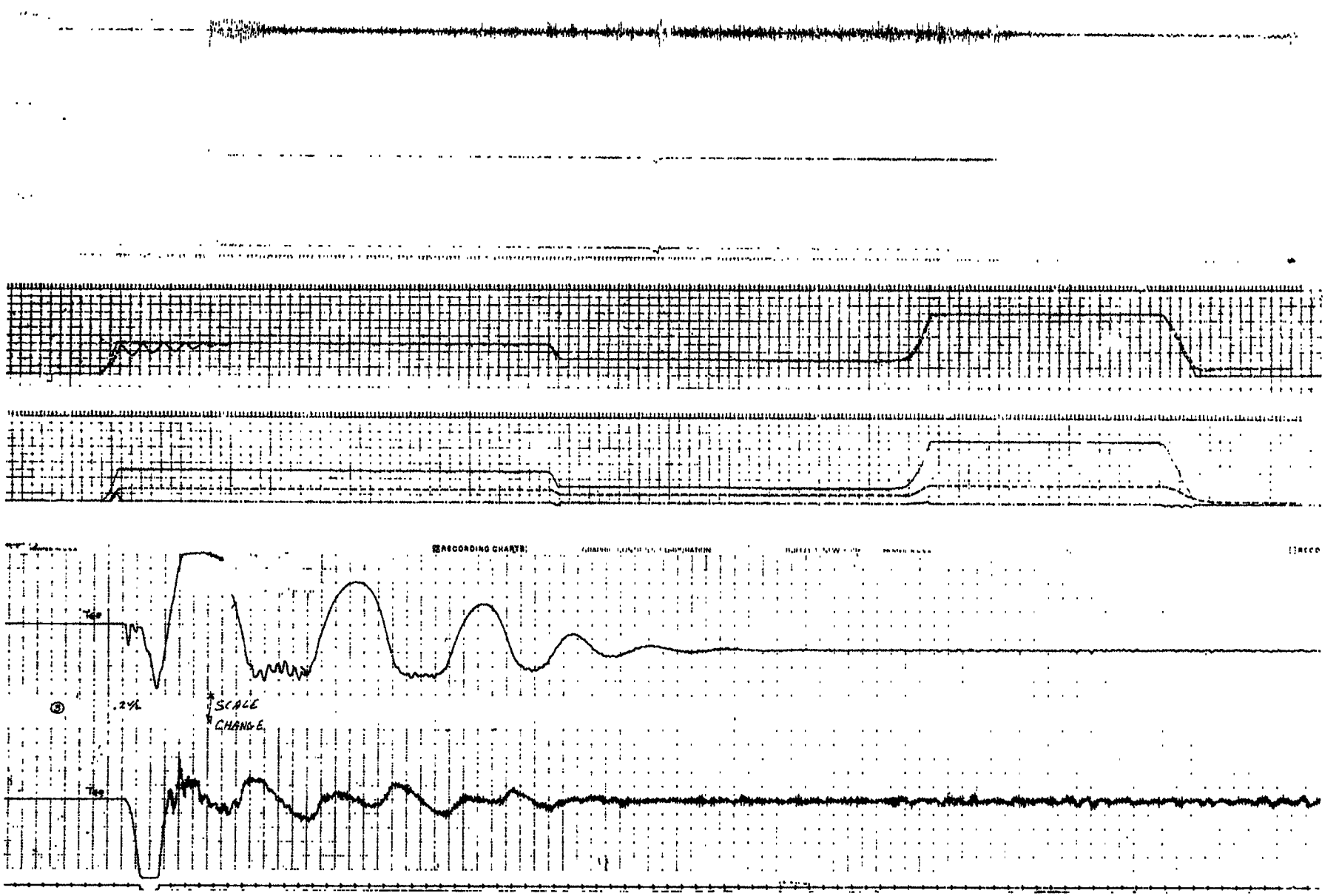
RECORDING CHARTS
.2%
SCALE
CHANGE

#4 (A70 - 1ST AXIS SAT.

#4 (A70

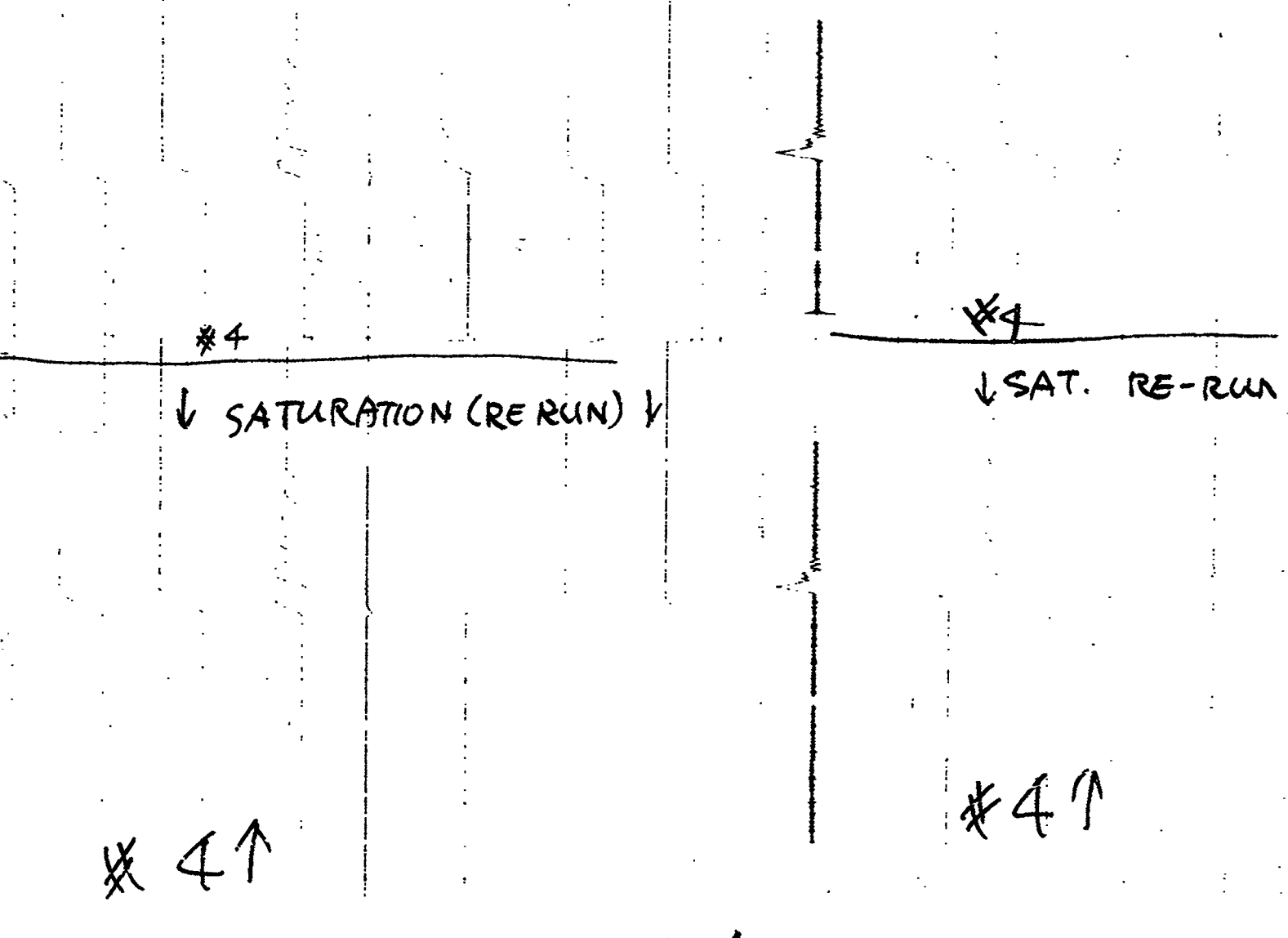

SAT.)

2

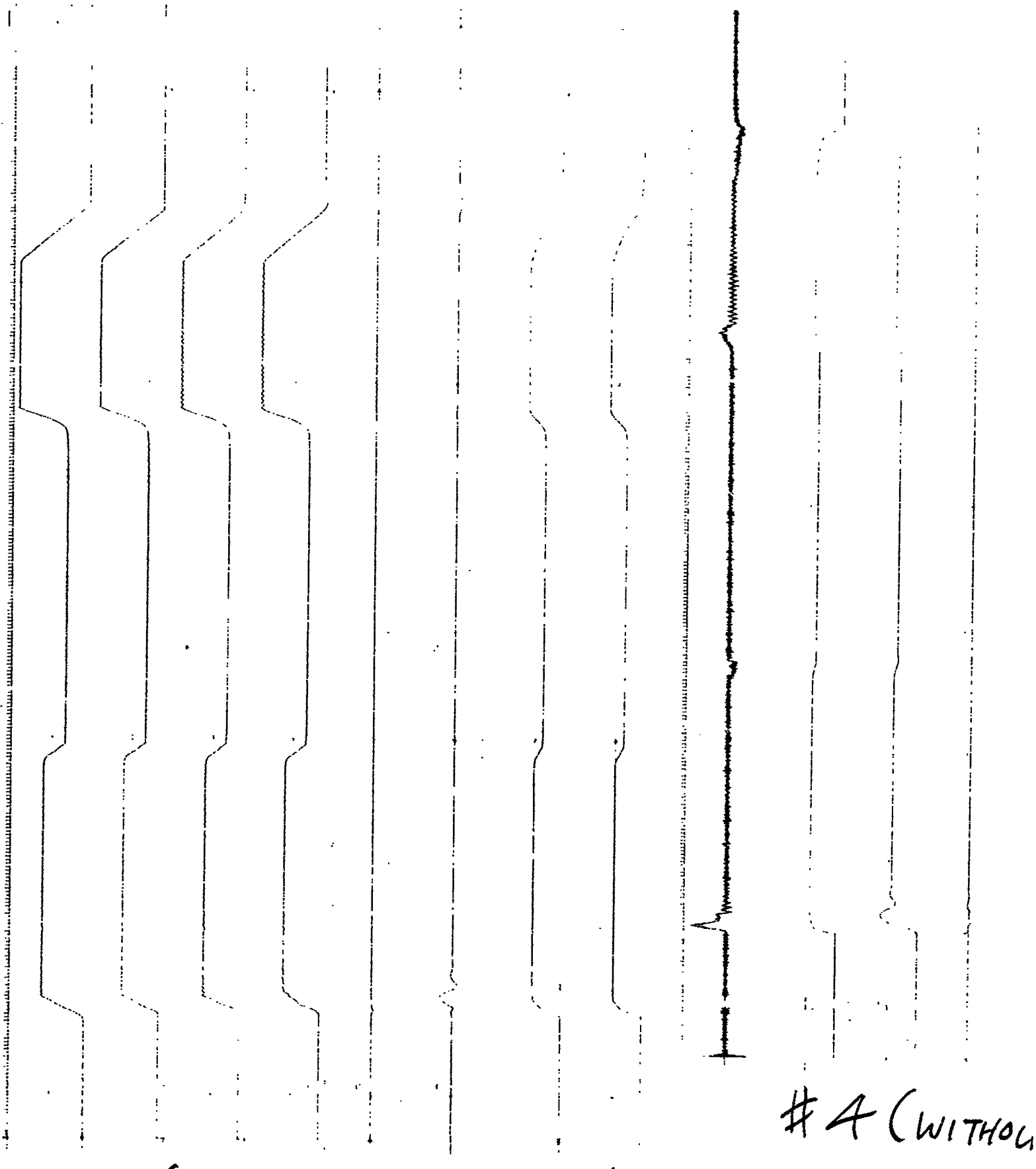

#4 (WITHOUT GYRO TORQ.)

#4 (WITHOU

/

IT GYRO TORQ.)

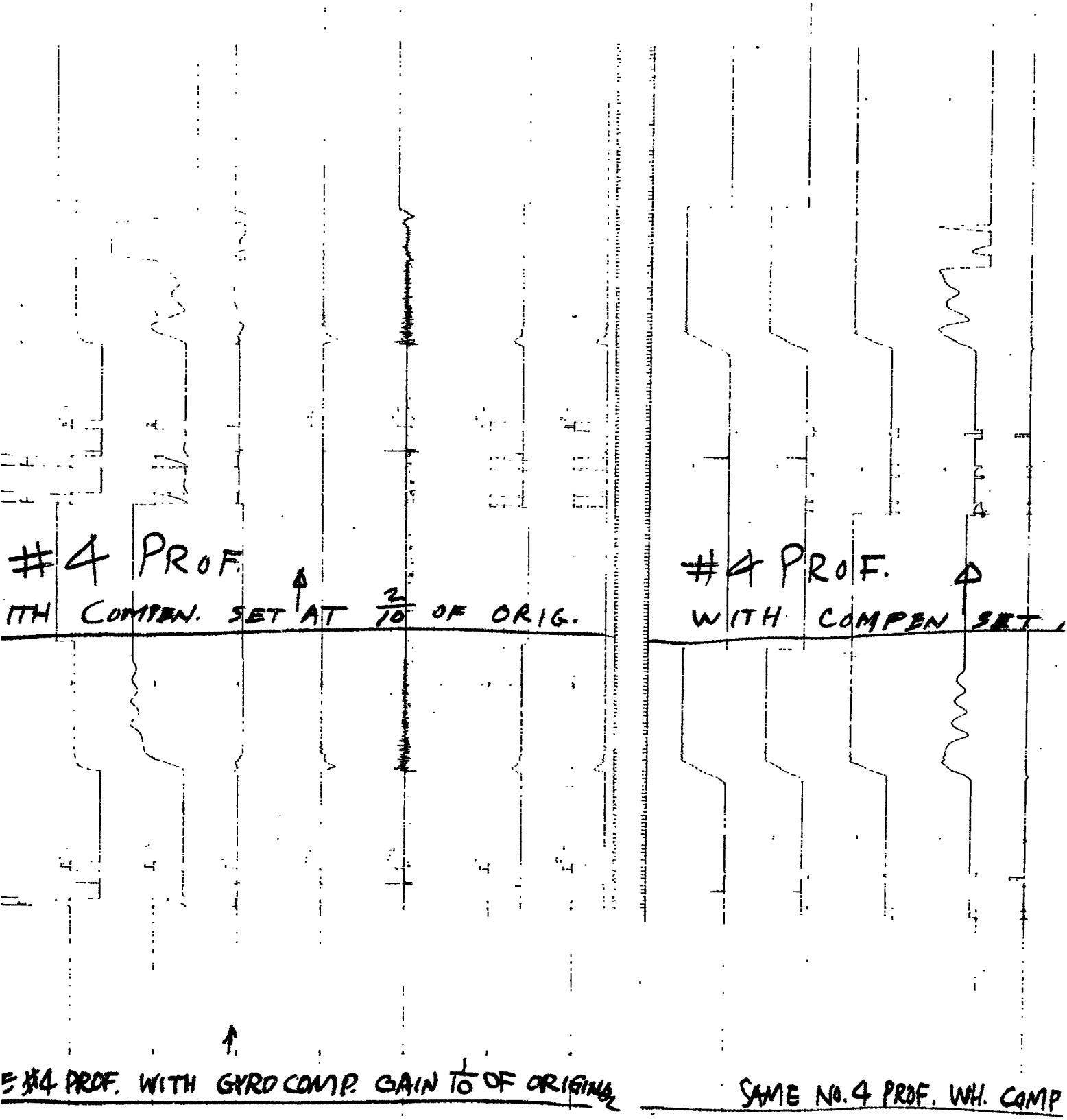
#4 PROF.
ITH COMPEN. SET AT 2/10 OF ORIG.
#4 PROF.
WITH COMPEN SET
E #4 PROF. WITH GYRO COMP. GAIN 1/10 OF ORIGINAL
SAME NO. 4 PROF. WH. COMP

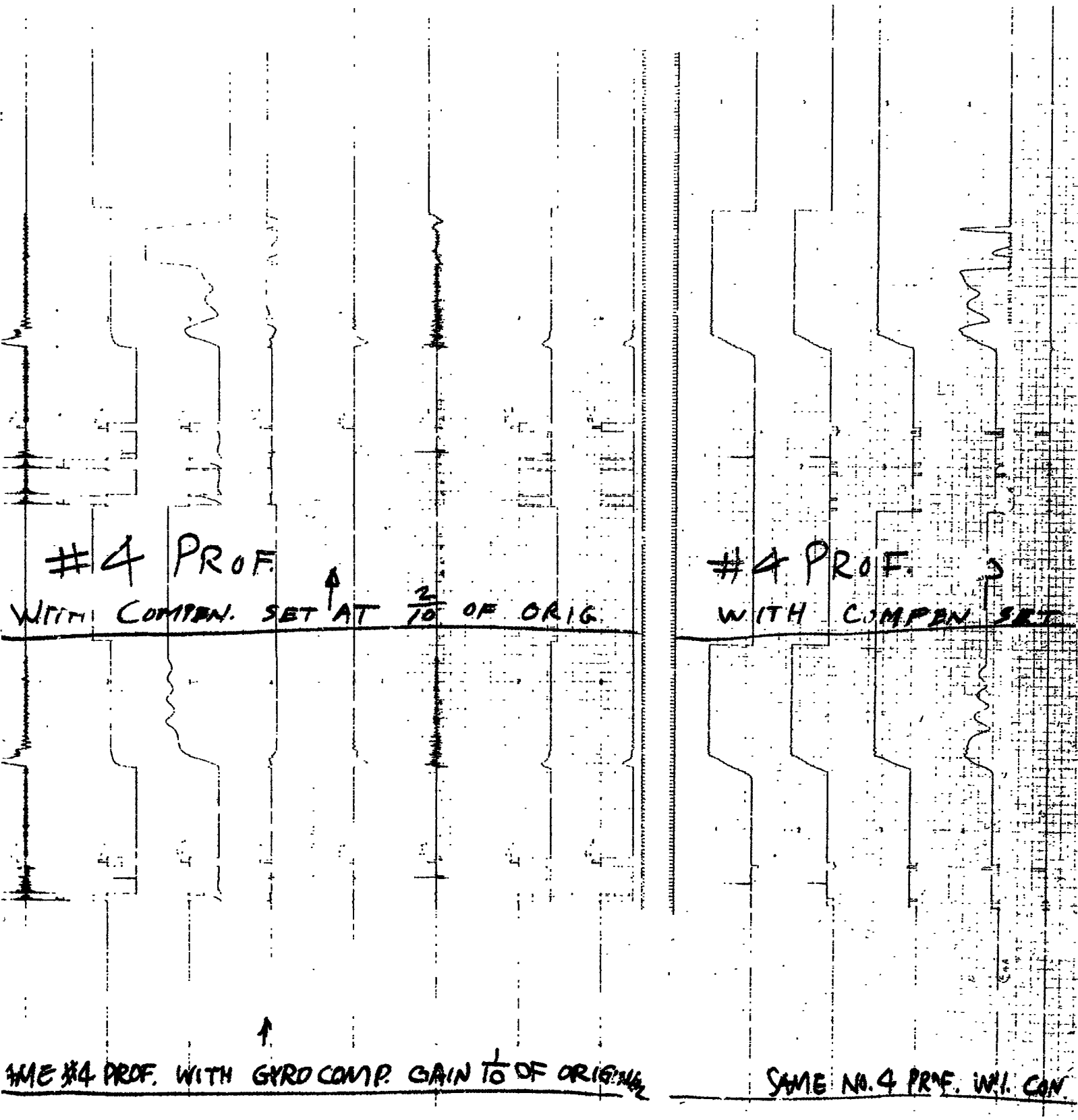
#4 PROF.
WITH COMPEN. SET AT 2/10 OF ORIG.
#4 PROF.
WITH COMPEN SET
SAME #4 PROF. WITH GYRO COMP. GAIN 1/10 OF ORIG.
SAME NO. 4 PROF. W.I. COM.

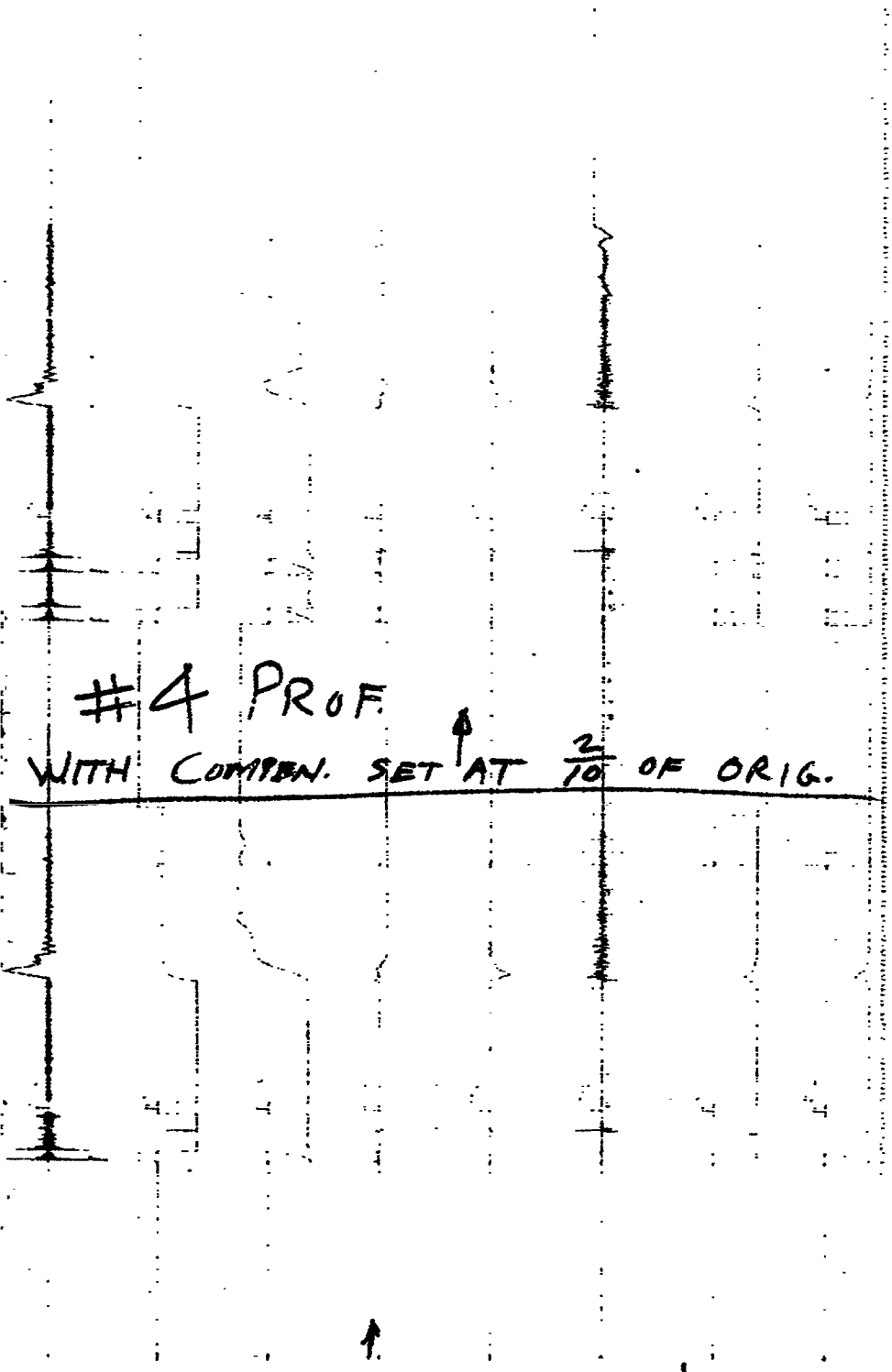
#4 PROF.
WITH COMPEN. SET AT 2/10 OF ORIG.

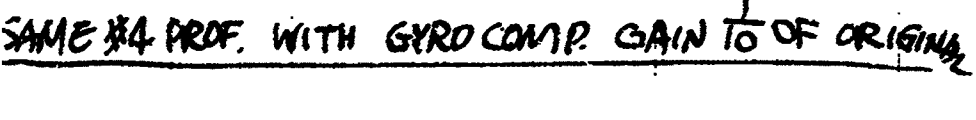
SAME #4 PROF. WITH GYRO COMP. GAIN 1/10 OF ORIGINAL

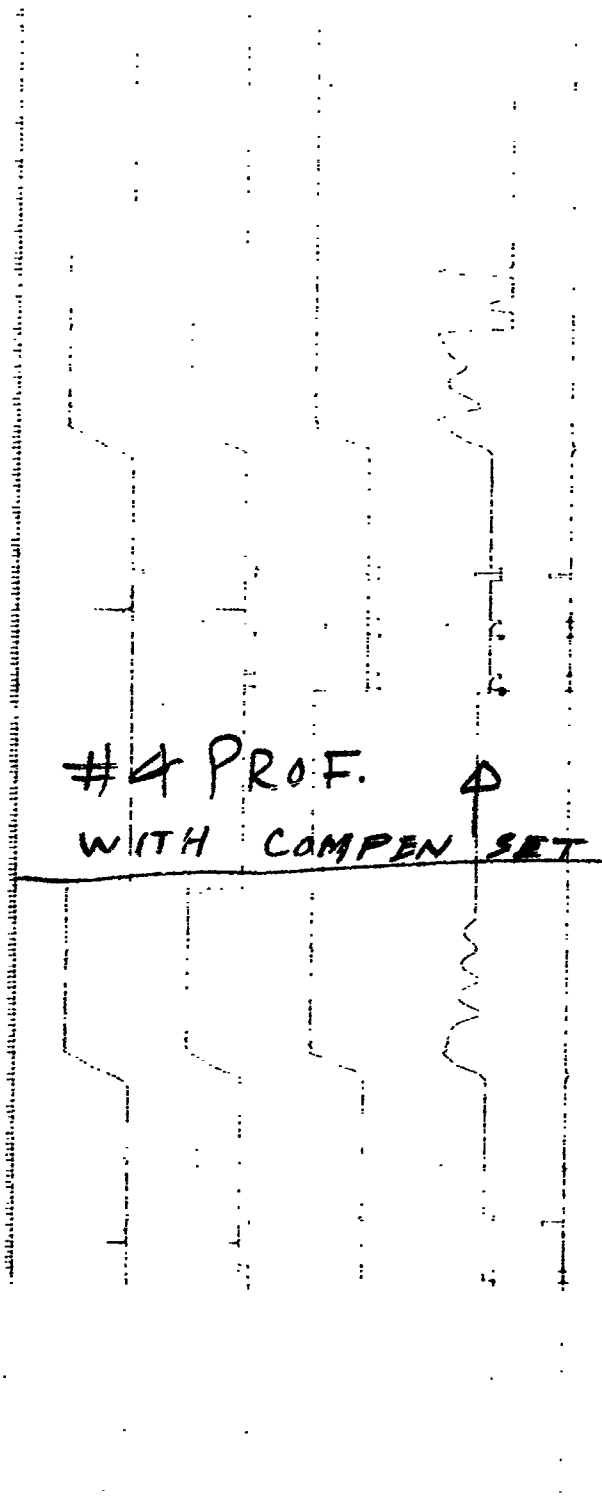
#4 PROF.
WITH COMPEN SET

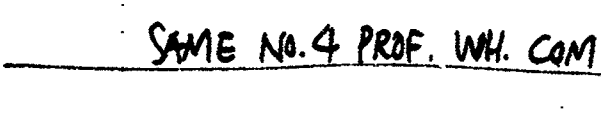
SAME NO. 4 PROF. WH. COM

/

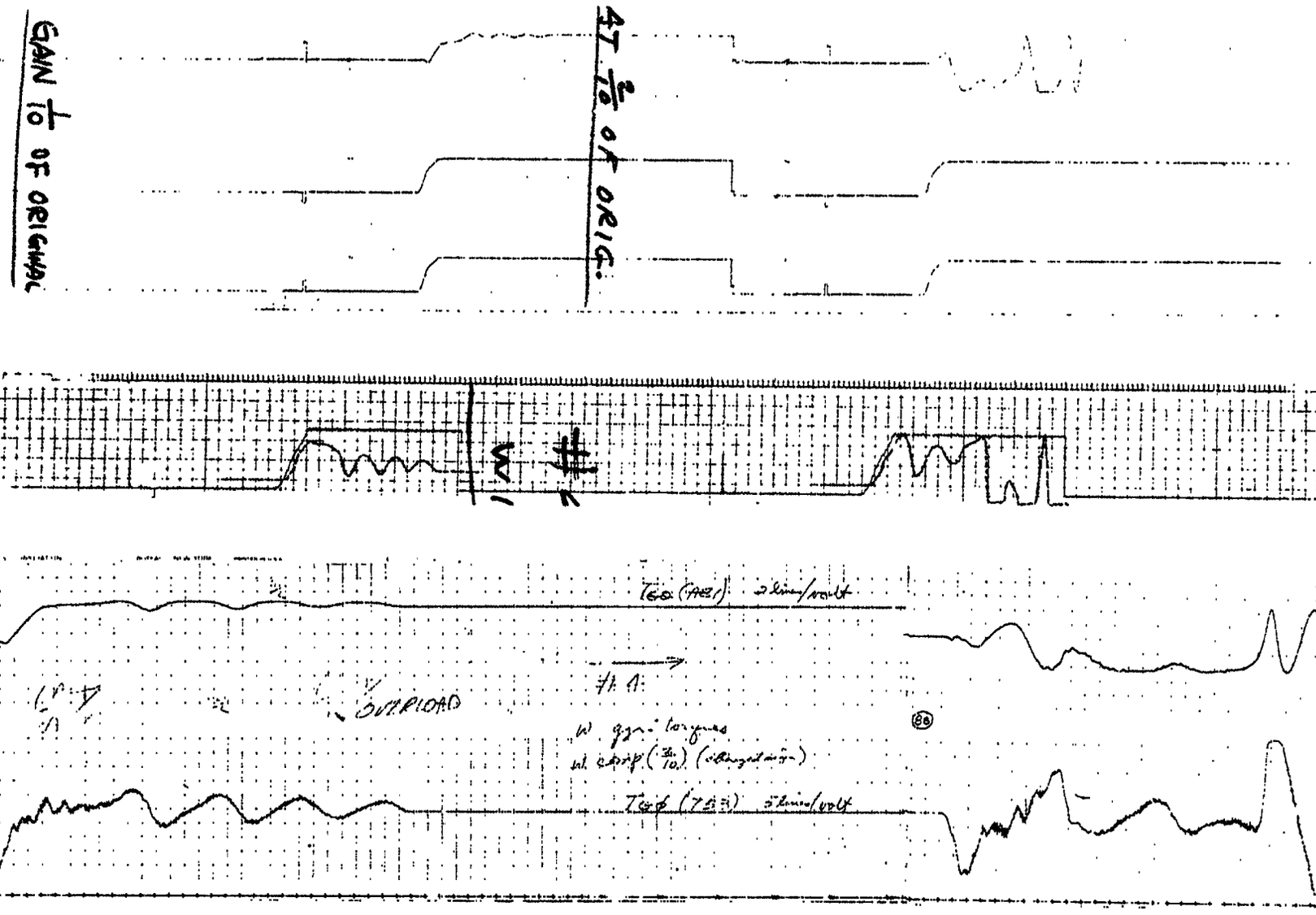
GAIN 1/10 OF ORIGINAL
AT 1/2 OF ORIG.
OVERLOAD

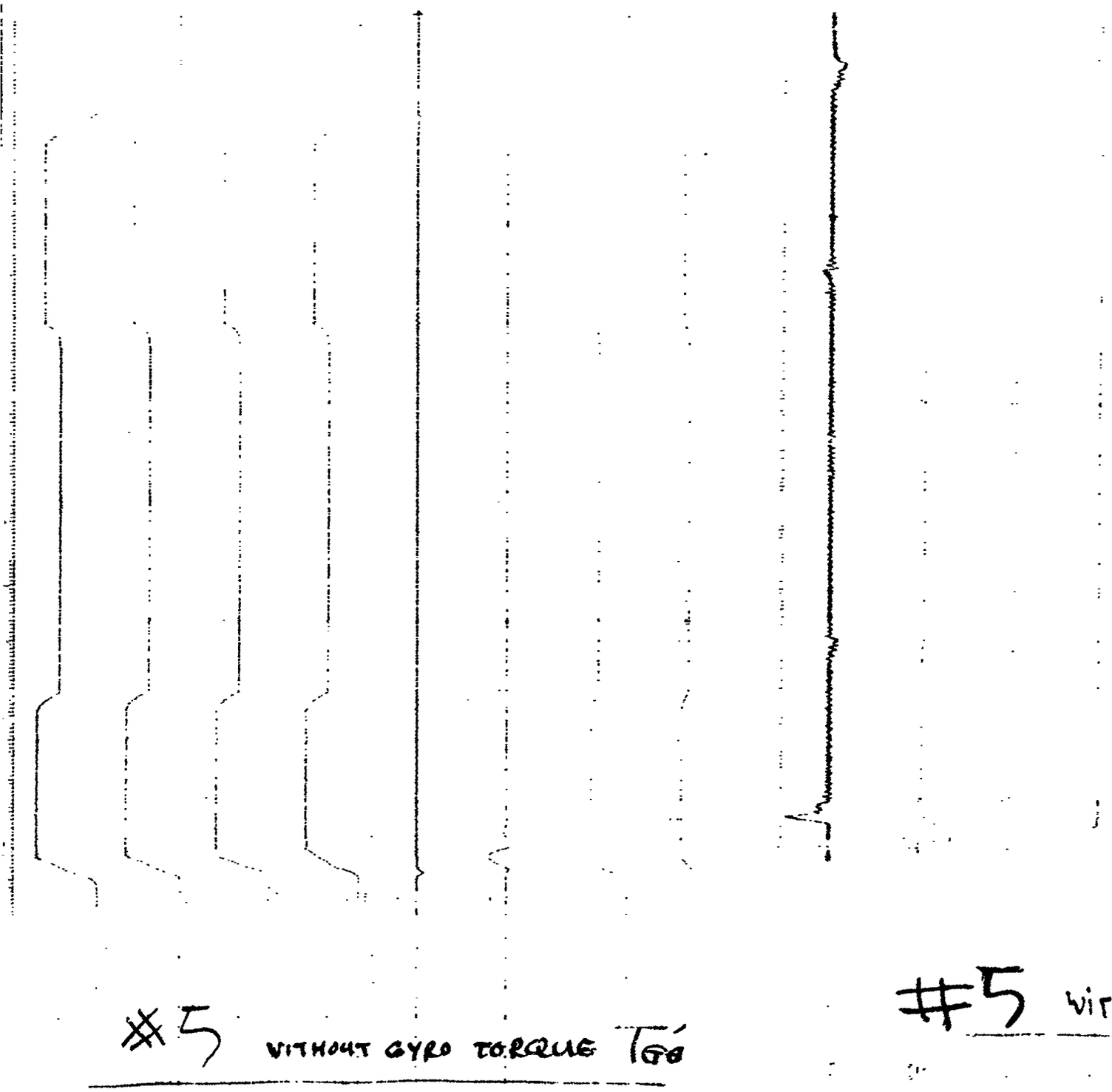

#5 WITHOUT GYRO TORQUE TG6

#5 WITHOU

1

GYRO TORQUE(T_{GO})

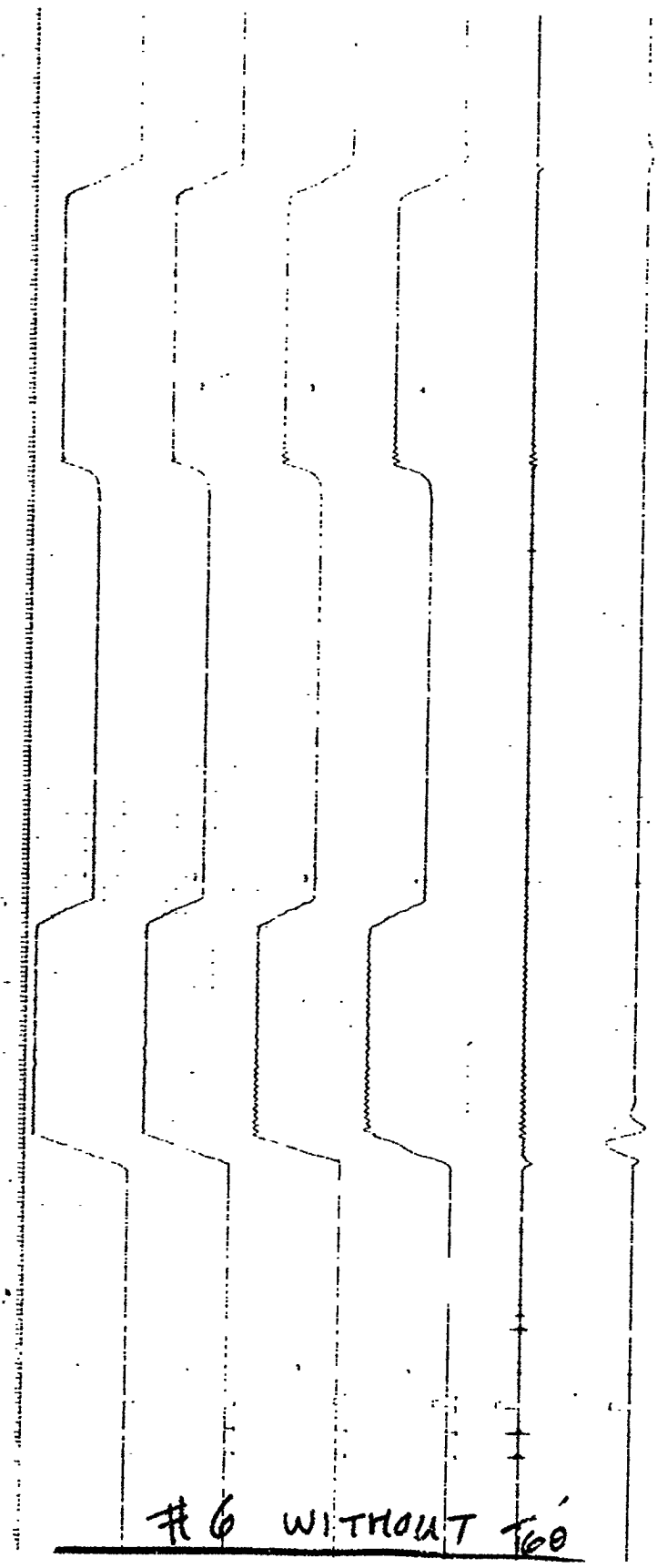
#6 WITHOUT T60

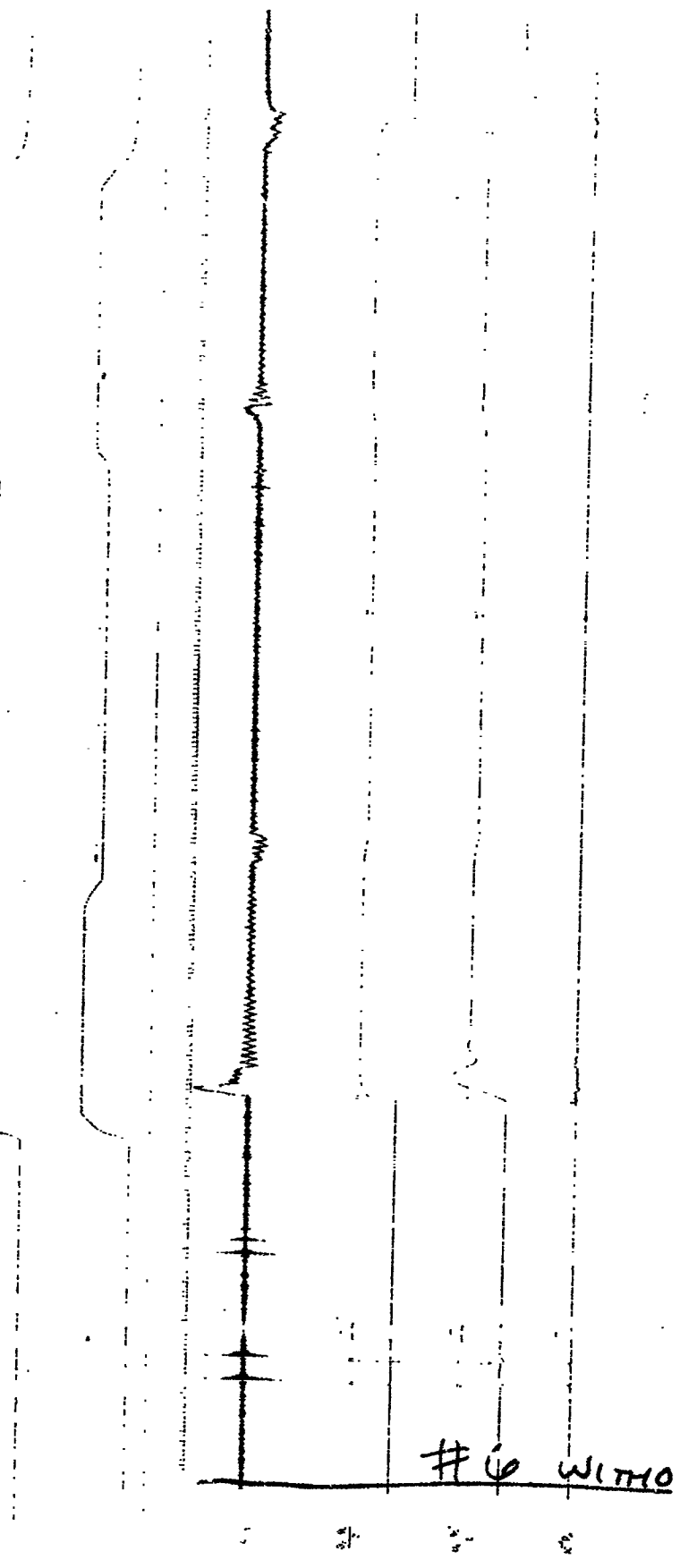
#6 WITHO

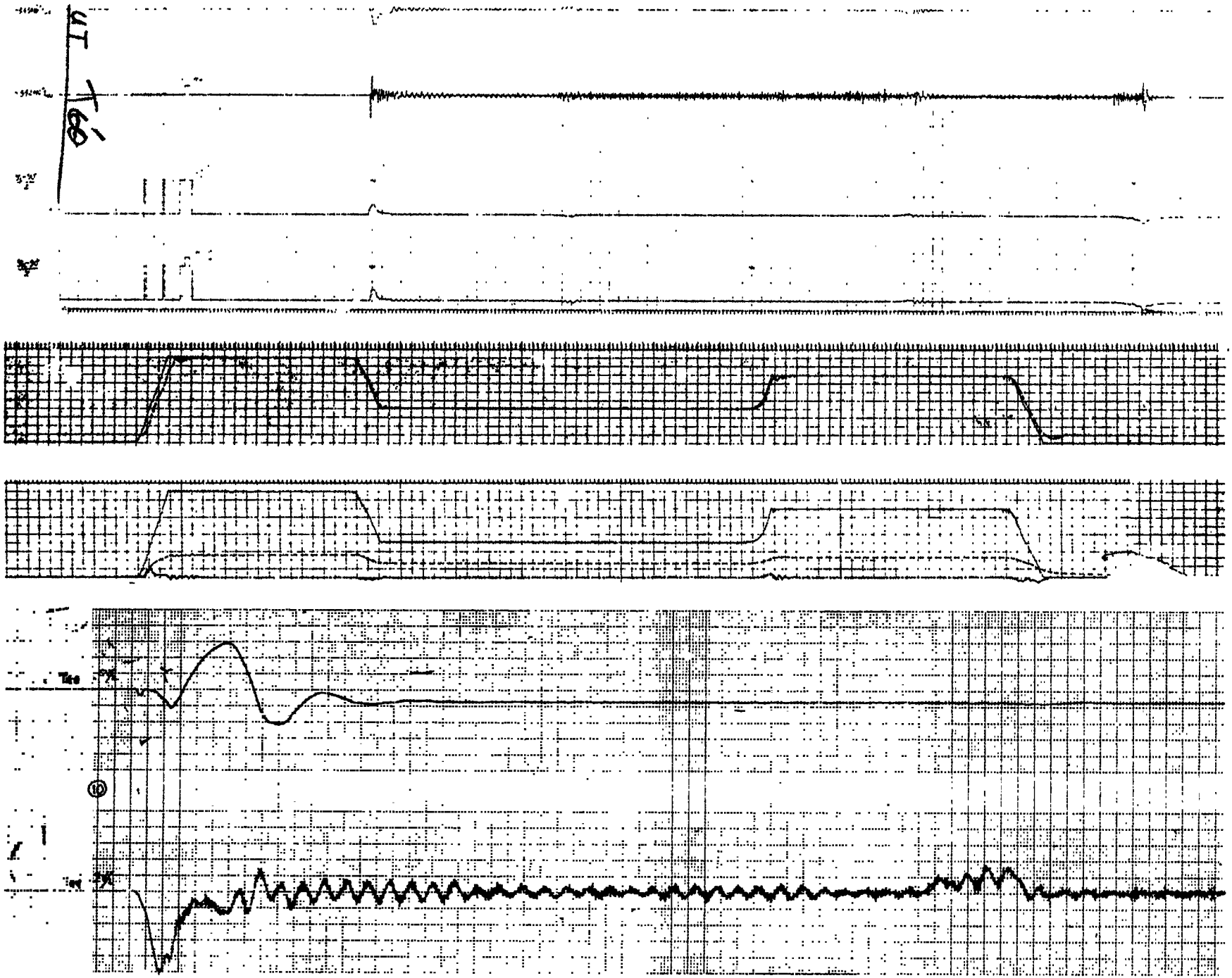
LT
T60
Tbo

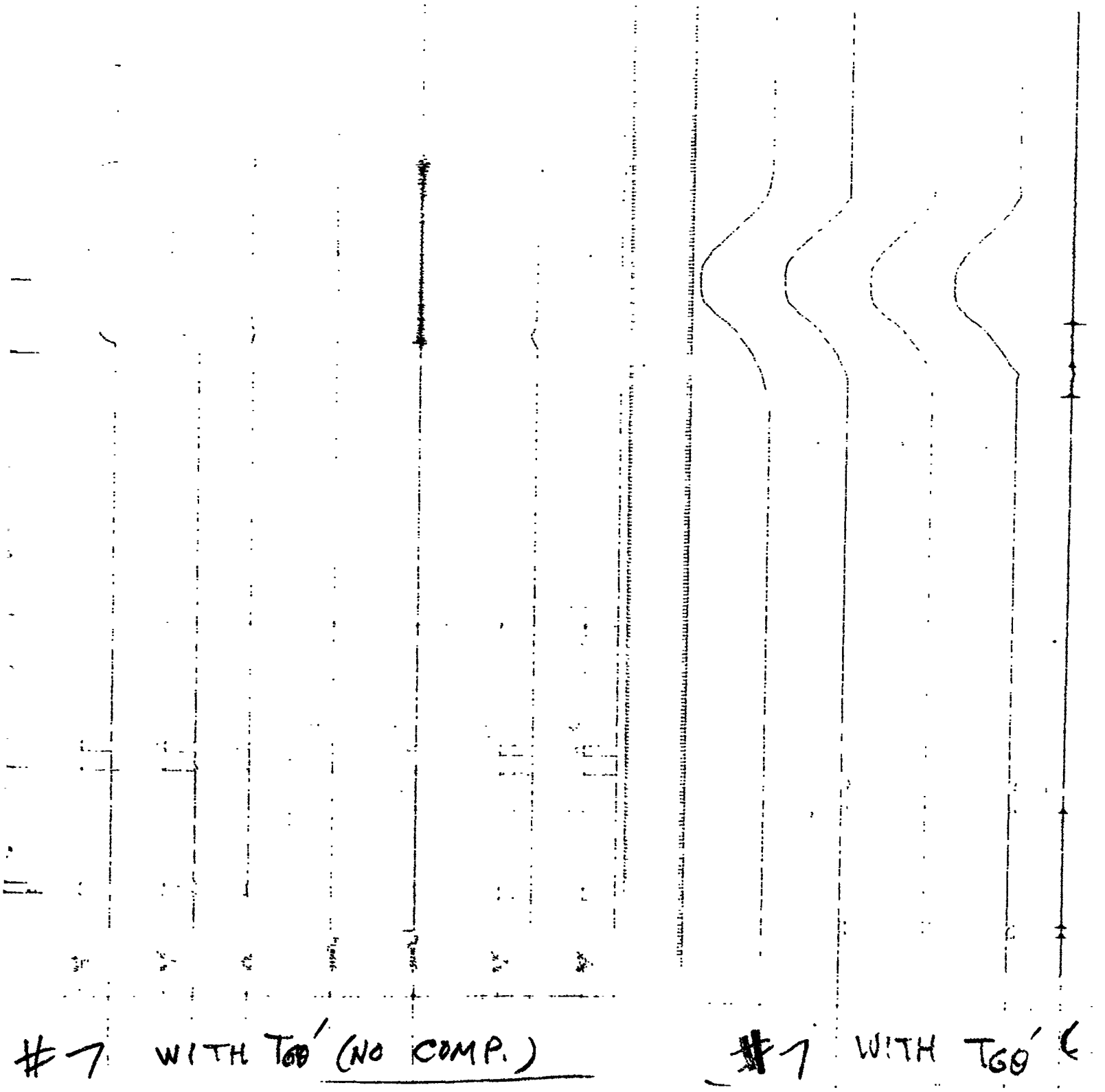

#7 WITH T_{60}' (NO COMP.)

#7 WITH T_{60}' (

#7 WITH T60' (NO COMP.)
#7 WITH T60'

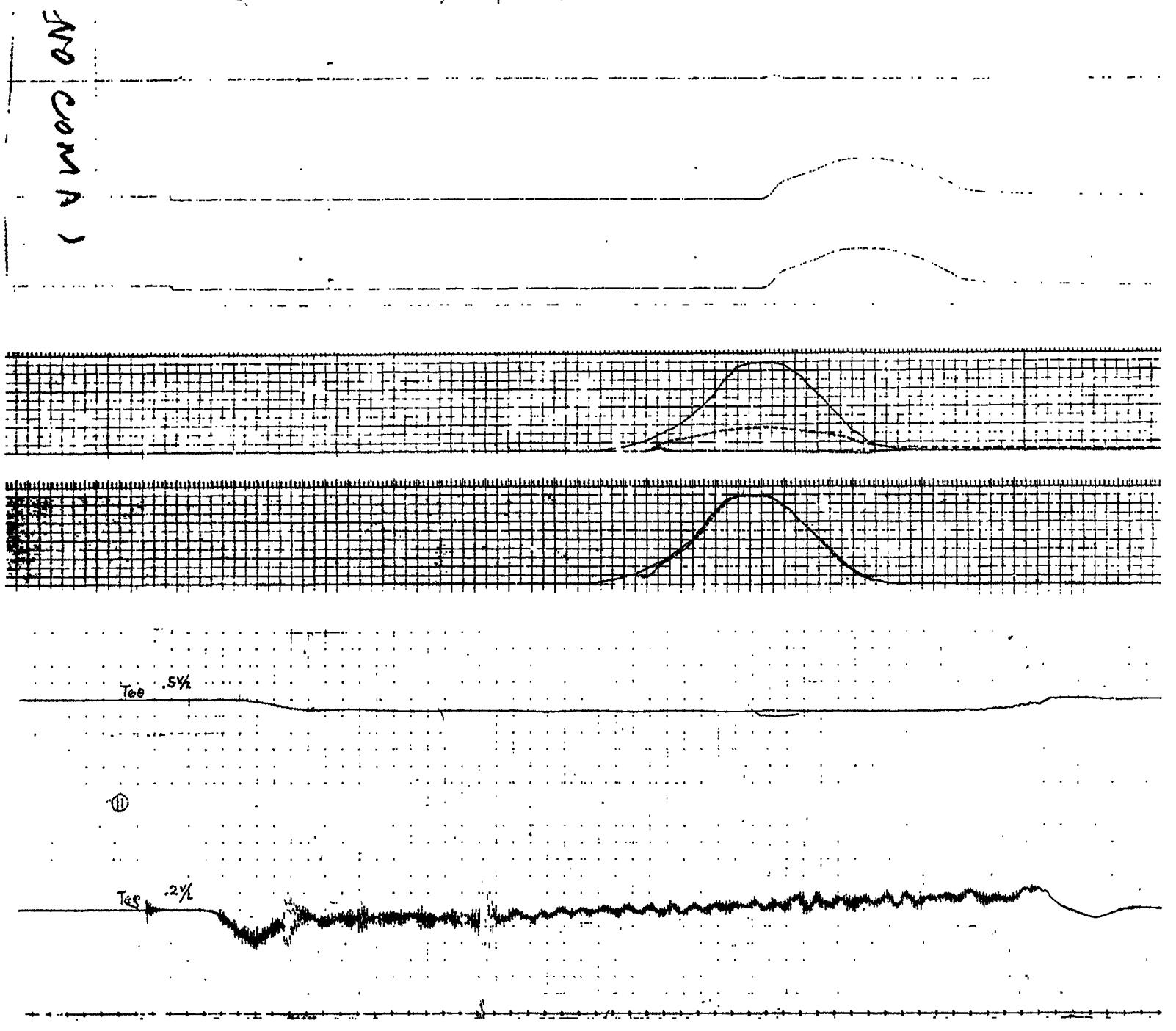
NO CONTACT
T66 .5%
T65 .2%

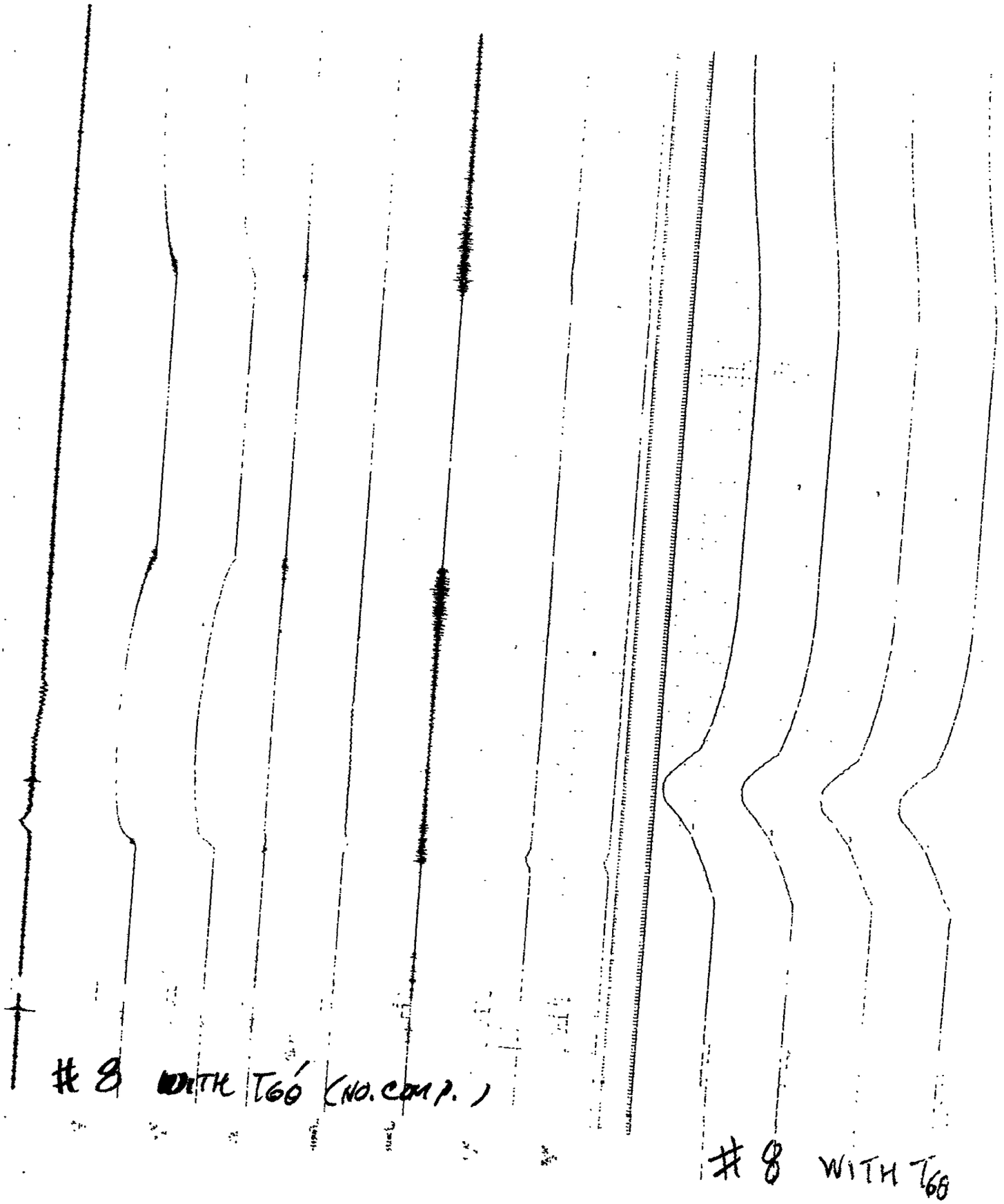
#8 WITH T66 (NO. COMP.)
#8 WITH T66

(no comp.)

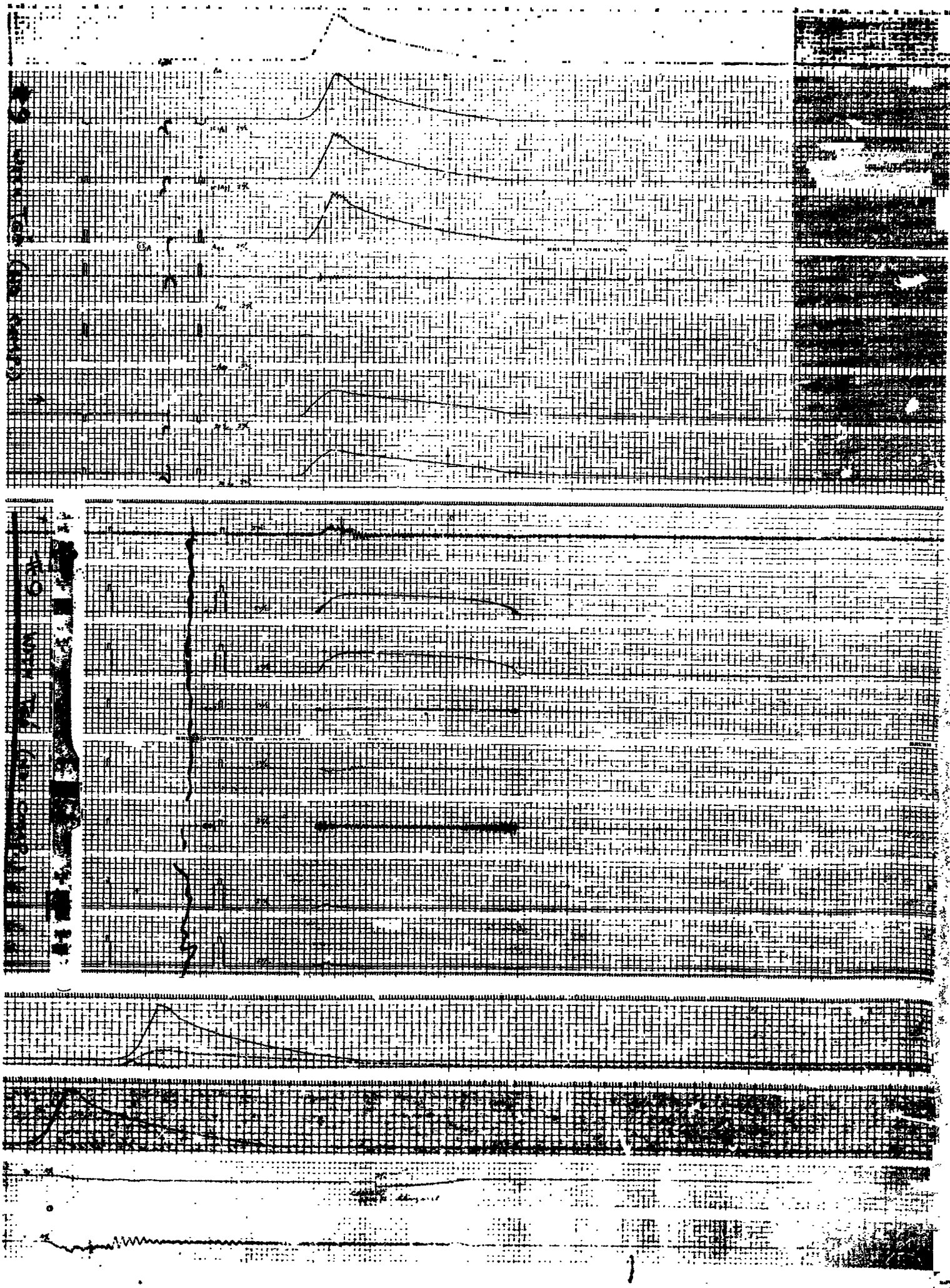

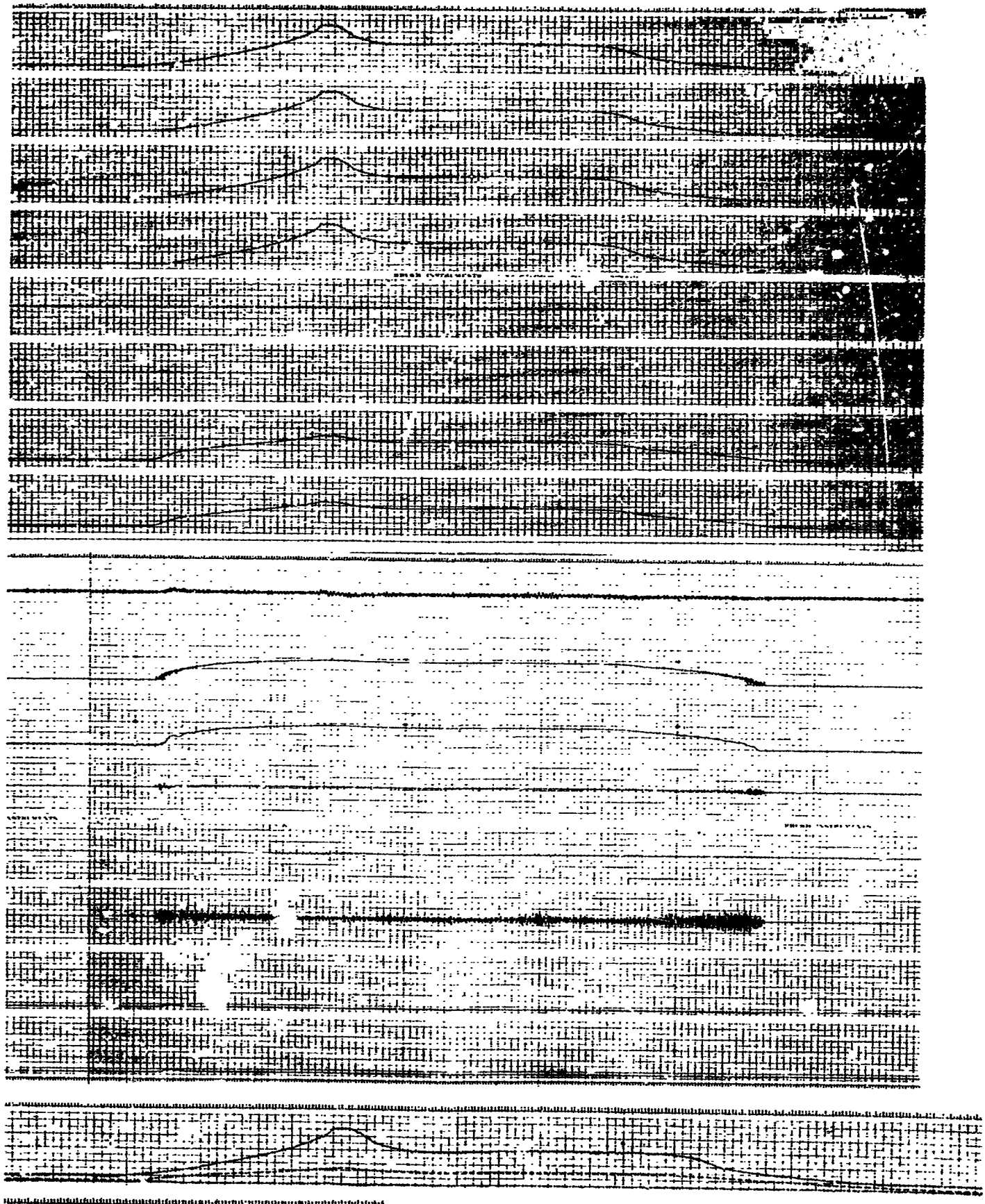

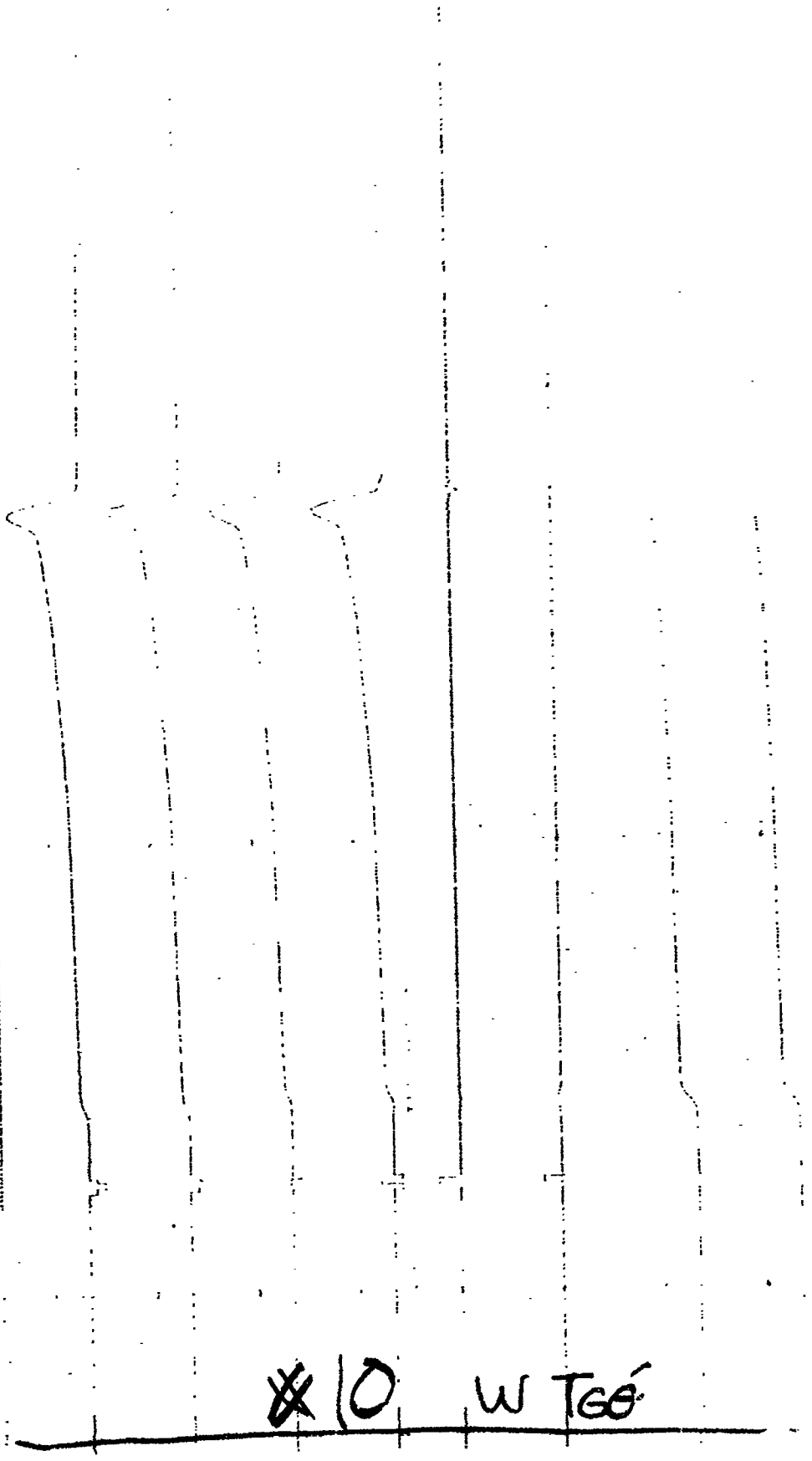
X10 W TGÓ

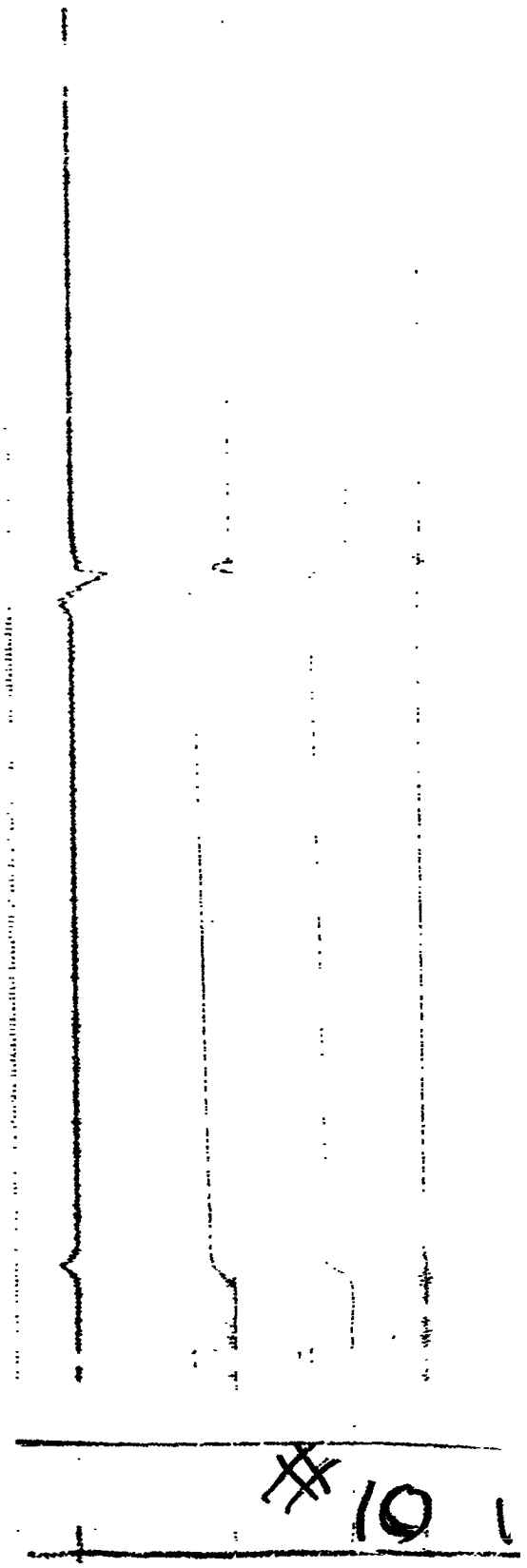
X10

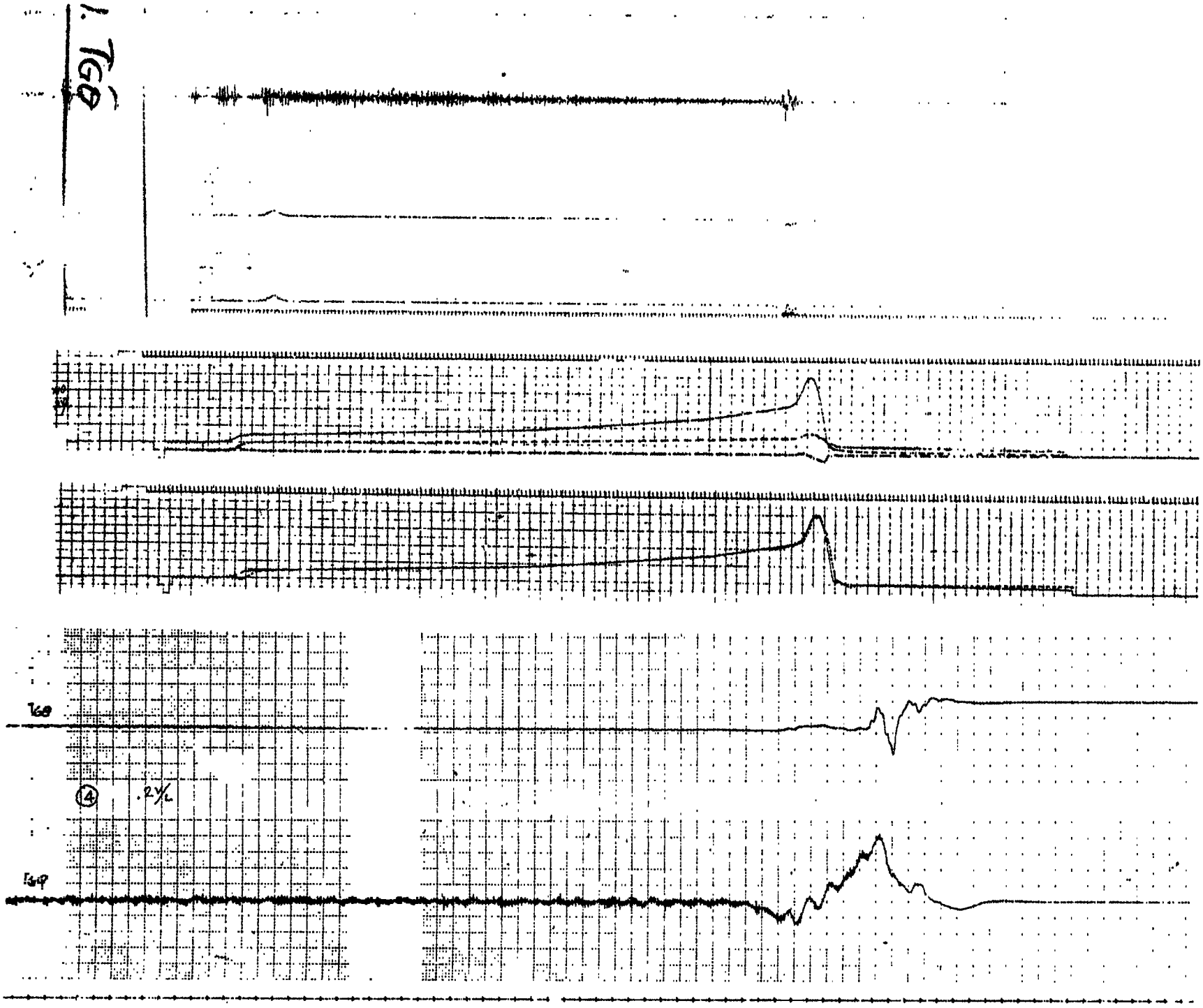
TGB
TGB
④ .2%
EKG

#11 W. Tea
#11 W. Tea

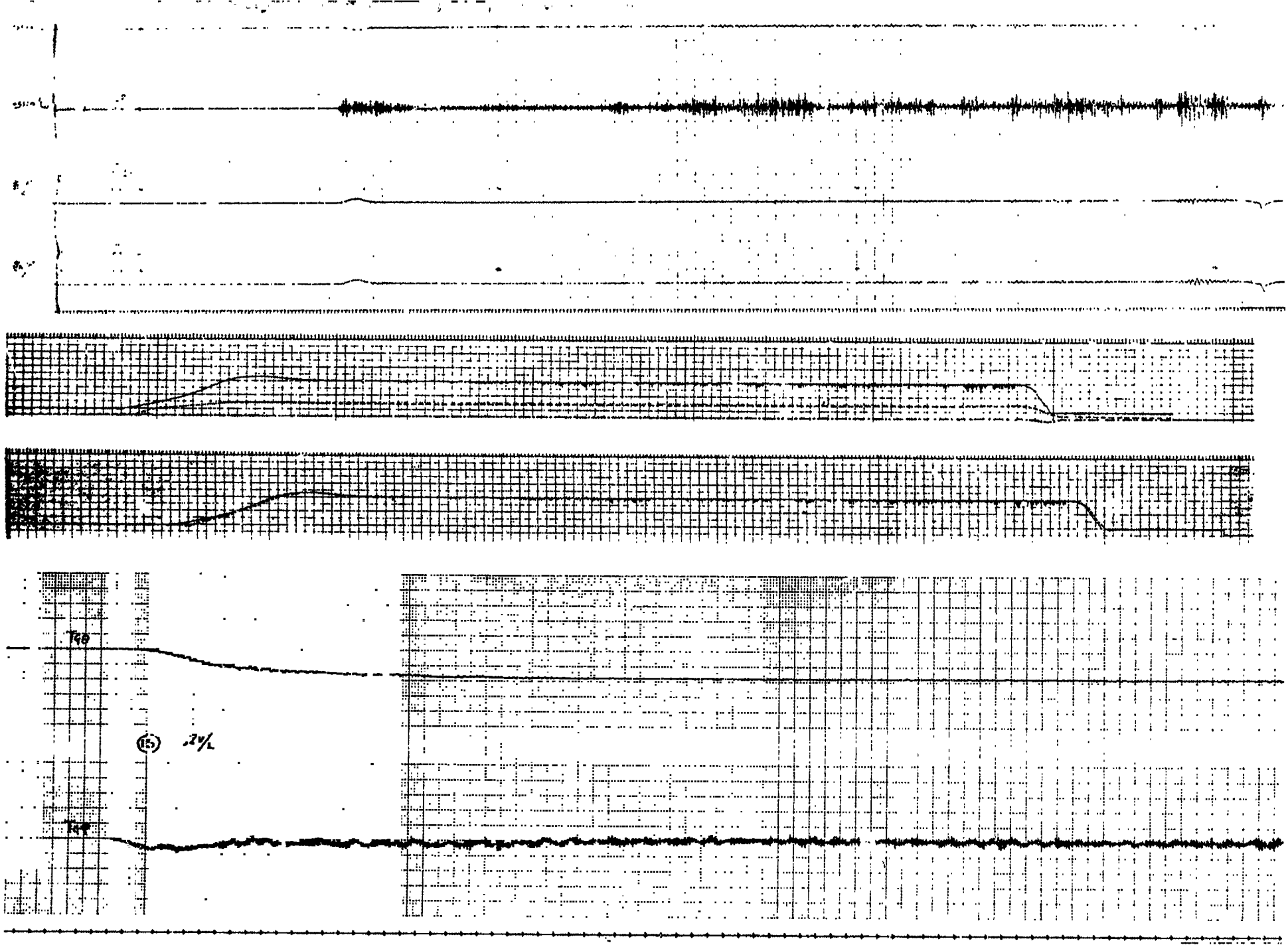
Tap
15
.2V/L

* 12 W TGO
* 12 W TGO

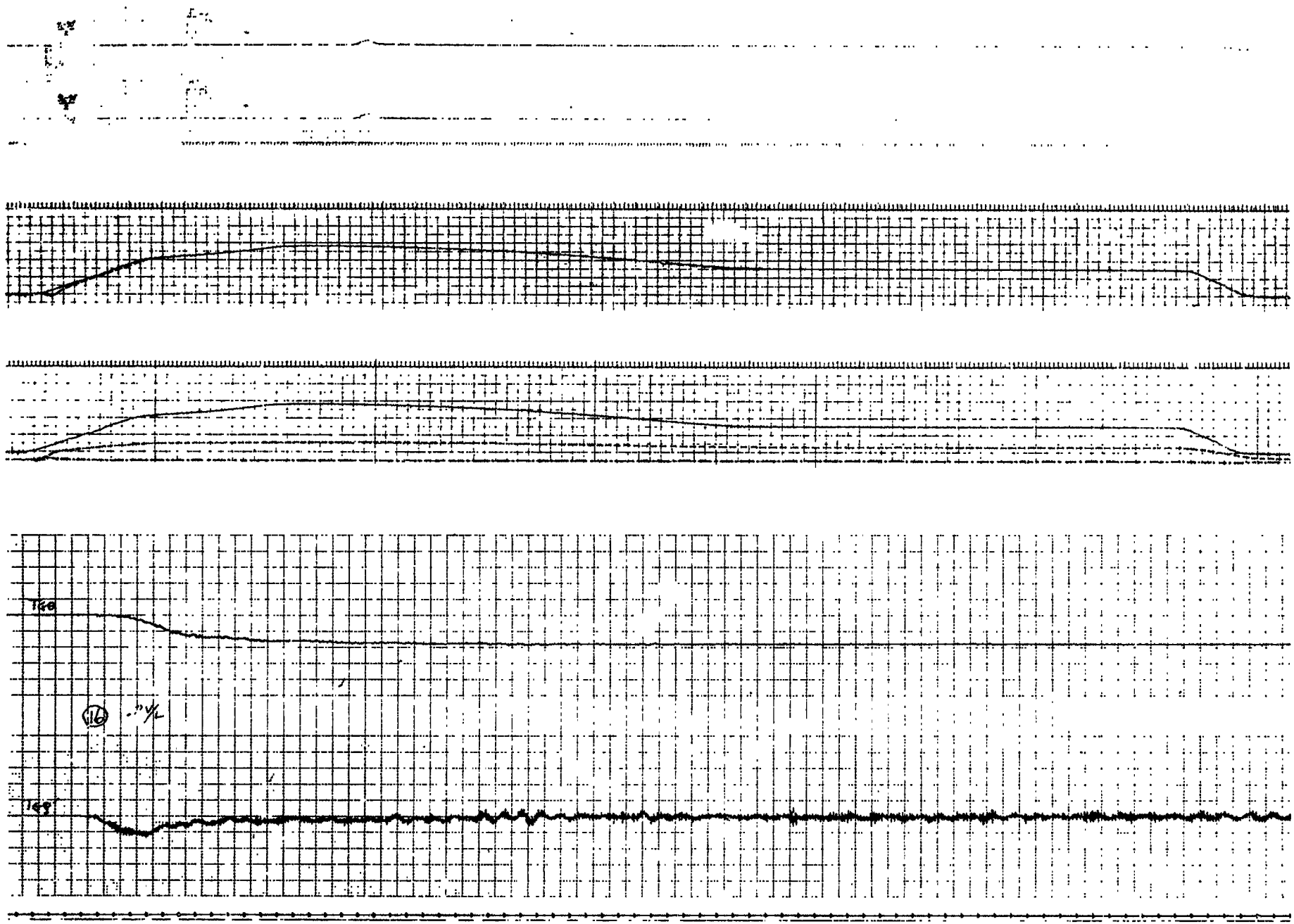
T66
T69

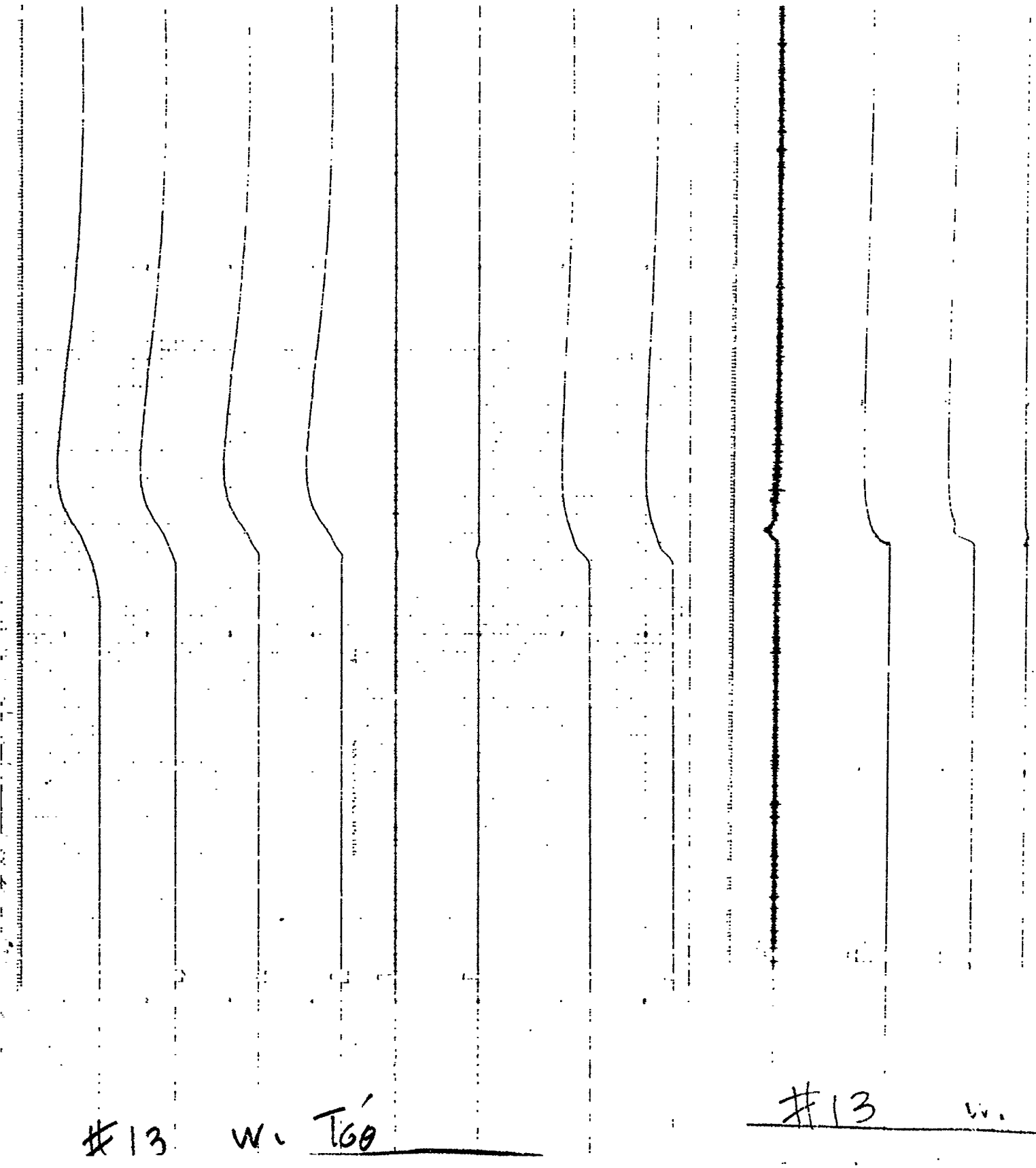
#13 W. TGB
#13 W. TC

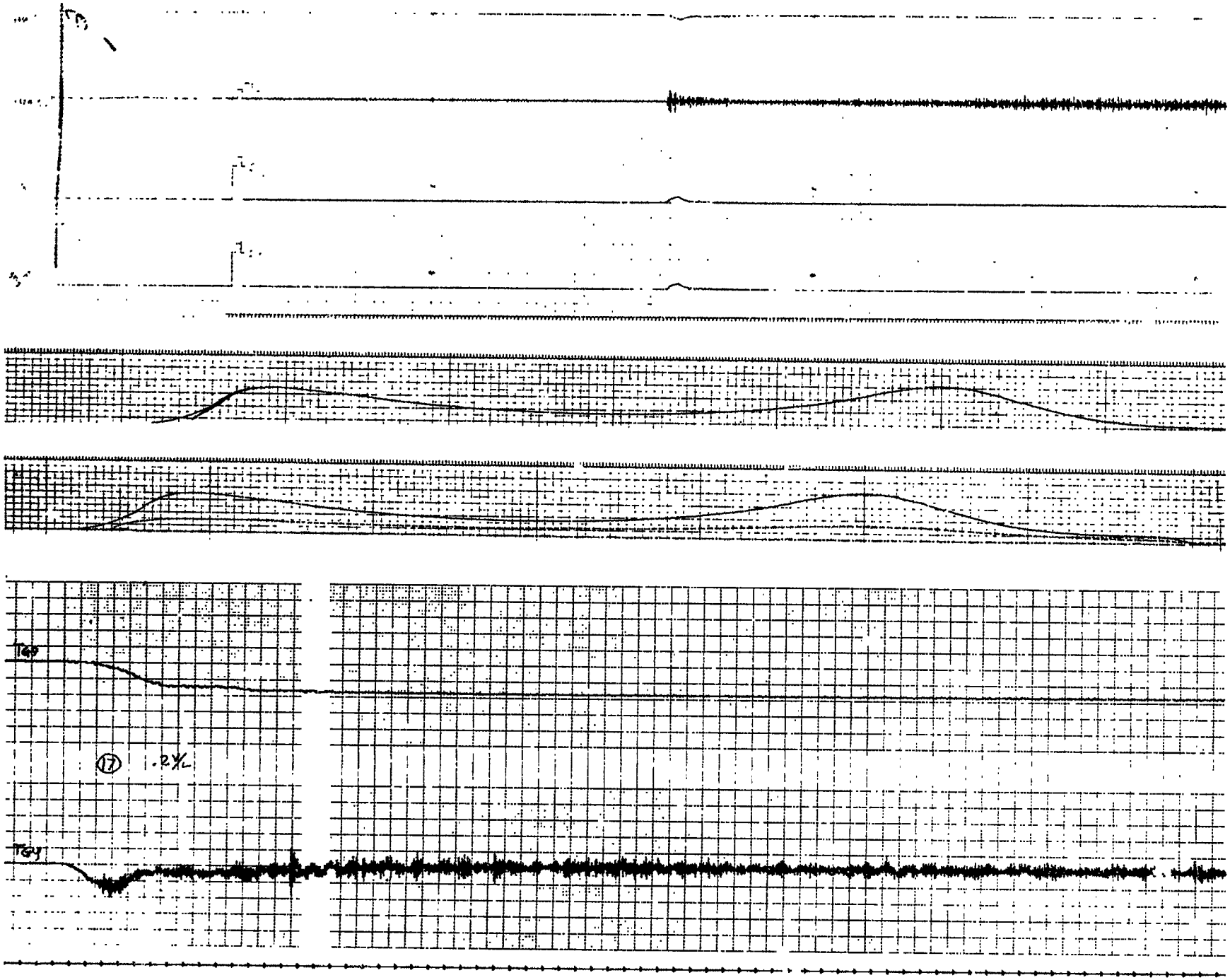
TG9
⑰ 1.2%
TG4

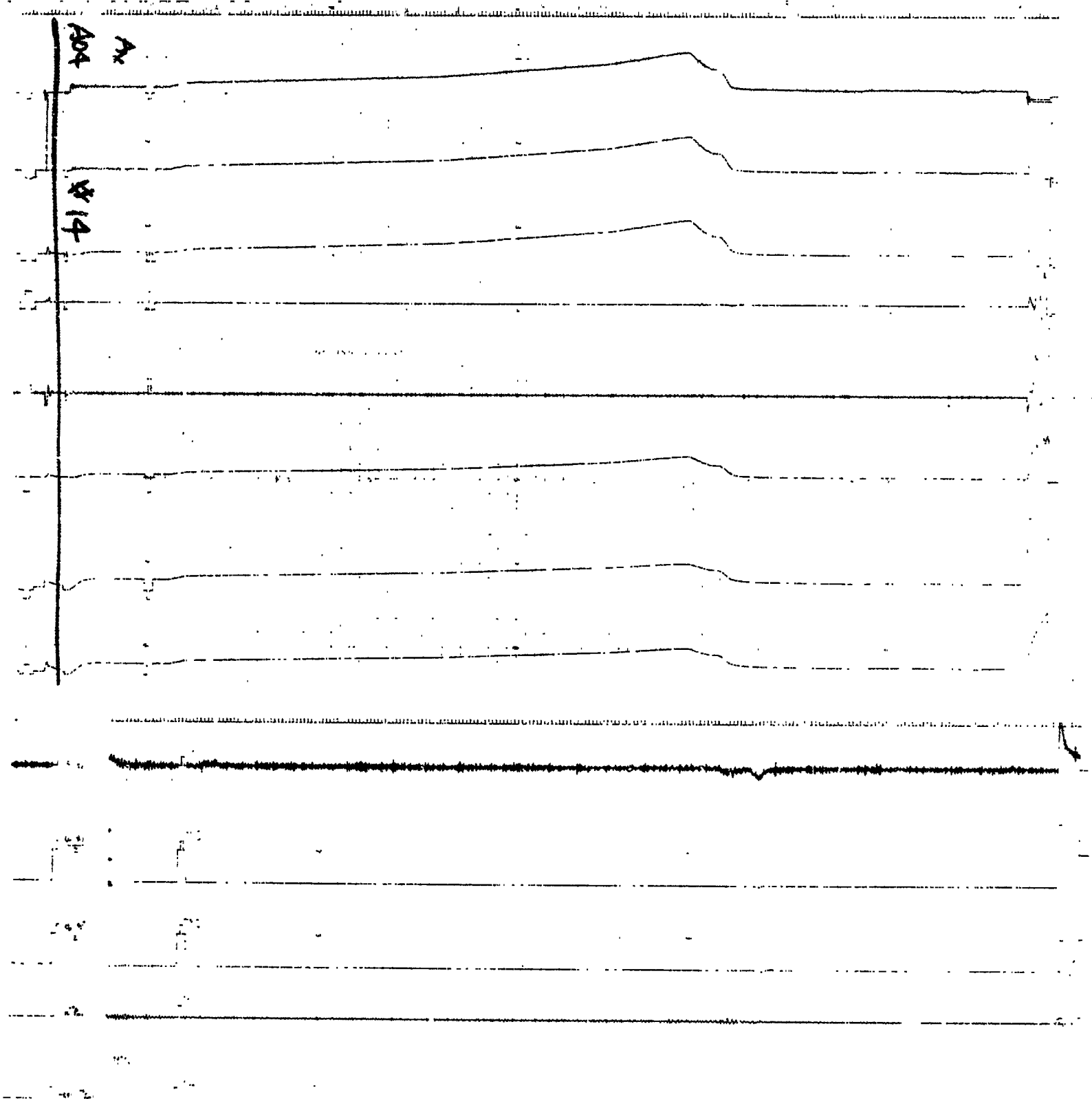
Ax
Ay

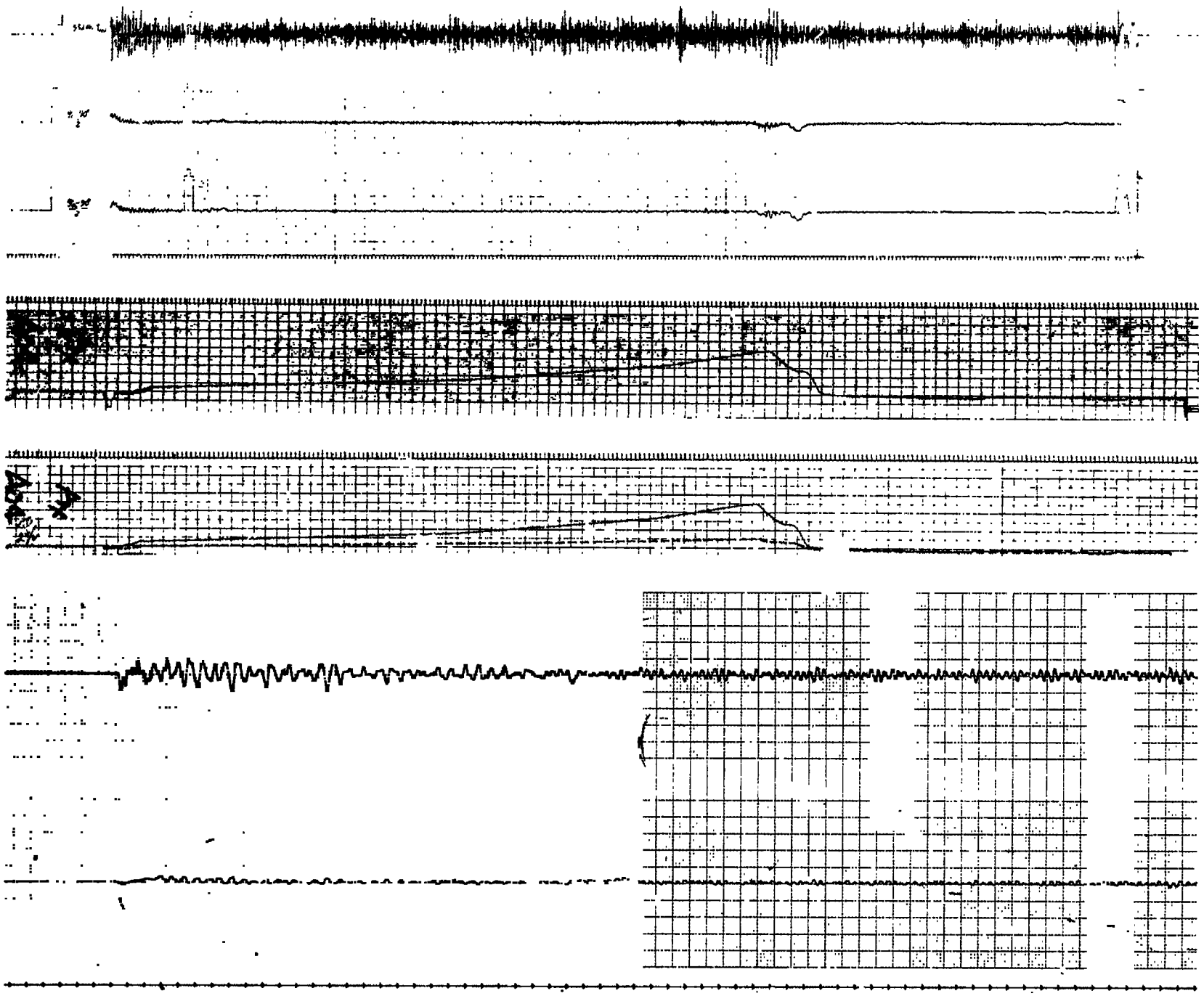

#15 RE-RUN
#15 RE-R

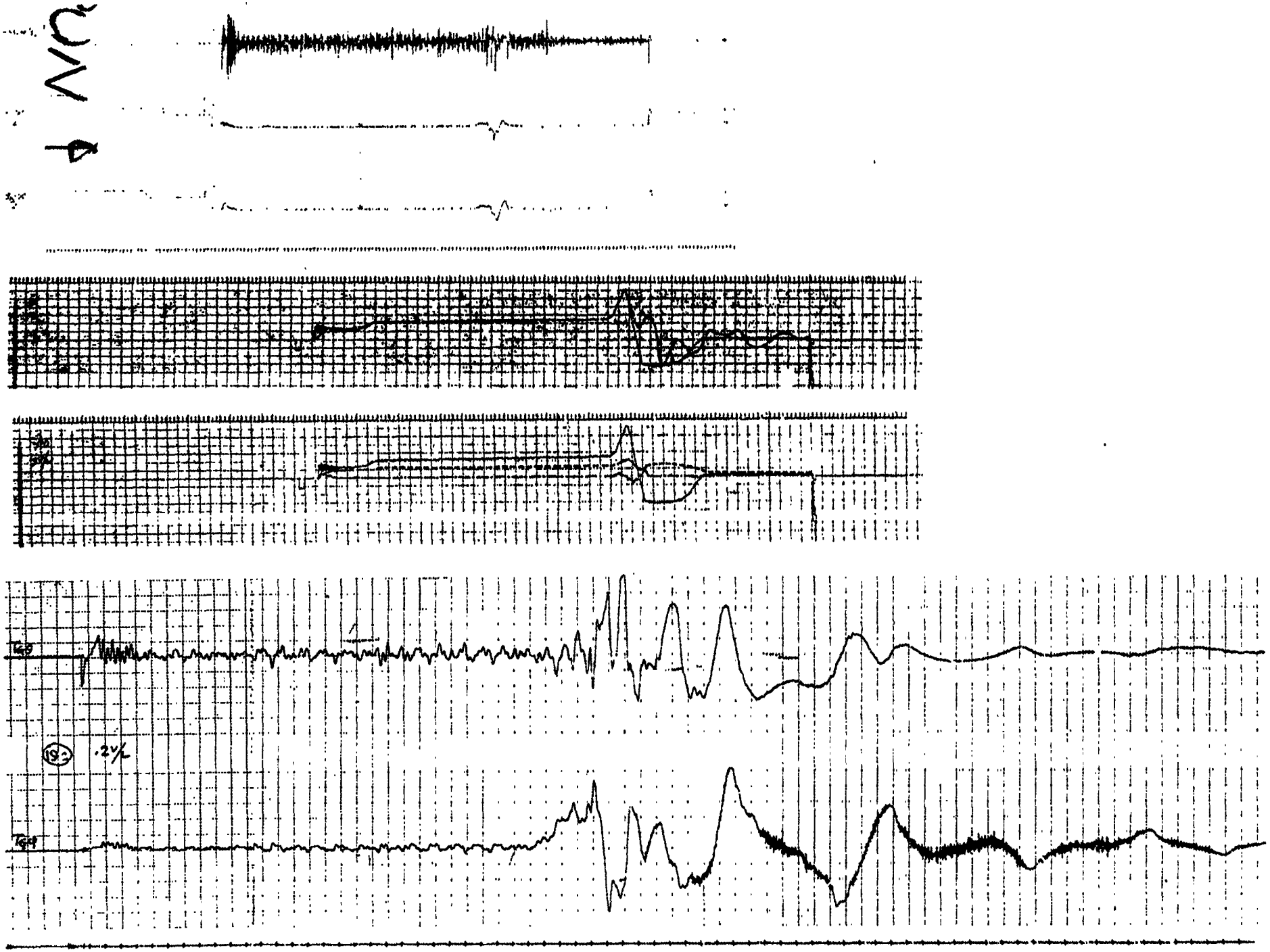
.2V/

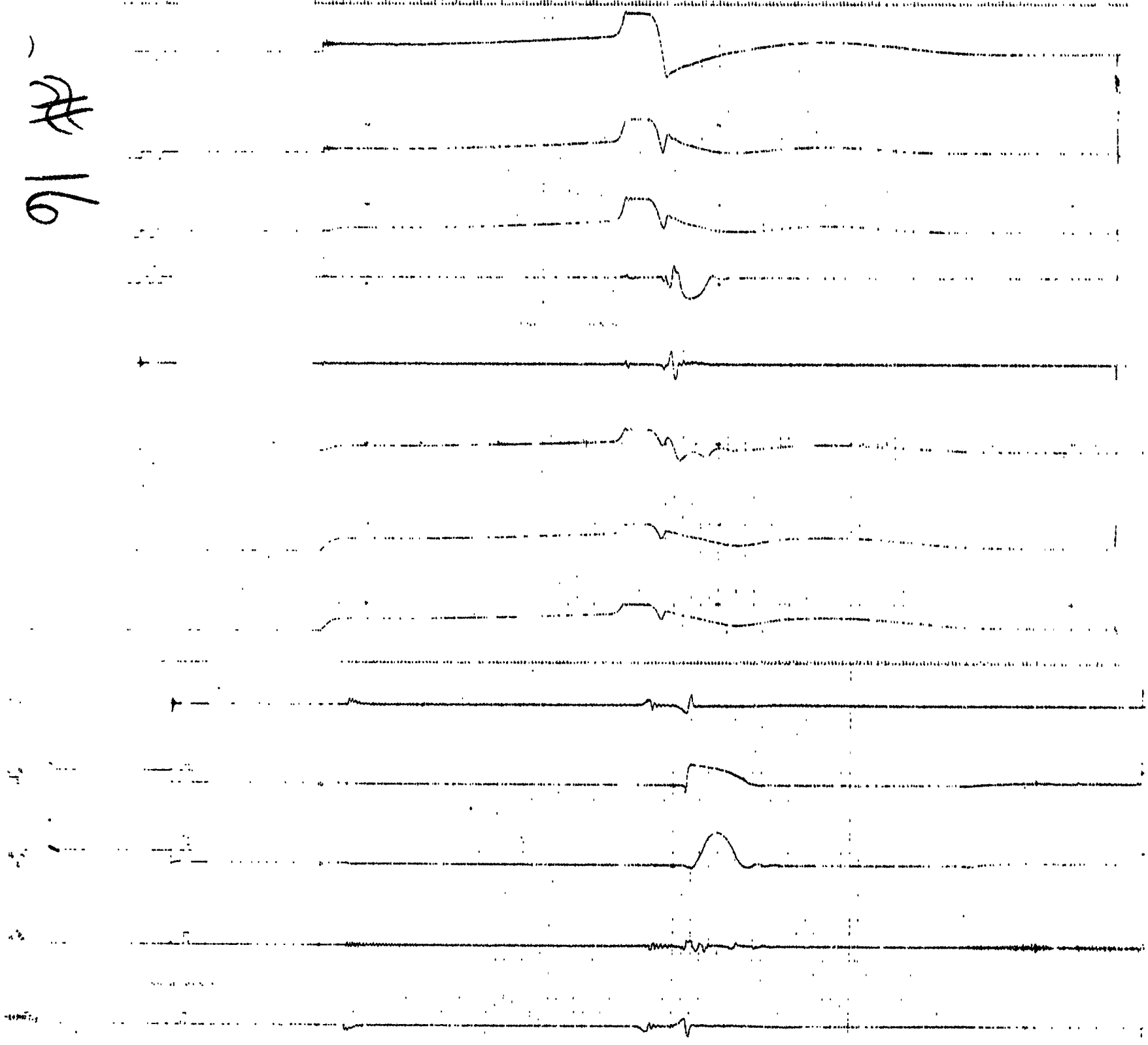

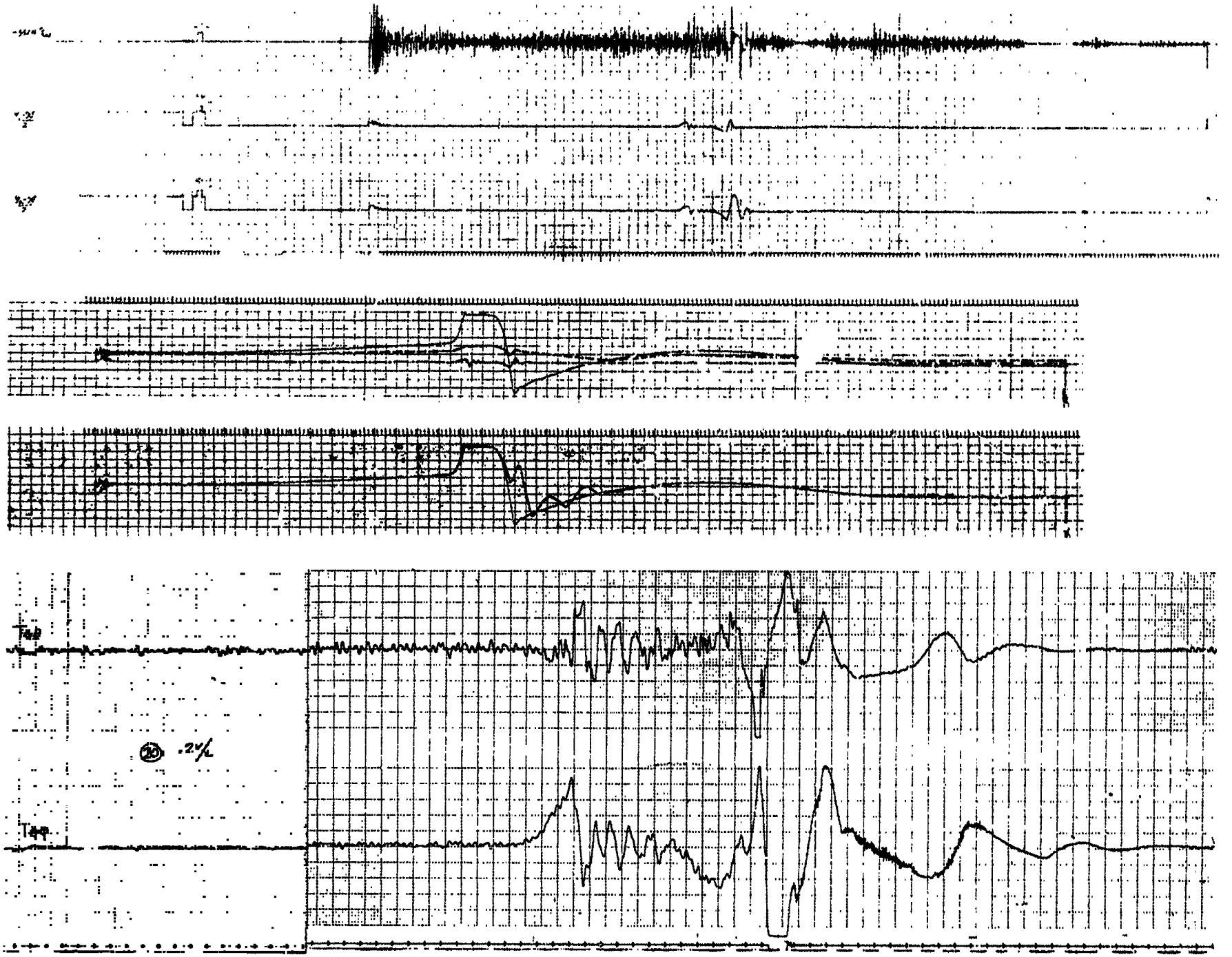

#10 RERUN
#10 RERUN

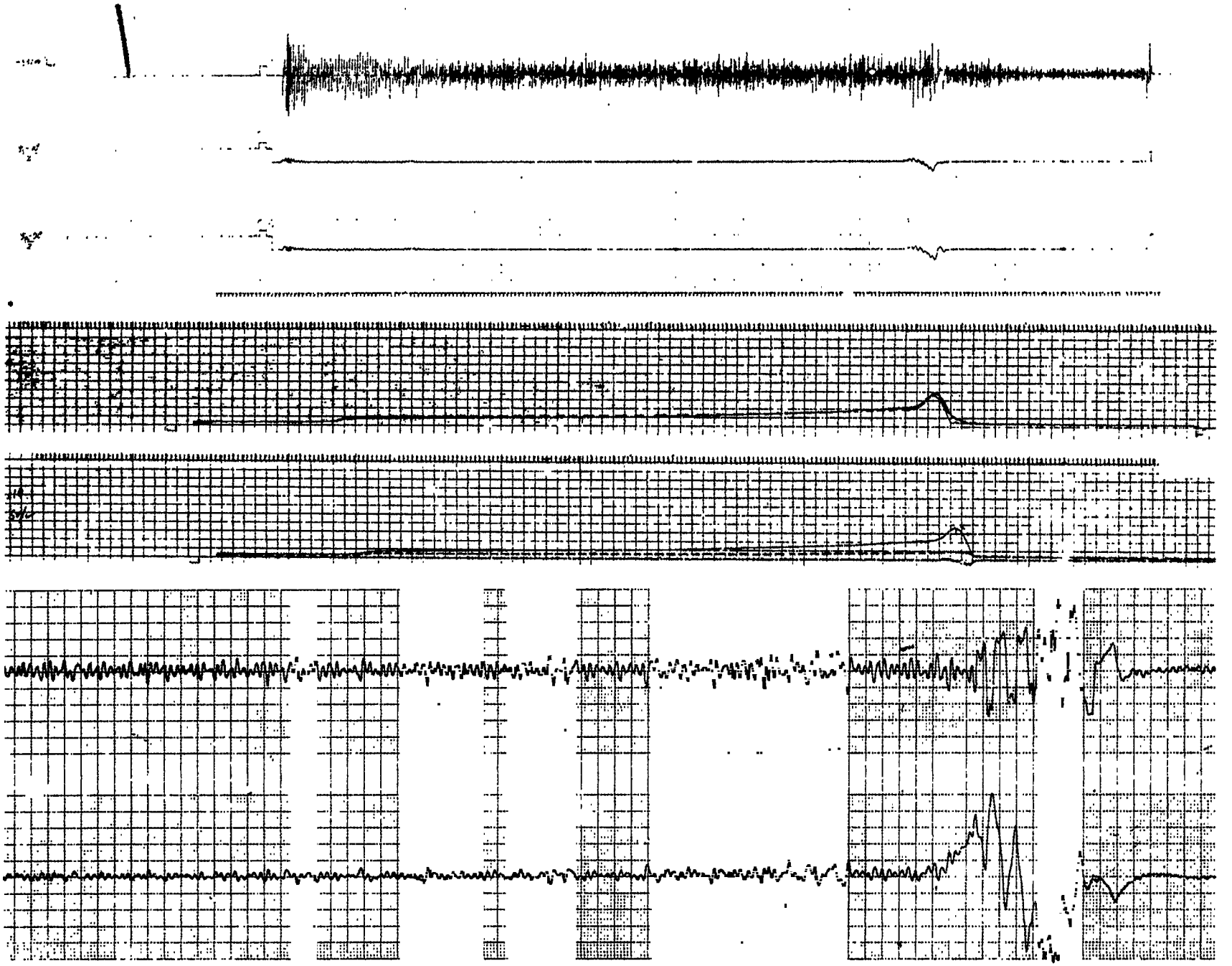

#26 of 27

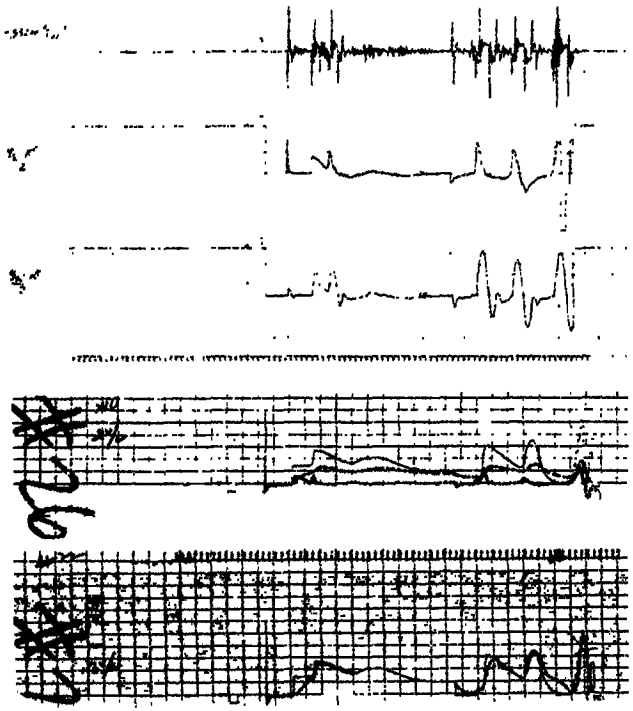

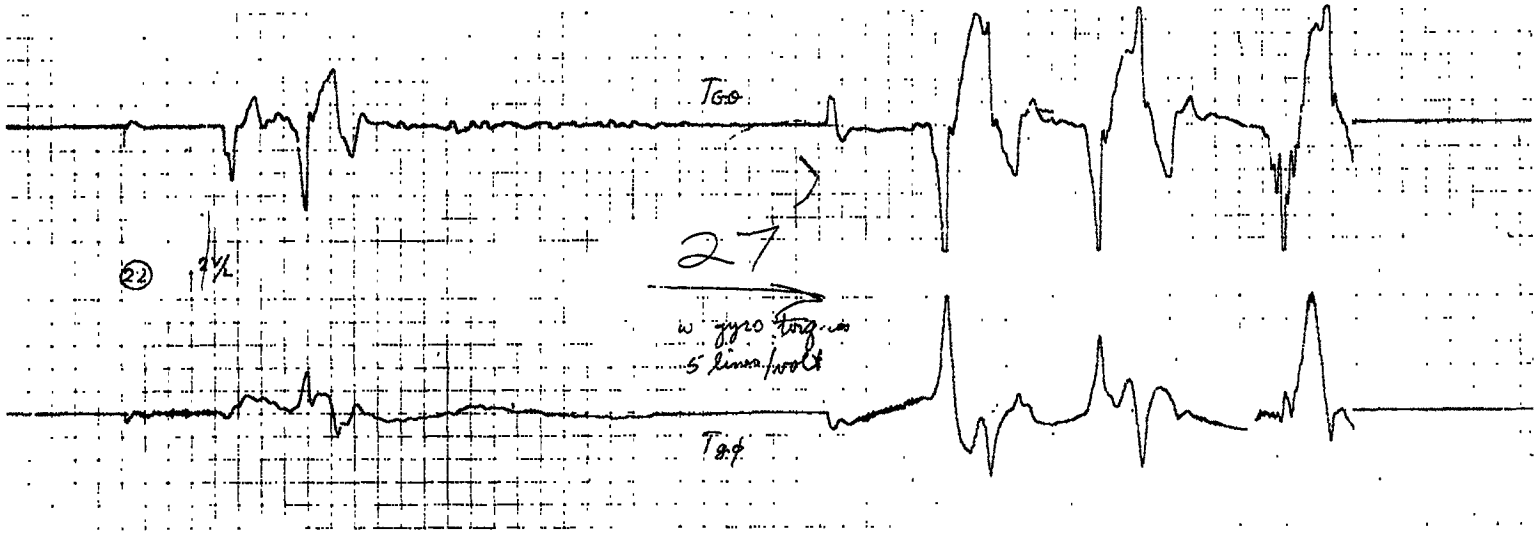
T60
27
w gyro freq.
5 lines/volt
T2.4

ANOTHER 23
ANOTHER 23

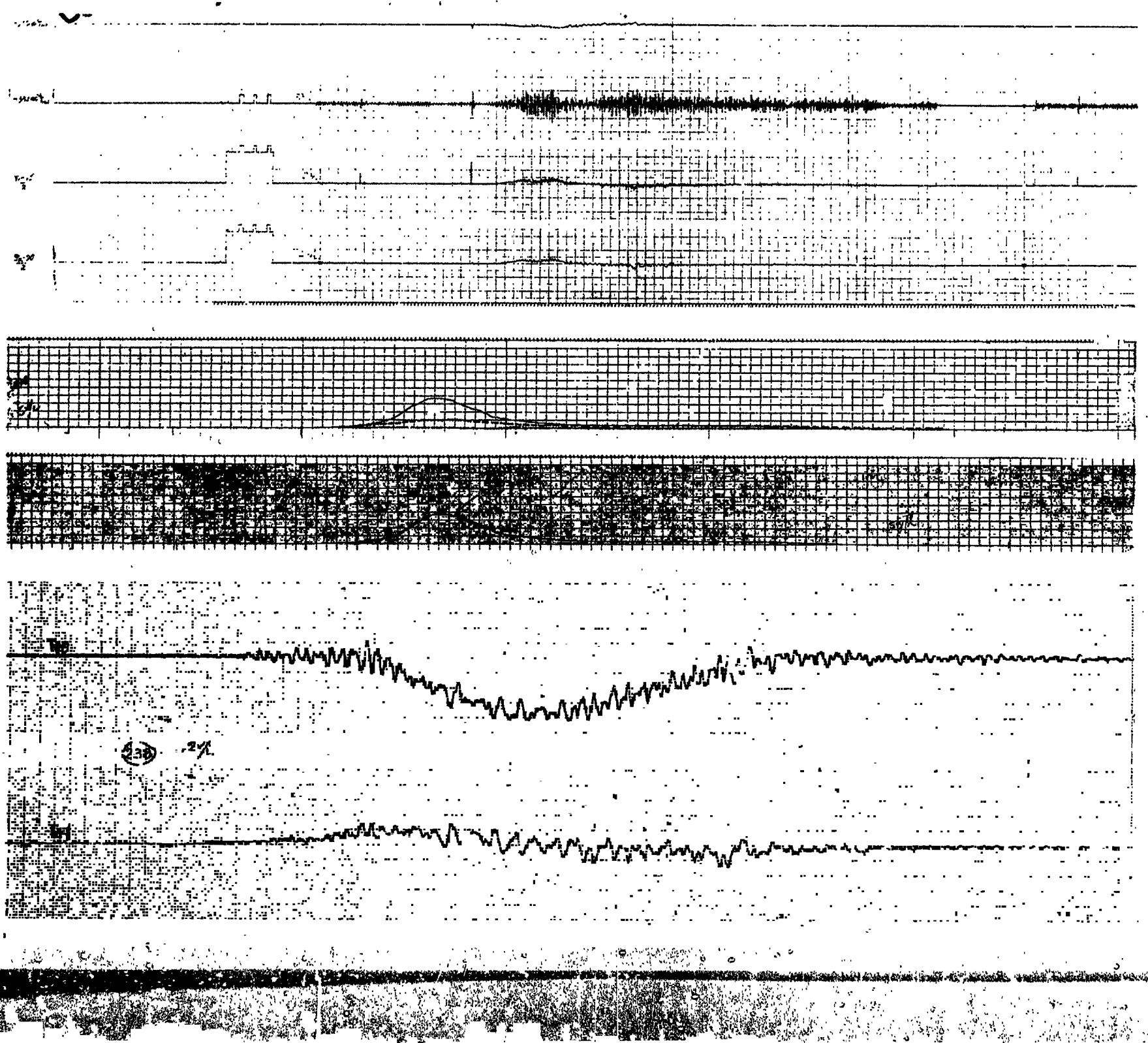

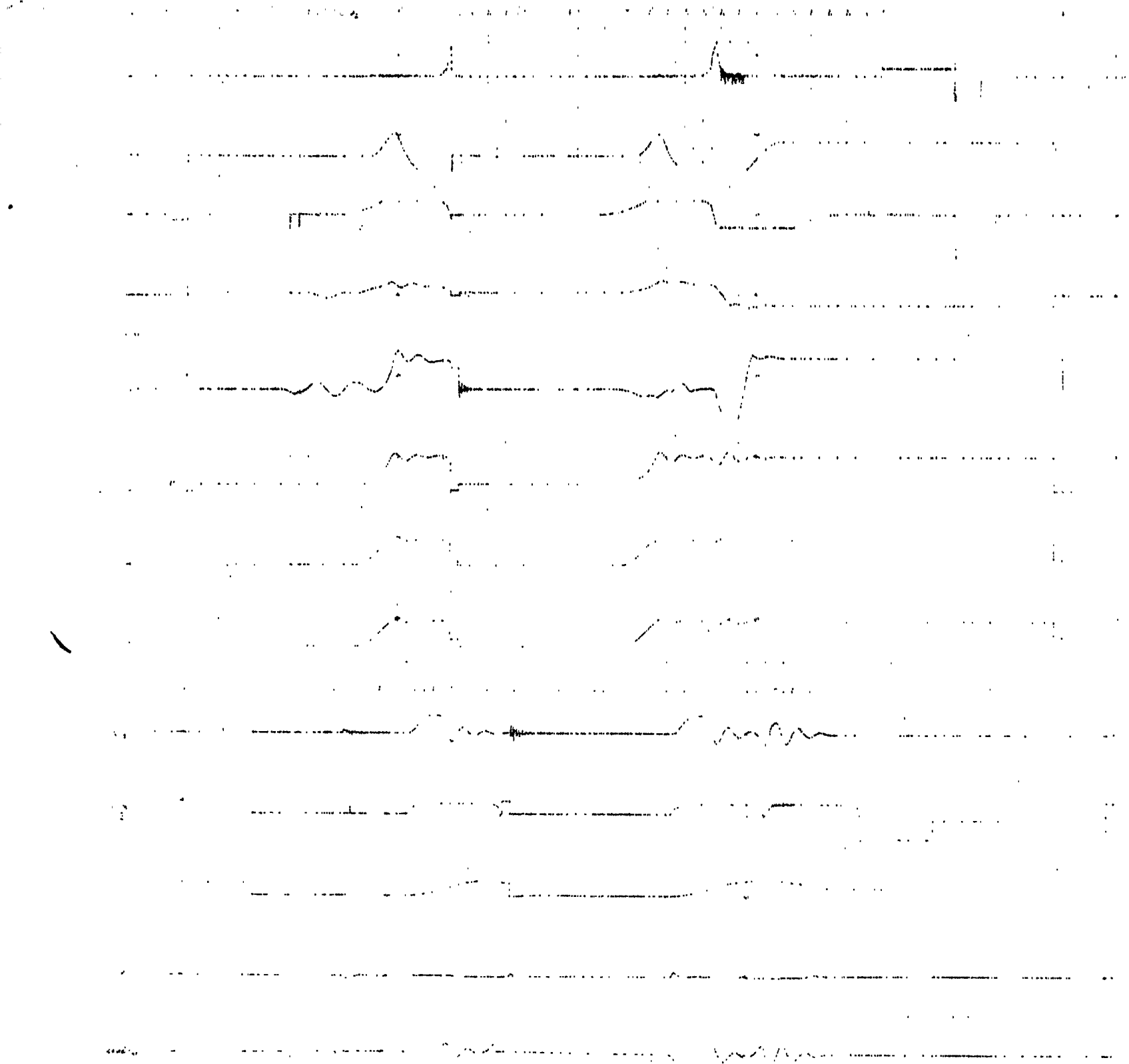

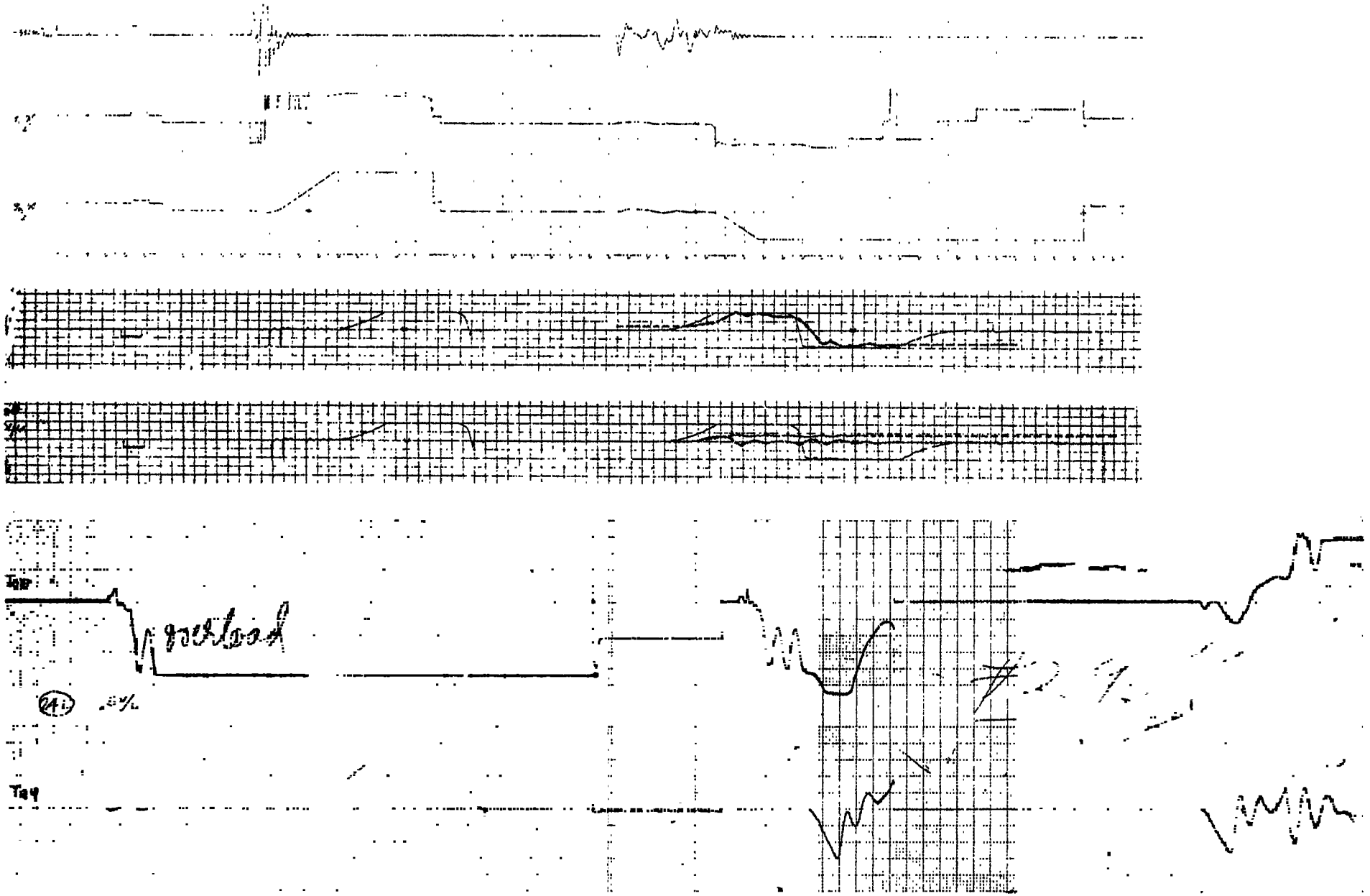
Tap
Tag

#18 ↓ WITH T60

#18 WITH T60

1

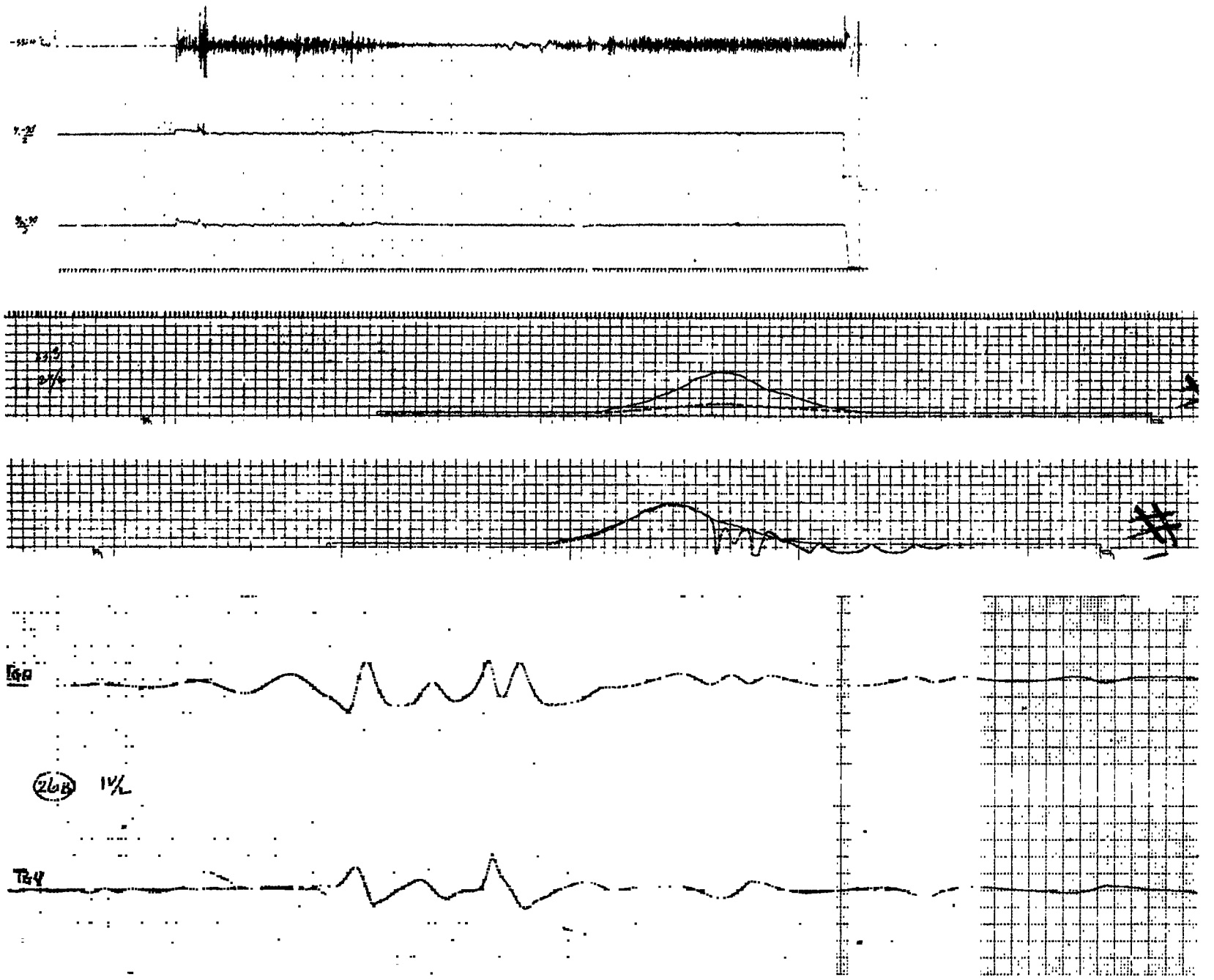
TGB
TB4

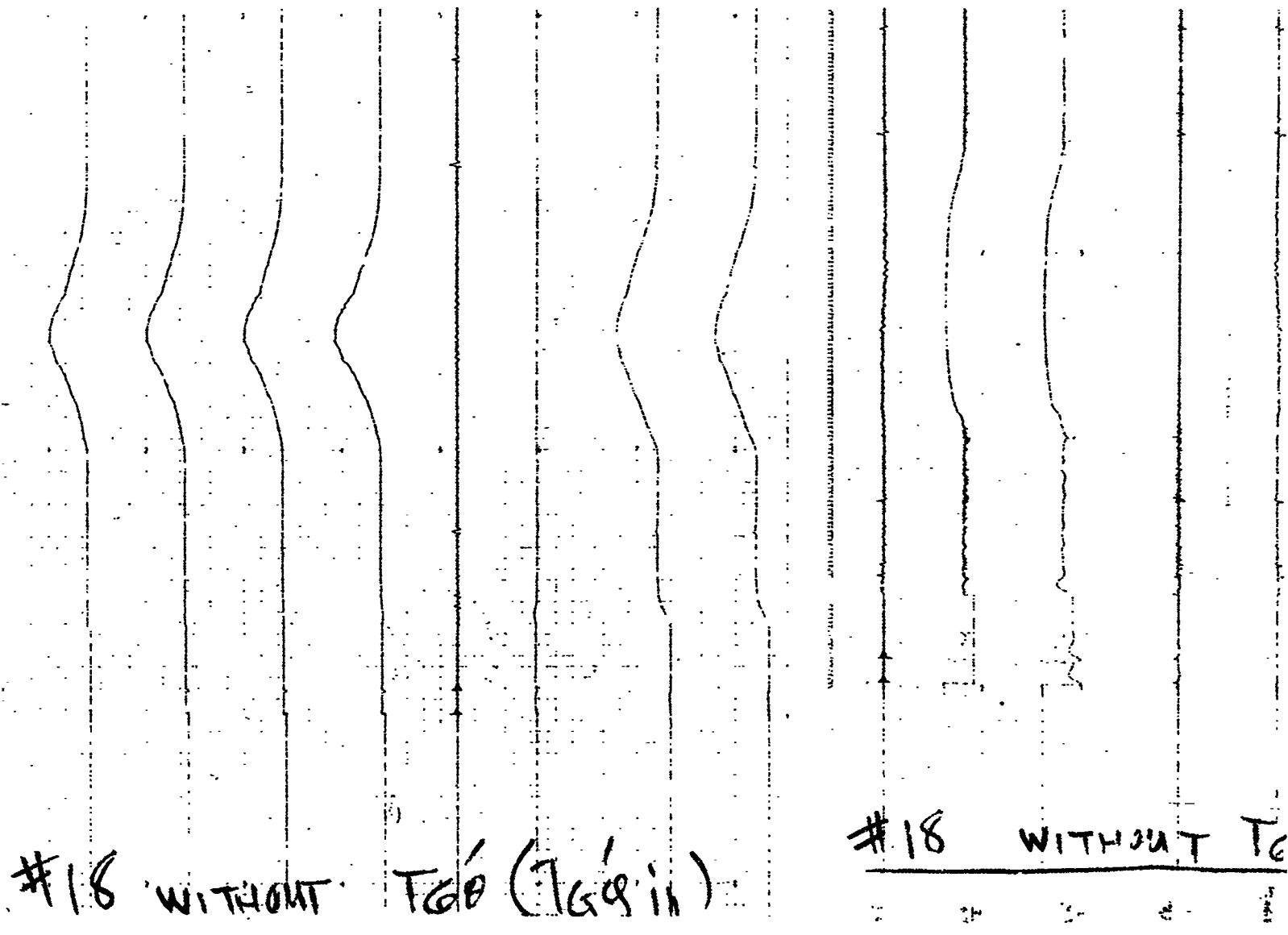
#18 WITHOUT TG6 (TG9'11)
#18 WITHOUT TG

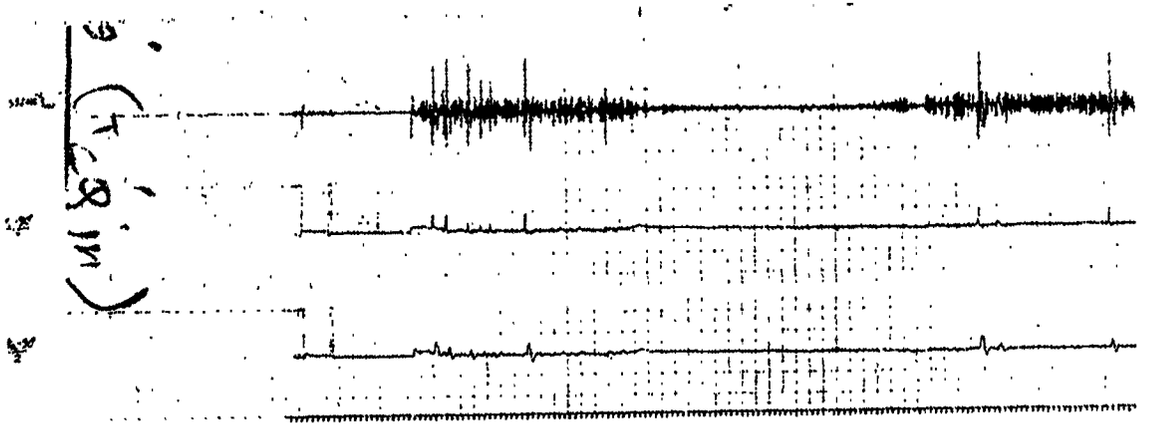

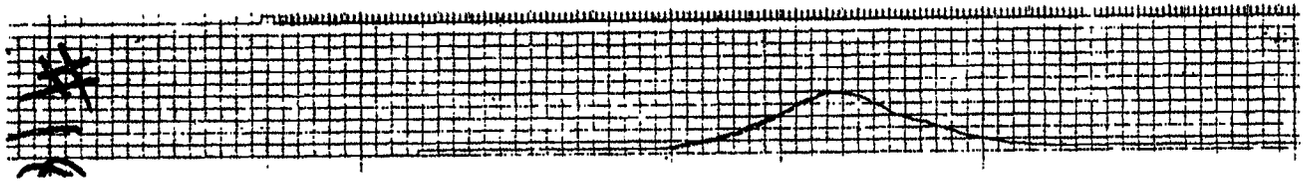

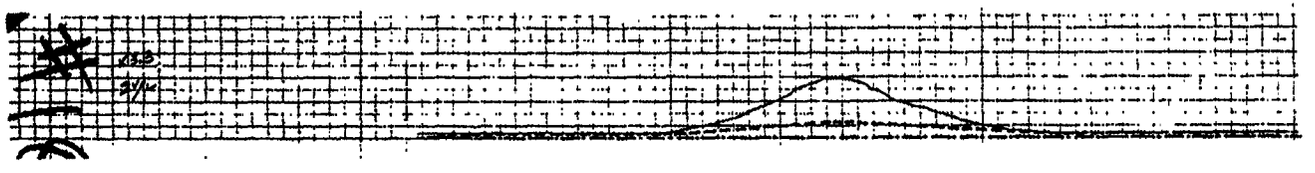

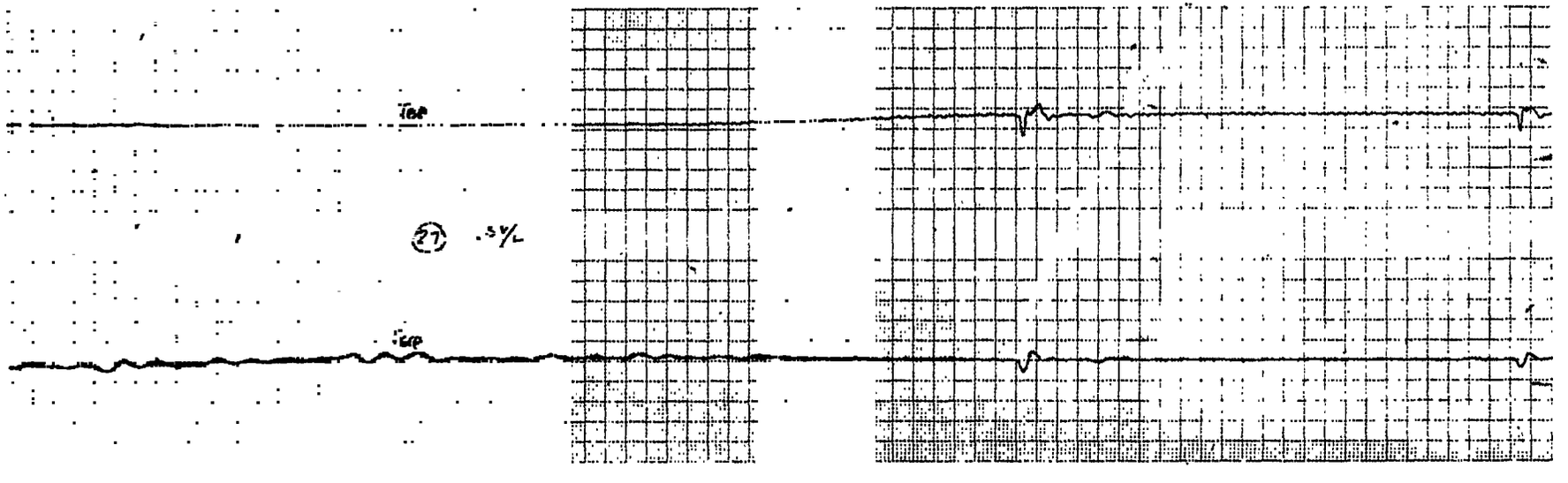
TOP
.5V/L
TOP

#19
WITHOUT

I-68
#19 WITHICH

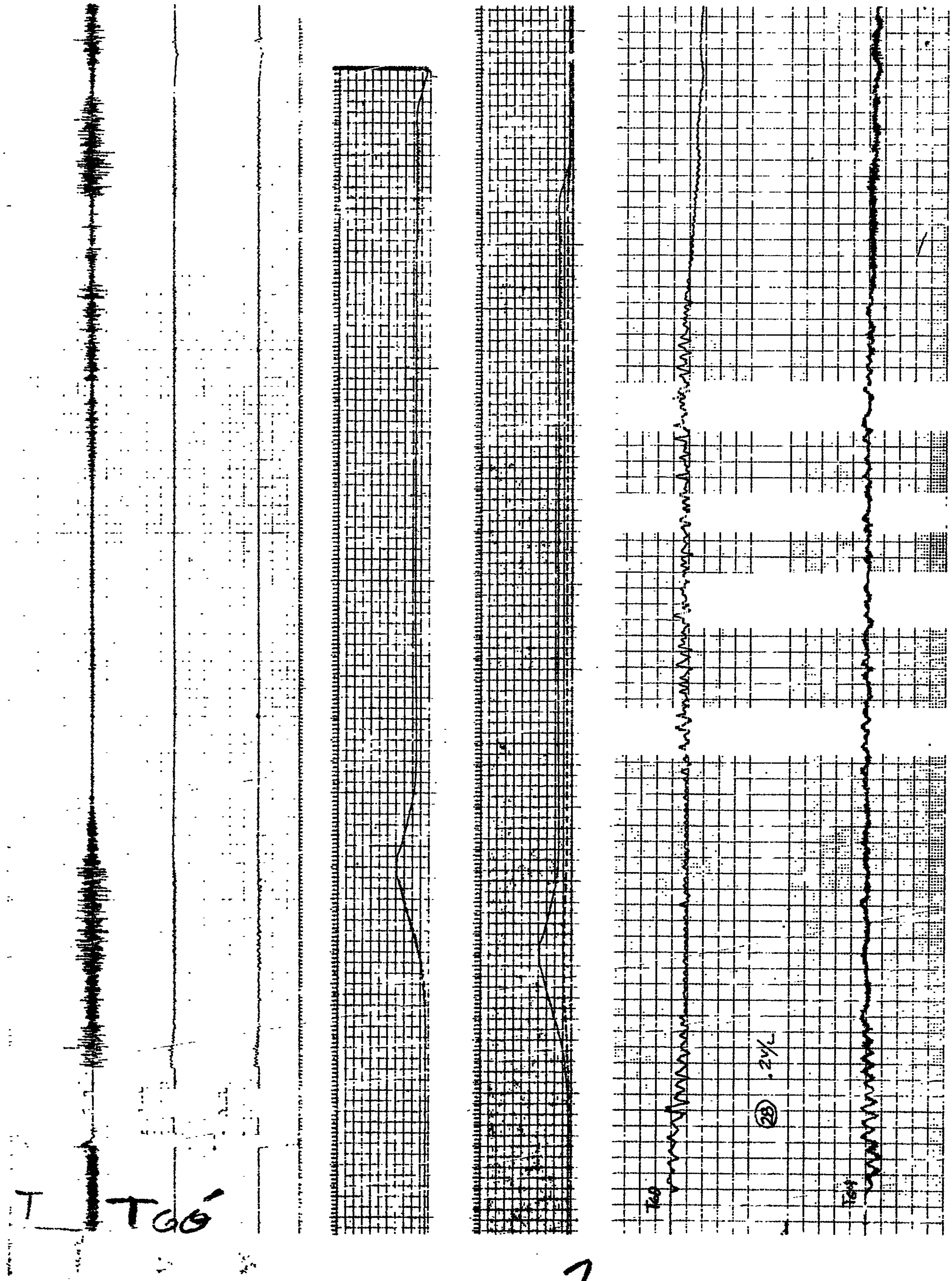
T
TGG'
T60
T64
28
.2V/L

#20
SAME

#1 20
SAME
2

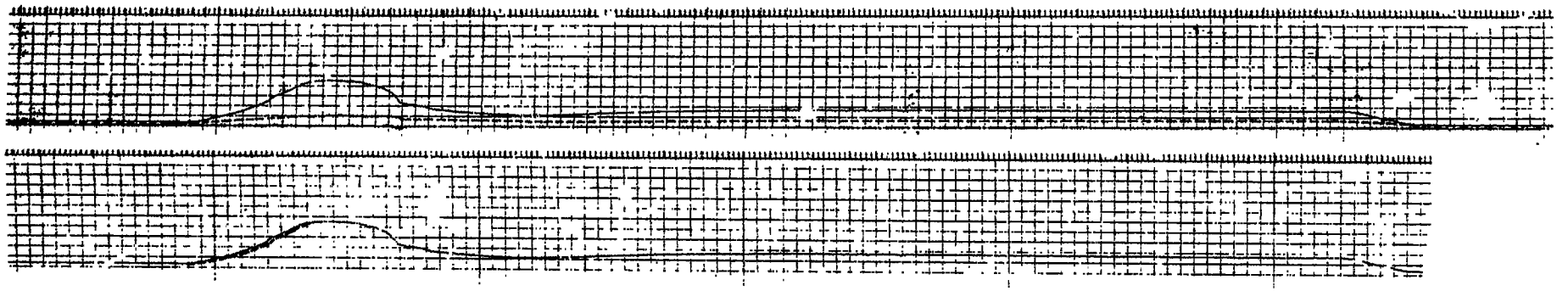

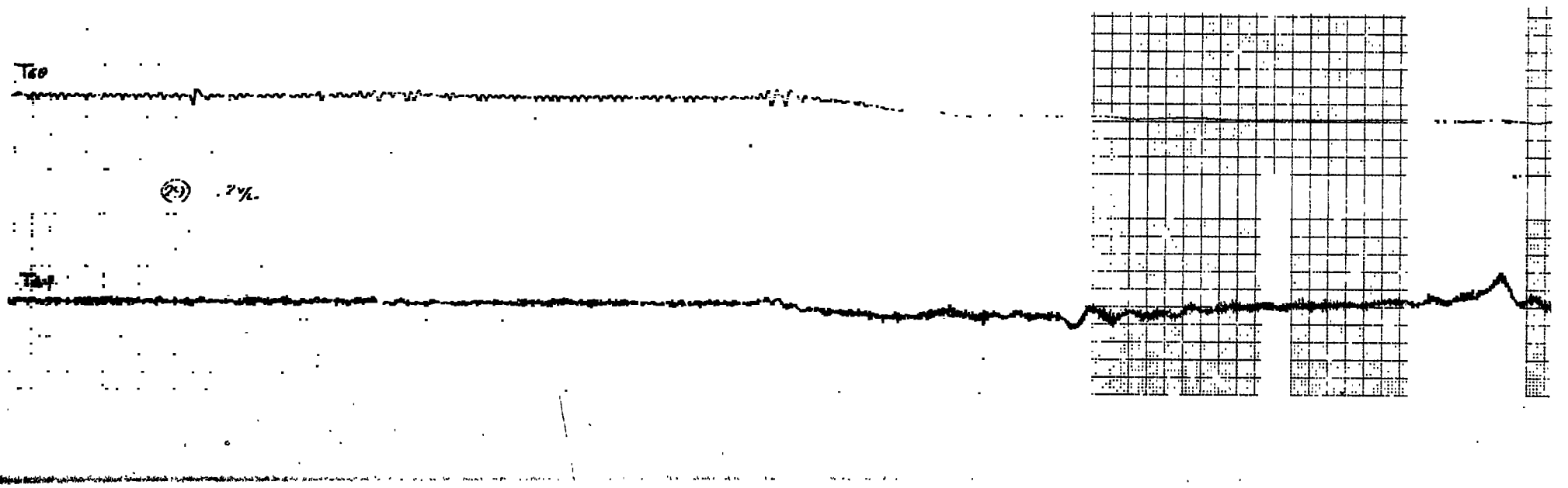
T60
.2%.

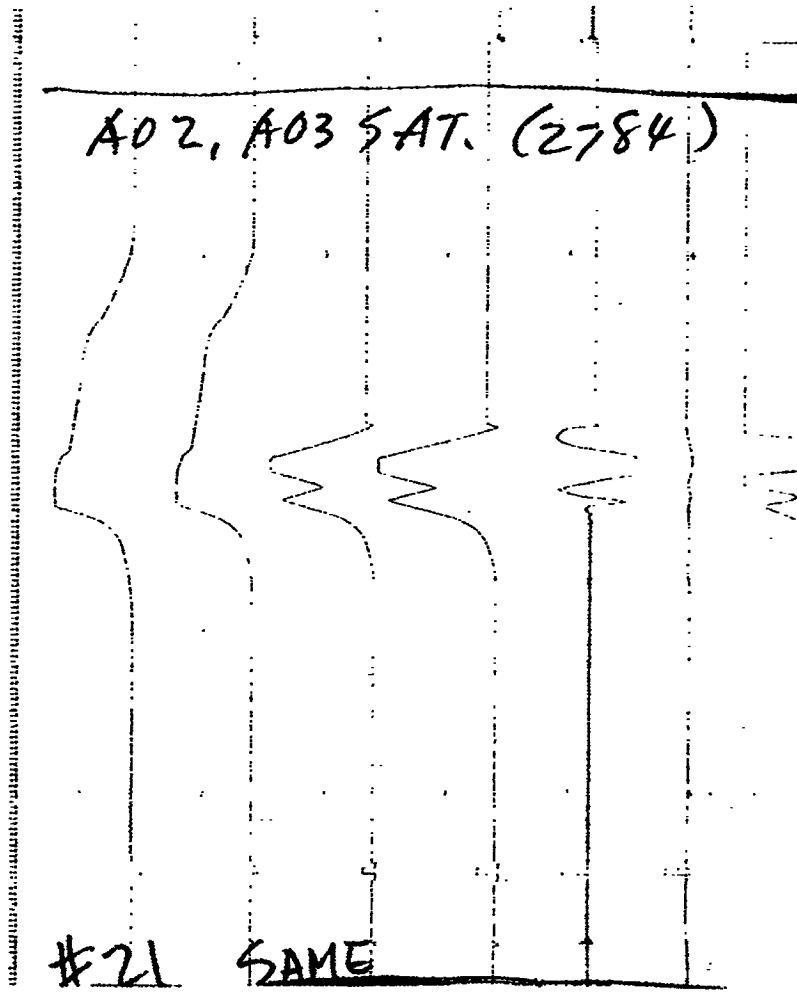
A02, A03 SAT. (2-84)
#21 SAME

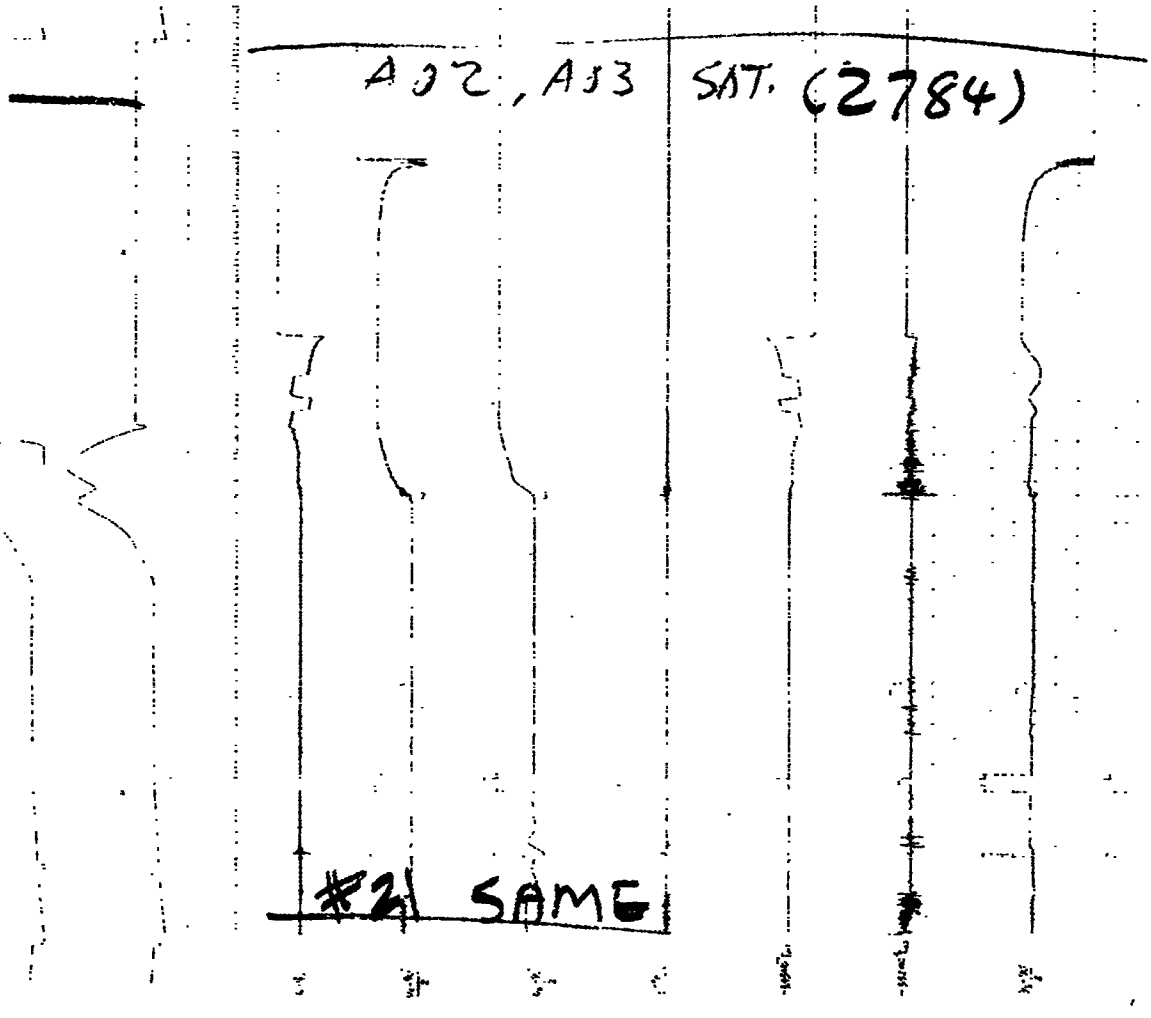
AJ2, AJ3 SAT. (2784)
#21 SAME

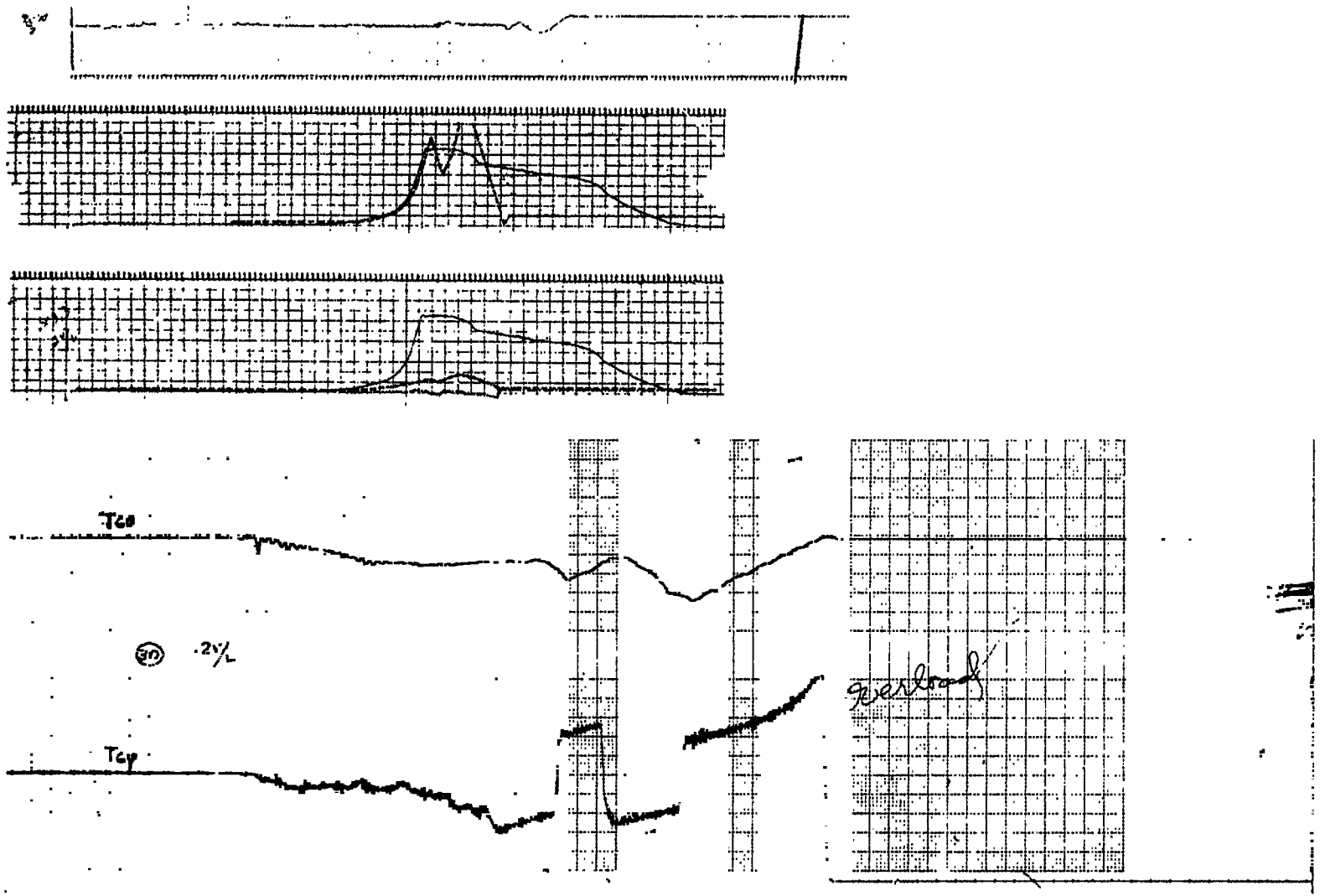
Tc0
Tcy
verbal

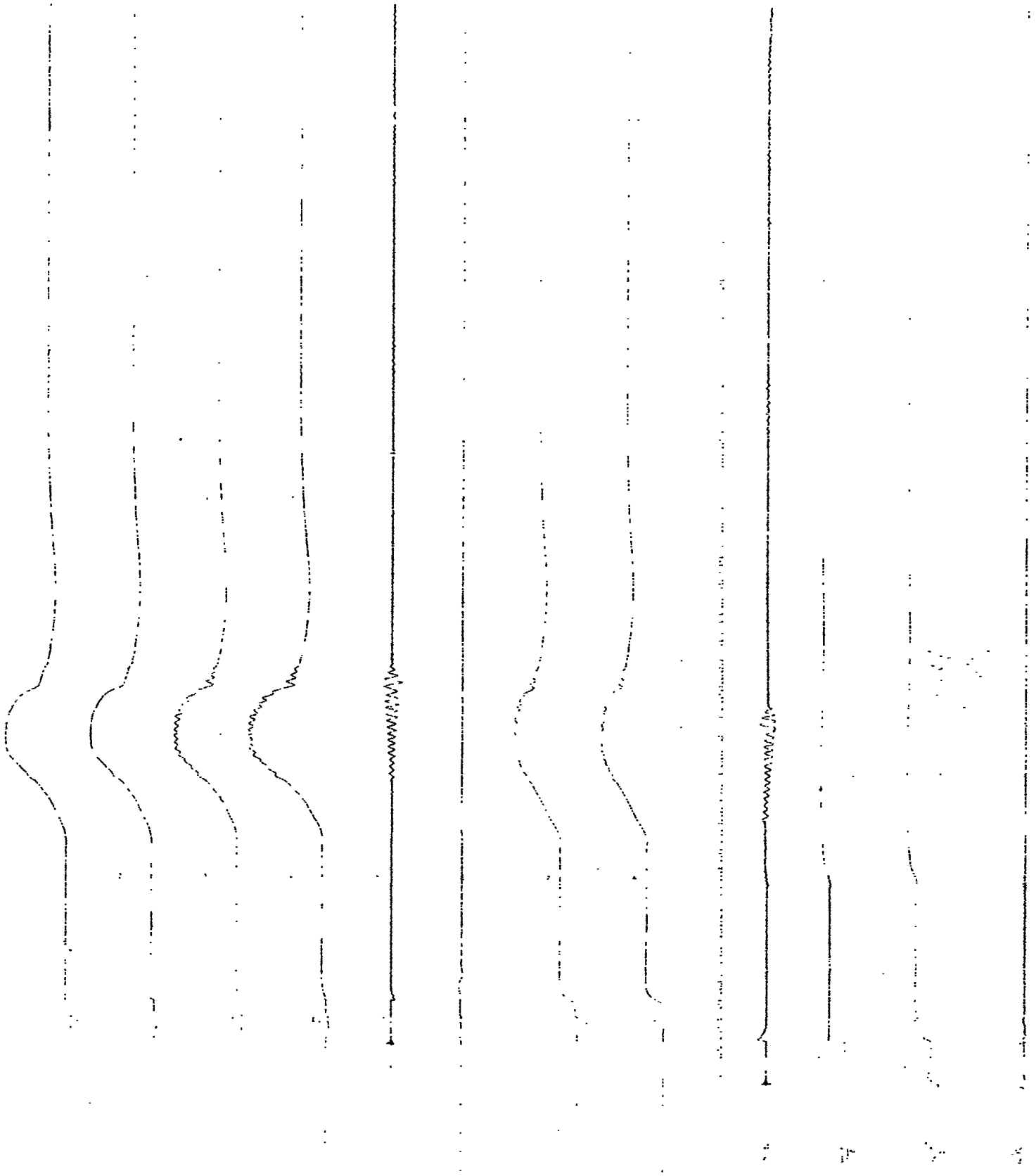

#20 WITHOUT 2·G level

#21 WITHOUT

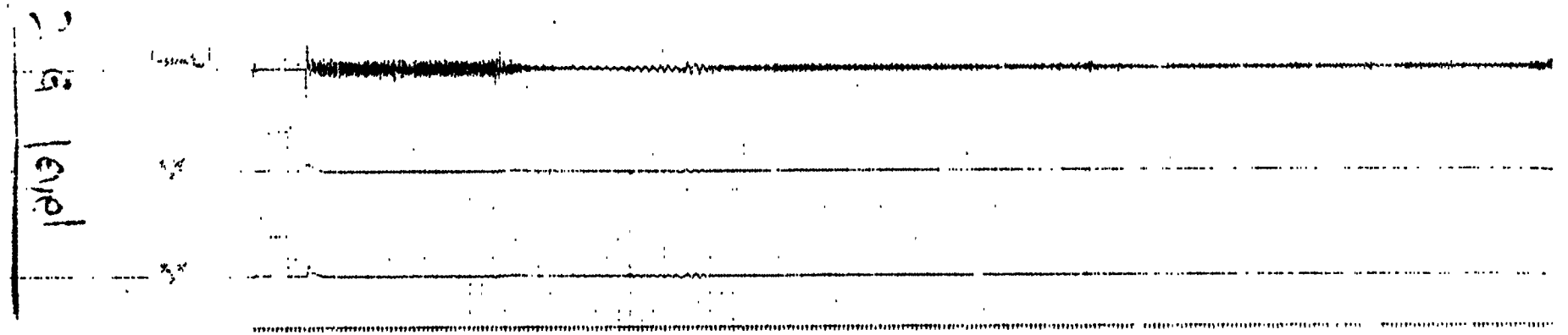

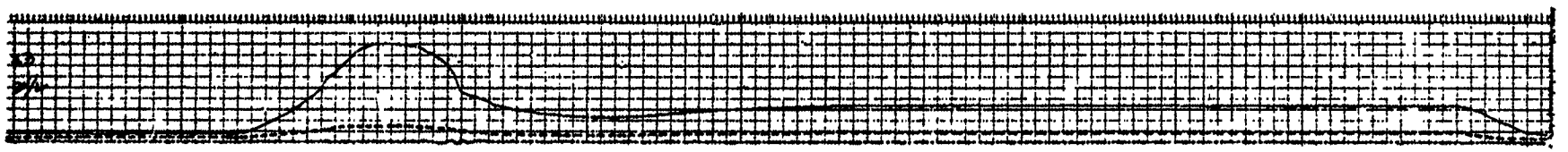

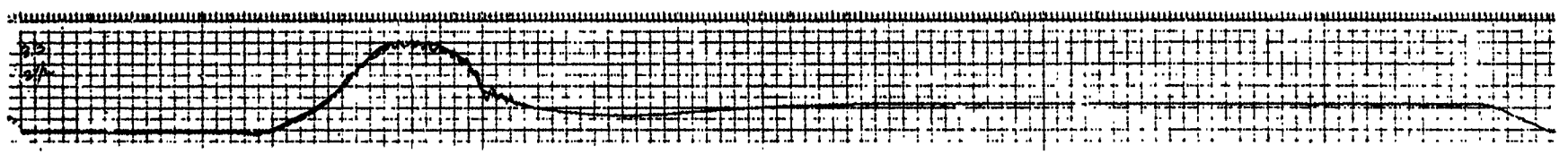

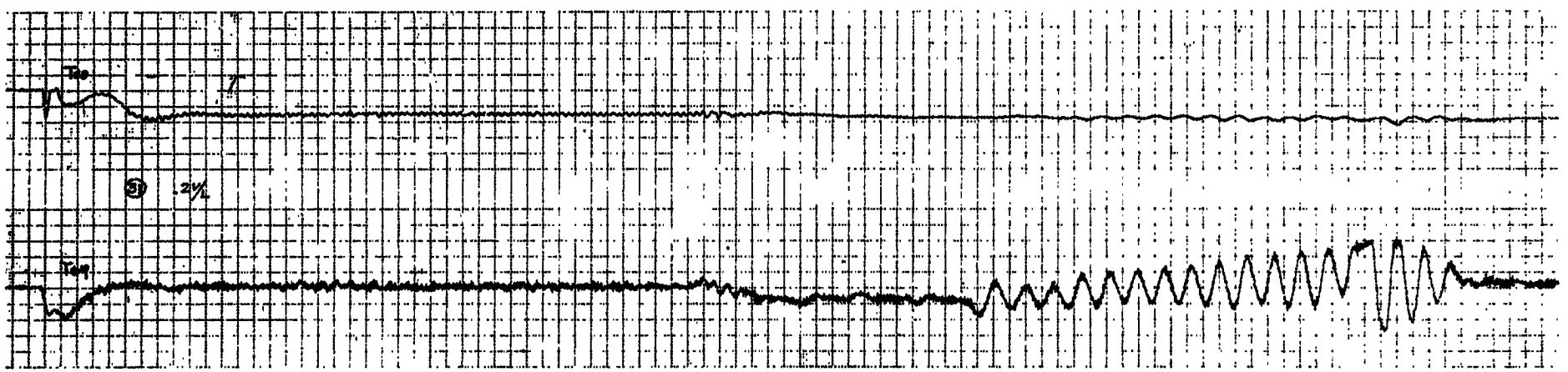
Tee
Tee

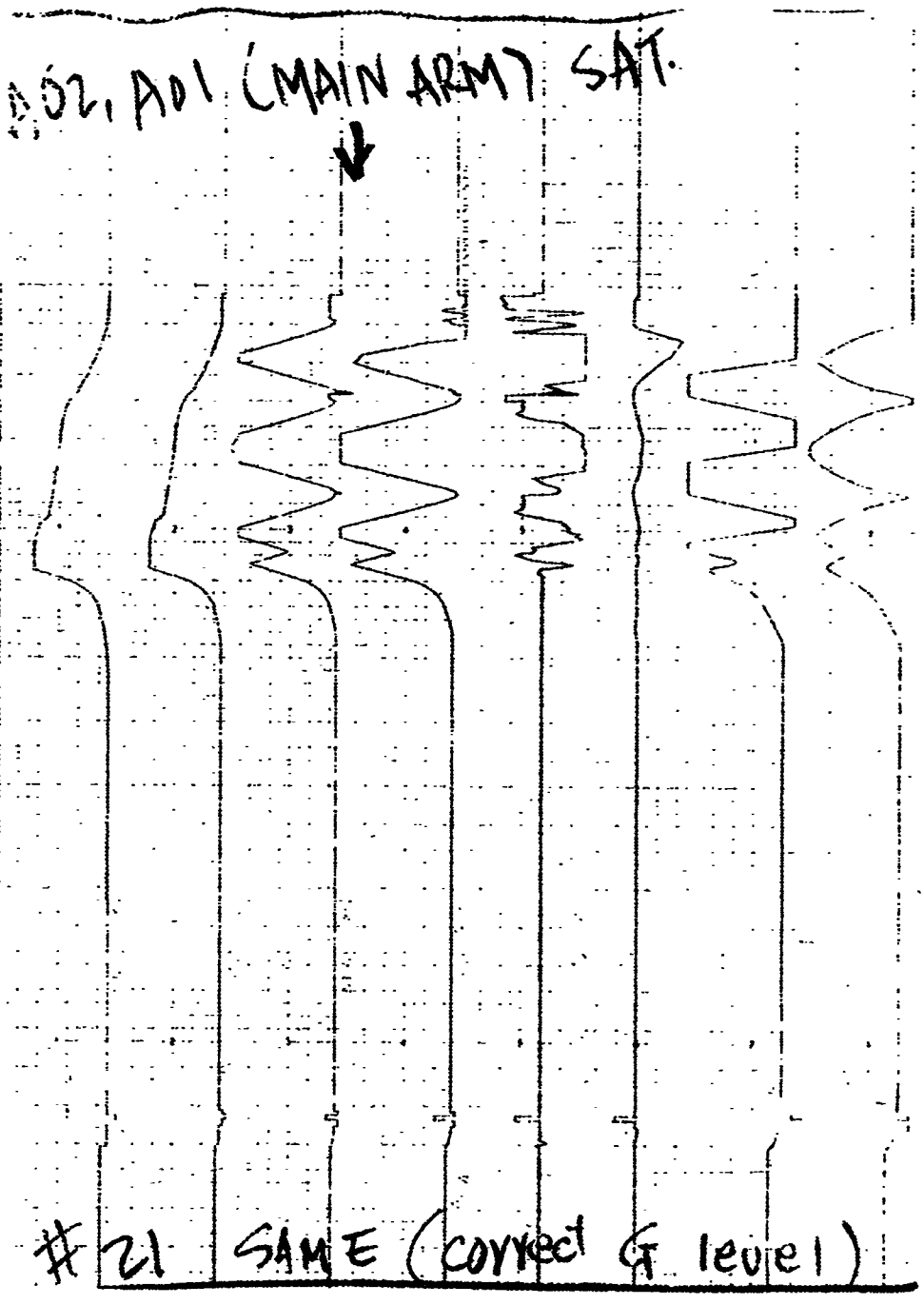
1:02, A01 (MAIN ARM) SAT.
#21 SAME (correct G level)

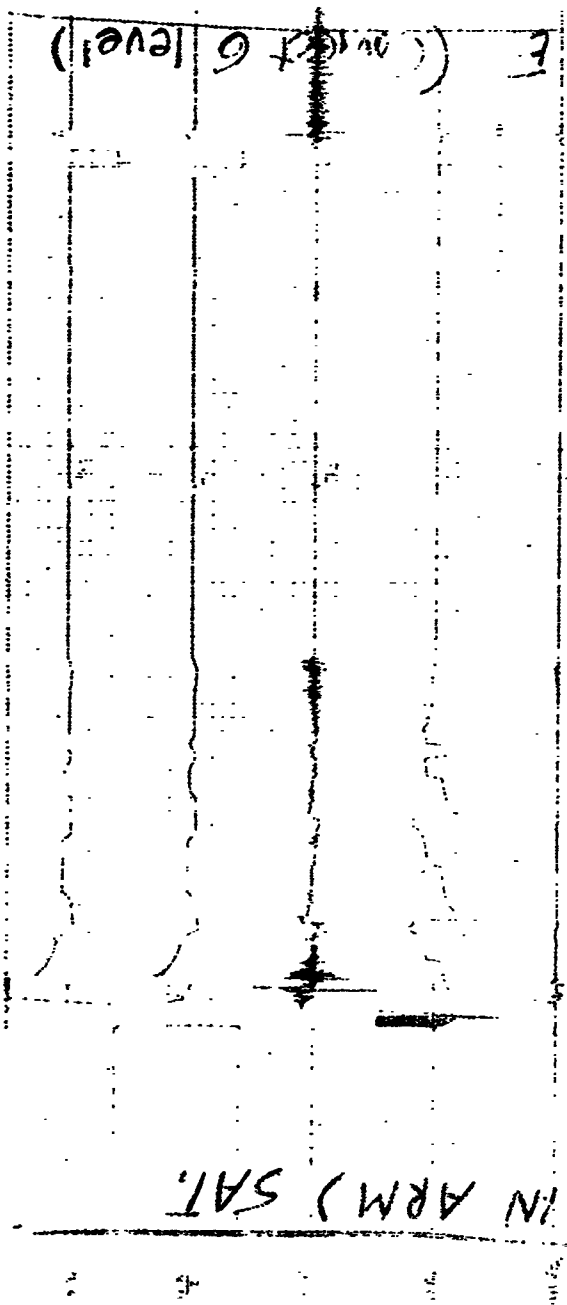
(correct G level)
IN ARM) SAT.

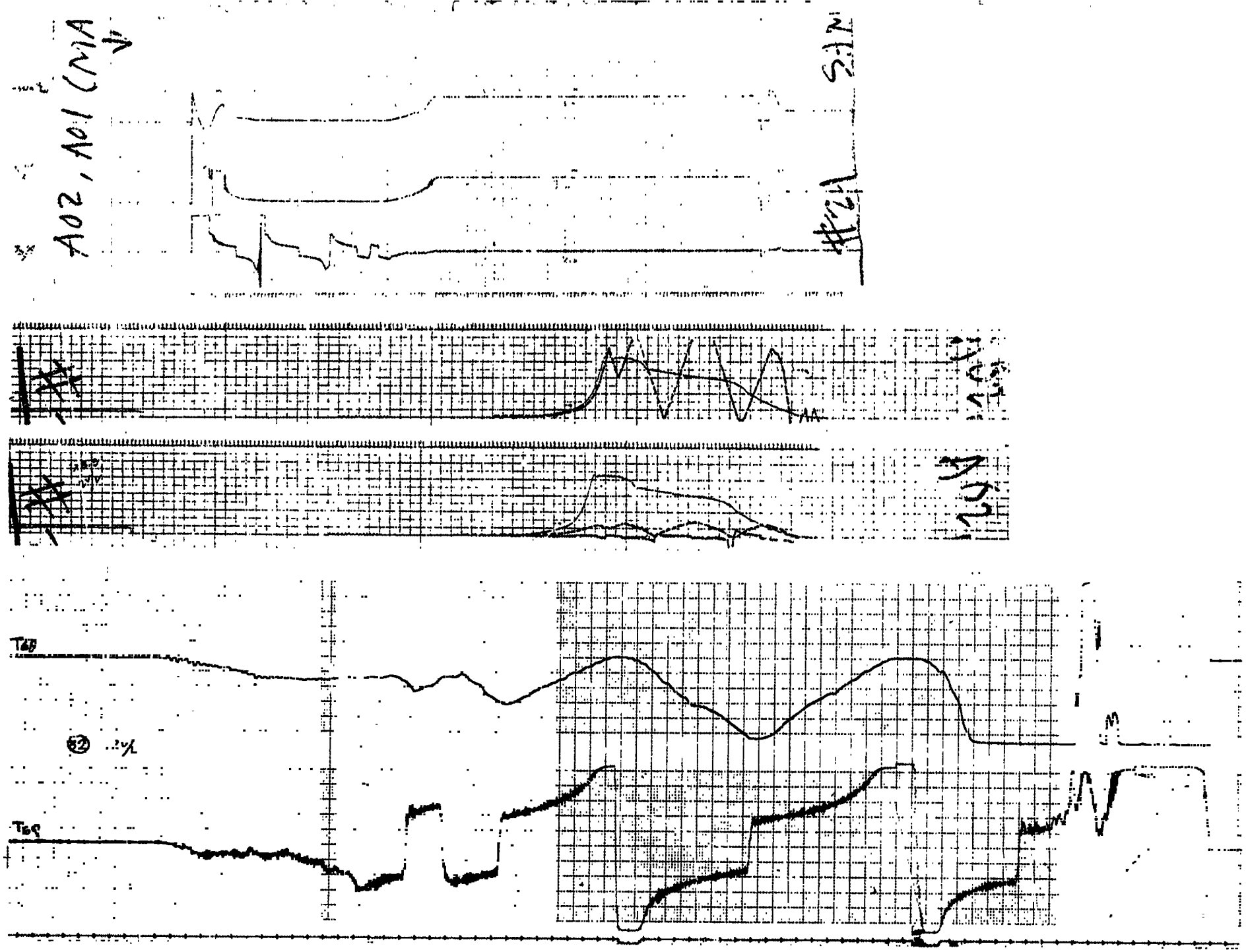
T&P

#22 (SAME)

#22 (SAME

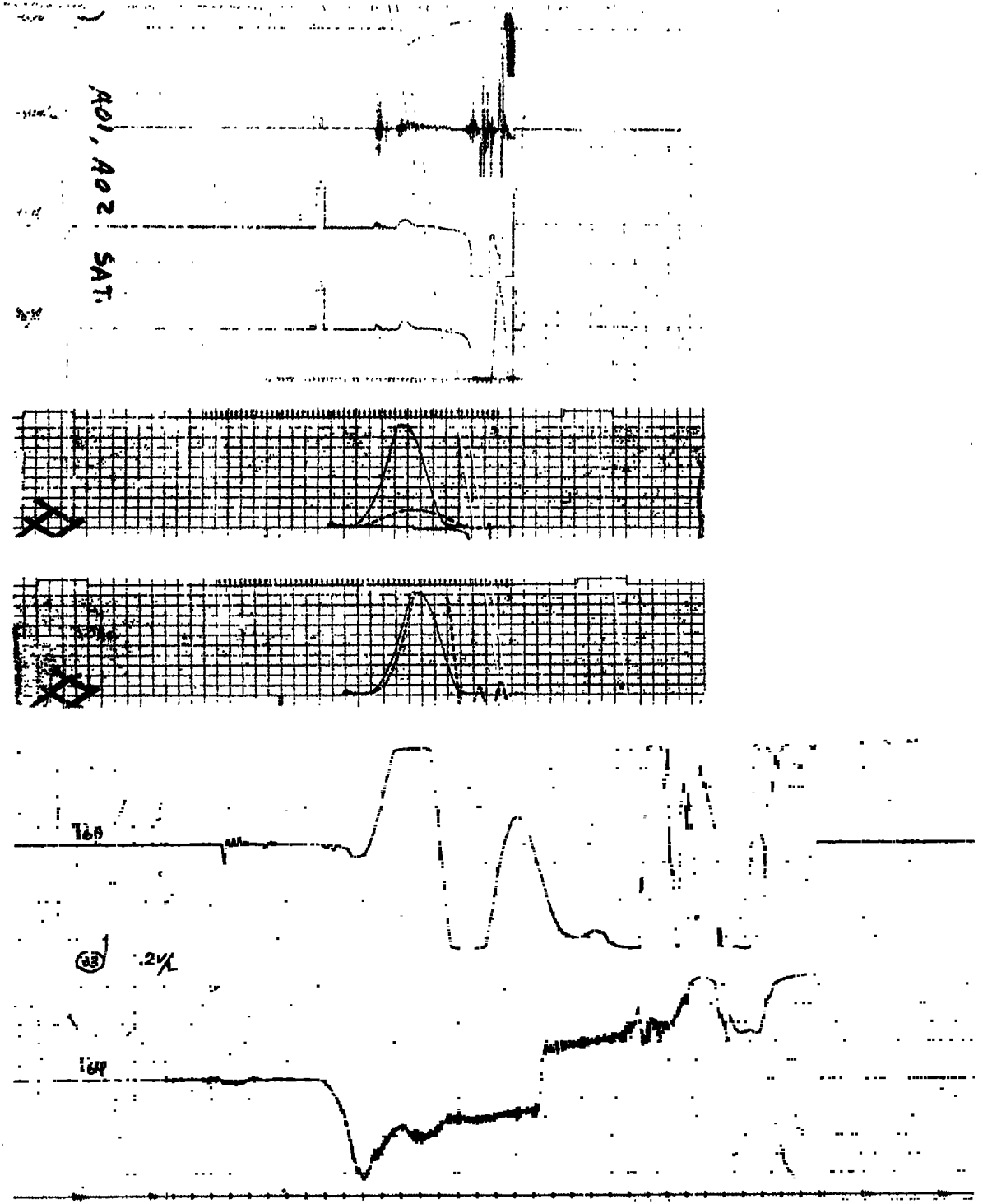

2

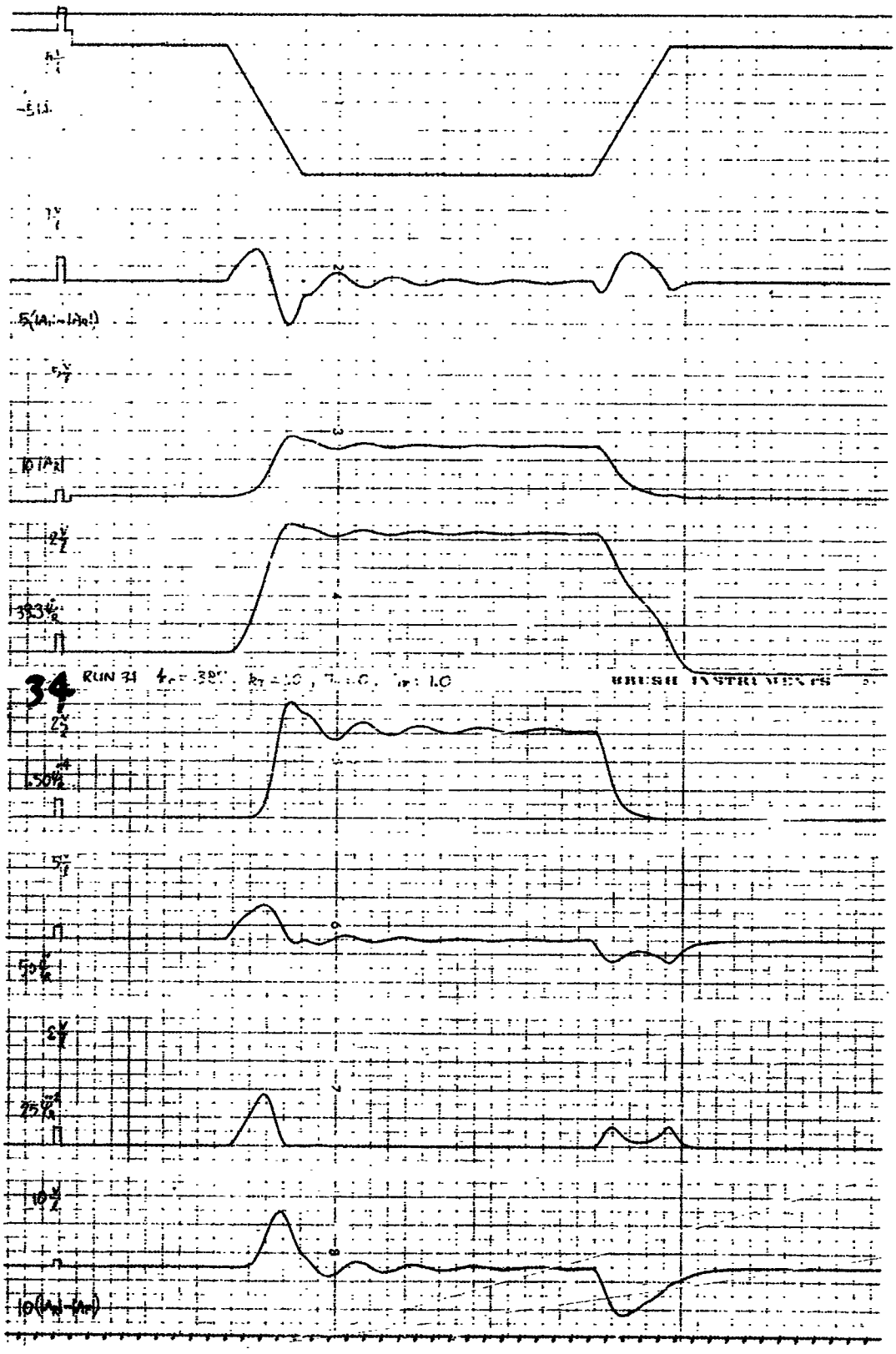
RUN 34
BRUSH INSTRUMENTS

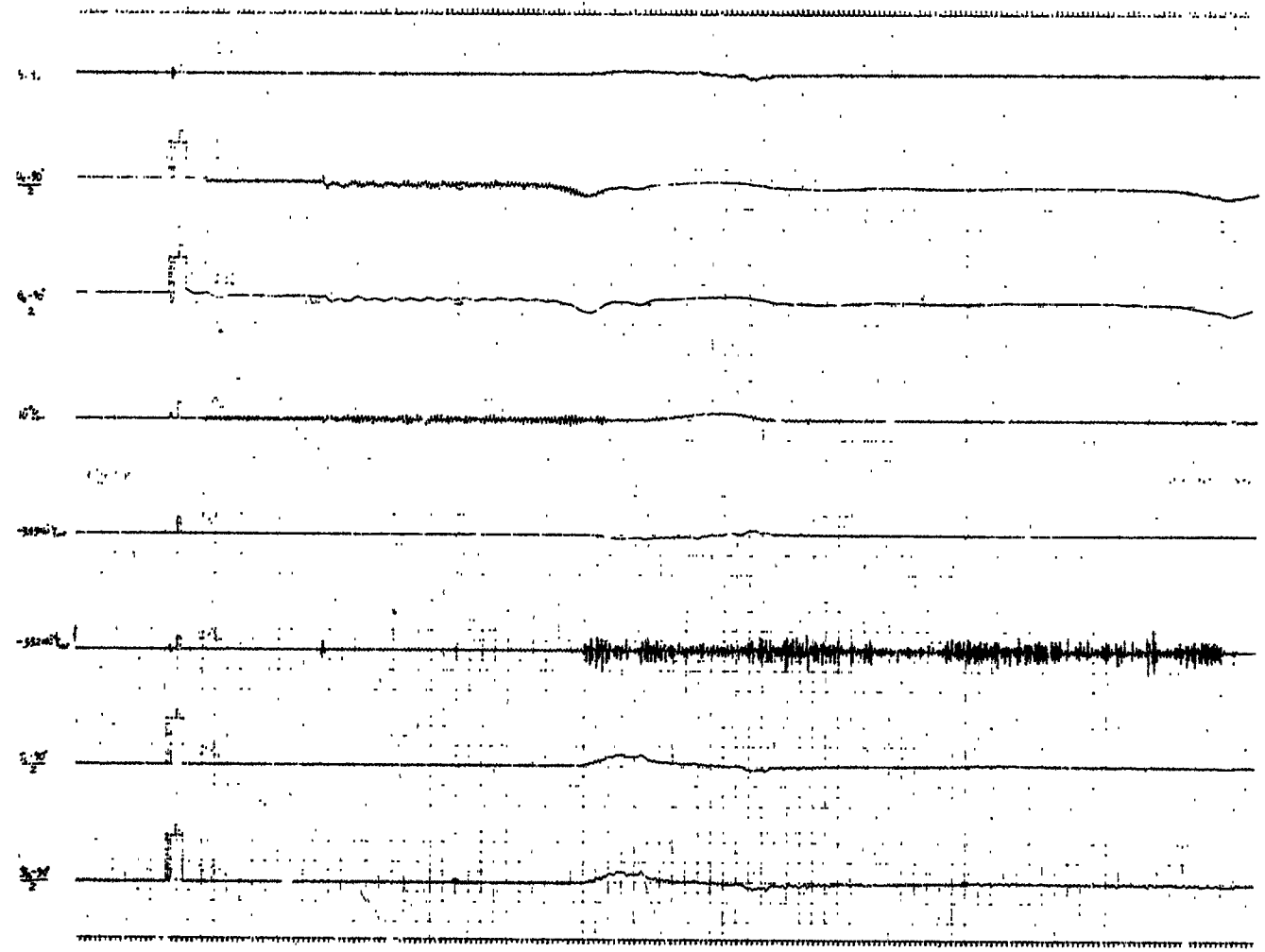

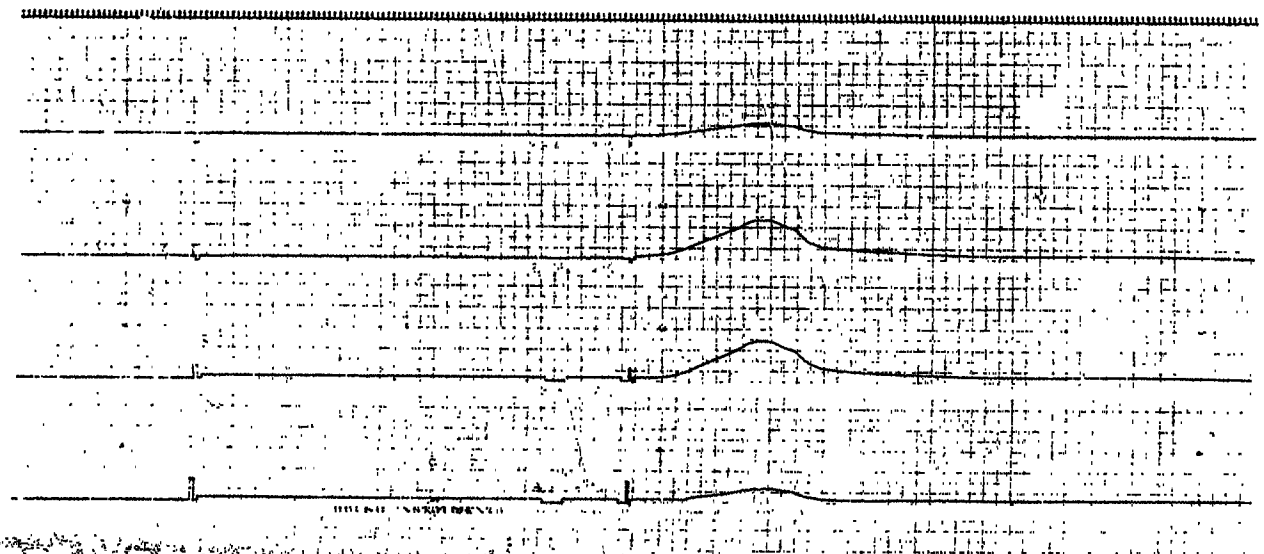

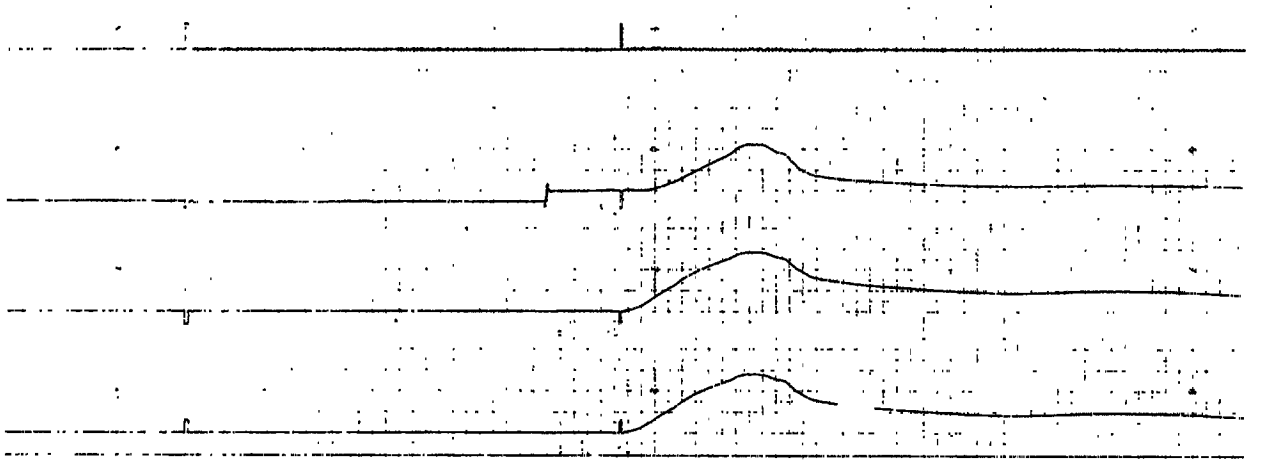

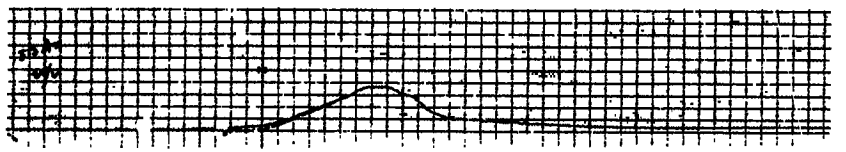

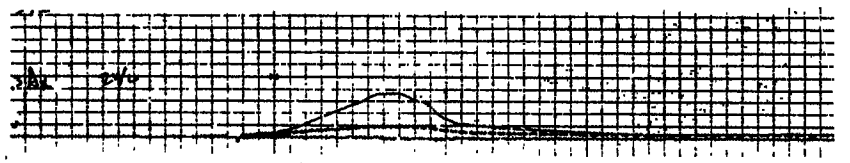

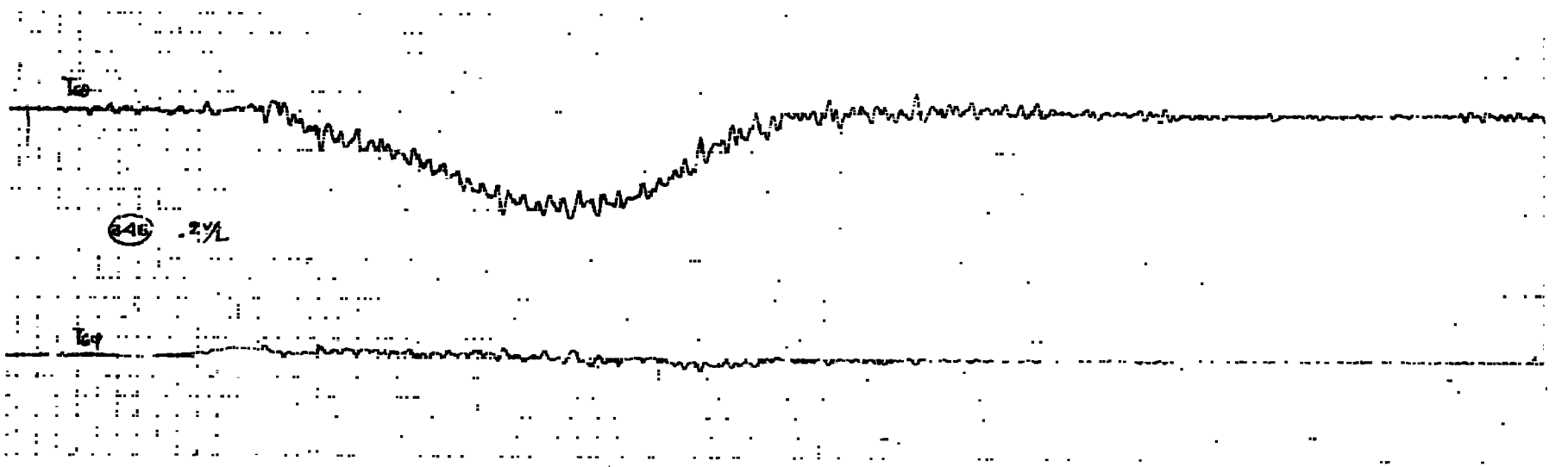
Tco
246
-2%
Tcg

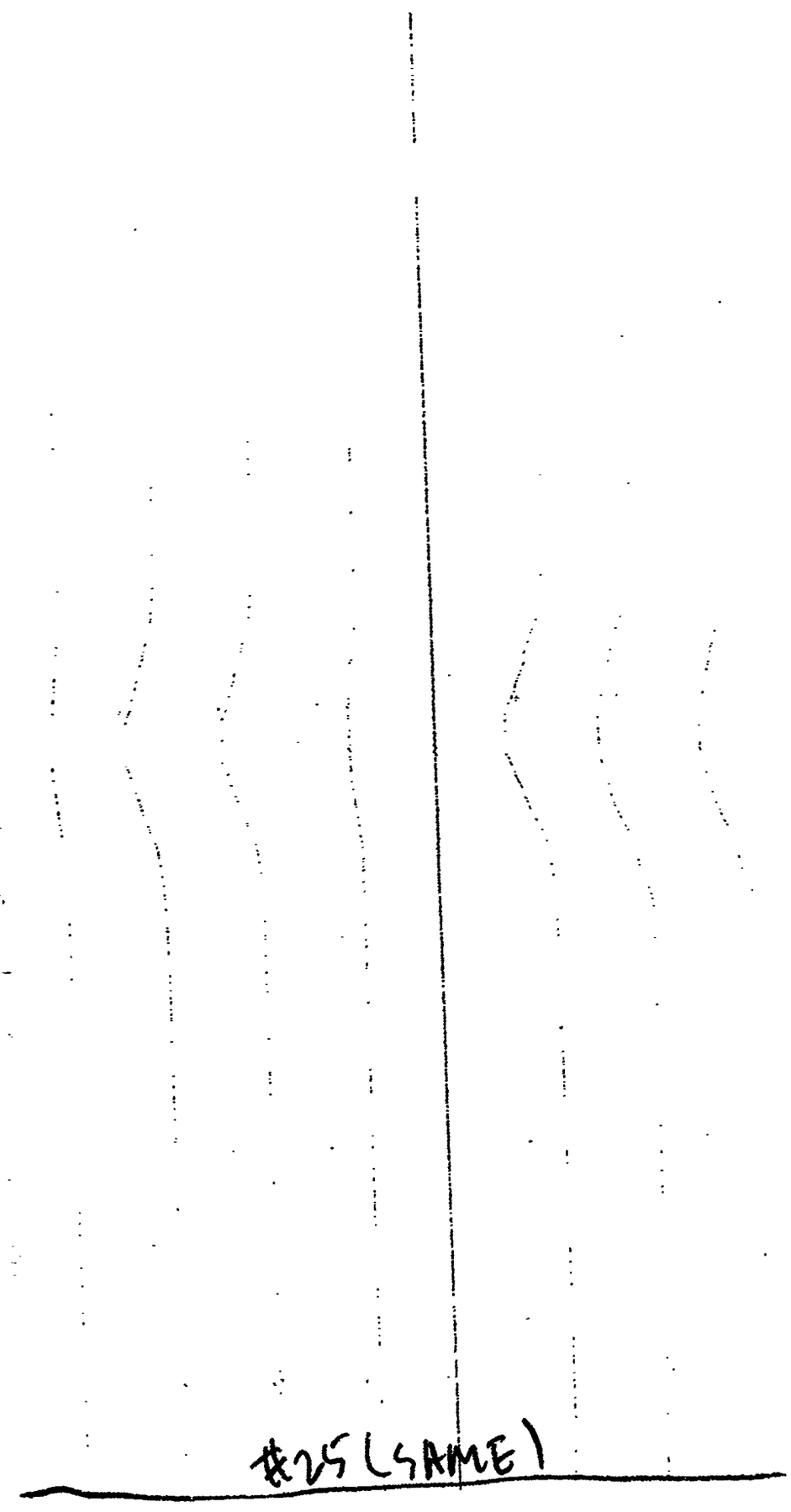
#25 (SAME)

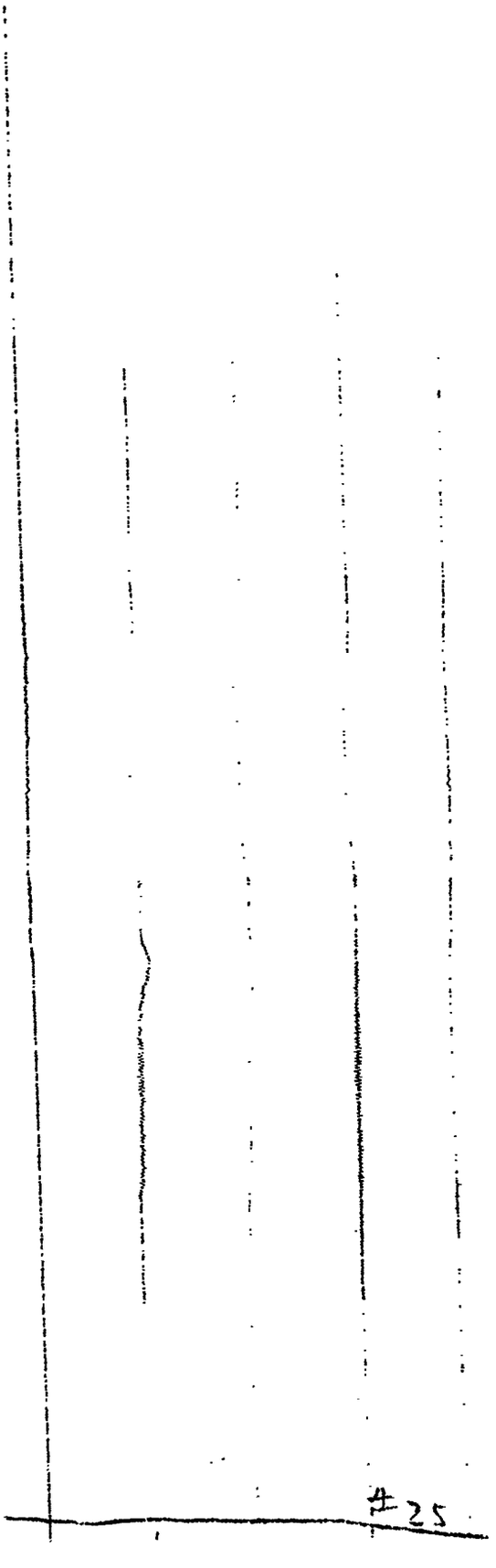
#25

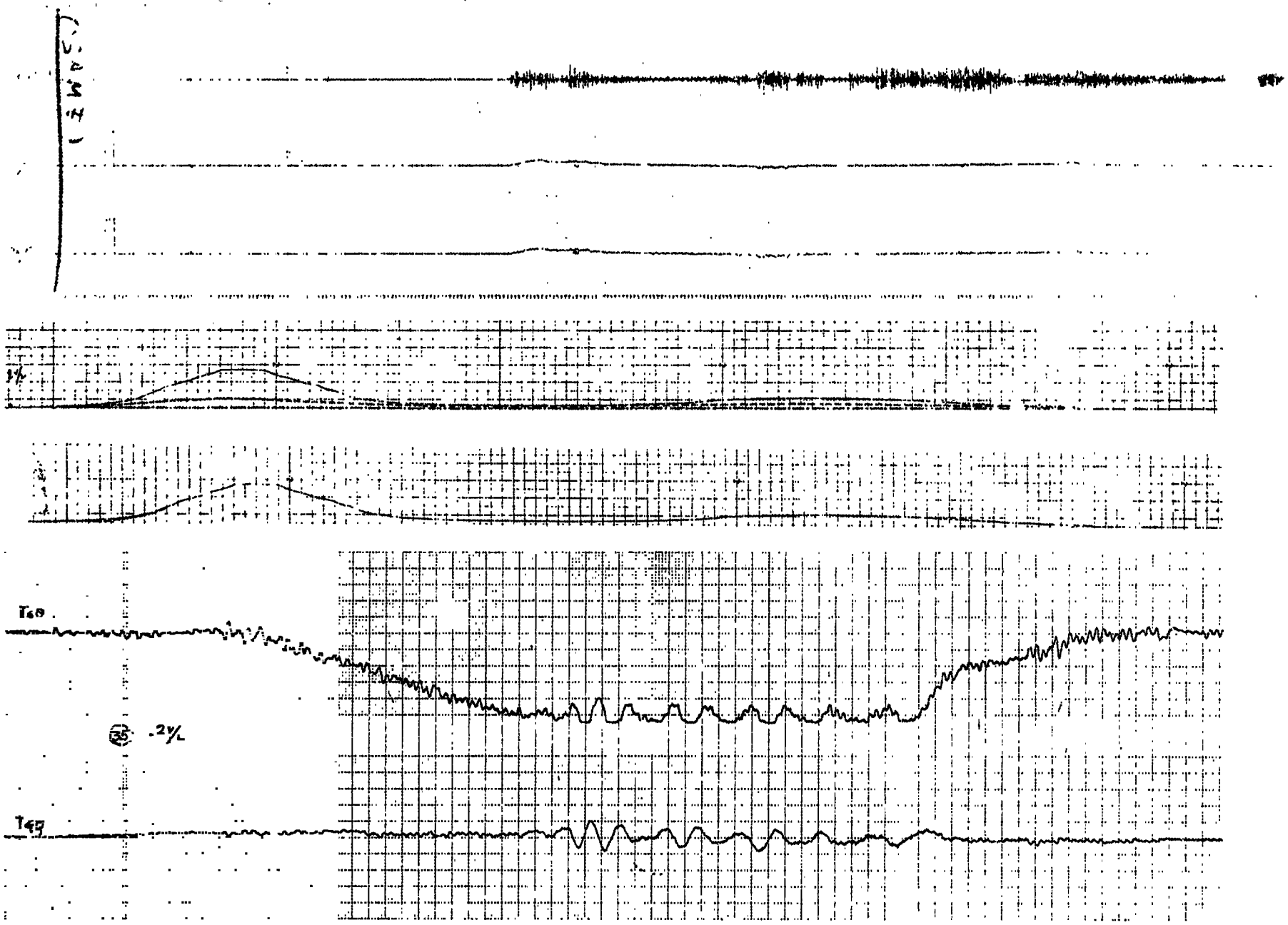
T60
35 -2%
T47

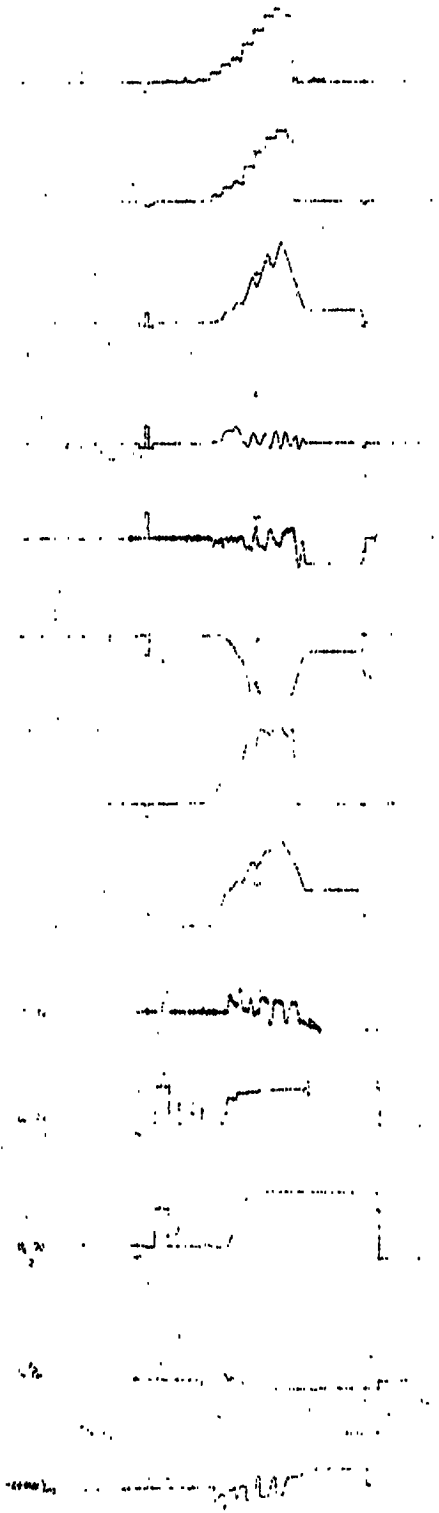

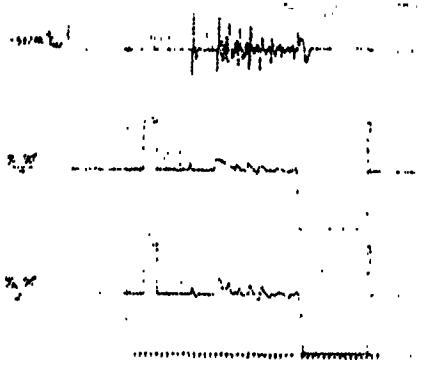

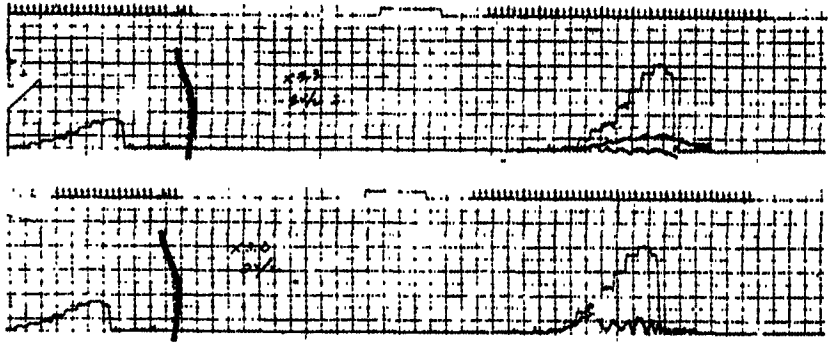

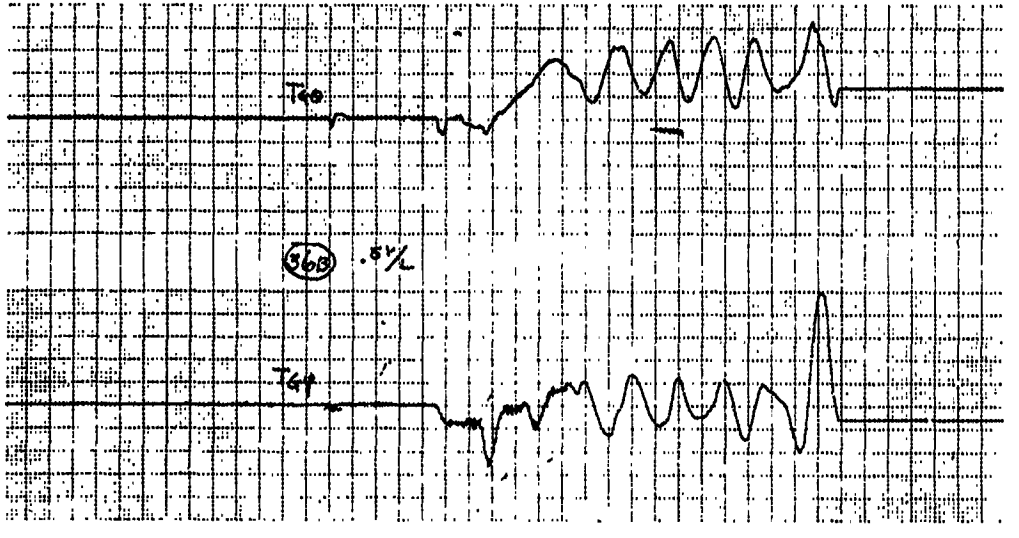
T40
360
.5 mV
T49

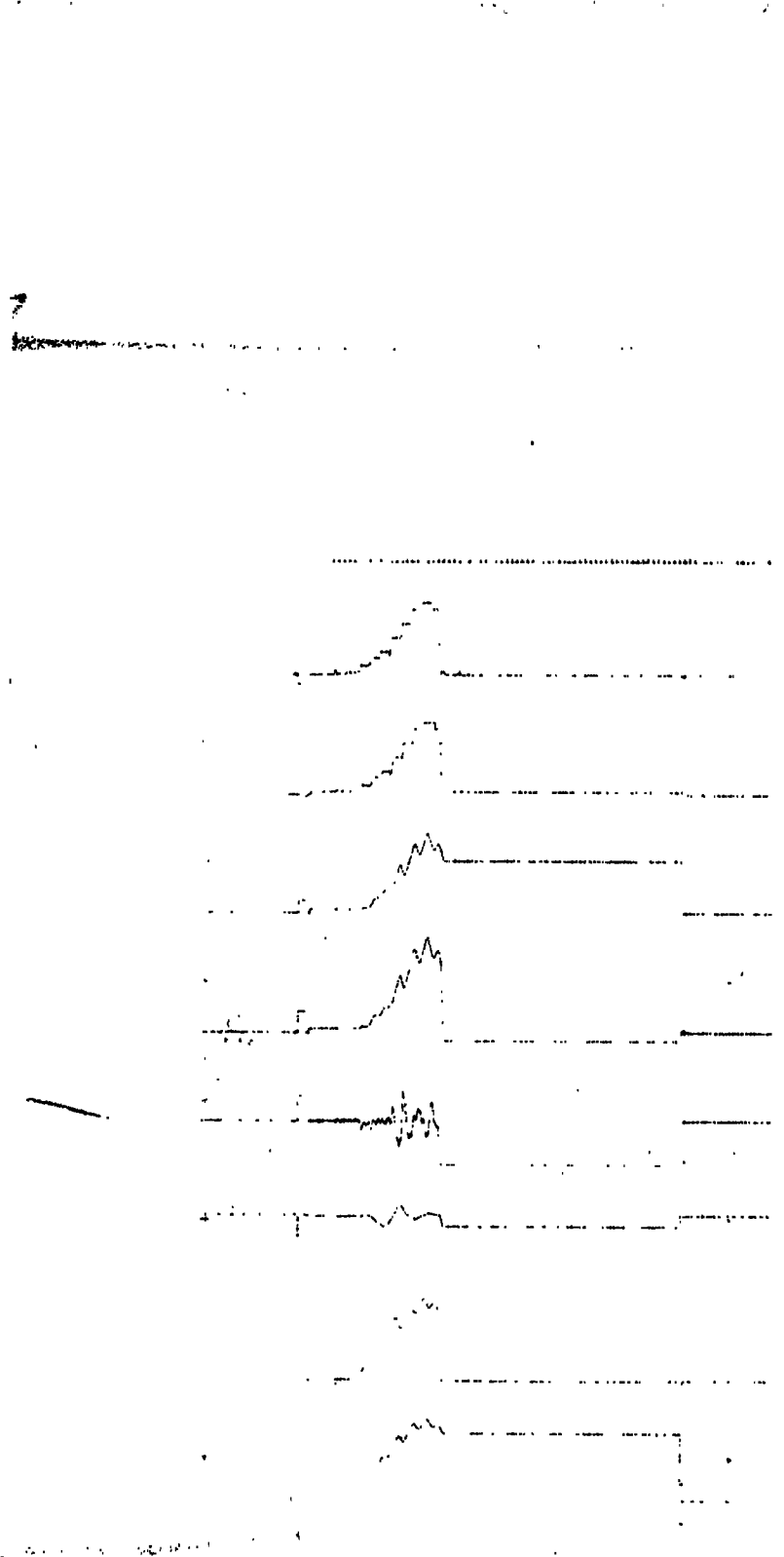

RERUN OF THE

Ch 2

LAST(#25)

@3

#30 RERUN (SAME)
#30
REI

RUN (SAME)

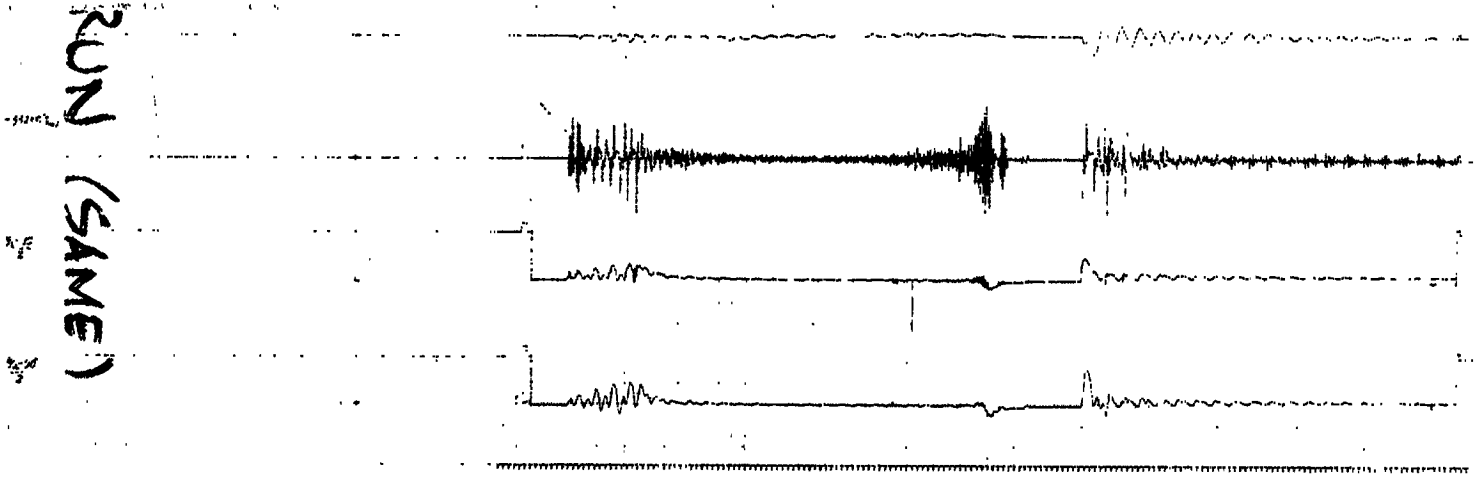

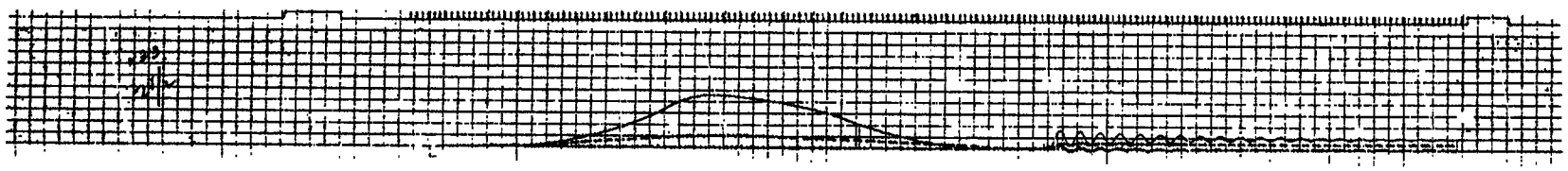

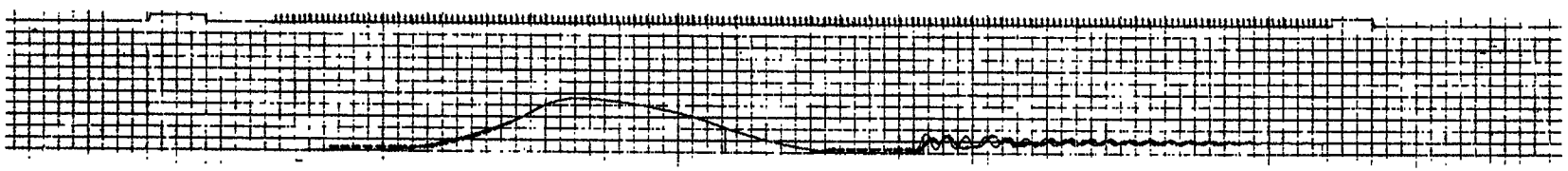

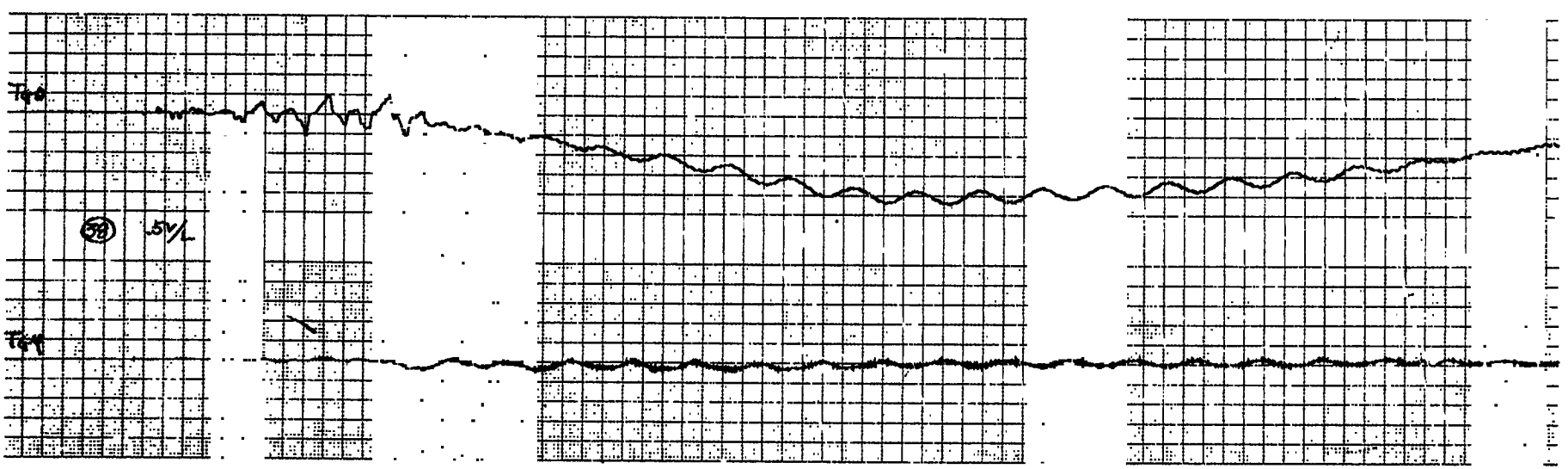

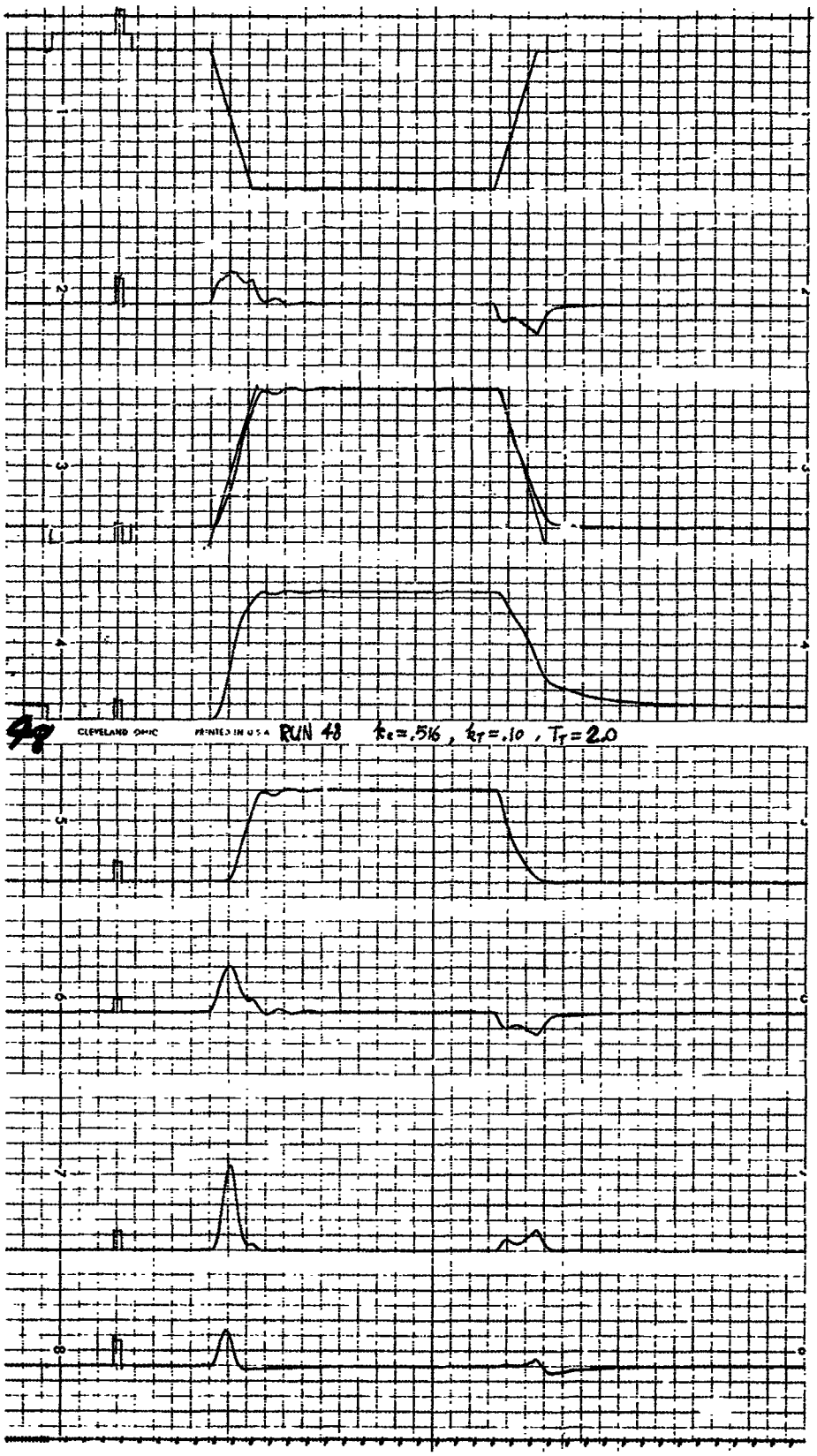
5 V/l
-5|A1|
1 V/l
5(|A1|-|AR|)
2 V/l
10|AR|
2 V/l
333 ψ̇R
CLEVELAND OHIO PRINTED IN U.S.A. RUN 48 kE = .516 , kT = .10 , TT = 2.0
2 V/l
1.50 ψ⁴R
5 V/l
50 ψ̈R
2 V/l
25 ψ̈²R
1 V/l
10(|AN|-|AR|)

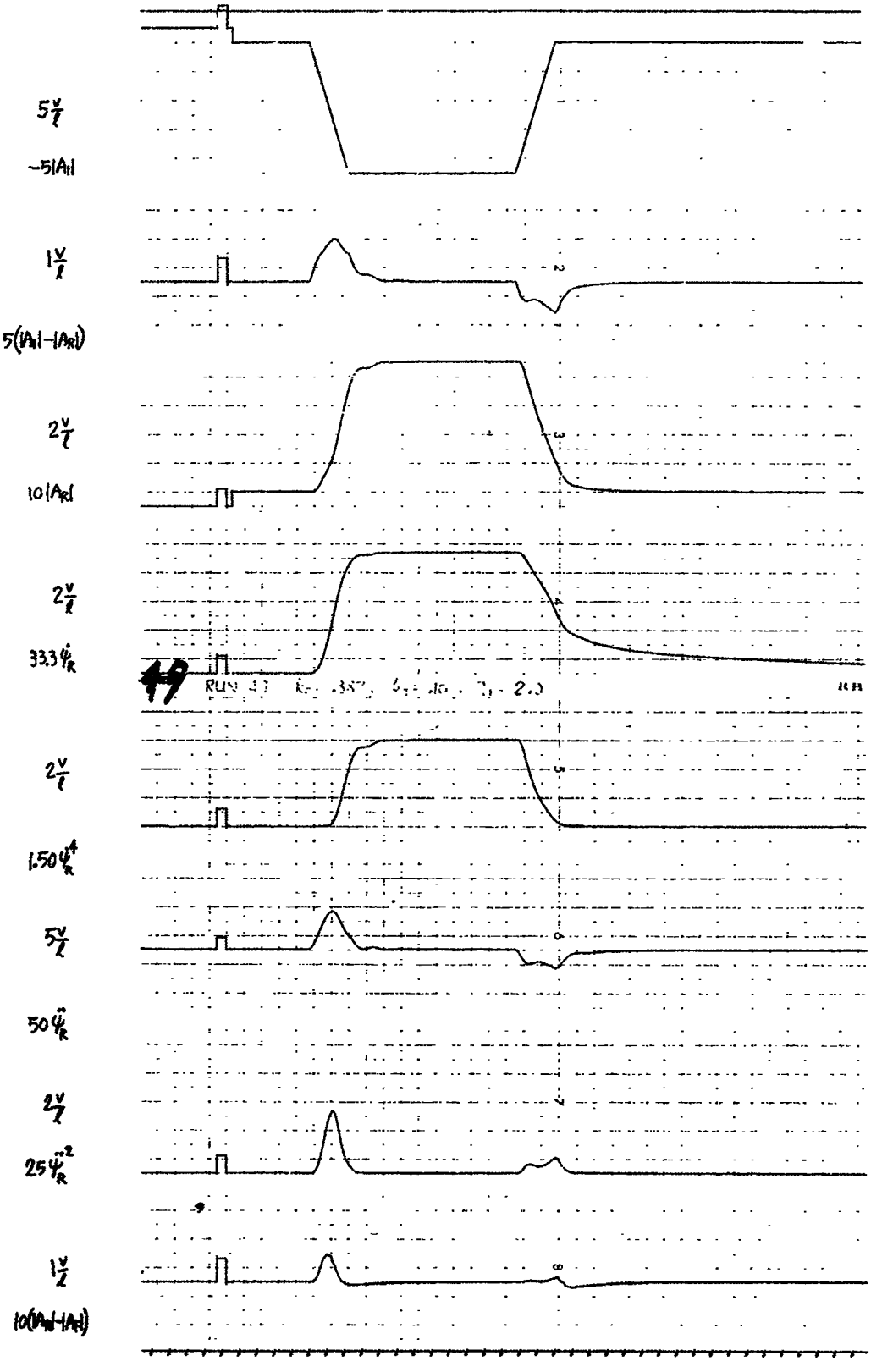
5 V/
−5|A11|
1 V/
5(|A21|−|A22|)
2 V/
10|A22|
2 V/
333 ψ̇R
49
RUN 47
2 V/
150 ψ̇R
5 V/
50 ψ̈R
2 V/
25 ψ̈R²
1 V/
10(|A12|+|A11|)

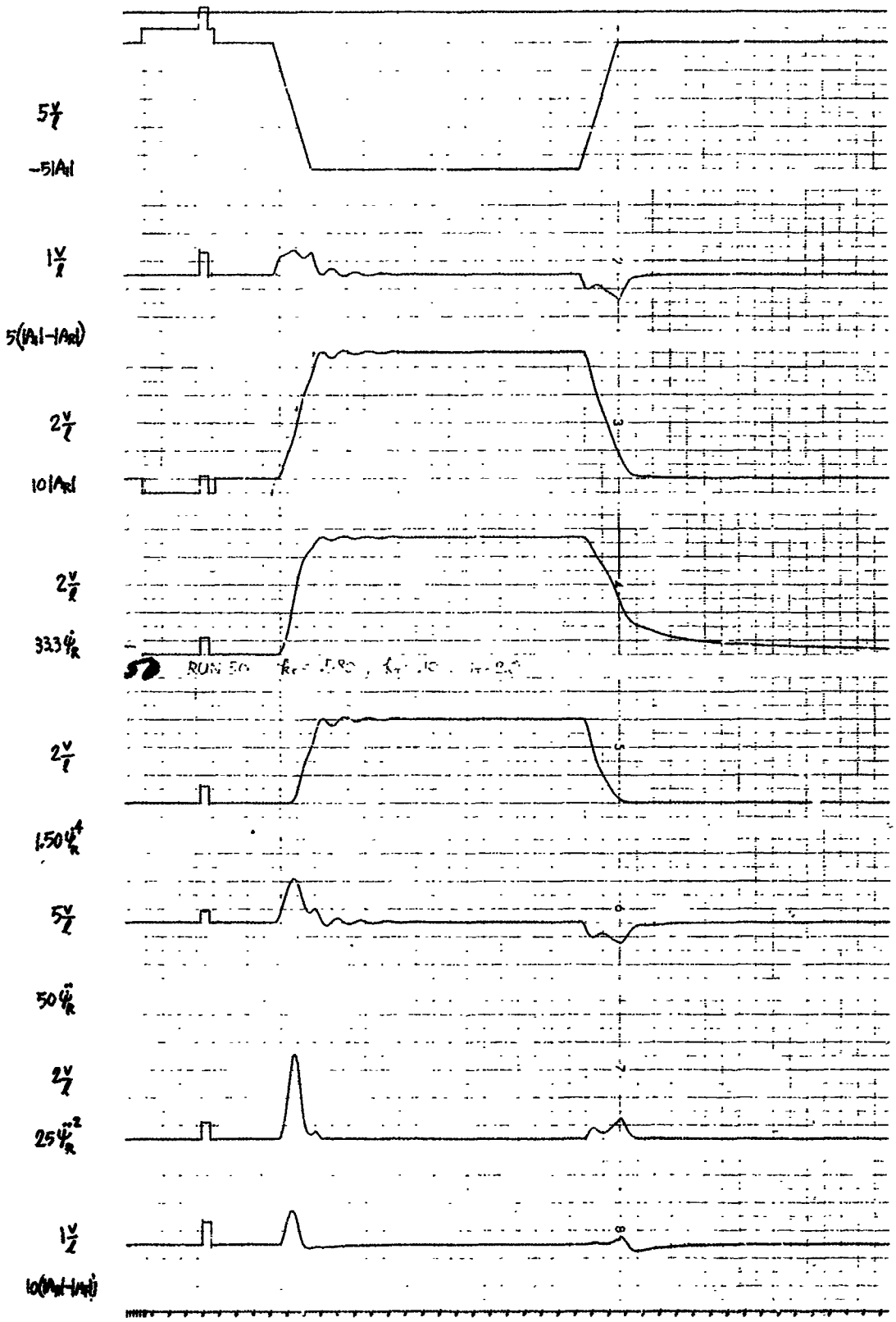
5 V/I
-5|A1|
1 V/I
5(|A1|-|A2|)
2 V/I
10|A2|
2 V/I
333 ψ̇R
RUN 50
2 V/I
1.50 ψ⁴R
5 V/I
50 ψ̈R
2 V/I
25 ψ̈²R
1 V/I
10(|A1|-|A2|)

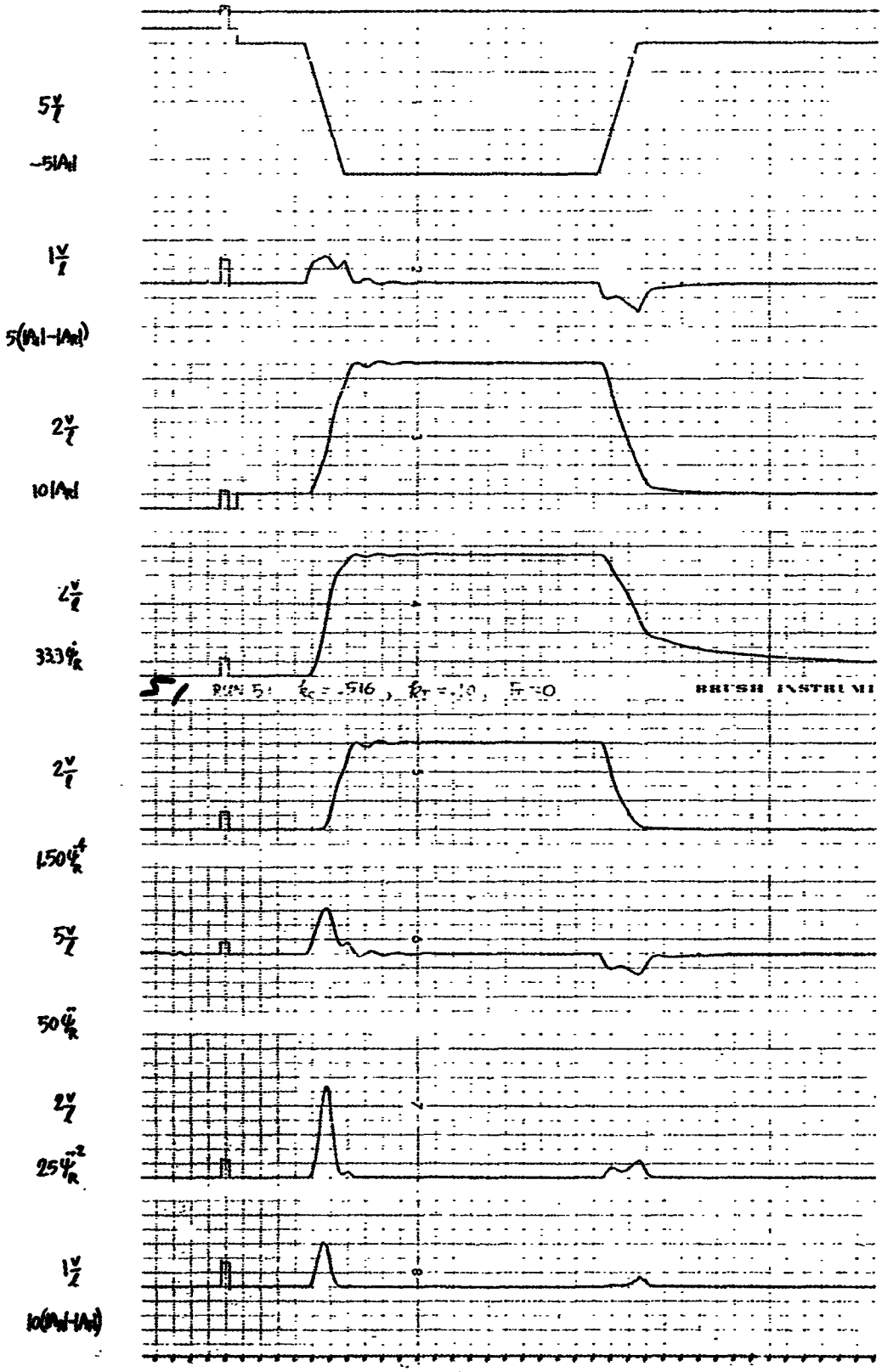
5 V/I
-5|A|
1 V/I
5(|A|-|A₀|)
2 V/I
10|A₀|
2 V/I
333 ψ̇R
RUN 5: kc = .516, kr = .10, F = 0
BRUSH INSTRUMENTS
2 V/I
150 ψ̈R
5 V/I
50 ψ̈R
2 V/I
25 ψ⃛R
1 V/I
10(|A₀|-|A|)

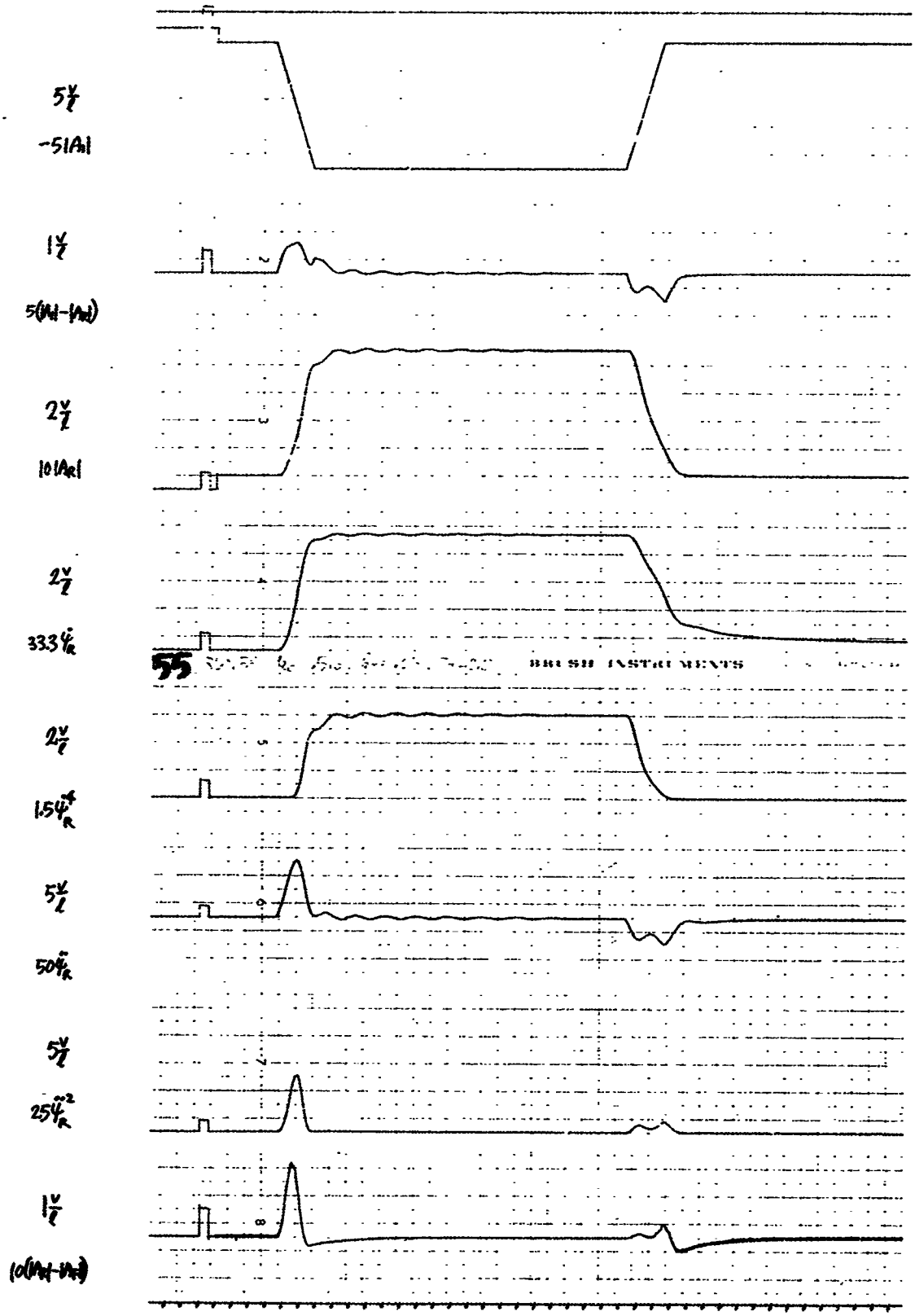
5V/
-5|A1|
1V/
5(N1-N2)
2V/
10|A2|
2V/
333Ψ²R
2V/
1.5Ψ⁴R
5V/
50Ψ⁶R
5V/
25Ψ⁸R
1V/
10(N1-N2)
55
BRUSH INSTRUMENTS

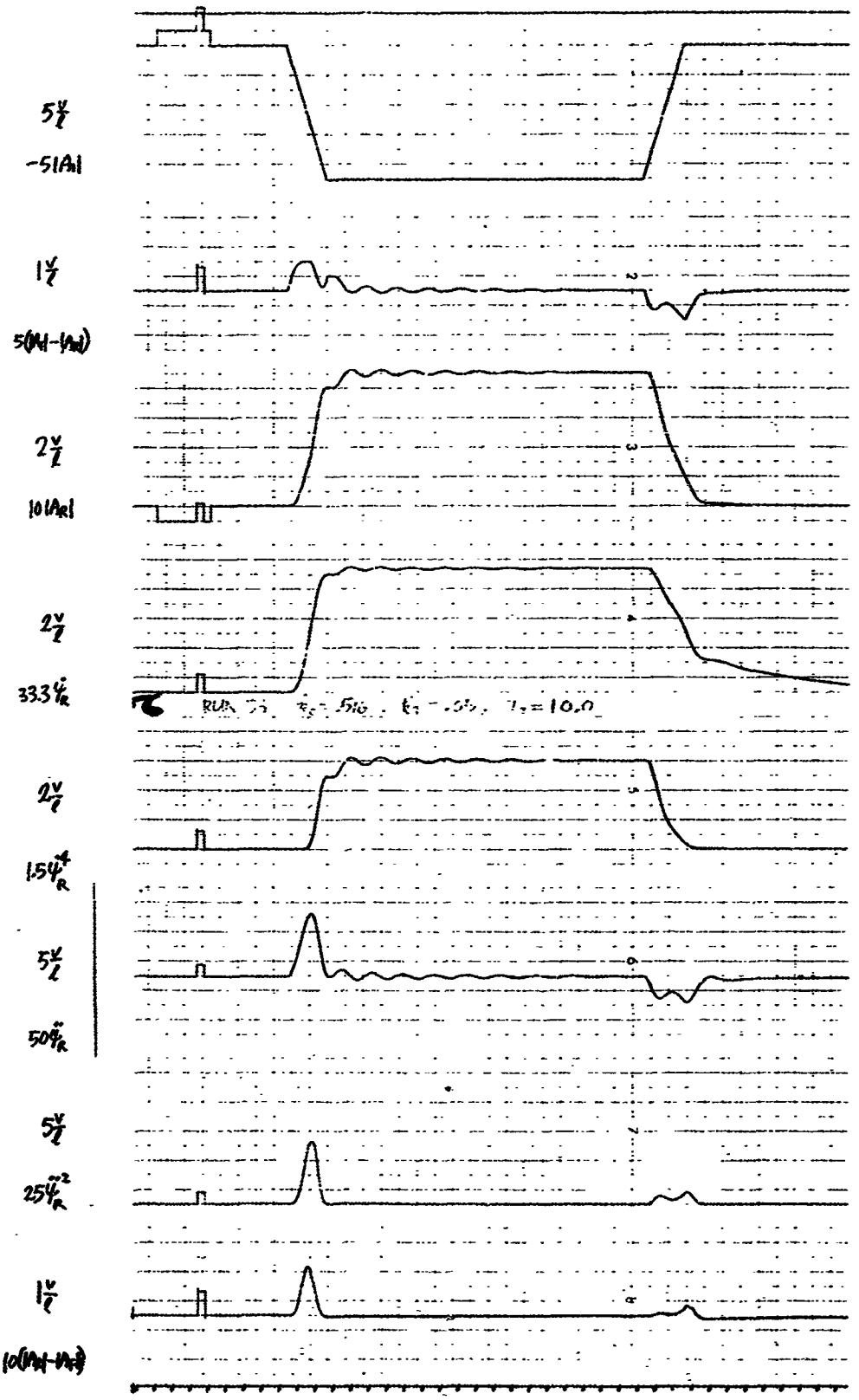
5V/
-5|A1|
1V/
5(M1-M2)
2V/
10|AR|
2V/
333Ψ̈R
RUN
2V/
154Ψ̈R
5V/
50Ψ̈R
5V/
25Ψ̈R²
1V/
10(M1-M2)

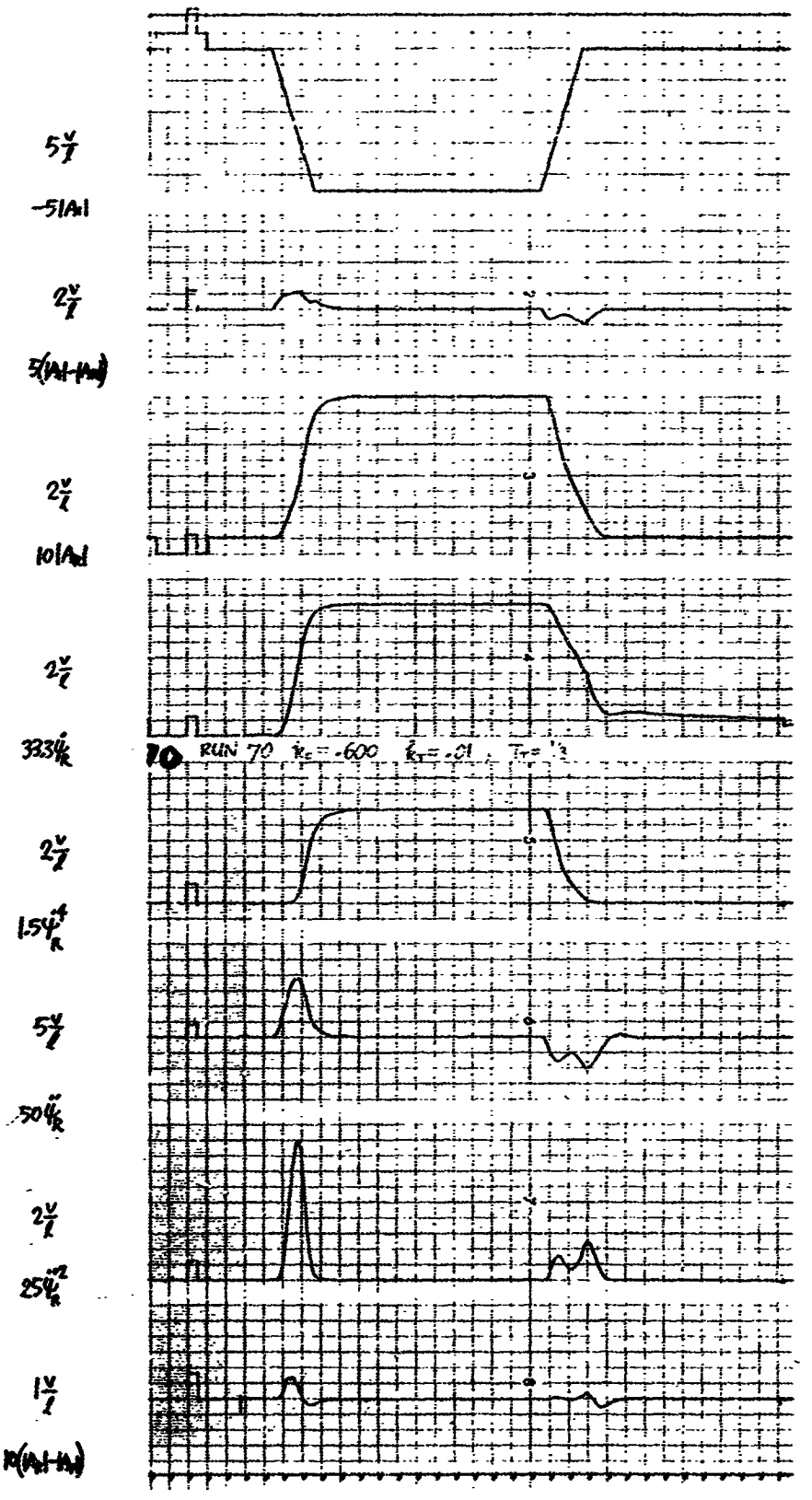
5 V/I
-5|A|
2 V/I
5(|A| - |A_0|)
2 V/I
10|A|
2 V/I
3334 ψ_R
RUN 70 k_c = .600 k_T = .01 T_F = 1/2
2 V/I
1.54 ψ_R^4
5 V/I
50 ψ_R^3
2 V/I
25 ψ_R^2
1 V/I
R(|A| - |A_0|)

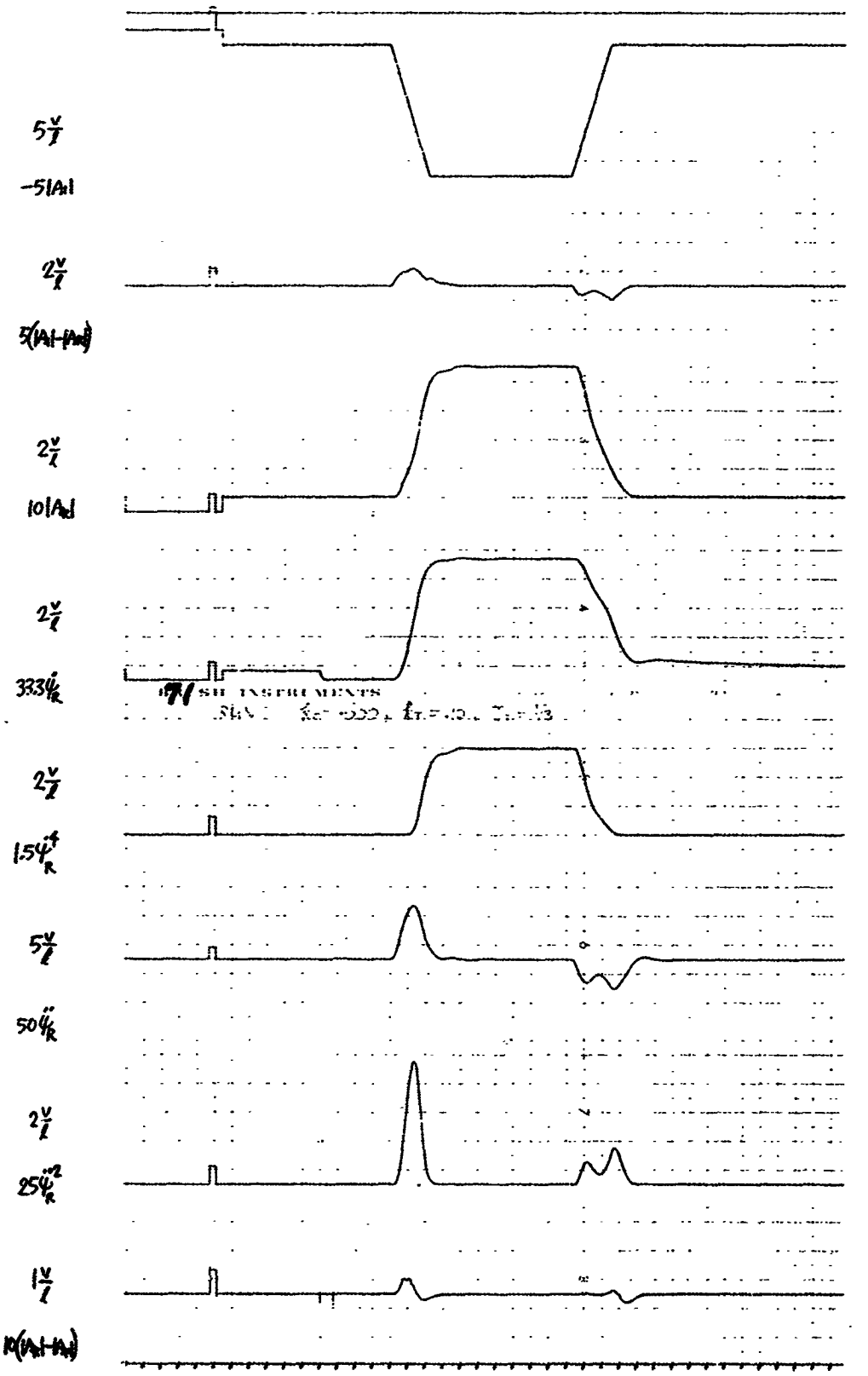
5 V/
-5|A1|
2 V/
5(|A1|-|A2|)
2 V/
10|A2|
2 V/
333 μR
2 V/
154 μR
5 V/
50 μR
2 V/
25 μR
1 V/
10(|A1|-|A2|)

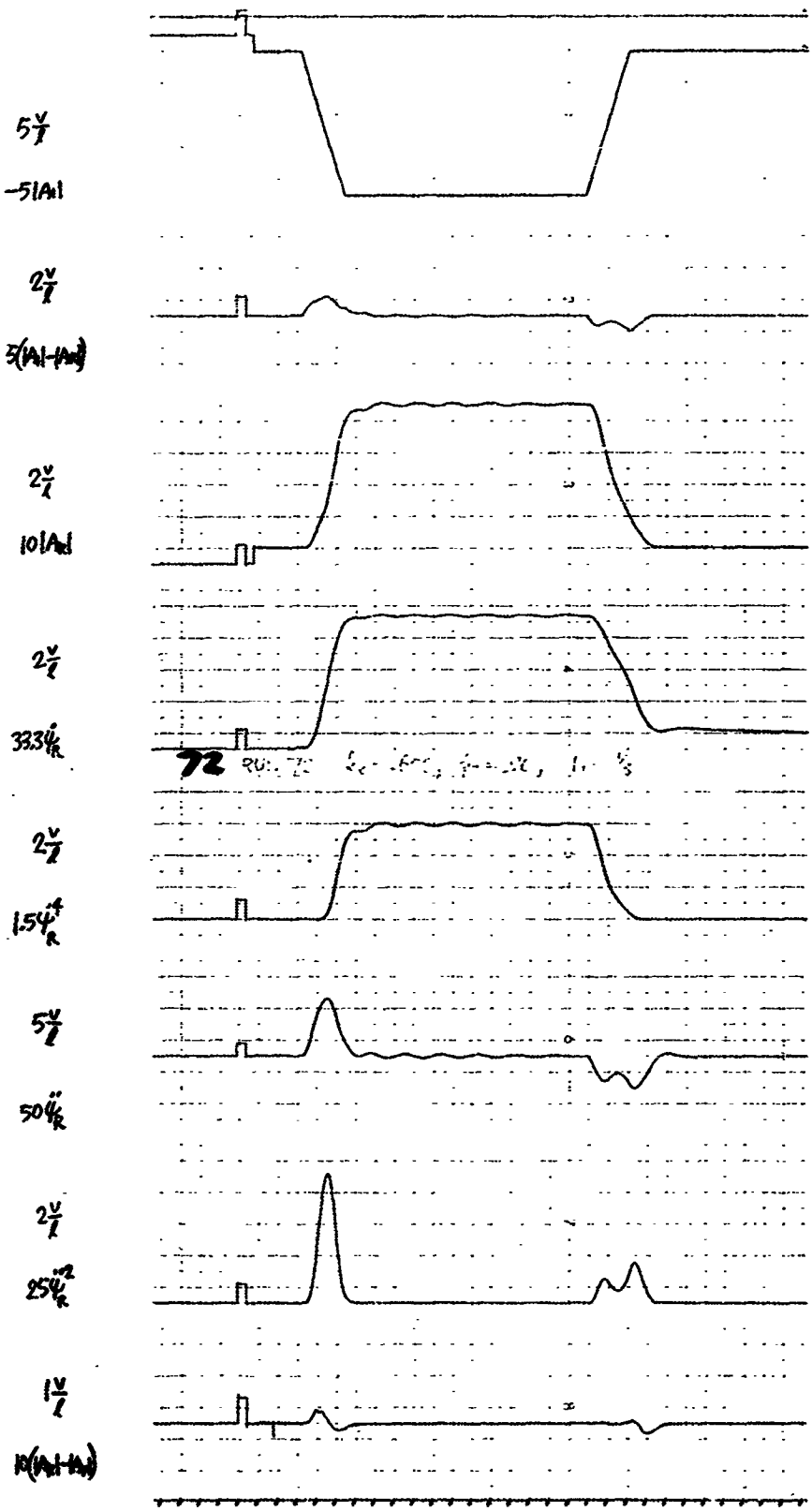
5 V/I
−5|A₁|
2 V/I
5(|A₁|−|A₂|)
2 V/I
10|A₂|
2 V/I
33.3ψ̇_R
72
2 V/I
15.4ψ̇_R
5 V/I
50ψ̈_R
2 V/I
25ψ̈²_R
1 V/I
10(|A₁|−|A₂|)